



Ianniciello, Angela (2019) *An investigation into the role of ULK1 in regulating chronic myeloid leukaemia stem and progenitor cell differentiation and sensitivity to tyrosine kinase inhibitors*. PhD thesis.

<https://theses.gla.ac.uk/77858/>

Copyright and moral rights for this work are retained by the author

A copy can be downloaded for personal non-commercial research or study, without prior permission or charge

This work cannot be reproduced or quoted extensively from without first obtaining permission from the author

The content must not be changed in any way or sold commercially in any format or medium without the formal permission of the author

When referring to this work, full bibliographic details including the author, title, awarding institution and date of the thesis must be given

Enlighten: Theses

<https://theses.gla.ac.uk/>  
[research-enlighten@glasgow.ac.uk](mailto:research-enlighten@glasgow.ac.uk)

**An investigation into the role of ULK1 in regulating  
chronic myeloid leukaemia stem and progenitor  
cell differentiation and sensitivity to tyrosine  
kinase inhibitors**

Angela Ianniciello

Thesis submitted to the University of Glasgow  
in accordance with the requirements for the degree of  
Doctor of Philosophy

Institute of Cancer Sciences  
College of Medical, Veterinary and Life Sciences  
University of Glasgow

September 2019



## Abstract

Chronic Myeloid leukaemia (CML) is a stem cell driven disease, and a paradigm for cancer stem cell biology and targeted therapy. The BCR-ABL oncoprotein is expressed in the most primitive leukaemic stem cells (LSCs) and drives myeloid expansion and accumulation of mature blood cells. Front line treatment for CML, using tyrosine kinase inhibitors (TKIs), still represents one of the most effective treatment for cancer. However, autophagy embodies a key role in LSC persistence following TKI treatment. Therefore, autophagy represents an attractive target for LSCs eradication. Our study using patient-derived CD34<sup>+</sup> CML cells indicates that ULK1, an autophagy-inducing kinase, is activated following TKI treatment, demonstrated by phosphorylation of its downstream target ATG13. Using a CRISPR-Cas9-mediated ULK1 knock-out (KO) we show that TKI treatment does not induce autophagy in ULK1 KO cells, thereby sensitising CML cells to TKI treatment *in vitro* and *in vivo*.

Here we also uncover a new combination treatment option, by exploiting a novel ULK1 kinase inhibitor (MRT403) that is under pre-clinical development. MRT403 treatment inhibited ULK1-mediated autophagy in a concentration-dependent manner, monitored by mitochondrial degradation in Parkin-dependent “enhanced mitophagy” assay. This correlates with increased mitochondrial respiration, measured by oxygen consumption rate, increased level of mitochondrial reactive oxygen species (ROS), and decreased level of glycolysis. Interestingly, using autophagy deficient cells (i.e. ATG7 KO) we show that while the effect of ULK1i treatment on mitochondrial respiration is autophagy-dependent, the effect on glycolysis is independent of autophagy.

Of clinical relevance, using robust patient-derived xenograft model, MRT403 targeted human CML CD34<sup>+</sup>133<sup>+</sup> LSCs *in vivo* when used in combination with TKI treatment.

Moreover, inhibiting ULK1 kinase activity in an inducible BCR-ABL mouse model promotes differentiation of LSCs when combined with imatinib. Loss of long-term leukaemic stem cells (LT-LSCs) resulted in increased megakaryocyte-erythroid progenitor (MEP) which contributed to rescue both disease and TKI-induced disfunction in erythroid maturation.

In conclusion, our findings describe a novel metabolic role for ULK1 in LSCs and provide a strong rationale for further clinical development of specific autophagy inhibitors as a therapeutic strategy to more effectively target TKI-resistant LSCs in CML patients.

# Table of Contents

Abstract .....	ii
List of Figures .....	ix
List of Tables .....	xii
Acknowledgements .....	xiii
Author's Declaration .....	xv
Declaration and permission of publication .....	xvi
Abbreviations .....	xvii
Chapter 1 Introduction .....	1
1.1 Haematopoiesis and haematopoietic stem cells (HSCs) .....	2
1.1.1 Ontogeny of haematopoiesis .....	2
1.1.2 HSCs hierarchy .....	2
1.1.3 HSCs isolation and identification .....	4
1.1.4 HSCs regulation .....	5
1.1.5 Stem cell proliferation and maintenance, a key role for fatty acid oxidation (FAO) .....	9
1.1.6 HSCs maintenance: Glycolysis versus OXPHOS .....	9
1.2 Leukaemic stem cells (LSCs) .....	10
1.2.1 Origin of LSCs .....	10
1.3 Chronic myeloid leukaemia (CML) is a stem cell driven cancer .....	11
1.3.1 CML epidemiology, diagnosis and disease progression .....	13
1.3.2 BCR-ABL signalling pathway .....	14
1.3.3 CML treatment: a historical point of view .....	15
1.3.4 TKI as a new treatment for CML .....	15
1.3.5 Imatinib resistance .....	18
1.3.6 Approaches to face imatinib resistance .....	19
1.3.7 LSCs persistence .....	21
1.3.8 LSCs metabolism .....	22
1.4 Autophagy .....	23
1.4.1 Overview .....	23
1.4.2 ULK1 initiation complex .....	25
1.4.3 VPS34 complex .....	29
1.4.4 Autophagosome completion .....	29
1.4.5 Autolysosome formation .....	30
1.4.6 Cargo receptor proteins: p62 .....	30
1.5 Autophagy and HSCs .....	31
1.5.1 Autophagy, key player in HSC maintenance .....	31
1.5.2 Autophagy and HSC cell cycle .....	31

1.5.3	Mitophagy .....	32
1.5.4	Mitophagy controls oxidative stress in HSCs .....	33
1.6	Autophagy and LSCs .....	35
1.6.1	Mitophagy and LSCs .....	35
1.6.2	Autophagy in the initiation of leukaemia .....	36
1.6.3	Autophagy in LSC drug resistance .....	36
1.6.4	CHOICES clinical trial and new generation of autophagy inhibitors. ....	36
1.6.5	Inhibition of ULK1 as a new emerging tool in the treatment of cancer and other diseases .....	37
1.7	Erythroid maturation.....	37
1.7.1	Autophagy and terminal erythropoiesis .....	39
Aims	.....	41
Chapter 2	Materials and methods.....	42
2.1	Human primary samples .....	43
2.1.1	Human primary sample origin .....	43
2.1.2	Enrichment of CD34 <sup>+</sup> cells from individuals diagnosed with CP-CML .....	44
2.1.3	Enrichment of Ph chromosome negative CD34 <sup>+</sup> cells.....	44
2.1.4	Thawing of primary cells .....	47
2.2	Human Long- and Short- Term Culture-Initiating Cell Assays .....	47
2.2.1	Colony Forming Cell (CFC) assay .....	47
2.2.2	Long-term culture-initiating cell (LTC-IC) assay .....	48
2.3	Erythroid maturation study using CD34 <sup>+</sup> CML cells .....	50
2.4	Culturing of cells .....	50
2.4.1	Maintenance of cell lines .....	50
2.4.2	Cryo-preservation of cell lines.....	50
2.4.3	Thawing of cell lines .....	50
2.5	Drugs preparation .....	51
2.6	Immunoblotting.....	51
2.6.1	Protein lysis and quantification .....	51
2.6.2	Hand casting polyacrylamide gels.....	52
2.6.3	SDS-PAGE separation of proteins .....	53
2.6.4	Transfer to PVDF membrane .....	54
2.6.5	Blocking and immunolabelling .....	54
2.7	Flow cytometry analyses .....	57
2.7.1	FACs staining procedure .....	58
2.7.2	Cell Trace Violet staining.....	58
2.7.3	Apoptosis staining .....	59
2.7.4	MitoSOX staining .....	59
2.8	NADPH measurements .....	59

2.9	Immunohistochemistry.....	61
2.10	RNA isolation and qPCR .....	61
2.10.1	RNA extraction .....	61
2.10.2	RNA isolation.....	61
2.10.3	RNA quantification and cDNA synthesis.....	62
2.10.4	qPCR reaction.....	62
2.11	Viral particles production and transfection .....	64
2.11.1	Viral particles production.....	64
2.12	Plasmid vectors.....	65
2.12.1	LentiCRISPR V2 vector Plasmid #52961 addgene .....	65
2.12.2	RFP-GFP LC3 puromycin vector Plasmid #84572 addgene.....	66
2.12.3	pLenti CMV V5-LUC blasticidin vector Plasmid #21474 addgene..	67
2.12.4	YFP-Parkin-IRES-zeocin Plasmid #61728 addgene .....	68
2.12.5	psPAX2 Plasmid #12260 addgene.....	69
2.12.6	pCMV-VSV-G Plasmid #8454 addgene.....	70
2.13	CRISPR cas9-mediated knock-out.....	71
2.13.1	Background.....	71
2.13.2	How to design Target Guide Sequence to generate knock-out....	71
2.13.3	Lentiviral vector digestion, oligo annealing and cloning .....	73
2.13.4	Transformation into Stbl3 bacteria.....	74
2.14	Parkin-enhanced mitophagy assay.....	75
2.15	Single cell cloning.....	75
2.16	Animal work.....	76
2.16.1	Ethical approval .....	76
2.16.2	Mouse models and in vivo studies.....	76
2.16.3	Plasma extraction from fresh blood.....	78
2.16.4	<i>In vivo</i> imaging of tumour-initiating CML cells.....	78
2.17	Live-cell Metabolic Assay using Seahorse Analyser.....	79
2.17.1	Basal respiration, maximal respiration and ATP linked analysis ..	81
2.17.2	Glycolytic function analysis .....	82
2.18	Cell viability assays .....	83
2.18.1	XTT assay.....	83
2.18.2	Resazurin assay.....	84
Chapter 3	Autophagy as a survival mechanism sustain LSPCs persistence .....	86
3.1	Introduction .....	87
3.2	Results .....	88
3.2.1	Second generation TKIs are not able to eradicate CML LSPCs .....	88
3.2.2	Autophagy level in normal and leukaemic stem cells .....	90
3.2.3	Nilotinib treatment induces protective autophagy in LSPCs .....	96

3.2.4	Deletion of ULK1 using CRISPR-Cas9 technology reduces autophagy levels in CML cells.....	104
3.2.5	ULK1 deficiency sensitises CML cells to TKIs treatment <i>in vitro</i> ...	104
3.2.6	Nilotinib fails to induce autophagy in ULK1 deficient cells .....	106
3.2.7	ULK1 deficiency sensitises CML cells to TKIs treatment <i>in vivo</i> ....	109
3.3	Discussion .....	116
Chapter 4	Using MRT921 to target CML LSPCs.....	118
4.1	Introduction .....	119
4.2	Results .....	121
4.2.1	MRT921 treatment inhibits CML cells proliferation in a concentration dependent manner.....	121
4.2.2	MRT921 induces cell death in WT and ULK1 deficient cells .....	123
4.2.3	ULK1 and ATG7 deficient CML cells exhibit lower level of basal and stressed-induced Parkin-dependent mitophagy .....	125
4.2.4	MRT921 treatment inhibits stressed-induced Parkin-dependent autophagy .....	128
4.2.5	MRT921 treatment increases accumulation of mitochondria and increases oxidative metabolism in CML cells .....	130
4.2.6	MRT921 treatment reduces glycolytic rate in CML cells .....	132
4.2.7	MRT921 treatment inhibits TKI-induced autophagy in CML.....	132
4.2.8	MRT921 treatment enhances TKIs effect in targeting CML cells....	135
4.2.9	MRT921 treatment affects cell viability of CD34 <sup>+</sup> CML cells in a concentration dependent manner .....	137
4.2.10	MRT921 inhibits TKI-induced autophagy in CD34 <sup>+</sup> CML cells .....	140
4.2.11	MRT921 enhances nilotinib-induced cell death in CD34 <sup>+</sup> cells....	142
4.2.12	MRT921 at 1 $\mu$ M has minimal effect on normal CD34 <sup>+</sup> CML cells .	145
4.3	Discussion .....	147
Chapter 5	Using MRT403 to target CML LSPCs.....	149
5.1	Introduction .....	150
5.2	Results .....	151
5.2.1	Validating new ULK1/2 inhibitors in CML .....	151
5.2.2	MRT403 further inhibits TKI-induced autophagy in ULK1 KO cells..	159
5.2.3	Discussion .....	162
5.2.4	Using MRT403 to inhibit TKI-induced autophagy and targeting of LSPCs using.....	163
5.3	Discussion .....	215
Chapter 6	Conclusion and future directions.....	218
6.1	Conclusions .....	219
6.1.1	Autophagy in HSCs and LSCs .....	219
6.1.2	TKI-induced autophagy in CML.....	221
6.1.3	Inhibition of autophagy induces phenotype changes in LSPCs .....	222

6.1.4 Inhibition of ULK1 to target TKI-induced autophagy and overcome TKI sensitivity in CML LSPCs .....	224
6.2 Future directions .....	225
Bibliography .....	228

# List of Figures

Figure 1.1: Schematic overview of haematopoiesis .....	3
Figure 1.2: Overview of metabolic features contributing to HSCs maintenance and differentiation in the endosteal niche. ....	8
Figure 1.3: Reciprocal translocation of BCR-ABL genes within LT-HSCs.....	12
Figure 1.4: CML patient's survival curve .....	17
Figure 1.5: Schematic representation of autophagy activation .....	24
Figure 1.6: ULK1 domain structure with location of phosphorylation sites.....	27
Figure 1.7: Overview of Parkin-dependent mitophagy.....	34
Figure 1.8: Erythrocyte maturation.....	40
Figure 2.1: Schematic diagram for selection and enrichment of BM-derived normal CD34 <sup>+</sup> cells. ....	46
Figure 2.2: Schematic diagram illustrating LTC-IC assay (adapted from <a href="https://cdn.stemcell.com/media/files/manual/MA28412Human_Long_Term_Culture_Initiating_Cell_Assay.pdf">https://cdn.stemcell.com/media/files/manual/MA28412Human_Long_Term_Culture_Initiating_Cell_Assay.pdf</a> ).....	49
Figure 2.3: Genome engineering using CRISPR cas9 .....	71
Figure 2.4: BsmBI digestion restriction fragment on lentiCRISPRv2.....	72
Figure 2.5: Example of oligos design. ....	72
Figure 2.6: lentiCRISPRv2 following BsmBI digestion.....	73
Figure 2.7: Serial dilution scheme for single cell cloning .....	76
Figure 2.8: Mitochondrial respiration profile.....	82
Figure 2.9: Glycolytic function profile .....	82
Figure 2.10: 1:2 serial dilution of compounds used for cell viability assay .....	85
Figure 3.1: Nilotinib only targets differentiate CML cells and enriches for CML LSPCs .....	89
Figure 3.2: Autophagic function in HSCs and LSCs.....	91
Figure 3.3: Primitive CML cells show a decrease in autophagy genes expression compared to normal cells. ....	93
Figure 3.4: CD34 <sup>+</sup> CML cells show lower level of autophagy flux than normal CD34 <sup>+</sup> cells.....	95
Figure 3.5: Mechanistic hypothesis of TKIs-induced autophagy in CML cells. ....	97
Figure 3.6: Efficiency of retroviral transfection in K562 cells. ....	98
Figure 3.7: Autophagy is induced in K562 following TKI treatment. ....	99
Figure 3.8: Primitive CML cells show an increase in autophagy genes expression following nilotinib treatment. ....	100
Figure 3.9: AMPK and mTOR regulates autophagy in CD34 <sup>+</sup> cells following nilotinib treatment. ....	103
Figure 3.10: Using CRISPR cas9 to knock-out ULK1 in CML cells.....	105
Figure 3.11: ULK1 deficient cells are more sensitive to TKIs treatment. ....	107
Figure 3.12: Nilotinib fails to induce autophagy in ULK1 deficient cells.....	108
Figure 3.13: Luminescence of CNTR. and ULK1 KO cells following transfection with luciferase expressing plasmid. ....	110
Figure 3.14: Xenografted NRGW41 mice with ULK1 deficient cells are more sensitive to imatinib treatment compared to mice receiving control cells. ....	111
Figure 3.15: Imatinib extend survival of NRGW <sup>41</sup> mice receiving ULK1 KO cells. ....	112
Figure 3.16: ULK1 KO cells significantly reduce number of tumours following imatinib treatment. ....	113
Figure 3.17: ULK1 deficient tumours show reduced level of autophagy following imatinib treatment. ....	115

Figure 4.1: MRT921 inhibits growth of TKI-sensitive and TKI-resistant CML cell lines .....	122
Figure 4.2: ULK1/2 inhibitor affects apoptosis and CFC in WT and ULK1 deficient CML cells.....	124
Figure 4.3: Over-expression of Parkin enhances mitophagy in CML cells .....	126
Figure 4.4: ULK1 and ATG7 deficient cells exhibit decreased Parkin-dependent mitophagy .....	127
Figure 4.5: MRT921 inhibits Parkin-dependent mitophagy .....	129
Figure 4.6: MRT921 induces accumulation of mitochondria and affects mitochondrial metabolism .....	131
Figure 4.7: MRT921 impairs glycolytic capacity in CML cells.....	133
Figure 4.8: MRT921 inhibits TKI-induced autophagy in CML cells .....	134
Figure 4.9: Combination treatment using nilotinib and MRT921 targets CML cells .....	136
Figure 4.10: MRT921 effect on inhibition of growth of CML CD34 <sup>+</sup> cells .....	138
Figure 4.11: MRT921 induces apoptosis and inhibits CFC in a concentration dependent manner in CML cells .....	139
Figure 4.12: MRT921 inhibits TKI-induced autophagy in patient-derived CD34 <sup>+</sup> CML cells.....	141
Figure 4.13: MRT921 targets CD34 <sup>+</sup> CML cells in combination with nilotinib ....	143
Figure 4.14: MRT921 targets LSPCs .....	144
Figure 4.15: Effect of MRT921 alone and in combination with nilotinib in CD34 <sup>+</sup> normal cells .....	146
Figure 5.1: New ULK1/2 inhibitor effect on viability of CML cells .....	152
Figure 5.2: Effect of ULK1/2 inhibition in KCL22 ULK1-deficient and ULK1-competent cells.....	153
Figure 5.3: Measurements of mitophagy inhibition using MRT993 and MRT016 ..	155
Figure 5.4: Using MRT403 to inhibit Parkin-dependent mitophagy.....	156
Figure 5.5: Using new generation ULK1/2 inhibitors to target TKI-induced autophagy .....	158
Figure 5.6: Validating new ULK1/2 inhibitors in combination with nilotinib to target CML cells .....	160
Figure 5.7: Effect of MRT403 treatment is dependent on ULK1 .....	161
Figure 5.8: MRT403 inhibits basal mitophagy in CD34 <sup>+</sup> CML cells .....	164
Figure 5.9: MRT403 treatment increases ROS levels and OCR in CD34 <sup>+</sup> CML cells .....	172
Figure 5.10: ULK1 and ATG7 KO cells exhibit an increase in mitochondrial respiration.....	173
Figure 5.11: MRT403 impairs glycolytic capacity and reduces NADPH in CD34 <sup>+</sup> CML cells.....	175
Figure 5.12: Pharmacological or genetical inhibition of ULK1 impairs glycolysis independently from autophagy inhibition. ....	176
Figure 5.13: MRT403 treatment reduces percentage of CD34 <sup>+</sup> and CD34 <sup>+</sup> CD133 <sup>+</sup> cells .....	178
Figure 5.14: MRT403 treatment drives an increase in CD44 <sup>+</sup> GlyA <sup>+</sup> cells.....	181
Figure 5.15: MRT403 treatment drives an increase in CD71 <sup>+</sup> GlyA <sup>+</sup> cells.....	182
Figure 5.16: MRT403 treatment drives an increase in CD36 <sup>+</sup> GlyA <sup>+</sup> cells.....	183
Figure 5.17: ULK1 deficient cells exhibit an increase in ROS levels and in erythropoiesis markers such as CD71 and GlyA <sup>+</sup> .....	184
Figure 5.18: MRT403 is well tolerated in NSG mice .....	186
Figure 5.19: Experimental plan of <i>in vivo</i> study treating DTG mice using MRT403 .....	189

Figure 5.20: MRT403 treatment reduces percentage of transplanted leukaemic cells without affecting myeloid cells .....	190
Figure 5.21: MRT403 treatment increases percentage of leukaemic MEP .....	192
Figure 5.22: MRT403 treatment increases number of Ter119 <sup>+</sup> cells in the BM of leukaemic mice .....	193
Figure 5.23: MRT403 treatment has marginal effect on LT- and ST-LSCs and on MPP subpopulation .....	195
Figure 5.24: MRT403 inhibits TKI-induced autophagy in CD34 <sup>+</sup> CML cells .....	197
Figure 5.25: MRT403 targets CD34 <sup>+</sup> CML cells in combination with nilotinib ....	199
Figure 5.26: MRT403 targets patient-derived stem and progenitor CML cells ...	200
Figure 5.27: MRT403 has minimal effect in normal stem and progenitor cells ..	202
Figure 5.28: MRT403 inhibits autophagy <i>in vivo</i> in transplanted hCD45 .....	204
Figure 5.29: Experimental plan of 2 independent PDX studies using 2 different CML samples .....	205
Figure 5.30: MRT403 targets human LSPCs <i>in vivo</i> in combination with TKI .....	207
Figure 5.31: MRT403 reduced percentage of leukaemic cells increasing ratio of normal cells as a single agent and in combination with TKI .....	209
Figure 5.32: MRT403 and imatinib combination treatment increases percentage of leukaemic MEP <i>in vivo</i> .....	211
Figure 5.33: MRT403 treatment increases number of Ter119 <sup>+</sup> cells in the BM of leukaemic mice .....	213
Figure 5.34: MRT403 treatment in combination with imatinib targets imatinib-resistant LT-LSCs <i>in vivo</i> .....	214
Figure 6.1: Inhibition of ULK1-dependent autophagy induces differentiation of LSCs potentiating TKI treatment and rescuing anaemia .....	226

## List of Tables

Table 1.1: Human haematopoietic stem and progenitor cell phenotypes .....	6
Table 1.2: List of known ULK1 substrates and function .....	28
Table 1.3: ULK1/2 inhibitors.....	38
Table 2.1: List of CML samples .....	43
Table 2.2: List of normal samples.....	44
Table 2.3: Preparation of PGF cocktail .....	45
Table 2.4: Drugs details .....	51
Table 2.5: Preparation of acrylamide-gels .....	53
Table 2.6: List of western blotting antibody .....	56
Table 2.7: List of FACS antibodies .....	60
Table 2.8: 2X RT MASTER MIX.....	62
Table 2.9: TaqMan qPCR mix .....	63
Table 2.10: Virus mix .....	64
Table 2.11: ULK1 and ATG7 oligo sequences .....	73
Table 3.1: Autophagy gene expression in CD34 <sup>+</sup> CML and normal cells measured by qPCR. ....	94
Table 3.2: Autophagy gene expression in CD34 <sup>+</sup> CML treated and untreated with nilotinib for 24h measured by qPCR. ....	101

# Acknowledgements

These past 4 years have been a great opportunity for me to learn and develop in the scientific field. I have met so many people during this path and the support received to make this thesis possible, I want to start by thanking my supervisor Dr Vignir Helgason for giving me the opportunity to undertake this PhD and to work on such a challenging and interesting project. I also would like to thank him for all the support and encouragement received during all the time I have spent in his lab. I would also like to thank all the members of Vignir's lab, Kevin, Martha, Amy, Lucie, Eric, Zuzanka, Elodie and Pablo for the many hours spent working all together and all the fun times we had as a team and friends.

Thanks also go to my second supervisor Dr David Vetrie for his support and the many chats we had about science. I would also like to thank all the members of his lab for the time shared in the lab and the great environment of the leukaemia team in Glasgow, in particular to Mary for her help with all the *in vivo* studies; Jake, Jane, Karim and Hassam with whom I started this PhD experience and for the friendship shared within all my PhD.

I would also thank our mentor Professor Tessa Holyoake for being a source of inspiration in science and in life.

I would like to thank Professor Kevin Ryan and all his team for the guidance and the advice received.

I would like to thank Dr Barbara Saxty for her advice, support and useful discussion during my studies on ULK1.

I would like to acknowledge all the people that made this work possible, Dr Mhairi Copland, Alan Hair and all the colleagues at the Paul O'Gorman Leukaemia research centre for the primary samples. Thanks to the Dr Alexis Smith and Selena McCafferty from the NHS bio-respiratory unit for providing all the normal samples. Thanks to Karen, Chris, and Evarest from the animal facility for their help with the mouse work. Thanks also go to Tom Gilbey for his great support at the FACs.

I also want to take the opportunity to thank all the friends made at the WWCRC in particular Alice for the many chats and coffee breaks shared and Jessica for her help at the confocal. A special thanks goes to Giusy, Holly and Ilaria for the great time we had together as scientists and friends.

My gratitude also goes to Tenovus Scotland for providing the funding for my PhD.

Thanks to my family for all the efforts made to always support me and encourage me.

Lastly, I want to thank George for all the support, patience and love towards those years.

## **Author's Declaration**

I declare that I am the author of this work, unless where explicit reference is made to the contribution of others. This dissertation, in whole or in part, has not been submitted for consideration of any other degree within the University of Glasgow or any other institution.

Angela Ianniciello

# Declaration and permission of publication

The work presented in this dissertation has contributed towards the following publication:

*The Ins and Outs of Autophagy and Metabolism in Hematopoietic and Leukemic Stem Cells: Food for Thought. Front. Cell Dev. Biol., 26 September 2018*

Ianniciello, Kevin M. Rattigan, G. Vignir Helgason

<https://www.frontiersin.org/articles/10.3389/fcell.2018.00120/full>

Frontiers in Cell and Developmental Biology publishes under [CC-BY license](https://creativecommons.org/licenses/by/4.0/), <https://creativecommons.org/licenses/by/4.0/>

**Copyright** © 2018 Ianniciello, Rattigan and Helgason. This is an open-access article distributed under the terms of the [Creative Commons Attribution License \(CC BY\)](https://creativecommons.org/licenses/by/4.0/). The use, distribution or reproduction in other forums is permitted, provided the original author(s) and the copyright owner(s) are credited and that the original publication in this journal is cited, in accordance with accepted academic practice. No use, distribution or reproduction is permitted which does not comply with these terms.

Permission to include part of this work within this dissertation is listed in the email below.

## **Angela Ianniciello (student)**

---

**From:** Frontiers in Cell and Developmental Biology <cellbiology@frontiersin.org>  
**Sent:** 29 October 2018 07:40  
**To:** Angela Ianniciello  
**Subject:** Re: Article reproduction in my dissertation

Dear Angela, if I may

Thank you for your query.

Please be aware that *Frontiers in Cell and Developmental Biology* is a Gold Open Access journal and thus, the entire content of all present and past journals is not only immediately and permanently accessible online free of charge but also published under the [CC-BY license](https://creativecommons.org/licenses/by/4.0/), which permits **unrestricted use, distribution, and reproduction in any medium, provided the original authors and the source are credited.**

Please note that this information can be found on every published article at the Copyright section at the bottom of the [article](#).

Should you have any further questions, please do not hesitate to contact me.

Best wishes and the best of luck with your PhD dissertation.  
Justyna

Frontiers | Editorial Office - Journal Development Team

Journal Development Manager: [Katie Powis](#), PhD  
Journal Development Specialist: [Justyna Lisowska](#), PhD

Frontiers  
[www.frontiersin.org](http://www.frontiersin.org)

Avenue du Tribunal-Fédéral 34  
1015, Lausanne, Switzerland  
Office T + 41 21 510 1700  
[Connect with us](#)

For technical issues, please contact [support@frontiersin.org](mailto:support@frontiersin.org)

## Abbreviations

7AAD	7 aminoactinomycin D
Ab	Antibody
ABC	ATP-binding cassette
ABL	Abelson murine leukaemia viral oncogene homolog
ACC	Acetyl-CoA carboxylase
Allo-SCT	Allogenic stem-cell transplantation
AKT	Protein kinase B
AML	Acute myeloid leukaemia
AMPK $\alpha$	5' AMP-activated protein kinase alpha
AP	Accelerated phase
APS	Ammonium persulfate
ATG	autophagy-related ( <i>ATG</i> ) genes
BC	Blast crisis
BIT	BSA-Insulin-Transferrin
BSA	Bovin serum albumin
BCR	Breakpoint cluster region
Baf	Bafilomycin A1
BM	Bone marrow
cDNA	Complementary DNA
C-KIT	Receptor tyrosine kinase
CCyR	Complete cytogenetic response
CFC	Colony forming cell
CHOICES	CHLoroquine and Imatinib Combination to Eliminate Stem cells
CHR	Complete haematological response
CYP	Cytochrome P450
CLP	Common lymphoid progenitor
CML	Chronic myeloid leukaemia
CMP	Common myeloid progenitor
CNS	Central nervous system
CNTR	Control
CP	Chronic phase
Crkl	Crk-like protein
	Class 2 Clustered Regularly Interspaced Short Palindromic Repeat
CRISPR	Repeat
CSC	Cancer stem cell
CTV	Cell trace violet
DMR	Deep molecular response
DMSO	Dimethylsulfoxide
DNA	Deoxyribonucleic acid
DTG	Double transgenic
DTT	Dithiothreitol
ECAR	Extracellular acidification rate
EDTA	Ethylenediaminetetraacetic acid
ELN	European Leukaemia Net
EPO	Erythropoietin

ESCC	Oesophageal squamous cell carcinoma
FAO	Fatty acid oxidation
FBS	Foetal bovine serum
FDA	Food and drug administration
G6PDH	Glucose-6-phosphate dehydrogenase
GCA	Grancalcin
GeCKO	Genome-scale CRISPR Knock Out
GF	Growth factor
GFP	Green Fluorescent Protein
G-CSF	Granulocyte-colony stimulating factor
Gy	Gray unit
GM-CSF	Granulocyte-macrophage colony-stimulating factor
GMP	Granulocyte-macrophage progenitor
GSK3	Glycogen synthase kinase 3
HBSS	Hank's buffered salt solution
HCQ	Hydroxychloroquine
HIF	Hypoxia-inducible factor-1 $\alpha$
HSC	Haematopoietic stem cells
KO	Knock-out
HSPC	Haematopoietic stem and progenitor cells
IFN- $\alpha$	Interferon-alpha
IL-3	Interleukin-3
IL-6	Interleukin-6
IMDM	Iscove's modified Dulbecco's media
IRIS	International Randomized Study of Interferon and ST1571
LC3	Microtubule-associated protein 1A/1B-light chain 3
LIF	Leukaemic inhibitory factor
Lin	Lineage
LIR	LC3-interacting region
LSC	Leukaemic stem cells
LSPC	Leukaemic stem and progenitor cell
LT-LSC	Long term leukaemic stem cell
LTC-IC	Long-term culture-initiating cell
MCyR	Major cytogenetic response
MEP	Megakaryocyte-erythroid progenitor
MFN2	Mitochondrial protein mitofusin 2
MIP- $\alpha$	Macrophage inflammatory protein - alpha
MMR	Major molecular response
MPP	Multipotent progenitor
MTG	MitoTrackerGreen
mTOR	Mammalian target of rapamycin
NAC	N-acetyl cysteine
NADP	Nicotinamide adenine dinucleotide phosphate
NCCN	National Comprehensive Cancer Network
NSG	NOD scid gamma
OCR	Oxygen consumption rate
OD	Optical density

ON	Over-night
ORP4L	Oxysterol binding protein-related protein 4L
OXPPOS	Oxidative phosphorylation
p-	phospho-
P-gp	P-glycoprotein
Pen/Strep	Penicillin/Streptomycin
PBS	Phosphate-buffered saline
PDK	Pyruvate dehydrogenase kinase
PE	Phosphatidylethanolamine
PFA	Paraformaldehyde
Ph	Philadelphia
PGF	Physiological growth factor
PI	Phosphatidylinositol
PI3K	Phosphoinositide 3-kinase
PI3P	Phosphatidylinositol-3'phosphate
Pink1	PTEN-induced putative kinase 1
PIP2	Phosphoinositide4,5-bisphosphate
PIP3	Phosphoinositide-3,4,5-trisphosphate
PMS	N-methyl dibenzo pyrazine methyl sulphate
PPAR $\delta$	Peroxisome proliferator-activated receptor delta
PTPMT1	Phosphatase protein tyrosine phosphatase 1
PVDF	Polyvinylidene difluoride
RBC	Red blood cells
RFP	Red Fluorescent Protein
RISP	Rieske iron sulphur protein
RNA	Ribonucleic acid
ROS	Reactive oxygen species
RT	Room temperature
SB	Sample buffer
SCF	Stem-cell factor
SDS	Sodium dodecyl sulfate
SFM	Serum free media
SOS	Son of Sevenless
SRT7	Sirtuin 7
ST-LSC	Short term leukaemic stem cell
TCA	Tricarboxylic acid
TEMED	Tetramethylenediamine
TKI	Tyrosine kinase inhibitor
TSC1	Tuberous sclerosis complex 1
ULK1	Unc-51 like autophagy activating kinase 1
UPRmt	Mitochondrial unfolded protein response
UT	Untreated
VPS34	Vacuole protein sorting 34
XTT	2,3-bis-(2-methoxy-4-nitro-5-sulphenyl)-(2H)-tetrazolium-5-carboxanilide

# Chapter 1 Introduction

## 1.1 Haematopoiesis and haematopoietic stem cells (HSCs)

### 1.1.1 Ontogeny of haematopoiesis

Haematopoiesis, as bound in the Greek αἷμα, "blood" and ποιεῖν "to make", is the process that leads to generation of the entire blood cell repertoire throughout an individual's lifetime. Human haematopoiesis first takes place in the yolk sac, in a process known as *primitive haematopoiesis*<sup>1</sup>. Evidence indicates that circulating blood cells during the yolk sac phase are short lived cells limited to the myeloid compartment, mainly erythrocytes to support high oxygen demand, lacking the lymphoid lineage<sup>2,3</sup>. The second phase of haematopoiesis occurs within the embryo in the aorta-gonad-mesonephros region, where the first multipotent myelo-lymphoid stem cells are generated<sup>3</sup>. Haematopoiesis is temporarily hosted in the liver to finally establish in the thymus and mainly in the bone marrow (BM) as *definitive haematopoiesis*<sup>4</sup>.

### 1.1.2 HSCs hierarchy

The mammalian hematopoietic system is maintained by self-renewal of quiescent long-term (LT)-HSCs, which subsequently can differentiate into short-term (ST)-HSCs or multipotent progenitors (MPPs), which no longer carry self-renewal potential. HSCs fate is dictated by their decision to undergo symmetric or asymmetric cell division when HSCs leave quiescence. Asymmetric division generates two daughter cells of which one will show same features of the initiator cell, such as self-renewal and quiescence, and the other will differentiate and enter the circulatory system. Otherwise, symmetric division will generate two daughter cells that will only be able to undergo cell cycling and differentiation.

MPPs can give rise to two different lineages, myeloid and lymphoid, depending on MPPs segregating into common myeloid progenitor (CMP) or common lymphoid progenitor (CLP) cell. CLPs can give rise to all cells within the lymphoid compartment such as B and T cells, natural killer and dendritic cells. From CMPs can originate MEPs, which will differentiate into platelets and mature reticulocytes, and granulocyte-macrophage progenitors (GMPs), which

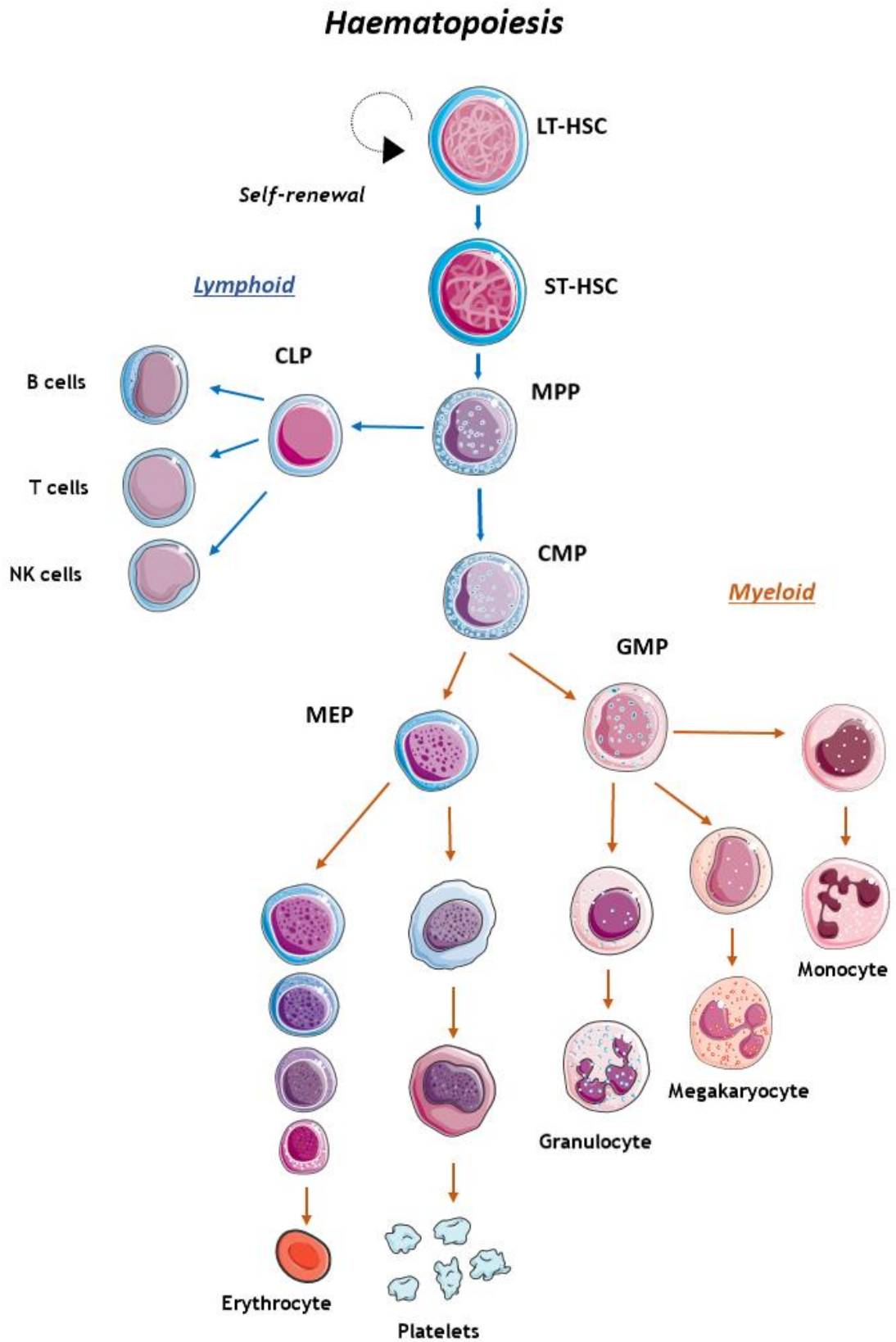


**Figure 1.1: Schematic overview of haematopoiesis**

Long-term haematopoietic stem cell (LT-HSC); short-term haematopoietic stem cell (ST-HSC); multipotent progenitor (MPP); common lymphoid progenitor (CLP); common myeloid progenitor (CMP); megakaryocyte/erythroid progenitor (MEP); granulocyte-macrophage progenitor (GMP).

differentiate into megakaryocytes, basophils, eosinophils, neutrophils, monocytes, macrophages and dendritic cells (Figure 1.1).

### 1.1.3 HSCs isolation and identification

Human haematopoietic stem and progenitor cells were identified, isolated and characterized using FACS analysis against surface markers (Table 1-1). *In vitro* colony forming cell (CFC) assay have helped to establish loss of quiescence and the ability of progenitor cells to proliferate and differentiate giving rise to specific type of colonies. As well, *in vivo* transplantation of human HSCs into immune-compromised recipient mice has established as a measure of BM repopulating ability of stem and progenitor cells.

First transplantation experiments used CD34<sup>+</sup> cells. However, *Baum et al.* demonstrated that cells expressing CD34 marker is a heterogeneous population. Of the CD34<sup>+</sup> cells only CD90<sup>+</sup>Lin<sup>-</sup> cells were able to generate both myeloid and lymphoid lineages following *in vivo* transplantation of CD34<sup>+</sup>CD90<sup>+</sup>Lin<sup>-</sup><sup>5</sup>. Following studies demonstrated that CD34<sup>+</sup>CD38<sup>-</sup> cells represents population enriched for LT-HSCs, able to repopulate both lineages respectively<sup>6</sup>.

Latest finding using single cell assays have however proposed a different representation of the hierarchical organization of haematopoiesis. Dick and Jacobsen studies indicate that during the first lineage restriction there isn't a complete separation between the myeloid and the lymphoid compartment but they propose a myeloid-lymphoid progenitor which shares features common to both lineages<sup>7-9</sup>. RNA-seq analysis on human bone marrow propose that lineage commitment doesn't require transition between different stages of progenitors but is a flow that occurs in uncommitted and unipotent HSPCs<sup>10</sup>. Together with that *Laurenti et al.* in a recent review propose a new representation of the haematopoietic tree, in which the destiny of a cell is dictated to an earlier stage than at the level of MPP<sup>11</sup>. However, combination of surface marker expression and functional assay together with single cell RNA-seq are still not exhaustive analysis to clarify specific lineage commitment.

## 1.1.4 HSCs regulation

### 1.1.4.1 Hypoxia, a key role in the regulation of HSCs quiescence

Because of their vital and long-term function, HSCs are provided with unique survival mechanisms. In this context, their localization in a complex endosteal niche, that is characterized by low levels of oxygen, is central<sup>12</sup>. Changes in the BM niche, such as increased production of growth factors and cytokines, as well as transplantation procedures and injuries, can stimulate HSCs to proliferate and differentiate. Once recovery is restored, HSCs return to a dormant state. Despite the fact that hypoxia tolerance in HSCs is poorly understood, it has been proposed to be responsible for the quiescence and slow cell cycling of HSCs<sup>13,14</sup>. *Takubo et al.* elucidated this mechanism by demonstrating that hypoxia-inducible factor-1 $\alpha$  (HIF-1 $\alpha$ ), a transcriptional factor that plays a central role in cellular response to oxygen levels, is stabilized by hypoxia in LT-HSCs<sup>15</sup>. In HIF-1 $\alpha$  deficient mice, loss of LT-HSCs numbers is directly proportional to loss of quiescence. This now raises the question: in what ways can hypoxia assume a protective role and assure LT-HSCs maintenance? HIF-1 $\alpha$  and hypoxia have in fact, been linked with the distinct metabolic phenotype of HSCs<sup>16</sup> (**Figure 1.2**).

### 1.1.4.2 HIF-1 $\alpha$ and the regulation of HSC metabolism

Metabolomic approaches indicate that LT-HSCs, when compared to MPPs and more differentiated cells, specifically upregulate glycolysis and repress influx of glycolytic metabolites into mitochondria, via regulation of pyruvate dehydrogenase kinase (PDK) activity by HIF-1 $\alpha$ <sup>17</sup>. Furthermore, glycolytic adenosine triphosphate (ATP) production, commissioned by the HIF-1 $\alpha$ /PDK regulatory system, is necessary to maintain HSCs during cell cycle quiescence. A recent discovery demonstrates that mitochondrial protein mitofusin 2 (MFN2), which has roles in mitochondrial fusion and in tying mitochondria to the endoplasmic reticulum, is essential for the maintenance of HSCs with wide lymphoid potential<sup>18</sup>. A different study identified that the mitochondrial unfolded protein response (UPR<sup>mt</sup>) is activated upon transition from quiescence

Cell type	Phenotype
<b>LT-HSC</b>	Self-renew <sup>high</sup> CD34 <sup>+</sup> CD38 <sup>-</sup> CD90 <sup>+</sup> CD45RA <sup>-</sup> Lin <sup>-</sup>
<b>ST-HSC</b>	Self-renew <sup>low</sup> CD34 <sup>+</sup> CD38 <sup>-</sup> CD90 <sup>-</sup> CD45RA <sup>-</sup> Lin <sup>-</sup>
<b>MPP</b>	Self-renew <sup>-</sup> CD34 <sup>+</sup> CD38 <sup>+</sup> CD90 <sup>-</sup> CD45RA <sup>-</sup> Lin <sup>-</sup>
<b>CLP</b>	CD34 <sup>+</sup> CD38 <sup>+</sup> CD123 <sup>low</sup> CD45RA <sup>+</sup> Lin <sup>-</sup>
<b>CMP</b>	CD34 <sup>+</sup> CD38 <sup>+</sup> CD123 <sup>low</sup> CD45RA <sup>-</sup> Lin <sup>-</sup>
<b>MEP</b>	CD34 <sup>+</sup> CD38 <sup>+</sup> CD123 <sup>-</sup> CD45RA <sup>-</sup> Lin <sup>-</sup>
<b>GMP</b>	CD34 <sup>+</sup> CD38 <sup>+</sup> CD123 <sup>+</sup> CD45RA <sup>+</sup> Lin <sup>-</sup>

**Table 1-1: Human haematopoietic stem and progenitor cell phenotypes**

## Chapter 1 Introduction

to proliferation in HSCs<sup>19</sup>. Remodelling the activity of sirtuin 7 (SIRT7), a component of the UPRmt, is translated into reduction of quiescence, higher mitochondrial unfolded protein stress, and insufficient self-renewal ability of HSCs. Furthermore, SIRT7 expression is lower in more mature HSCs whose regenerative capacity is improved following upregulation of SIRT7<sup>20</sup>. *Kim et al.*, using a cationic fluorescent dye that selectively accumulates in the mitochondria of eukaryotic cells, demonstrated that HSCs have relatively less mitochondria when compared to proliferating progenitors<sup>21</sup>. A subsequent study showed that differentiation of primary human HSCs (quantified by CD34 loss) is connected with increased mitochondrial content<sup>22</sup>. In agreement with this, *Simsek et al.* showed that LT-HSCs are characterized by low mitochondrial potential and utilize cytoplasmic glycolysis for ATP production<sup>23</sup>. Contrarily, cells that need to cycle and expand do not rely on anaerobic glycolysis. This may be because pyruvate produced during glycolysis will generate only 2 ATPs per molecule of glucose following anaerobic respiration (with lactate being the by-product), while it will produce 32 ATPs per molecule of glucose upon entering in the mitochondria to be used for oxidative phosphorylation (OXPHOS). However, *de Almeida et al.* using dye-independent methods, such as mitochondria DNA quantification and enumeration of mitochondria nucleoids, have recently suggested that while HSCs have high mitochondrial content, they have compromised respiratory and turnover capacity, concluding that mitochondria may perform an essential and yet unknown function in HSCs, which may not be directly linked with ATP production<sup>16,24</sup>.

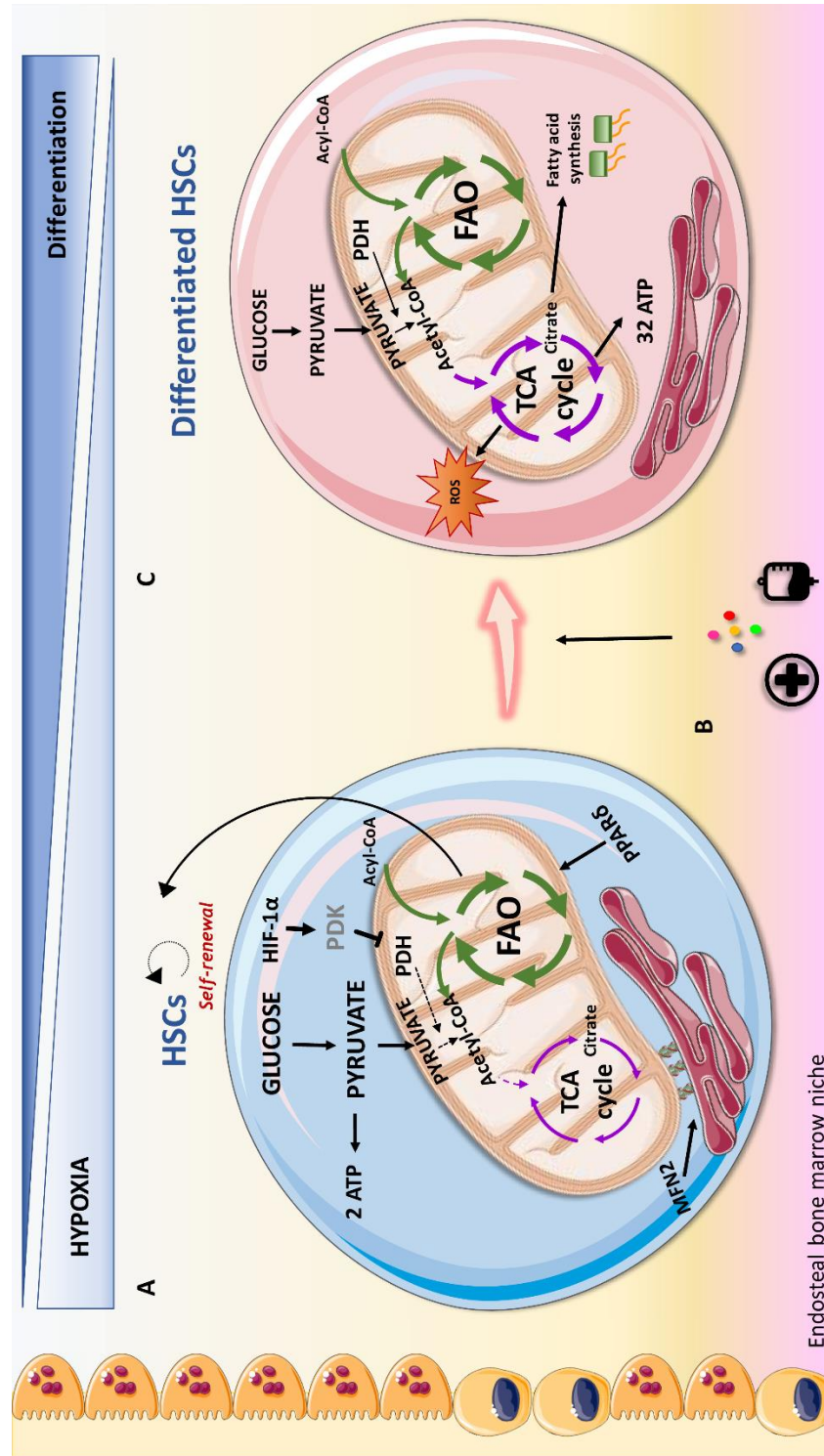


**Figure 1.2: Overview of metabolic features contributing to HSCs maintenance and differentiation in the endosteal niche.**

HSCs are characterized by the expression of the surface marker CD34 and utilize anaerobic glycolysis and fatty acid oxidation (FAO) as the sources of energy. Nutrient sensor peroxisome proliferator-activated receptor delta (PPAR $\delta$ ) promotes FAO, contributing to their self-renewal capacity. HIF-1 $\alpha$  represents a fundamental feature in regulating oxidative metabolism via regulation of pyruvate dehydrogenase kinase (PDK) (a). Transplantation procedures, cytokines and injuries can promote HSCs to proliferate and differentiate (b). Differentiated HSCs lose their stemness surface marker CD34 and adapt their energy source to address energy demand for proliferation. CD34<sup>+</sup> haematopoietic cells, rely on increased oxidative metabolism that provides a higher production of ATP compared to anaerobic glycolysis. Oxidative metabolism can result in increased production of reactive oxygen species (ROS), which can contribute to differentiation. PDH, pyruvate dehydrogenase; MFN2, mitofusin 2 (c). Image from *Ianniciello et al.*<sup>16</sup>

### **1.1.5 Stem cell proliferation and maintenance, a key role for fatty acid oxidation (FAO)**

LT-HSC glycolytic phenotype can be seen as a protective mechanism to reduce reactive oxygen species (ROS) generation, which would cause oxidative stress and induce differentiation<sup>25</sup>. Based on this, a recent study demonstrated that while mitochondrial complex III subunit Rieske iron sulphur protein (RISP), in foetal HSCs is not essential for mitochondrial membrane potential maintenance, it is crucial for stem cell genes and multilineage potential retainment<sup>26</sup>. Based on the critical role of mitochondria in driving cell differentiation, RISP null foetal HSCs were unable to generate an adequate number of MPPs indicating compromised HSC differentiation. In addition, products of the tricarboxylic acid (TCA) cycle, such as citrate, could be exported to the cytosol to contribute to lipid metabolism that is required for cell growth, proliferation and differentiation<sup>27</sup>.

FAO, which occurs in the mitochondria, also plays an important role in HSCs maintenance. FAO metabolism prevents HSC exhaustion when HSC proliferation and division are required, resulting in asymmetric division and thus assuring self-renewal<sup>28</sup>. A role for peroxisome proliferator-activated receptor delta (PPAR $\delta$ ), which is a member of a nuclear receptor superfamily of transcription factors that controls nutrient sensing and FAO, has been reported in HSCs. PPAR $\delta$  deletion or pharmacological inhibition of FAO stimulates the symmetric commitment of HSCs leading to stem cell depletion, while PPAR $\delta$  activation, via use of an agonist, increased asymmetric cell division. In agreement with this, a subsequent study showed that weakening the mitochondrial phosphatase protein tyrosine phosphatase 1 (PTPMT1), drives the conversion from glycolysis and FAO to mitochondrial aerobic metabolism, resulting in unsuccessful haematopoiesis<sup>29</sup>. This is linked with accumulation of HSCs unable to differentiate due to increased entry of quiescent stem cells into the cell cycle and a following pause at the G1 phase<sup>16</sup>.

### **1.1.6 HSCs maintenance: Glycolysis versus OXPHOS**

As introduced above, HSC maintenance is affected by a balance between HSC metabolic status and ROS levels. In fact, dormant HSCs seem to rely on glycolysis to avoid a decline in HSC maintenance and HSCs with defective glycolysis will

switch to a mitochondrial metabolic profile with increased production of ROS<sup>30</sup>. ROS have been largely found to contribute to BM failure and are one of the main sources for DNA damage and genome instability<sup>31</sup>, thus ROS can play a role as sensor dictating HSCs fate. Mitochondria, which are the main source of energy and indirectly of ROS, are considered as minor player in the maintenance of HSCs maintenance. However, HSCs highly rely on mitochondria when a metabolic switch is required (i.e., HSCs need to increase their proliferation rate). FOXO3, a transcriptional factor that shows multiple functions associated with longevity, is a regulator of HSCs metabolism. Loss of FOXO3 alters mitochondria function, inducing deleterious accumulation of ROS<sup>32,33</sup>. Specifically, deletion of FOXO3 in HSCs compromise DNA repair pathway leading to DNA damage, which compromises HSCs function. Mutation in tuberous sclerosis complex 1 (TSC1), a negative regulator of mTOR and a key regulator for cellular metabolism, induces levels of ROS and loss of quiescence in HSCs<sup>34</sup>. Additionally, mTOR activity contributes to erythroid differentiation favouring mitochondria activity and is also increased with aging<sup>35,36</sup>. Moreover, mTOR is one of the main regulators of autophagy, a process that itself has a critical role in HSCs biology<sup>16</sup>.

## **1.2 Leukaemic stem cells (LSCs)**

### **1.2.1 Origin of LSCs**

The ground-breaking discovery of the HSCs niche was made by Schofield (1978)<sup>37</sup>. Since then, significant advances have been made in describing what orchestrates HSC maintenance, as previously described. Mutagenesis or epigenetic changes in HSCs, together with fluctuations in the BM microenvironment, are important events to cause blood malignancies as leukaemia. Based on functional and immunophenotypic investigation of various subtype of cells, the existence of cancer stem cells (CSCs) was firstly described in the haematopoietic system and it is proposed that leukaemia is a stem cell disorder, initiated by as little as a single LSC. These cells can originate either from rare transformed HSCs or from more abundant and more differentiated progenitor cells. The origin of LSCs can vary with the stage of the disease, whether the leukaemia is chronic or acute, its immunophenotype, myeloid or lymphoid, and the nature of the transforming event. HSCs are equipped with intrinsic self-renewal activity that persists for the whole life of an individual. In this context, HSCs have much higher chance to

accumulate mutations than less primitive cells, which are not as long lived. LSCs initiation and maintenance is based on enhanced self-renewal activity<sup>38,39</sup>. In the case of leukaemic cells, they could potentially originate from more restricted progenitors by acquiring mutations that allow them to self-renew, or from HSCs that accumulate genetic and epigenetic changes that down-regulate cell death and maintain their self-renewal capability<sup>16</sup>.

### **1.3 Chronic myeloid leukaemia (CML) is a stem cell driven cancer**

CML is a myeloid-proliferative disease that originates from a LT-HSCs, making it an ideal model to study CSCs (Figure 1.3).

Almost 100% of CML patients are positive for the Philadelphia (Ph) chromosome, a shortened chromosome 22 that arises from a reciprocal translocation  $t(9q34,22q11)$ <sup>40,41</sup>. The Ph chromosome is the hallmark of the disease, in which fusion of *BCR* and *ABL* genes encode for a constitutively active protein kinase<sup>42,43</sup>. Since BCR-ABL fusion can occur in myeloid, B lymphoid, erythroid and sporadically T lymphoid cells in the majority of CML patients, the consensus is that the original translocation takes place in LT-HSCs<sup>44</sup>. The presence of BCR-ABL in endothelial cells originating from CML patient, raises the question: does the aberration take place even in more primitive cells than LT-HSC<sup>45</sup>? An elegant experiment conducted by *Fialkow et al.* using patterns of inactivation in X-linked genes, showed that erythrocytes and myeloid cells in female CML patients with heterozygous X-linked glucose-6-phosphate dehydrogenase (G6PDH) had the same single isoenzyme type for G6PDH in contrast to normal cells, which were heterogeneous<sup>46,47</sup>. These results suggested that both erythrocytes and granulocytes share a common stem cell, demonstrating that CML is a clonal disease

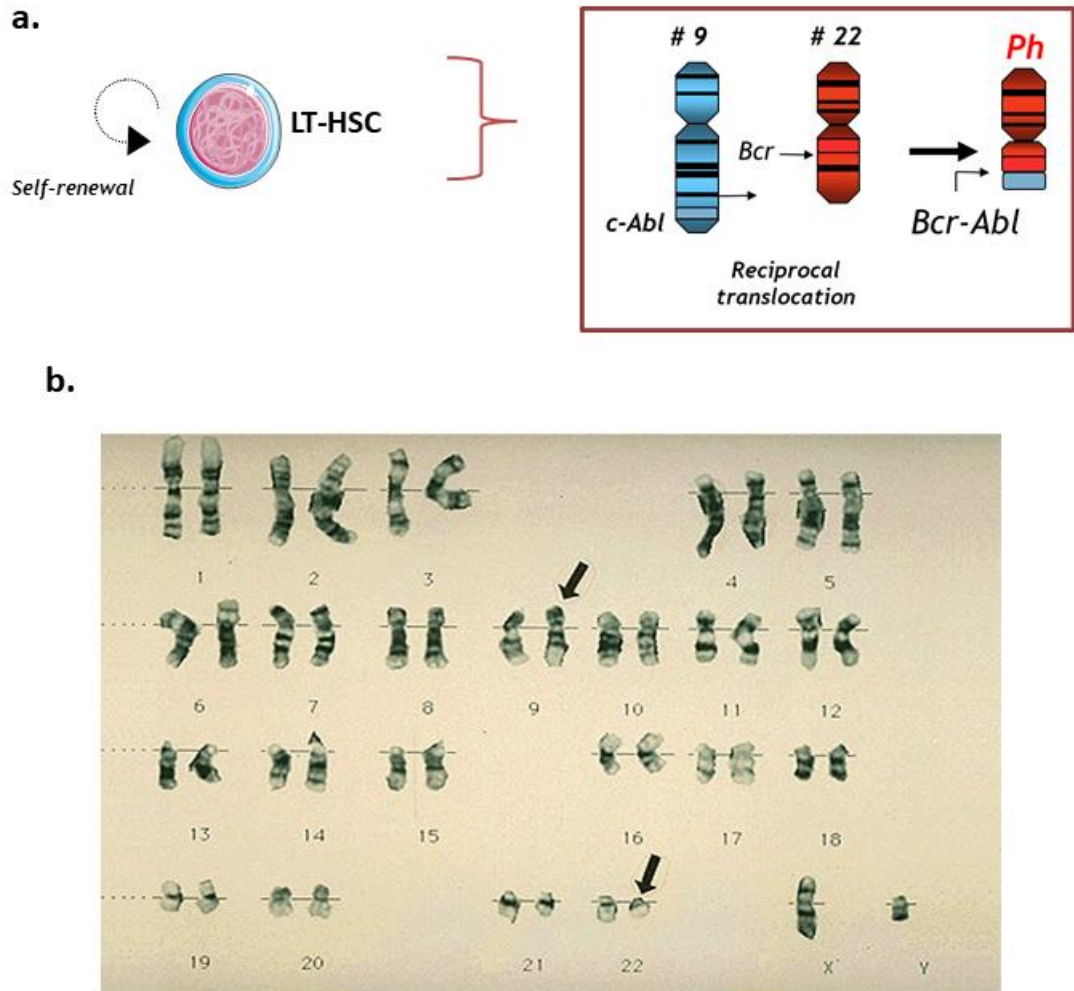


**Figure 1.3: Reciprocal translocation of BCR-ABL genes within LT-HSCs**

Representation of BCR-ABL reciprocal translocation within LT-HSC (a). Human chromosomes panel highlighting gene translocation between chromosome 9 and 22. Font <https://webpath.med.utah.edu/jpeg2/CYTOG010.jpg> (b).

with a stem cell origin. A recent study showed that while BCR-ABL expressing progenitor cells were eliminated following imatinib treatment (discussed below) in patients with a major molecular response (MMR), BCR-ABL expressing LSCs were still detectable<sup>48</sup>. In chronic phase (CP), the leukaemic clone seems to be maintained by a small number of BCR-ABL positive CD34<sup>+</sup>CD38<sup>-</sup> cells, a population enriched for LSCs<sup>44</sup>. These LSCs differentiate normally and proliferate slowly like normal HSCs. However, as these cells progress into intermediate phases of lineage restriction, their progeny proliferate losing their primitive marker CD34. By analysing different subpopulation of primitive CML cells it has been shown that an unusual autocrine IL-3-granulocyte colony-stimulating factor mechanism can provide a strong rationale for the unusual performance of BCR-ABL expressing stem and progenitor cells<sup>49,50</sup>. This mechanism only moderately offsets the *in vivo* signals, which maintain normal HSCs quiescence but, when active in BCR-ABL expressing LSCs, drives their differentiation at the expense of their self-renewal. In less primitive CML progenitors, the same mechanism has a more potent mitogenic effect that is then quenched when the cells progress into the final phases of differentiation.

### 1.3.1 CML epidemiology, diagnosis and disease progression

Occidental countries have a record of CML incidents between 0.7 and 2.0 cases/100.000 persons each year<sup>51</sup>. CML is not a genetic disease and no evidence of factor of risk that could increase chances to develop CML are available. Pesticides and benzene exposure, as well as the radiation exposure as the atomic bomb, increases the chance to develop leukaemia including CML<sup>52,53</sup>. The diagnosis of CML is more prevalent in males with an age average between 45 and 55 years old<sup>51</sup>. Most of the patients have no evident symptoms of the disease and diagnosis often occurs during routine check-ups. Minor symptoms are represented by fatigue, fever and loss of weight. Presence of the Ph chromosomes, blood counts and cytogenetic analysis of the BM, splenomegaly and anaemia, confirm diagnosis of CML. CML develops as an expansion of myeloid lineage, with myeloid cells losing their ability of fully differentiation into a mature granulocyte, resulting in accumulation of immature blasts in the blood stream.

Most of CML patients are diagnosed as CP CML. CML is in fact a tri-phase disease. Mild symptoms previously described are characteristic of CP, with patients and a

10% of blasts accumulation in the peripheral blood<sup>54,55</sup>. CP can advance in accelerated phase (AP), characterised by a 10% increase in blast's accumulation in the blood compared to CP, together with increased basophil and white blood cells counts. However, if left untreated, most patient will progress to blast crisis (BC) phase, with 20% increase in immature blast compared to CP with enhanced proliferation and ability to evade cell death<sup>56</sup>. Progression to BC is also increased by genomic instability and accumulation of chromosomal aberrations as trisomy 8<sup>40</sup>. Over-expression of BCR-ABL in committed progenitors, can lead to CML progression. This can result in altered signalling pathways which normally would control tumour suppression such as p53 and PP2A, apoptosis and differentiation<sup>57</sup>.

### **1.3.2 BCR-ABL signalling pathway**

ABL is a tyrosine kinase which transfers a phosphate from ATP to a tyrosine residue of a protein, switching on or off a signal pathway. In CML, ABL kinetic activity is constitutively active, up- or down-regulating a wide range of signalling pathways.

BCR-ABL binding with GRB2 and Son of Sevenless (SOS) forms a complex which leads to activation of Ras, responsible for cell growth, cell survival, cell migration and adhesion<sup>58</sup>. Activation of Ras leads to activation of MAPK signalling. Effects on MAPK results in mis-regulation of cell cycle, promoting tumour expansion and advancement in a more severe phase of the disease. As well, Ras induces activation of phosphoinositide 3-kinase/protein kinase B (PI3K/AKT) pathway, which switches off apoptotic stimuli endorsing cell survival<sup>59</sup>. PI3K is an intracellular lipid kinase that phosphorylates phosphatidylinositol converting phosphoinositide 4,5-bisphosphate (PIP<sub>2</sub>) to phosphoinositide-3,4,5-trisphosphate (PIP<sub>3</sub>). PIP<sub>3</sub> can bind AKT leading to its activation. Within all AKT functions, its activity on mTOR represents a major driver for leukemogenesis, increasing cell proliferation and growth<sup>60</sup>. Even though Crkl function for CML is still unknown, Crkl interacts with BCR-ABL working as a protein adaptor<sup>61</sup>. One of the hypotheses is that Crkl can be involved in cytoskeleton re-organization signalling pathway through interaction with paxillin<sup>62</sup>. BCR-ABL also functions as a growth factor mimicking, supporting cell proliferation and malignant transformation<sup>59</sup>.

### **1.3.3 CML treatment: a historical point of view**

In the first place, due to limited knowledge of CML and restricted option to treat CML patients, anti-malaria agents such as arsenic and quinine were thought to have some potential for treatment of CML<sup>63</sup>. Both regimen gave poor response and since World War II weapons had some anti-myeloproliferative effect, mustard gas was used for leukaemic patients<sup>64</sup>. Despite the fact it resulted with a wide range of toxic effects making it not applicable to treat cancer patients, it reduced blood cell counts which encouraged researchers to develop alkylating agents and microtubule destabilizers with reduced toxicity to treat CML patients. This led to the introduction of agents such as busulfan and hydroxyurea<sup>65</sup>. Both treatments were combined with the use of radiotherapy to reduce spleen size. While x-ray reduced splenomegaly, chemotherapeutic agents did not seem to have significant effect in reducing progression of the disease to BC phase.

At the time, allogenic stem-cell transplantation (allo-SCT) represented the only option for CML patients. Even though allo-SCT still remains the only cure for CML patients, transplantation success still remains very poor<sup>66</sup>. In first instance, uniquely patients below 60 years old and with no history of comorbidities, are eligible for allo-SCT and in most cases it is very difficult to find a donor<sup>67</sup>. However, most of patients with an available donor, are still associated with a high risk of transplantation rejection, infections and host/graft reactions.

In the early 1980s, interferon-alpha (IFN- $\alpha$ ) had shown anti-proliferative effect against other malignancies, making it a good candidate for cancer treatment. Leukopenia effect shown using IFN- $\alpha$ , led the cytokine to be tested against CML as well<sup>68</sup>. IFN- $\alpha$  significantly increased survival rates of CML patients, making it together with allo-SCT the only option to sustain complete cytogenetic response (CCyR) following discontinuation of treatment<sup>69</sup>. However, long-term treatment using IFN- $\alpha$  resulted in adverse effect probably due to its effect in enhancing an immune-response.

### **1.3.4 TKI as a new treatment for CML**

Since prognosis for CML patients was very low, in the late 1980 biochemists Lydon and Matter from Novartis, introduced new projects to identify molecules with a

kinase inhibitor effect. Success from those studies came in the late nineties when the attachment of a highly polar side chain, N-methyl-piperazine for solubility, made imatinib a new promising treatment for CML patients.

Imatinib (STI571, Gleevec®, Glivec®, formerly CGP 57148B) has high boundary affinity with the catalytic centre of ABL, making kinase ABL inactive when bound to the inhibitor and inhibits autophosphorylation and the subsequent phosphorylation of key downstream substrates.

*In vitro* and *in vivo* data sustained imatinib efficacy to inhibit BCR-ABL oncoprotein, which resulted in anti-proliferative and apoptotic effect on CML cells<sup>70,71</sup>. A randomized phase III study in 2001, The International Randomized Study of Interferon and ST1571 (IRIS), proved higher efficacy of imatinib versus IFN- $\alpha$ . A 400 mg/day dose of imatinib or the standard treatment of IFN- $\alpha$  and cytarabine, an inhibitor of DNA synthesis, was achieved in patients<sup>72</sup> (**Figure 1.4**). Following 19 months trial, the 1106 patients recruited from 16 different countries, showed that imatinib arm resulted in 87% major cytogenetic response (MCyR) versus 34.7% in the IFN- $\alpha$  and cytarabine treated arm. Furthermore, 76% of the imatinib arm had achieved CCyR compared to the 14% of the IFN- $\alpha$  and cytarabine arm. The impressive results together with increased tolerability and reduced toxicity effect, made imatinib the front-line therapy for CML patients<sup>73,74</sup>.

To assess treatment response, blood counts, splenomegaly and quantification of mRNA levels of BCR-ABL, are routinely performed on CML patients. Treatment response has been officially categorised by the European Leukaemia Net (ELN) and the U.S. National Comprehensive Cancer Network (NCCN) guidelines. Complete haematological response (CHR) is achieved when white blood cell counts are below  $1 \times 10^4/\text{mm}^3$  with non-palpable spleen are maintained for at least 4 weeks<sup>75</sup>.

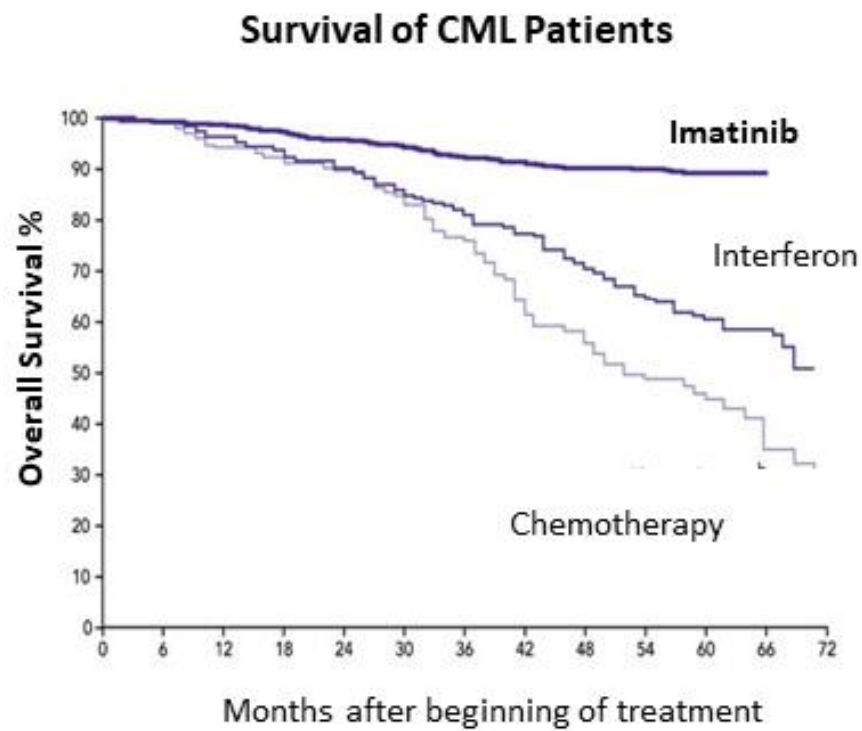


**Figure 1.4: CML patient's survival curve**

Overall CML patient's survival curve following treatment using standard chemotherapeutics, interferon or imatinib. Adapted from *Tura et al.* and *Druker et al.*<sup>73,76</sup>

## Chapter 1 Introduction

MCyR is achieved when BCR-ABL transcript is less than 35% in the BM. CCyR is defined as BCR-ABL transcript is non-quantifiable or non-detectable in the BM.

Major molecular response (MMR) is achieved when BCR-ABL transcript is less than 0.1% in the BM<sup>77</sup>.

The ELN has also offered guidelines for time frame expected to reach a specific response and warning for suboptimal response or relapse. CHR is expected

following 3 months imatinib treatment, and CCyR and MMR should be achieved within six and twelve months of treatment.

### 1.3.5 Imatinib resistance

Nowadays, CML is a malignancy with the most successful treatment history. However, even though the majority of patients respond to front line treatment using imatinib, some cases do not respond or acquire resistance following treatment.

Resistance mechanism can be classified as BCR-ABL dependent mechanism, which include:

- *Point mutations in the BCR-ABL catalytic domain:* are found in 80% of resistant patients, causing conformational changes in the catalytic domain, impeding binding with imatinib, impairing efficacy of the treatment. The most common point mutation is the substitution of threonine to isoleucine at position 315 (T315I), also known as the 'gatekeeper' mutation<sup>78,79</sup>.
- *BCR-ABL oncogene amplification:* it does not represent a major form of imatinib resistance since it has been assessed in few CML patients<sup>80</sup>. Analysis in those patients indicated a higher copy of BCR-ABL with increased level of BCR-ABL signalling and genomic instability, making standard imatinib dose to be ineffective against the increased signal.

Other forms of resistance mechanism are classified as BCR-ABL independent, which include:

- *Pharmacokinetics adverse effect:* cytochrome P450 (CYP) system is in charge of imatinib metabolism. Differences in levels of the CYP between patients affects plasma level of imatinib, leading to a shortage of delivery of the compound in the BM and imatinib resistance<sup>81</sup>.
- *Drug efflux:* Member of the ATP-binding cassette (ABC) transporter family, such as P-glycoprotein (P-gp; ABCB1), is particularly high in CML cells<sup>82</sup>. It has been reported that ABC proteins can actively export imatinib from the intracellular compartment, leading to a decrease in the intracellular concentration of the compound, resulting in reduced cytogenetic response.

Clonal evolution has been associated with genome instability promoting CML progression from CP to BC. Most recurrent genomic instability are represented by trisomy 8 and 19, aberration of chromosome 17q, loss of p53 and presence of a second copy of the Ph chromosome<sup>83</sup>.

Epigenetic aberrations play a critical role in modulating imatinib treatment response which could leading to resistance<sup>84</sup>. Epigenetic modifications include DNA methylation, histone acetylation, deacetylation and phosphorylation. Using histone deacetylation inhibitor has shown to improve treatment for CML<sup>85</sup>.

### **1.3.6 Approaches to face imatinib resistance**

As described in the previous paragraphs, many are the reason that could cause imatinib resistance.

One of the approaches to overcome imatinib resistance is represented by treating CML patients with increased dose of TKI. Daily rising imatinib dose from 400 to 600 and 800 mg has resulted in increasing patients' response and reduced chance to progress from CP to BC<sup>86</sup>. However, in most cases, specifically in the event of point mutations, imatinib dose escalation was not beneficial, which lead to development of 2<sup>nd</sup> and 3<sup>rd</sup> generation TKIs.

#### **1.3.6.1 Nilotinib, a 2<sup>nd</sup> generation TKI**

Nilotinib (Tasigna) was developed by Novartis to overcome imatinib resistance. It is structurally very similar to imatinib, except for the additional of an N-methyl-

piperazinyl group, which conferred to nilotinib the ability of better fit within the kinase domain of BCR-ABL, increasing affinity to BCR-ABL of 30 times compared to other kinases. The ENESTnd phase III clinical trial compared nilotinib treatment versus imatinib in newly diagnosed CP CML patients. A 2-year follow-up from the study proves that 86% of the patients treated with nilotinib achieved CCyR against the 74% in the imatinib arm<sup>87</sup>. A 5-year follow-up further underlined nilotinib efficacy with more than 50% of the patients achieved deep molecular response (DMR) compared to the 30% in the imatinib arm<sup>88</sup>. Based on the high impact of patient's response, food and drug administration (FDA) approved nilotinib treatment for patients diagnosed with CP CML. However, nilotinib did not seem to have efficacy against T315I mutation and in eradicating LSCs<sup>89</sup>.

### **1.3.6.2 Dasatinib, a 2<sup>nd</sup> generation TKI**

Dasatinib (Sprycel®; Bristol Myers Squibb) is a 2<sup>nd</sup> generation TKI that is 325 times more potent inhibitor than imatinib against BCR-ABL. The increased potency confers to dasatinib a more stringent binding to the kinase pocket, being able to bind both active and inactive conformation of ABL catalytic fraction. Dasatinib has been proved to target imatinib resistant cells with the exception of T315I mutation. DASISION phase III clinical trial measured the efficacy of dasatinib versus imatinib in newly diagnosed CP CML patients<sup>90</sup>. A 2-year follow-up indicated that 77% of patients treated with dasatinib achieved CCyR against 66% of the imatinib treated arm<sup>91</sup>. A 5-year follow-up study confirmed higher efficacy of dasatinib compared to imatinib in increasing both CCyR and MMR, leading the compound to approval from FDA as a new treatment for newly diagnosed CP CML patients and patients resistant or not responding to imatinib treatment<sup>92</sup>.

### **1.3.6.3 Bosutinib, a 2<sup>nd</sup> generation TKI**

Bosutinib is a 2<sup>nd</sup> generation TKI developed by Pfizer which inhibits ABL and SRC kinases. Compared to imatinib, bosutinib shows increased ability to target ABL at much lower concentration. Bosutinib targets unmutated and mutated BCR-ABL cells with the exception of T315I mutation<sup>93</sup>. Phase III BELA clinical trial indicated no difference in CCyR between bosutinib and imatinib treatment, however, bosutinib treated patients achieved a 40% MMR rate compared to 25% in the imatinib treated arm<sup>94</sup>. A different trial instead proved that bosutinib raised MCyR

to 60% in imatinib non-responding patients<sup>95</sup>. Bosutinib was approved by FDA in 2012 as second line treatment for imatinib non-responding CML patients.

#### **1.3.6.4 Ponatinib, a 3<sup>rd</sup> generation TKI**

The development of imatinib and 2<sup>nd</sup> generation TKI was an extraordinary success for CML treatment. However, a major challenge remained and was represented by the T315I mutation. Ponatinib, formally developed by ARIAD, together with inhibiting BCR-ABL and targeting imatinib resistant cells, also showed efficacy in targeting T315I mutated cells, making ponatinib a pan-TKI, targeting all forms of known ABL mutation<sup>96</sup>. Phase II clinical trial, PACE, showed that 45% of patient non-responding to imatinib achieved CCyR and 34% achieved MMR<sup>97</sup>. However, a subsequent phase III clinical trial, EPIC, was terminated in advance due to heart complications and cardiovascular risk in the ponatinib treated patients<sup>98</sup>. Due to these side effects, ponatinib was withdrawn from the market in 2013, but re-introduced few months later as treatment option for CML patients with T315I mutation and non-responding to other available TKIs.

#### **1.3.6.5 Omacetaxine**

A 40 years development history led to introduction of omacetaxine. It was firstly introduced by Chinese as an anti-cancer herbal extract from the bark of species of the Chinese plum yew, *Cephalotaxus harringtonia*<sup>99</sup>. Omacetaxine is an inhibitor of protein translation and has also properties to induces cell cycle arrest, two mechanism highly upregulated in cancer cells. Omacetaxine, even though it targets imatinib resistant and T315I mutated cells, is proposed as an ultimate option for non-responding patient or acquire resistance to other available TKIs, due to its adverse effect on normal cells.

#### **1.3.7 LSCs persistence**

Despite the fact that a wide range of TKIs have been developed to overcome TKIs resistance in CML, LSCs persistence and relapse following TKIs treatment has raised the question if treatment of TKIs allows complete LSCs eradication<sup>100,101</sup>. Both patients with MMR and CMR still exhibit the presence of BCR-ABL. Evidence indicates in fact that TKIs fail to target LSCs which may explain the presence of BCR-ABL<sup>+</sup> cells in the BM of patients with MMR and CMR and in the cases in which

BCR-ABL is not detectable its thought to be because of technical limitation. This has raised the question if LSCs might be addicted to BCR-ABL signalling. However, *Corbin et al.* indicate that LSCs are not dependent on BCR-ABL expression and can survive in a BCR-ABL independent manner<sup>102</sup>. This evidence was further supported by other studies were removal or inhibition of BCR-ABL showing that persistence occurs in absence of the oncogene<sup>103,104</sup>. Understanding which are the survival mechanism that CML activates to persist might result in discover new promising combination treatment to eradicate LSCs<sup>105,106</sup>. Inhibiting of BCR-ABL re-localises transcriptions factors FOXO1 and FOXO3a in the nucleus resulting in anti-apoptotic effect and cell cycle arrests<sup>107-109</sup>. The signal pathway activated by BCR-ABL is a source of ROS, causing genomic instability and DNA damage. Furthermore, BCR-ABL also prevents mismatch repair, enhancing an anti-apoptotic effect in BCR-ABL expressing cells<sup>110</sup>. Among those, modulation of immune-response and the bone marrow micro-environment also have been proposed as a mechanism that LSCs use to escape eradication<sup>111</sup>. Upregulation of autophagy following BCR-ABL inhibition has also been indicated as a mechanism that CML LSCs use to sustain survival<sup>112</sup>.

### **1.3.8 LSCs metabolism**

LSCs as most CSCs are highly proliferating cells exhibiting increased metabolism to sustain their energy demand. Also, since HSCs exhibit a unique metabolic phenotype, with low mitochondrial metabolism to repress differentiation, LSCs instead seem to have an opposite metabolic profile.

#### **1.3.8.1 Mitochondrial metabolism and LSCs**

LSCs are resilient cells and able to exploit multiple metabolic pathways in order to survive. In fact, LSCs can, in addition to glucose, utilize fatty acids and amino acids such as glutamine in order to provide precursors of the TCA cycle to sustain mitochondrial metabolism in LSCs. Most CSCs that are dependent on OXPHOS generally upregulate this energy source. For this reason, CSCs can be sensitive to mitochondrial inhibition. Since higher oxysterol binding protein-related protein 4L (ORP4L) is associated with higher OXPHOS rate and it is upregulated in 80% of CML cases, CML cells are thought to have higher levels of oxidative metabolism compared to their normal counterparts<sup>113</sup>. This was further investigated by *Kuntz*

*et al.*<sup>114</sup>. Performing metabolic analyses on both stem cell-enriched CD34<sup>+</sup>CD38<sup>-</sup> and CD34<sup>+</sup> and differentiated CD34<sup>-</sup> cells derived from patients with CML, the authors demonstrated that most primitive LSCs have higher mitochondrial activity than more differentiated LSCs and normal CD34<sup>+</sup>CD38<sup>-</sup> cells. Importantly, they show that primitive CML cells are reliant on higher rates of oxidative metabolism for their survival.

## 1.4 Autophagy

### 1.4.1 Overview

Autophagy, from the Greek *auto*-self and *-phagy* eating, is an evolutionally conserved process first described in mammalian cells in 1963 by Christian de Duve. Studies from the recent nobel prize Ohsumi, clarified the role of autophagy unravelling the key regulators of the process in yeast<sup>115-117</sup>. It is a lysosomal catabolic process that has several functions. First of all, it has a role as a cell cleaner by reducing the chance of cell malfunction due to accumulation of damaged cellular components and organelles. It is also involved in microbe's demolition and sustains metabolism during stressful situations, such as starvation, providing building blocks for energy production and cellular homeostasis. Autophagy is also associated with a subtype of non-apoptotic cell death, known as type II programmed cell death<sup>118</sup>.

The assembly of the catabolic machinery of autophagy takes place in the cytoplasm, in double membrane vesicles known as autophagosomes. The origin of the autophagosomes in mammalian cells most of the time starts within an extension of the endoplasmic reticulum known as omegasome<sup>119</sup>. Other potential sources of the double membranes are the mitochondrial outer membrane, the plasma membrane and the nuclear envelope<sup>120,121</sup>. Numerous autophagy-related

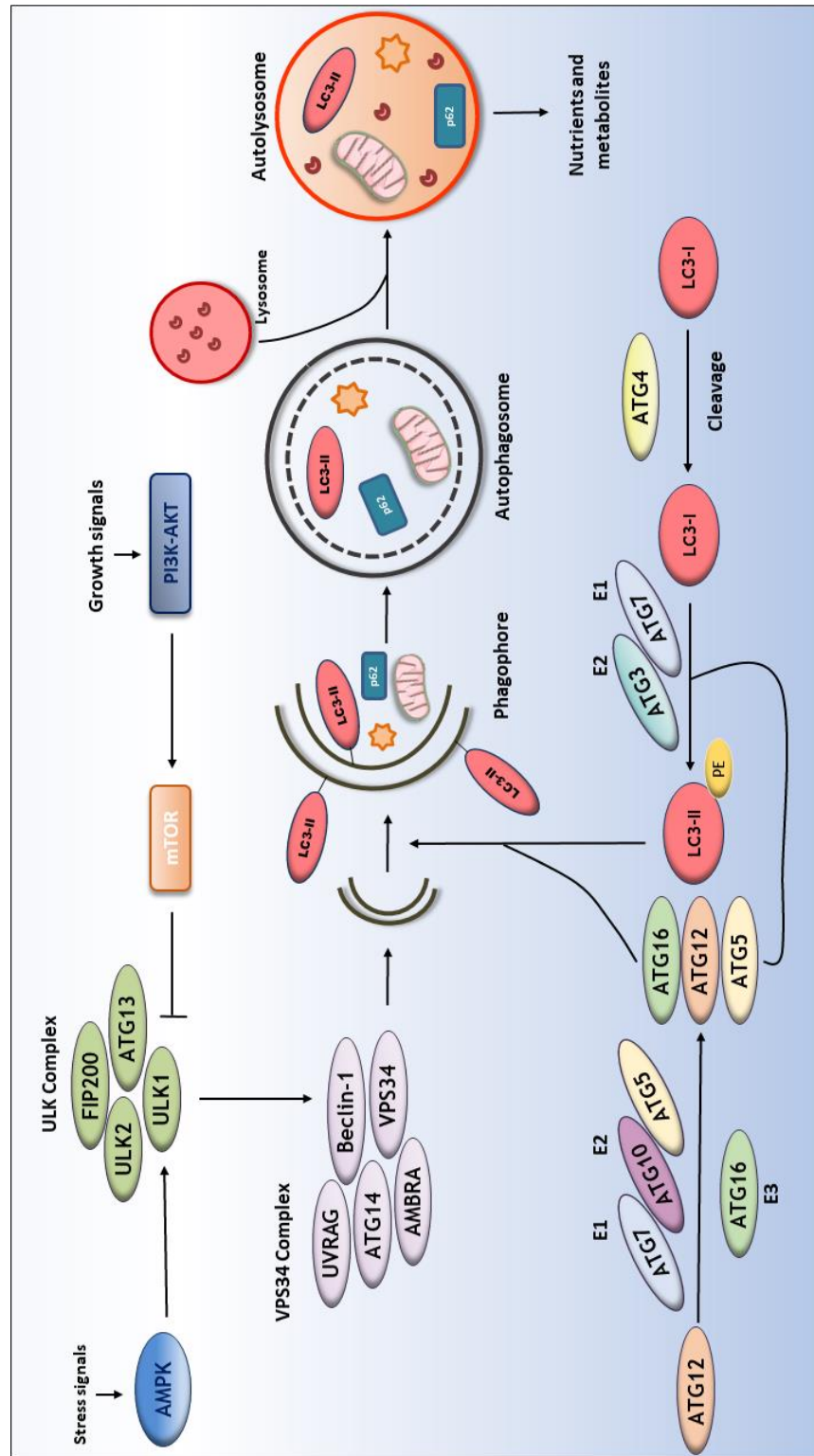


**Figure 1.5: Schematic representation of autophagy activation**

Following stress and/or growth signals, AMPK and mTOR guide autophagosome formation through regulation of ULK1 activity. Active ULK Complex drives early stages of autophagy (initiation and early elongation) and the recruitment of the VPS34 Complex. Sealing and LC3-II attachment to the double membrane require two ubiquitin-like conjugation systems. Firstly, ATG12 is activated by the E1 like enzyme, ATG7. Activated ATG12 is then conjugated to ATG5 in a process that requires ATG10 acting as an E2-like enzyme. ATG5-ATG12 then forms a complex with ATG16, which functions as an E3 enzyme in the next ubiquitin-like conjugation system. LC3-II is produced as a “pro-protein” that is cleaved by ATG4 and then activated by the E1-like ATG7 and is conjugated to phosphatidylethanolamine (PE) in the autophagosomal membrane by ATG3 and the ATG5-ATG12-ATG16 complex. Fusion with lysosomal provides the necessary enzymes for autophagosomal content degradation.

(ATG) genes are involved in their biogenesis and function that can be organized in three main stages<sup>122</sup>. The very first step consists in the autophagy initiation and formation of the phagophore. Signals of cellular nutrient status are sensed by the unc-51 like autophagy activating kinase 1 (ULK1) initiation complex which then activates autophagy and recruits a second complex, known as vacuole protein sorting 34 (VPS34) complex, resulting in the formation of a flat unique membrane known as phagophore<sup>123,124</sup>. Phagophores will then elongate and expand leading to autophagosomal maturation. The last step is represented by their fusion with lysosomes where proteases will be in charge of their content demolition.

### 1.4.2 ULK1 initiation complex

The ULK1 complex controls the initiation of the autophagosomal formation and is mainly regulated by ULK1/2 (yeast ATG1), ATG13 and FIP200 (yeast ATG17)<sup>125</sup>.

ULK1 activity it's dictated by mTOR and AMPK, two sensors of the nutritional status of the cell. mTOR signalling pathways integrate biosynthetic pathways to stimulate protein translation and cell growth. AMPK is a main regulator of cellular metabolism which senses changes in level of nucleotides such as ATP, AMP and ADP, promoting pathways that will lead to ATP synthesis and breakdown to support energy demand<sup>129</sup>. mTOR and AMPK can have an opposite function in regulating central metabolism. Abundant nutrients conditions lead to interaction between ULK1 and mTORC1<sup>128</sup>. In this scenario, mTOR represses autophagy with an inhibitory phosphorylation of ULK1 on ser757 and ATG13<sup>123,127</sup> (**Figure 1.6**). During conditions of low nutrients, AMPK directly inhibits mTORC1 to mainly repress waste of energy for protein synthesis. AMPK repression of mTOR also releases ULK1 inhibition from mTOR itself. Furthermore, AMPK directly phosphorylates ULK1 on ser555 activating it, triggering the initiation of the autophagic cascade<sup>130</sup> (**Figure 1.6**). Furthermore, inhibition of mTOR can also result in localising the E3-ligase TRAF6 to ULK1, where K63 ubiquitylate and stabilise ULK1, which results active<sup>131</sup>. Activation of ULK1 can also occur independently from mTOR or AMPK. Activation of acetyl transferase TP60 by glycogen synthase kinase 3 (GSK3), induces activation of ULK1 following its acetylation<sup>132</sup>. Insulin it is proposed to be a regulator of ULK1 phosphorylation on ser774 through an AKT-dependent phosphorylation<sup>133</sup>. Once ULK1 is active, it phosphorylates and interacts with ATG13 and FIP200, which leads to recruitment of the ULK1-complex to the

## Chapter 1 Introduction

phagophore formation site within the cytoplasm <sup>134</sup> (**Figure 1.5**). Auto-phosphorylation on T180 in its kinase domain it's a key phosphorylation for ULK1 activation<sup>133,135</sup>. ULK1 activation, however, has also been associated with autophagy-independent mechanism. As indicated in (**Table 1-2**) ULK1 can phosphorylates different substrates, leading to autophagy induction but also regulation of glycolytic flux and cellular homeostasis<sup>124,133,136-151</sup>. Nowadays 5 homologues of ULK1 have been identified (ULK1, ULK2, ULK3, ULK4 and STK36). Among them, only ULK1 and ULK2 have been proposed as regulator of autophagy. They are also the most similar and ULK2 can compensate loss of ULK1.

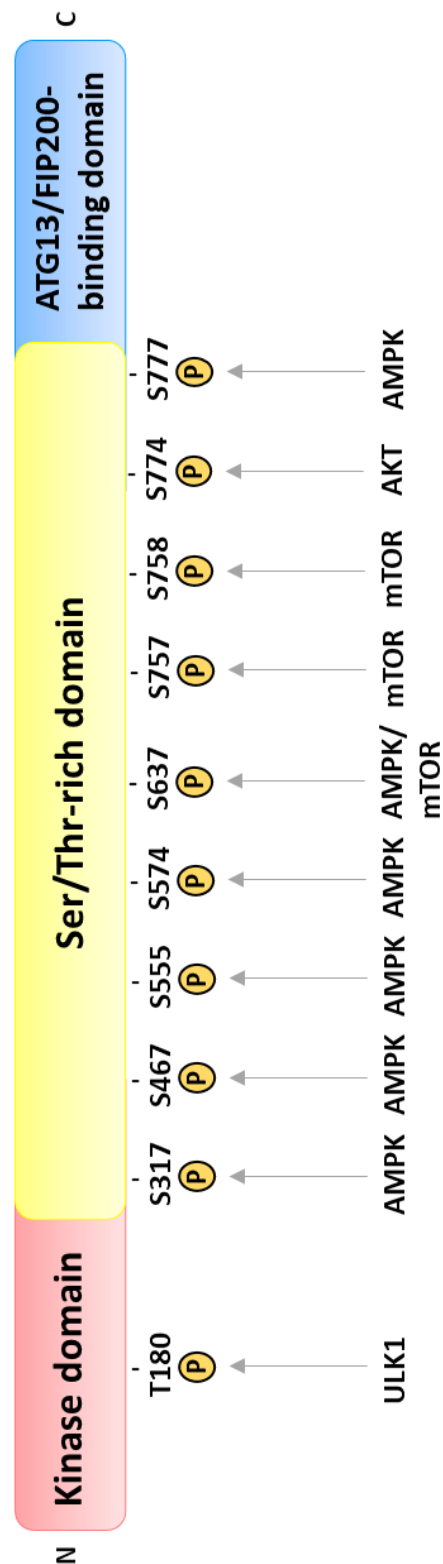


**Figure 1.6: ULK1 domain structure with location of phosphorylation sites**

AMPK phosphorylation of ULK1 on S317, S467, S555, S574 and S777 is necessary for the kinase activity of ULK1; AMPK phosphorylation of ULK1 on S555 is necessary for ATG13-ULK1 interaction and for autophagy mediated by ULK-complex; mTOR phosphorylation of ULK1 on S757 prevents ULK1 interaction with AMPK; mTOR phosphorylation of ULK1 on S758 facilitates ULK1 interaction with AMPK; AKT phosphorylation of ULK1 on S774 activates ULK1; mTOR and AMPK phosphorylation of ULK1 on S637 facilitates ULK1 interaction with AMPK. Auto-phosphorylation on T180 important for ULK1 activation.

Protein	Residue(s)	Function
AMBRA1	S465, S635	Induces dissociation of AMBRA1 from the dynein complex in favour of its interaction with the ULK1-complex
AMPK $\alpha$ 1	S360/S368, S397 S486/T488	Negatively regulates AMPK
AMPK $\beta$ 2	S38, T39, S68, S173	Negatively regulates AMPK
AMPK $\gamma$ 1	S260/T262, S269	Negatively regulates AMPK
ATG4B	S316	Inhibits AT4B activity during LC3 conjugation
ATG9	S14	Promotes ATG9 trafficking in response to starvation
ATG13	S318, S355	S318 required for clearance of depolarized mitochondria
ATG14L	S29	Promotes autophagy by increasing VPS34 complex activity
ATG101	S11, S203	Unknown
BECLIN-1	S14	Activates VPS34
Cdc37	S339	Disrupts Cdc37 client proteins stability
DENND3	S554, S572	Activates Rab12 to facilitate autophagosome trafficking
ENO1	S282	During amino acid and growth factor starvation in order to maintain homoeostasis of cellular energy and redox levels
FBP1	S63	During amino acid and growth factor starvation in order to maintain homoeostasis of cellular energy and redox levels
FUNDC1	S17	Promotes mitophagy by enhancing FUNDC1 binding to LC3
FIP200	S943, S986, S1323	Unknown
HK1	S124	During amino acid and growth factor starvation in order to maintain homoeostasis of cellular energy and redox levels
p62/SQSTM1	S409	Promotes aggregate clearance during proteotoxic stress
PFK1	S762	During amino acid and growth factor starvation in order to maintain homoeostasis of cellular energy and redox levels
Raptor	S855, S859, S792	Inhibits mTORC1 during starvation
Sec23A	S207, S312	Inhibits ER to Golgi trafficking during starvation
Smrc8	S400, S492, S562, T666	Unknown
Sting	S366	Inhibits excessive transcription of innate immune genes during their activation by cyclic dinucleotides
ULK1	T180, S1042, T1046	T180 important for ULK1 kinase activity. S1042 and T1046 regulate ULK1 ubiquitylation and degradation during prolonged starvation
VPS34	S249	Unknown

**Table 1-2: List of known ULK1 substrates and function**

Adapted from Zachari *et al.*<sup>152</sup>

### 1.4.3 VPS34 complex

Upon activation of ULK1, it phosphorylates Beclin-1 and AMBRA to recruit a new complex to autophagosome formation, known as the VPS34 complex<sup>140</sup>. The main component of this complex is a class III PI3K VPS34, a lipid kinase that phosphorylates phosphatidylinositol (PI) to form phosphatidylinositol-3'phosphate (PI3P)<sup>153,154</sup>. Inhibition of autophagy is associated with the interaction of the BH3 domain of Beclin-1 with the anti-apoptotic protein BCL-2. However, starvation condition will release Beclin-1 from BCL-2 making it available to form a complex with VPS34. Other members of the complex are UVRAG and ATG14, that positively regulate autophagy (**Figure 1.5**).

### 1.4.4 Autophagosome completion

The final stages to enclose the double membranes vesicles, leading to autophagosomes maturation, depends on two ubiquitin like conjugation system. The process of ubiquitin conjugation occurs when a small protein modifier, ubiquitin, is directly conjugated to substrate proteins by three sequential enzymatic activities. The first conjugation system occurs by transfer of PE (phosphatidylethanolamine) to ATG8, yeast orthologues of LC3 (microtubule associated protein 1 light chain 3), converting the cytoplasmic isoform of LC3, LC3-I, to the PE conjugated isoform bound to the autophagosomal membrane, LC3-II<sup>155</sup> (**Figure 1.5**). ATG8 is firstly cleaved by ATG4 to reveal a C-terminal glycine residue. This is then activated by ATG7, an E1 ubiquitin-activating enzyme, and is conjugated to PE membrane by ATG3, an E2 ubiquitin-conjugating enzyme. The second conjugation system is represented by the complex ATG12-ATG16-ATG5 (**Figure 1.5**). The process begins with ATG7, an E1, which activates the C-terminal glycine of ATG12, which ATG10, an E2, conjugates with a covalent binding to ATG5<sup>156</sup> (**Figure 1.5**). The ATG12-ATG5 system finally conjugates with a non-covalent binding to ATG16, forming a ubiquitin like conjugation system, which is directed to the double membrane and acts as an E3 ubiquitin ligase enzyme, binding LC3-II to the autophagosomal membrane. ATG4, in a process known as de-lipidation, cleaves LC3 removing it from the outer membrane.

In human have been described at least 6 orthologues of ATG8 which can be organised in two distinct families. GABARAPs family (members GABARAP,

GABARAPL1 and GABARAPL2/GATE-16) and LC3 family (members LC3A, LC3B and LC3C). LC3 function has been strongly investigated and together with GABARAB and GATE-16 is a ubiquitin like protein which their function is mainly linked with the previous described autophagosomal conjugation system. Less is understood about whether there are divergent functions for other Atg8 orthologues<sup>157</sup>.

### **1.4.5 Autolysosome formation**

The completion of the autophagic biogenesis requires the fusion of the outer membrane of autophagosomes with lysosomes, organelles that contain pH-sensitive proteases, to form autolysosomes. Within autolysosomes, the inner single membrane of the autophagosome and its content are lysed by lysosomal hydrolases, especially cathepsins. This fusion process between autophagosomes and lysosomes to generate autolysosomes is not fully understood, although it has been shown to require LAMP-2, the small GTPase RAB7 and UVRAG<sup>158</sup>. However, signalling pathway such as the PI3K/Akt/mTORC1, seem to have a major role.

### **1.4.6 Cargo receptor proteins: p62**

During autophagy, a class of cargo receptors act as a bridge to conjugate cargos to lipidated LC3 on the double membrane. The most abundant class of cargo receptors for selective autophagy are related by the presence of one or more linear peptide motifs that mediate direct interaction with LC3-II, called LIR motifs (LC3-interacting region).

p62 (also known as sequestosome-1, SQSTM1) is an autophagy cargo receptor involved in the removal of protein aggregates, mostly associated in neurological and hepatic diseases such as mutant Huntingtin and Lewy bodies<sup>159</sup>. p62 interacts with LC3-II within its LIR motif and is able, with its C-terminal ubiquitin associated domain, to recognise protein aggregates which are highly ubiquitinated. This double interaction allows delivery of ubiquitinated substrates to the autophagosome for autophagic degradation. Since LC3-II is also internalised in the double membrane, this internalisation involves also cargo receptors and cargo proteins destined to degradation. For this reason, p62 is a major marker for autophagy flux.

## 1.5 Autophagy and HSCs

Although, keeping LT-HSCs in their hypoxic niche seems to satisfy maintenance of their “dormant” state, it may not be the only factor that contributes to their metabolism adaptation. Lately, autophagy has been shown to be essential in preserving the organization and the welfare of this small cell compartment<sup>160,161</sup>. The maintenance of cell health and prevention of stem cell aging is also vital for haematopoiesis, and the role of autophagy in degrading damaged cellular components and organelles may be essential in this context. Furthermore, autophagy flux negatively correlates with cell decline in several cell subtypes including HSCs<sup>162</sup>.

### 1.5.1 Autophagy, key player in HSC maintenance

The fact that HSCs have a slow turnover decreases the chance to reduce or dilute damaged cellular components and autophagy might be indispensable for the necessary increase in catabolic rate. Several studies propose that autophagy can sustain glycolytic flux, protecting HSCs from metabolic stress and expansion stimulus in the BM, thereby reducing the chance of HSCs exhaustion. FOXO3a, a transcriptional factor that shows multiple functions associated with longevity, regulates levels of autophagy in HSCs in case of metabolic stress<sup>163</sup>. Specifically, FOXO3a deficient mice showed a pronounced reduction in autophagy capacity in protecting HSCs. FIP200, a component of the ULK1 initiation complex, has also been associated with maintenance of HSCs<sup>164</sup>. This study found that mice depleted of FIP200 resulted in increased HSC proliferation, in which mitochondrial mass was higher when compared with HSC with no depletion. ATG7, whose role is only associated with autophagy, regulates mitochondrial homeostasis of HSCs, as well as ROS production and cell differentiation<sup>165</sup>. Deleting ATG7 in the hematopoietic compartment results in the loss of normal HSCs functions and severe myeloid-proliferation, causing mice death. The authors also show that the HSPC compartment exhibit accumulation of mitochondria and ROS, in addition to an increased proliferation rate and DNA impairment.

### 1.5.2 Autophagy and HSC cell cycle

Orientating HSCs to quiescence and a slow cell cycle ensure preservation and health of long-lived stem cells. Fewer replication cycles with minimum telomere

shortening ensure that HSCs age more slowly<sup>166</sup>. Despite the fact that cyclin D family members, including cyclins D1-D3, are expressed at different levels in HSPCs, Cao *et al.*<sup>167</sup> showed that only cyclin D3 responds to nutrient stress and identified autophagy as a driving force for cell cycle entry. Therefore, they suggest that the lower levels of autophagy activity observed in aged mice may be due to lower cyclin D3 levels, and thus a postponed HSCs entry into the cell cycle. This ultimately results in a defect in self-renewal. The most common way to test HSCs ability to undergo self-renewal is represented by serial transplantation of murine HSCs from an original donor to a recipient, whose own HSCs are ablated before transplantation. Recent studies indicate that autophagy is an essential process for self-renewal. Ho *et al.*<sup>168</sup>, demonstrated that mice with hematopoietic-specific deletion of the essential autophagy factor ATG12 had increased numbers of cells in the peripheral blood and spleen. The authors then performed serial transplantation of ATG12 deficient HSCs into recipient mice. The mice receiving the ATG12 deficient HSCs showed dramatically impaired engraftment and reduced number of regenerated HSCs.

### 1.5.3 Mitophagy

Nowadays, mitophagy is one of the most investigated process for mitochondrial clearance<sup>169</sup>. The term mitophagy was proposed in the late nineties by Klionsky and within the years its critical function has been clarified<sup>170</sup>. The removal of mitochondria using the autophagic machinery is used by a cell not only for the removal of damaged and aged mitochondrion but also to sustain several conditions such as cellular stress, differentiation and cell death as well as it's implicated in several diseases such as Parkinson<sup>171-173</sup>. Multiple signal events are required to induce autophagy, of which signals of eat me or ubiquitin-dependent receptors such as Parkin and PTEN-induced putative kinase 1 (Pink1).

#### 1.5.3.1 Parkin dependent mitophagy

Parkin is a cytosolic E3 ubiquitin ligase that is mutated in familial forms of Parkinson disease<sup>174</sup> which is required to address mitochondrial clearance. Together with Parkin, Pink1 is an essential kinase required to mitochondrial degradation<sup>175</sup>. Pink1 is a serine/threonine kinase that functions with a protective role towards cells against stressed induced following mitochondrial dysfunction.

Physiologically, Pink1 expression and its kinase activity recruits Parkin to depolarized mitochondria inducing mitophagy<sup>176</sup>. Using agents that depolarise and reduce the mitochondria membrane potential, force the exposure of Pink on the cytoplasmic side of the mitochondrial membrane, enhancing its effect on Parkin recruitment<sup>177</sup>. Furthermore, *Baudot et al.* demonstrated that overexpressing Parkin enhances mitophagy, making Parkin-enhanced mitophagy as a suitable assay to measure autophagy flux<sup>178</sup> (Figure 1.7).

### 1.5.4 Mitophagy controls oxidative stress in HSCs

It is likely that to maintain latency in HSCs, it is fundamental to have low mitochondrial activity. A phenomenon known as mitophagy is the only known process for mitochondrial clearance, and this function has been demonstrated to control levels of oxidative stress. One of the key regulators of mitophagy is Pink1 that interacts with the outer mitochondrial membrane and with Parkin, an E3 ubiquitin ligase, guiding mitochondria to autophagosomal degradation<sup>178,179</sup>. In their study, *Jin et al.*<sup>180</sup> reported that ATAD3A is a major regulator of mitophagy. During mitophagy in the haematopoietic system, ATAD3A functions as a bridge between the translocase of the outer membrane complex and the translocase of the inner membrane complex to facilitate the import of Pink1 into mitochondria. Deletion of ATAD3A results in enhanced mitophagy with mitochondria depletion and blockage in differentiation, restoring HSCs pool. Another study showed that PPAR-FAO pathway mediates clearance of damaged mitochondria, an important process in the self-renewing population expansion of Tie2<sup>+</sup> HSCs in mice<sup>181</sup>. Tie2, a receptor tyrosine kinase, expression on HSCs is a marker of quiescence<sup>182,183</sup>. Additionally, ATG5 and ATG7 have been shown to regulate mitophagy and oxidative stress<sup>184</sup>. A robust increase in mitochondrial mass is detected in mice with conditional depletion of ATG5 or ATG7. This is translated in increased production of ROS and higher DNA damage in ATG7 deficient cells than that of their wild-type counterparts. Authors therefore highlight mitophagy as a critical mechanism for normal HSPC function. Furthermore, it has been reported that mice deficient in ULK1 have compromised mitochondrial clearance during the stages of erythrocyte maturation<sup>185</sup>. As previously mentioned, ROS have a major role in HSCs decline. Since mitochondria are the main source for ROS, mitophagy might also represent a crucial regulator for HSCs aging. Reducing oxidative stress via

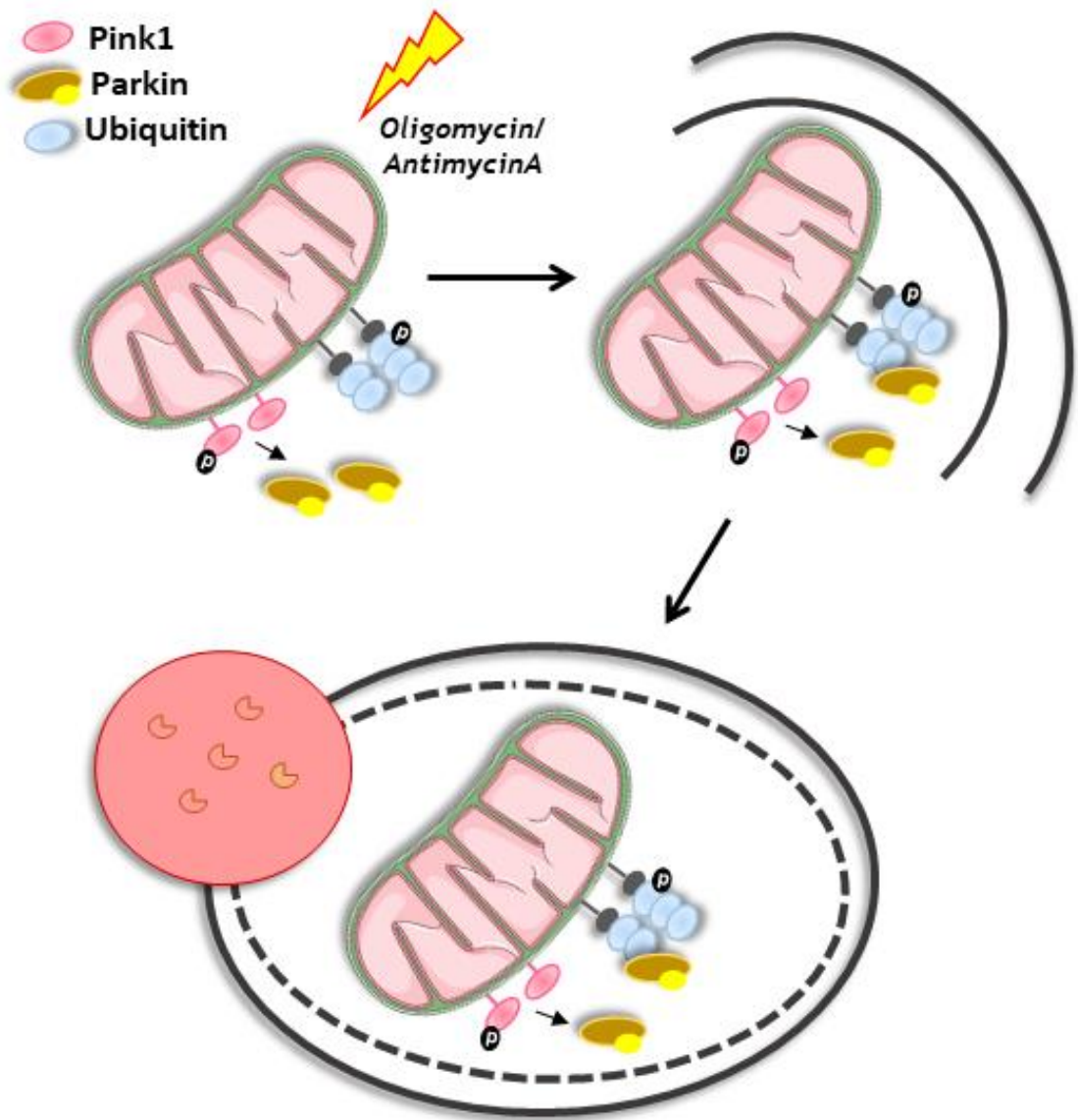


**Figure 1.7: Overview of Parkin-dependent mitophagy**

Overexpression of Parkin mediates autophagy-dependent mitochondrial degradation, mitophagy, upon mitochondrial damage induced with oligomycin/antimycin A treatment. Recruitment of Parkin to damaged mitochondria requires kinase activity of Pink1.

mitochondria degradation might therefore prevent HSCs exhaustion and immature aging, although further investigation to address this hypothesis is needed.

## 1.6 Autophagy and LSCs

In the last few decades the hypothesis that LSCs, as many other CSCs, have a high-energy demand has been supported by the results of a large number of studies. High rates of metabolism also correspond to high levels of cellular stress and this can damage cellular components. In this scenario, LSCs take advantage of the survival “sustainer” process, autophagy, by using it as a building block provider to address their metabolic requirements. As well as this, autophagy contributes to keeping cells healthy by reducing oxidative stress. *Watson et al.*<sup>186</sup> indicated that human and mouse HSPCs exhibited lower mitochondrial stress and increased mitochondrial clearance due to increased autophagy when compared to more differentiated cells. Loss of ATG7 impaired glycolysis and induced a distinctive mitochondrial metabolism profile, and the subsequent induction of ROS encouraged differentiation of CD34<sup>+</sup> CML cells in the erythroid lineage. Further investigations are still required to understand the metabolic profile of LSCs, which will also provide additional tools to elucidate the role of autophagy in sustaining leukaemic metabolism.

### 1.6.1 Mitophagy and LSCs

As described previously, mitochondrial metabolism is one of the main sources of energy for LSCs. To ensure that oxidative metabolism can meet LSCs energetic demand, their mitochondria need to be conformed to meet this. We have previously indicated mitophagy as the mechanism that removes injured mitochondria and, in this context a high demand for mitophagy will probably assure the replenishment of functioning mitochondria. However, this still remains to be investigated in detail. One of the few studies conducted in leukaemia regarding mitophagy is a recent study in acute myeloid leukaemia (AML)<sup>187</sup>. In their manuscript authors indicate that AML LSCs have increased level of mitophagy compared non-LSCs. However limited evidence is available about CML LSCs.

### **1.6.2 Autophagy in the initiation of leukaemia**

Understanding what are the main features in the initiation of leukaemia is still of high importance. Remodelling of autophagy function hasn't been largely investigated in the transformation of HSCs to LSCs. Autophagy genes are upregulated in CML and loss of autophagy in CD34<sup>+</sup> CML cells results in compromised initiation of leukaemia<sup>188,189</sup>. A high-energy demand is also required for leukaemia expansion. *Ianniciello et al.*<sup>190</sup> indicates that CD34<sup>+</sup> LSCs when exit hypoxia have increased autophagy compared to normal cells.

### **1.6.3 Autophagy in LSC drug resistance**

Several studies have shown that LSCs escape from drug treatment by upregulating autophagy. TKIs, the front-line treatment of CML, inhibit the oncogenic BCR-ABL tyrosine kinase activity and this induces autophagic flux<sup>191-194</sup>. Arsenic trioxide is an alternative way to remove BCR-ABL, which requires induction of the cathepsin B, a lysosomal protease<sup>195,196</sup>. Interestingly, CML LSCs balance autophagy between a survival and apoptotic function. Autophagy is induced for BCR-ABL degradation upon TKIs treatment and at the same time promotes leukaemic cell recovery following cessation of treatment<sup>197</sup>. Additionally, Helgason *et al.*<sup>198</sup> highlighted autophagy inhibition with TKIs treatment as a strategic approach to eradicate LSCs.

### **1.6.4 CHOICES clinical trial and new generation of autophagy inhibitors**

The relevance of combining current treatment with autophagy inhibition in LSCs have come to a phase II clinical trial. The name of the study is CHOICES (CHLOroquine and Imatinib Combination to Eliminate Stem cells) and combines first line treatment for CML patients with HCQ. However, HCQ is a non-specific autophagy inhibitor and high doses are required to target autophagy in patients that might not be achievable, thus there is a need to develop more specific autophagy inhibitors to target autophagy in patients. ULK1 and VPS34 inhibitors have been established and *in vitro* results are promising<sup>138,193,199,200</sup>. However, further analysis and *in vivo* studies using suitable robust pre-clinical models are still necessary to validate their ability to target autophagy in cancer patients and specifically in the context of leukaemia.

### 1.6.5 Inhibition of ULK1 as a new emerging tool in the treatment of cancer and other diseases

The implication of autophagy in cancer resistance has been of high debates in the past years and evidence gives a crucial role to ULK1 in the process. ULK1 plays a critical role in induction of protective autophagy in oesophageal squamous cell carcinoma (ESCC)<sup>201</sup>. ULK1-mediated autophagy has been proved to be responsible in the resistance of AML LSCs following treatment using BET inhibitors<sup>202</sup>.

A better understanding of the function and the mechanism regulated by ULK1 has led in adopting pharmacological and genetical inhibition of ULK1 approach to target autophagy in the treatment of cancer and other disorders. At the moment, a wide range of small molecules to target ULK1 are available (**Table 1-3**).

The importance of targeting ULK1 has now been highlighted in recent publications. *Radhi et al.* indicates that targeting ULK1 using both MRT68921 or SBI-0206965 leads to inhibition of autophagy and reduced *Staphylococcus* ability of infection and induce death of the host<sup>203</sup>. Inhibition of ULK1 using ULK1-101 sensitise KRAS mutated lung cancer cells to nutrient stress<sup>204</sup>. *Zhang et al.* also show the importance of targeting ULK1 in the treatment of triple negative breast cancer<sup>205</sup>. Using approach to target components of the early stages of autophagy such ULK1 and VPS34, results in enhancing BRAF inhibitors in the treatment of central nervous system (CNS) tumours<sup>206</sup>.

## 1.7 Erythroid maturation

Erythropoiesis from the Greek *ερυθρο*, red and *ποίηση*, to make, is a physiological process originating within the BM that gives rise to mature red blood cells (RBCs). The process starts from HSCs, that differentiating lose their self-renewal ability, commit to erythroid lineage first as multipotent progenitors and then as MEP. From a MEP every second 2 million of RBCs are produced in an adult person<sup>207</sup>. The transition from MEP to RBCs is a fine regulated process, involving several cell divisions steps, removal of intracellular compartment and acquiring a red phenotype due to increased concentration of haemoglobin.

Compound	Targets	Potency	Reference
<b>SBI-0206965</b>	ULK1 and ULK2	ULK1: IC <sub>50</sub> of 108 nM ULK2: IC <sub>50</sub> of 711 nM	<i>Egan et al.</i> <sup>138</sup>
<b>MRT67307</b>	ULK1 and ULK2	ULK1: IC <sub>50</sub> of 45 nM ULK2: IC <sub>50</sub> of 38 nM	<i>Petherick et al.</i> <sup>200</sup>
<b>MRT68921</b>	ULK1 and ULK2	ULK1: IC <sub>50</sub> of 2.9 nM ULK2: IC <sub>50</sub> of 1.1 nM	<i>Petherick et al.</i> <sup>200</sup>
<b>Compound 1</b>	ULK1 and ULK2	ULK1: IC <sub>50</sub> of 5.3 nM ULK2: IC <sub>50</sub> of 13 nM	<i>Lazarus et al.</i> <sup>135</sup>
<b>Compound 3</b>	ULK1	ULK1: IC <sub>50</sub> of 120 nM	<i>Lazarus et al.</i> <sup>135</sup>
<b>SR-17398</b>	ULK1	ULK1: IC <sub>50</sub> of 22 nM	<i>Wood et al.</i> <sup>203</sup>
<b>SR-20295</b>	ULK1	ULK1: IC <sub>50</sub> of 45 nM	<i>Wood et al.</i> <sup>203</sup>
<b>ULK-101</b>	ULK1 and ULK2	ULK1: IC <sub>50</sub> of 8.3 nM ULK2: IC <sub>50</sub> of 30 nM	<i>Martin et al.</i> <sup>289</sup>

**Table 1-3: ULK1/2 inhibitors. Adapted from *Limpert et al.*<sup>208,209</sup>**

## Chapter 1 Introduction

More in details, the maturation process of MEP occurs in the erythroblastic islands, a specialised region of the BM mainly populated by immature erythroblasts and macrophages. In this defined area, MEP starts decreasing cell volume, with a total of five cell division cycles. MEP first becomes a pro-erythroblast, to gradually move to basophilic, polychromatophilic and ortho-chromatophilic erythroblasts (**Figure 1.8**). Within those morphological changes, there is a gradual decrease in ribosomes, which causes a reduction in basophilia, followed by removal of mitochondria and other cytoplasmic organelles. Chromatin becomes increasingly denser until the nucleus presents a pyknotic appearance and is finally extruded from the cell, with reticulocytes become mature and terminal erythrocytes. Macrophages that populate the erythroblastic islands, feeds on extruded organelles<sup>209</sup>. Furthermore, macrophages interact with the erythroblasts to provide iron, which will facilitate proliferation and terminal differentiation preventing premature erythroblastic death.

Many cytokines are involved in the process, but erythropoietin (EPO), a growth factor produced in the kidneys, promotes the synthesis of globin, the protein counterpart of haemoglobin, essential during RBCs maturation<sup>210</sup>.

### **1.7.1 Autophagy and terminal erythropoiesis**

Autophagy appears to play a major role during RBCs maturation, contributing to clearance of organelles such as ribosomes and mitochondria (mitophagy). ULK1 and ATG7 dependent mechanism are involved in organelles removal during terminal erythropoiesis, with ULK1 and ATG7 deficient mice showing signs of anaemia and deficiency in maturation of reticulocytes<sup>184,185,211</sup> However, evidence indicate that autophagy-independent mechanism can occur when canonical autophagy is impeded<sup>212,213</sup>. Furthermore, *Karvela et al.* indicate that inhibition of autophagy using HCQ or removal of ATG7 promote erythropoiesis in the contexts of CML<sup>189</sup>. However further studies are required to fully elucidate this process.

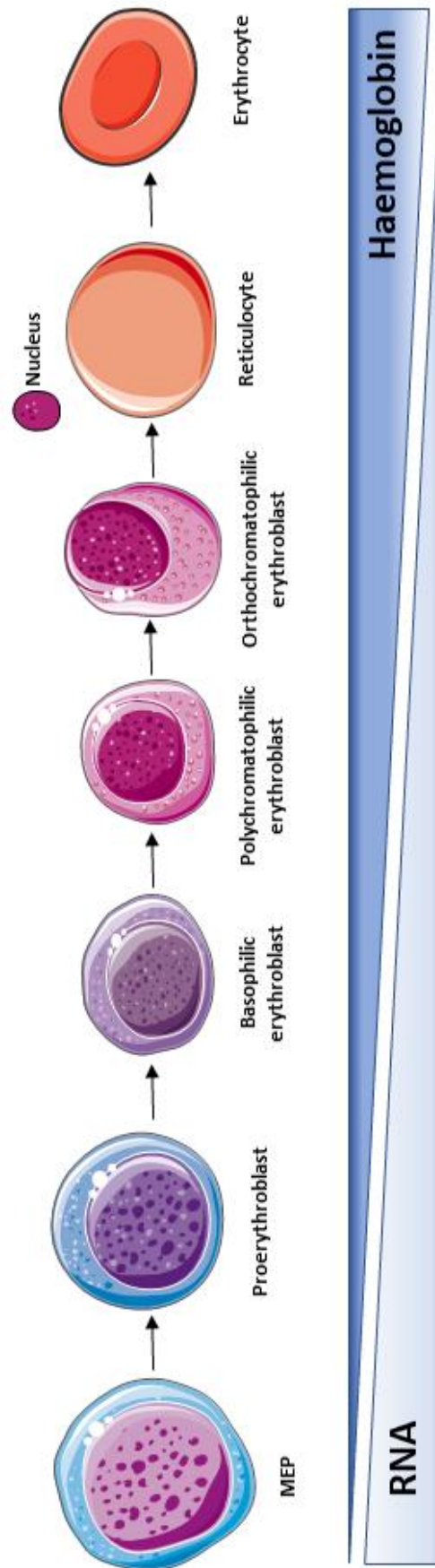


**Figure 1.8: Erythrocyte maturation**

Summary of erythroid maturation during which changes in cellular size and morphology occurs, including loss of nucleus reaching the terminal stage of erythrocyte. Increase in haemoglobin concentration and RNA level is recorded during erythropoiesis.

## Aims

The aims of this study were to:

1. Identify targetable mediators of TKI-induced autophagy in LSPCs
2. Target TKI-induced autophagy using pharmacological approaches
3. Unravel the role that ULK1 plays in regulating LSPCs' "function"

## Chapter 2 Materials and methods

## 2.1 Human primary samples

### 2.1.1 Human primary sample origin

Prior to use surplus human tissue in my research (REC 10/S0704/60) and for bank human tissue (REC 15/WS/0077), ethical approval has been given. CML samples were leukapheresis products from patients in CP-CML at the time of diagnosis, with informed consent in accordance with the Declaration of Helsinki and approval of the National Health Service Greater Glasgow Institutional Review Board (Table 2-1). Normal samples were: i) surplus cells collected from femoral head BM, surgically removed from patients undergoing hip replacement (with written patient consent and approval from the NHS Greater Glasgow and Clyde Biorepository), or ii) leukapheresis products from patients with non-myeloid Ph chromosome-negative haematological disorders (Table 2-2). The presence of the Ph chromosome in CML samples was confirmed by cytogenetic analysis.

Sample	Patient sample	Age	Gender	Disease and Phase	BCR-ABL
CML454	#1	58	Male	CML-CP	+
CML380	#2	69	Male	CML-CP	+
CML470	#3	-	-	CML-CP	+
CML483	#4	46	Male	CML-CP	+
CML407	#5	63	Female	CML-CP	+
CML456	#6	-	-	CML-CP	+
CML476	#7	-	-	CML-CP	+
CML465	#8	46	Male	CML-CP	+
CML484	#9	-	-	CML-CP	+
CML461	#10	52	Female	CML-CP	+
CML468	#11	-	-	CML-CP	+
CML462	#12	68	Male	CML-CP	+
CML472	#13	-	-	CML-CP	+
CML465	#14	62	Male	CML-CP	+
CML349	#15	40	Male	CML-CP	+
CML428	#16	-	-	CML-CP	+
CML482	#17	-	-	CML-CP	+
CML480	#18	-	-	CML-CP	+

Table 2-1: List of CML samples

Sample	Patient sample	Age	Gender	BCR-ABL
HIP57	1			-
HIP41	2			-
HIP55	3			-
BB171281	4	40	Female	-
BB171030	5	50	Male	-
BB171229	6	72	Male	-
BB180071	7	68	Male	-
BB171535	8	51	Male	-
BB180300	9	62	Male	-
BB180092	10	77	Female	-
PGT	11	-	-	-
BB181041	12	65	Male	-
BB181959	13	51	Female	-

Table 2-2: List of normal samples

### 2.1.2 Enrichment of CD34<sup>+</sup> cells from individuals diagnosed with CP-CML

Leukapheresis bag containing peripheral blood from patients diagnosed with CML were used to isolate CD34<sup>+</sup> cells using CD34 Microbeads Kit or Clini-MACS. Following isolation, samples were stained with anti-human CD34 Ab (APC) and positivity of cells was confirmed by FACs. Cells were freshly used or stored in the Paul O’Gorman Leukaemia Research Centre bio-bank at -80° C

### 2.1.3 Enrichment of Ph chromosome negative CD34<sup>+</sup> cells

#### Solutions

##### DAMP buffer

For 500 mL:

2 mL DNase I (2500U/mL) (*Roche#11284932001*)

1.25 mL Magnesium chloride (400X, 1.0 M)

53 mL Trisodium citrate (0.155M) (*Sigma#s5770*)

25 mL Human Serum Albumin (20%, Scottish National Blood Transfusion Service)

419 mL PBS (*Invitrogen#14190*)

**SFM**

For 50 mL:

500  $\mu$ L of Pen/Strep (10000 U/mL<sup>-1</sup>/10000  $\mu$ g/mL<sup>-1</sup>) (*Invitrogen#15140-122*)10 mL BIT (*Stem Cell Tech.#09500*)200  $\mu$ L low density lipo-protein (10mg/mL) (*Sigma#L4646*)2 Mercapto-ethanol (50nM) (*Invitrogen 31350-010*)25  $\mu$ L LIF (0.05ng/mL) (*PeptoTech#300-05*)34  $\mu$ L PGF cocktail (**Table 2-3**)39 mL IMDM (*Invitrogen#12440-053*)

GF	Supplier	Cat. Number	Stock conc. $\mu$ g/mL	Required conc. ng/mL	Volume x 50 mL SFM
SCF	Biolegend	#573902	5	0.2	2
G-CSF	Biolegend	#578602	20	1	2.5
GM-CSF	Biolegend	#572902	1	0.2	10
IL6	Biolegend	#570802	5	1	10
MIP- $\alpha$	PeptoTech	#300-08	1	0.2	10

**Table 2-3: Preparation of PGF cocktail**

BM sample, obtained from femoral head of individuals undergoing hip replacement, was used to isolate normal CD34<sup>+</sup> cells (**Figure 2.1a**). BM tissue was crushed using a mortar and pestle and resuspended in DAMP buffer (**Figure 2.1b**). Following spin, a 1200rpm/10min cells were resuspended in 6 mL of DAMP buffer and accurately resuspended in 15 mL tube containing 6 mL Histopaque (*Sigma#H8889*) proceeding with a ficoll separation at 400g/30 min without break (**Figure 2.1c**). Mononuclear layer of cells was collected and washed in 20 mL of DAMP buffer (**Figure 2.1d**). Cells were then resuspended in 5 mL DAMP buffer and stained with CD34<sup>+</sup> beads (*MiltenyiBiotec#130-100-454*) for 30 min at 4°C. Cells were then washed in 15 mL DAMP buffer and purified using magnetic separation (**Figure 2.1e**). LS column (*MiltenyiBiotec#5180608045*) was washed with 3 mL of PBS and cell suspension was applied onto the column. Following 2 washes with 5 mL PBS, column was placed into a 15 mL tube and 7 mL of PBS were pipetted in the column and cells immediately flushed out of the column by firmly pushing a plunger into the column (**Figure 2.1f**). This step was repeated twice. Positivity of cells expressing CD34 marker was assessed by FACs (**Figure 2.1g**).

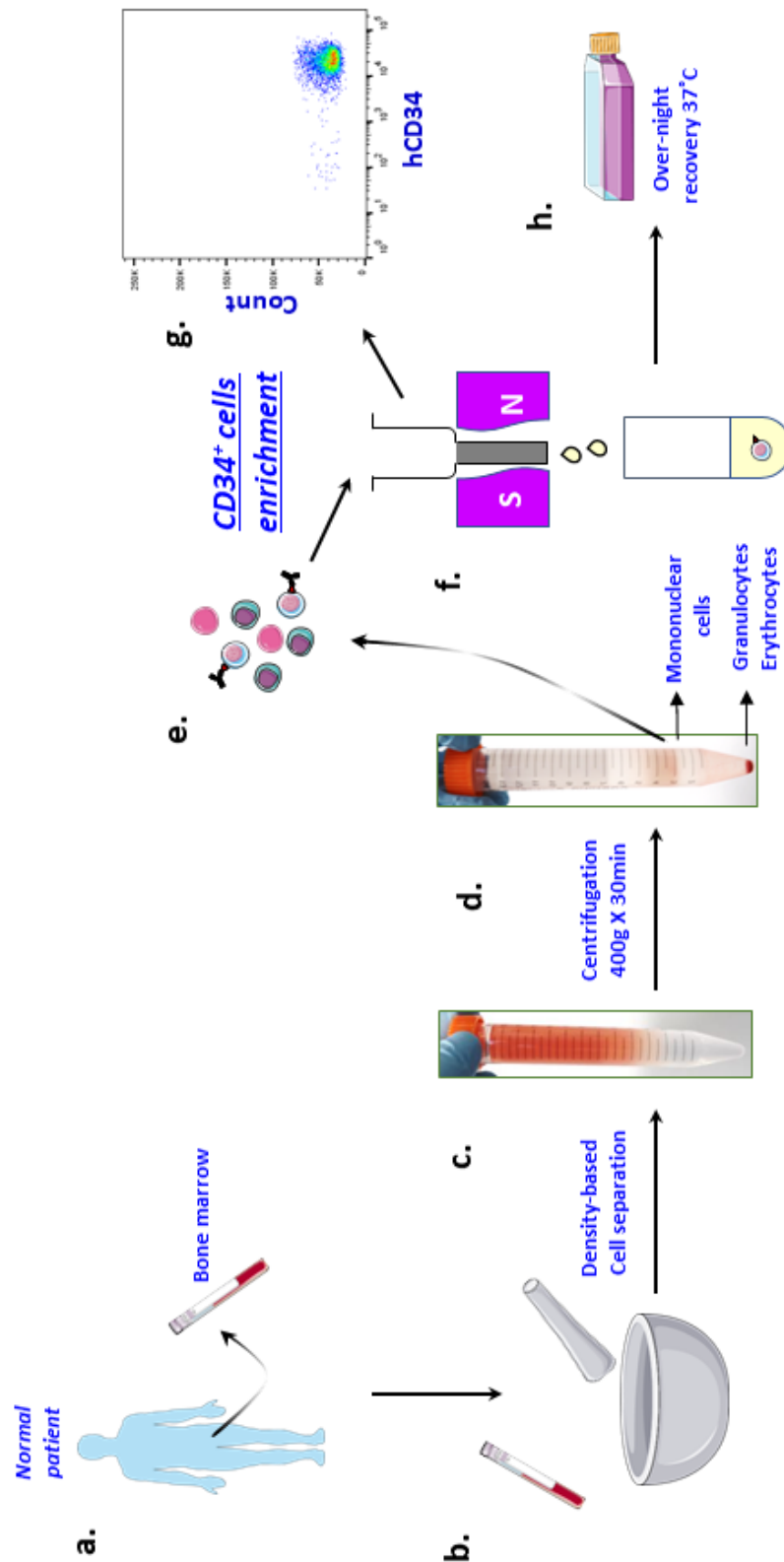


**Figure 2.1: Schematic diagram for selection and enrichment of BM-derived normal CD34<sup>+</sup> cells.**

BM was collected from residual tissue obtained from patient undergoing hip replacement (a). BM cells were extracted using a mortar and pestle (b), resuspended in PBS and placed on top of histopaque solution (c). Mononuclear cells were separated from the rest of the cells (d) and CD34<sup>+</sup> cells were enriched using beads (e, f). Positivity to CD34 expression was assessed by FACs (g). Cells were left recover ON at 37°C (h)

## Chapter 2 Materials and methods

Cells were centrifuged at 1200 rpm/10min and resuspended in serum free media (SFM Enrichment of CD34<sup>+</sup> cells from leukapheresis bag isolated from patient diagnosed with CMLCD34<sup>+</sup> cells were isolated using CD34 Microbeads Kit or CliniMACS; the flow through consisting of CD34<sup>-</sup> cells. For positive selection of human CD34 cells with Microbeads, cells were centrifuged at 1200 rpm/10 min in 5 mL DAMP buffer and stained with CD34<sup>+</sup> beads for 30 min at 4°C. Cells were then washed in 15 mL DAMP buffer and cells were purified using magnetic separation. LS column was washed with 3 mL of PBS and cell suspension was applied onto the column. Following 2 washes with 5 mL PBS, column was placed into a 15 mL tube and 7 ml of PBS were pipetted in the column and cells were immediately flushed out of the column by firmly pushing a plunger into the column. This step was repeated twice. Cells were centrifuged at 1200 rpm/10min and resuspended in SFM ON to recover.

### 2.1.4 Thawing of primary cells

Human CD34<sup>+</sup> cells were defrosted in a 37°C water bath. The cell suspension was then transferred to a 50 ml falcon tube. DAMP solution was added drop by drop (10 ml DAMP +10% FB (*Invitrogen#10500064*) was added over 20 min) while gently shaking. The cells were then centrifuged at 1200 rpm/10 min and washed with DAMP. This procedure was repeated twice. The cells were then suspended in SFM at a concentration of  $1.0 \times 10^6$  cells/ml for ON recovery.

## 2.2 Human Long- and Short- Term Culture-Initiating Cell Assays

### 2.2.1 Colony Forming Cell (CFC) assay

Colony-forming cell (CFC) assay is *invitro assay that is commonly used* in the hematopoietic field to study hematopoietic stem cells. The assay measures the ability of hematopoietic progenitors to proliferate and differentiate into colonies in a semi-solid media in response to cytokine stimulation.

Primary CML and normal cells were seeded at a concentration of  $2.0 \times 10^5$  cells/mL in SFM and treated for 3 days in the presence of indicated drugs. After 3 days,  $3 \times 10^3$  cells in the untreated arm were counted and transferred in 1.5 mL of semi-solid medium, Methocult H4034 Optimum, (*StemCell#04034*) and vortexed. The

same volume as the untreated was harvested from the rest of the conditions. The mixture of cells and semi-solid media was transferred to a 35 mm dish and incubated for 12-14 days at 37°C, 5% CO<sub>2</sub>, following which colonies were then manually counted.

CFC was also performed using CML cell lines. Following 3 days treatment, 1x10<sup>3</sup> cells were harvested and seeded for 13-14 days in Methocult 4230 (*StemCell#04230*).

### 2.2.2 Long-term culture-initiating cell (LTC-IC) assay

Long-term culture-initiating cell (LTC-IC) assay measures the ability of primitive haematopoietic cells to generate progenitor cells capable of initiate and sustain myelopoiesis for 5 weeks *in vitro*.

Genetically engineered mouse cell lines expressing human cytokines, specifically M2-10B4 (expressing IL-3 and G-CSF) and S1/S1 (expressing IL3 and SCF) were selected using hygromycin B (final concentration 62.5µg/mL for M2-10B4 and 125µg/mL for S1/S1 fibroblasts) and G418 (final concentration 400µg/mL for M2-10B4 and 800µg/mL for S1/S1 fibroblasts) in DMEM using Collagen I coated plate (Thermo#A1142802) (**Figure 2.2**). Following selection, both cell lines were irradiated at a dose of 80 Gy to inhibit cellular expansion. One day prior the assay, 7x10<sup>4</sup> cells from each feeder cell line were resuspended in 500 µL myelocult supplemented with hydrocortisone and let adhere ON (**Figure 2.2**). The following day, 5x10<sup>4</sup> primary CML cells (pre-treated for 6 days) were harvested, resuspended in 500 µL of Myelocult H5100 (*StemCell#05150*) and seeded on top of the feeder cell layer (**Figure 2.2**). Feeder cells and primary cells were cultured for additional 5 weeks with a weekly refresh of half of the media (**Figure 2.2**). Both feeder and CML cells were then harvested and transferred to 1.5 mL of semi-solid medium, Methocult H4034 Optimum, (*StemCell#04034*) and vortexed (**Figure 2.2**). The mixture of cells and semi-solid media was transferred to a 35 mm dish and incubated for 12-14 days at 37°C, 5% CO<sub>2</sub>, and colonies manually counted (**Figure 2.2**).

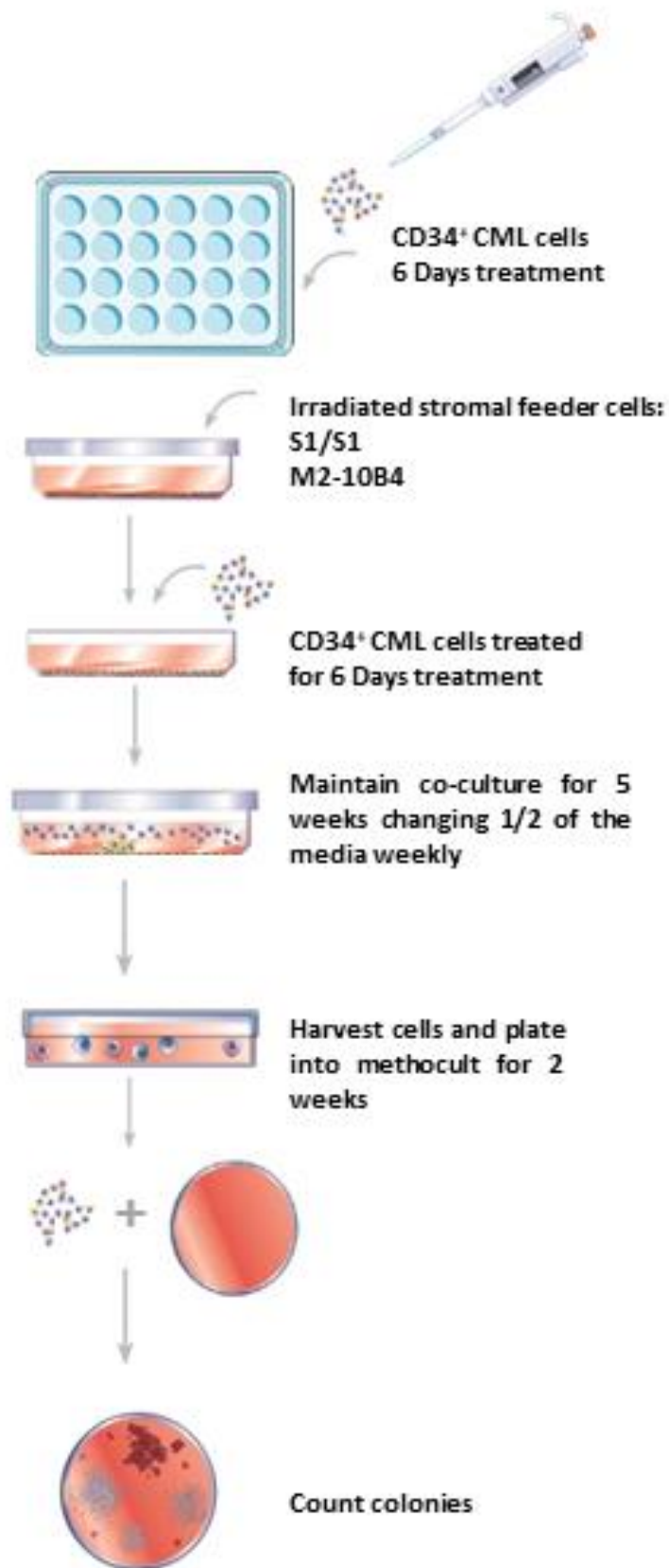


Figure 2.2: Schematic diagram illustrating LTC-IC assay (adapted from [https://cdn.stemcell.com/media/files/manual/MA28412Human\\_Long\\_Term\\_Culture\\_Initiating\\_Cell\\_Assay.pdf](https://cdn.stemcell.com/media/files/manual/MA28412Human_Long_Term_Culture_Initiating_Cell_Assay.pdf))

## 2.3 Erythroid maturation study using CD34<sup>+</sup> CML cells

CD34<sup>+</sup> CML cells were seeded at a concentration of  $2.0 \times 10^5$  cells/mL in SFM supplemented with 3 u/mL of erythropoietin (EPO). Cells were treated for 3, 6 and 9 days, and media was refreshed every 3 days. A positive control using 10 u/mL of EPO was performed and treatment with N-acetyl cysteine (NAC) was used to rescue erythroid maturation.

## 2.4 Culturing of cells

### 2.4.1 Maintenance of cell lines

#### RPMI

For 500 mL:

5 mL of Pen/Strep ( $10000 \text{ U mL}^{-1} / 10000 \text{ } \mu\text{g mL}^{-1}$ )

5 mL of Glutamine (200 mM)

50 mL of FBS

440 of RPMI (*Thermo#11875-093*)

K562 and KCL22 CML cell lines were cultured in RPMI at a concentration of  $2 \times 10^5$ /mL and passaged every 2-3 days. Cells were maintained at 37°C with 5% CO<sub>2</sub>.

### 2.4.2 Cryo-preservation of cell lines

#### Freezing media

90% FBS

10% DMSO

Cell lines were resuspended in freezing media at an approximate concentration of  $5 \times 10^6$  cells/ml and 1 ml aliquoted into individual cryovials. The cryovials were rapidly transferred into the Cool-Cell to allow a steady decrease in temperature and placed into a -80°C freezer for 24h before transfer into liquid nitrogen.

### 2.4.3 Thawing of cell lines

Cryovials were placed into in a 37°C water bath for approximately one minute. The cell suspension was then transferred into a 15mL tube containing 10 ml of pre-warmed complete growth media. Cells were centrifuged and then suspended in complete growth media at a concentration of  $2.5 \times 10^5$  cells/ml.

## 2.5 Drugs preparation

For *in vivo* study, drugs were freshly prepared twice per week and stored at 4° C. For *in vitro* assays, compounds were resuspended in specified (**Table 2-4**) vehicle and stored ad -20° C.

Drug	Company/Supplier	Vehicle	Required conc.	Dose x Day	Route of administration
MRT403 <i>in vitro</i>	Supplied by LifeArc	DMSO	1 to 10 $\mu$ M	-	-
MRT921	Supplied by LifeArc	DMSO	1 to 10 $\mu$ M	-	-
MRT016	Supplied by LifeArc	DMSO	1 to 10 $\mu$ M	-	-
MRT993	Supplied by LifeArc	DMSO	1 to 10 $\mu$ M	-	-
SBI-0206965	Sigma	DMSO	1 to 10 $\mu$ M	-	-
HCQ	USP	PBS	10 $\mu$ M	-	-
BAF	Donation from Kevin Ryan lab.	DMSO	100 nM	-	-
Nilotinib	LC Laboratories	DMSO	0.3 - 3 $\mu$ M	-	-
Omacetaxin	Sigma	DMSO	10 nM	-	-
Imatinib	LC Laboratories	Water	50 mg/Kg	2	Oral gavage
MRT403 <i>in vivo</i>	Supplied by LifeArc	DMSO	40 mg/Kg	1	Oral gavage

**Table 2-4: Drugs details**

## 2.6 Immunoblotting

### 2.6.1 Protein lysis and quantification

Prior to protein lysis, stock solutions were made as indicated below.

#### SDS 10%

Dissolve 10g SDS (*Sigma#L5750*)  
in 100mL deionized water

#### PhoshoSTOP solution

Dissolve 1 tablet PhosphoSTOP (*Roche#04906837001*)

## Chapter 2 Materials and methods

in 1mL deionized water

### **Complete Solution**

Dissolve 1 tablet Complete (*Roche#05892970001*)  
in 1mL deionized water

### **Ripa buffer mix**

Ripa buffer (*Thermo#89901*)  
10% PhosphoSTOP solution  
10% Complete solution  
10% SDS 10%

Cells were harvested from each condition in a 15 ml tube and counted. Following centrifugation at 1200 rpm/5min, media was discarded, and cell pellet was washed with PBS and placed in a fresh 1.5 ml Eppendorf. Cells were spin at 1200 rpm/5min, PBS was accurately removed, and cells were resuspended in RIPA buffer mix and place in ice. The use a syringe and 25G needle facilitated cell lyses. Lysates were centrifuged at 16000 rpm/30min at 4 °C and collected in a fresh 1.5 ml Eppendorf and stored at -80 °C. Quantification of protein was evaluated using Bicinchoninic acid (BCA) protein assay. Following defrosting of lysates on ice, 2 µL x3 of each sample was place into a 96 well plate. Standard curve was generated using 0-0.1-0.25-0.5-0.75-1.0-1.5-2.0 mg of standard albumin. For protein quantification, the Pierce™ BCA Protein Assay Kit (*Thermo#23228*) was used according to manufacturer's instructions. In brief, 98% (v/v) Reagent A was mixed with 2% (v/v) Reagent B and 198 µl of the Reagent A+ Reagent B was distributed into each sample previously spread in a 96-well plate. Following incubation of the plate at 37 °C for 30 min, absorbance was measured at OD 562 nm using a spectrophotometer plate reader. The concentration of each samples was determined by interpolating their absorbance values with the standard curve. Equal amounts of proteins (5-20 µg) were resuspended in Nupage SB4X (*Invitrogen#NP007*) and appropriate amount of water was added to each sample to dilute SB to 1X and 0.1% DTT (*Sigma#43819*) for a final volume of 30µL respectively.

### **2.6.2 Hand casting polyacrylamide gels**

Prior to gel preparation, stock solutions were made as indicated below.

#### **Stock solutions**

## Chapter 2 Materials and methods

### 1.5 M Tris-HCl pH 8.8

18.15 g Tris (*Sigma#T1378*)

60 mL deionized water

Adjust to pH 8.8 with HCl

Make to 100mL with deionized water

### 0.5 M Tris-HCl pH 6.8

6g Tris

60 mL deionized water

Adjust to pH 6.8 with HCl

Make to 100mL with deionized water

### APS 10%

1g APS (*Sigma#2486-14*)

10ml deionized water

Components	Stacking gel 4%	Resolving gel			
		7.50%	12%	15%	X%
30% Acrylamide ( <i>Biorad#88520</i> )	1.98 mL	3.75 mL	6.0 mL	7.5 mL	0.33*XmL
0.5 M Tris-HCl pH 6.8	3.78 mL	-	-	-	-
1.5 M Tris-HCl pH 8.8	-	3.75 mL	3.75 mL	3.75 mL	3.75 mL
10% SDS	150µL	150µL	150µL	150µL	150µL
Deionized water	9 mL	7.28 mL	5.03 mL	3.5 mL	11.03-(0.33*X) mL
TEMED ( <i>Sigma#T9281</i> )	15µL	15µL	15µL	15µL	15µL
10% APS	15µL	15µL	15µL	15µL	15µL
<b>Total volume</b>	<b>15 mL</b>	<b>15 mL</b>	<b>15 mL</b>	<b>15 mL</b>	<b>15 mL</b>

**Table 2-5: Preparation of acrylamide-gels**

Resolving gel acrylamide solution was prepared following recipe in **Table 2-5**. Quickly pore solution in an empty cassette (*LifeTech.#NC2015*) and use 2-Propanol (*Sigma#24137*) to help remove bubbles and initiate polymerization. Allow polymerization for at least 20 min. After that, properly remove 2-Propanol and prepare stacking acrylamide 4% gel solution and pore on top of the resolving solution. Add a comb and let polymerize for at least 20 min. Store at 4°C for no longer than a week. In specific cases, pre-cast gels were used (*Invitrogen#NP0321-2*).

### 2.6.3 SDS-PAGE separation of proteins

Prior to protein separation, stock solutions were made as indicated below.

#### Running buffer

For 1L 10X stock solution:

## Chapter 2 Materials and methods

Dissolve 30.3 g Tris and 144.1 g of glycine (*Sigma#G8898*) in 800 mL deionized water. Use a magnetic stir to help powder to dissolve. Adjust volume to 1L with deionized water. Previous to use dilute stock solution to 1X and add 10 mL of 10% SDS.

Samples were defrosted and placed at 95 °C for 5 min for denaturation. Pre-made gels were placed into running buffer and comb was removed. For pre-cast gels Nupage Mes buffer was used (*Invitrogen#2010944*). Samples were accurately spun down for few second and then loaded in each well, reserving one well for protein size marker (*Biorad#161-0377*). Any empty well was filled with 1xSB. Proteins were allowed to separate for 1.5-2 h.

### 2.6.4 Transfer to PVDF membrane

Prior to protein transfer, stock solutions were made as followed indicated.

#### Transfer buffer

For 1L solution (made fresh at the time of use):

700 mL of deionized water

100 mL methanol (*Fisher#67-56-1*)

100 mL running buffer

2 mL SDS 10%

Activate PVDF membrane (*Thermo#88520*) for 5 min in 5 mL methanol. Following protein separation, proteins were transferred to a PVDF membrane enclosed in a western blot « sandwich » made as follows: 1 sponge - 2 Whatman paper - PVDF membrane - 2 Whatman paper - 2 sponge. All components were soaked in transfer buffer before assembly of the « sandwich ». The proteins were then transferred for 2 h at 400 mA.

### 2.6.5 Blocking and immunolabelling

Prior to membrane blocking and immunolabelling, stock solutions were made as followed indicated.

#### TBS10x

For 1L solution:

## Chapter 2 Materials and methods

Dissolve 6.05g Tris and 8.76g NaCl (*WWR#7647-14-5*) in 800 mL of deionized water. Use a magnetic stir to mix the solution and accelerate powder dissolving. Adjust pH to 7.5 with HCl. Adjust volume to 1L with deionized water

### **TBST1X**

For 1L solution:

Dilute TBS10x to TBS1x using deionized water and add 1ml of TWEEN (*Sigma#P1379*) for 1 L solution.

### **Blocking solution**

For 250 mL solution:

Dissolve 2.5 g BSA (*Sigma#A7906*) in TBST1x. Use a magnetic stir to accelerate BSA dissolve.

Membrane was incubated for 1 h with 5 mL blocking buffer at RT followed by ON incubation with primary Ab diluted in blocking solution (**Table 2-6**). The following day, membranes were washed 3 times 15 min each in TBST1x and incubated for 1 h RT with specific secondary Ab, appropriately diluted in blocking solution. Membranes were then washed 3 times 15 min each in TBST1x and revealed by chemiluminescence using LICOR. Precisely, the membrane was incubated for 1 min with a working solution made of equal part of luminol-enhancer and peroxide solution using Pierce™ ECL Western Blotting Substrate (*Thermo#32106-34095*). When occurred, membrane was stripped in Ponceau red solution (*Sigma#P7170*) and re-incubated ON with primary Ab. When occurred, quantification was performed using Image studio software [https://www.licor.com/bio/products/software/image\\_studio/](https://www.licor.com/bio/products/software/image_studio/).

## Chapter 2 Materials and methods

Target	Species	Supplier	Cat. Number	Usage
<b>Primary</b>				
ACC	Rabbit	Cell signalig	#3662	IB: 1 : 1000
AMPK $\alpha$	Rabbit	Cell signalig	#2532	IB: 1 : 1000
Arginase-1	Rabbit	Cell signalig	#93668	IB: 1 : 1000
ARA70	Mouse	SANTA CRUZ	#sc-373739	IB: 1 : 500
ATG13	Rabbit	Cell signalig	#13468	IB: 1 : 1000
ATG7	Rabbit	Cell signaling	#8558	IB: 1 : 1000
c-ABL	Rabbit	Cell signaling	#2862	IB: 1 : 500
Cruk1	Rabbit	Cell signaling	#3182	IB: 1 : 500
GAPDH	Rabbit	Cell signaling	#5174	IB: 1 : 1000
GFP	Mouse	Roche	#118144600001	IB: 1 : 1000
LC3B	Rabbit	Cell signaling	#2775	IB: 1 : 500
MT-CO2	Mouse	Thermo Fisher Scientific	#A-6404	IB: 1 : 2000
MTOR	Rabbit	Cell signaling	#2983	IB: 1 : 500
NBR1	Mouse	ABNOVA	#H00004077-M01	IB: 1 : 500
OXPPOS cocktail	Mouse	Abcam	#ab110413	IB: 1 : 2000
P62	Mouse	BD	#610833	IB: 1 : 1000
p-ACC <sup>ser79</sup>	Rabbit	Cell signaling	#3661	IB: 1 : 1000
p-AMPK <sup>tyr172</sup>	Rabbit	Cell signaling	#2531	IB: 1 : 1000
p-ATG13 <sup>ser318</sup>	Rabbit	ABNOVA	#PAB19948	IB: 1 : 1000
p-Cruk1 <sup>tyr207</sup>	Rabbit	Cell signaling	#3181	IB: 1 : 1000
p-MTOR <sup>ser2448</sup>	Rabbit	Cell signaling	#2971	IB: 1 : 500
p-S6 <sup>ser240/244</sup>	Rabbit	Cell signaling	#5364	IB: 1 : 1000
p-ULK1 <sup>ser757</sup>	Rabbit	Cell signaling	#6888	IB: 1 : 500
S6	Rabbit	Cell signaling	#2317	IB: 1 : 1000
ULK1	Rabbit	Cell signaling	#8054	IB: 1 : 1000
Flotillin1	Rabbit	Abcam	#ab41927	IB: 1 : 1000
TSG101	Rabbit	Abcam	#ab30871	IB: 1 : 1000
$\beta$ -tubulin	Rabbit	Cell signaling	#2146	IB: 1 : 1000
<b>Secondary</b>				
Mouse IgG	HRP	Cell signaling	#7076	IB: 1 : 5000
Rabbit IgG	HRP	Cell signaling	#7074	IB: 1 : 5000

**Table 2-6: List of western blotting antibody**

## 2.7 Flow cytometry analyses

Flow cytometry analysis are used to determine morphological and phenotypical parameters of single cells. Based on fluidic system, flow cytometers separate cell samples into a flow stream, allowing system of optics and filters to identify size and granularity of single cells. Flow cytometers are also composed of lasers that can be used to resolve expression of extracellular or intracellular markers using specific fluorophore-labelled antibodies.

### Solutions

#### **Fc block**

1  $\mu$ L Fc block  
49  $\mu$ L PBS 2% FBS (v/v)

#### **Lin<sup>-</sup> cocktail MIX1**

0.8  $\mu$ L Biotin anti-mouse CD4  
1.6  $\mu$ L Biotin anti-mouse CD5  
1.6  $\mu$ L Biotin anti-mouse CD8a  
6.2  $\mu$ L Biotin anti-mouse Mac-1  
6.2  $\mu$ L Biotin anti-mouse CD45R/B220  
25  $\mu$ L Biotin anti-mouse TER119  
12.5  $\mu$ L Biotin anti-mouse GR-1  
71.1  $\mu$ L PBS

1  $\mu$ L Streptavidin  
100  $\mu$ L 2% FBS (v/v)

#### **Lin<sup>-</sup> cocktail MIX2**

6.2  $\mu$ L Biotin anti-mouse Mac-1  
12.5  $\mu$ L Biotin anti-mouse GR-1  
106.3  $\mu$ L PBS

1  $\mu$ L Streptavidin  
100  $\mu$ L 2% FBS (v/v)

#### **Murine ST/LT/MPP HSC-LSC mix**

11  $\mu$ L Pacific Blue Lin<sup>-</sup> cocktail MIX1  
1  $\mu$ L Sca anti-mouse PeCy7  
1  $\mu$ L cKit anti-mouse APC/780  
3.2  $\mu$ L CD48 anti-mouse PE  
1  $\mu$ L CD150 anti-mouse APC  
1  $\mu$ L FITC anti-mouse CD45.1  
3  $\mu$ L PerCP/Cy5.5 anti-mouse CD45.2  
17.8  $\mu$ L PBS

#### **Myeloid progenitors mix**

11  $\mu$ L Pacific Blue Lin<sup>-</sup> cocktail

## Chapter 2 Materials and methods

1  $\mu$ L cKit anti-mouse APC-Cy7  
3.2  $\mu$ L CD48 anti-mouse PE  
1  $\mu$ L CD16/32 anti-mouse APC  
1  $\mu$ L PE anti-mouse CD45.1  
3  $\mu$ L PerCP/Cy5.5 anti-mouse CD45.2  
16.8  $\mu$ L PBS

### **Murine myeloid cells mix**

1  $\mu$ L FITC anti-mouse CD45.1  
2  $\mu$ L PerCP/Cy5.5 anti-mouse CD45.2  
1  $\mu$ L APC anti-mouse GR-1  
0.5  $\mu$ L PeCy7 anti-mouse Mac-1  
1  $\mu$ L FITC anti-mouse TER119

### **Murine erythroid cells mix**

1  $\mu$ L PE anti-mouse CD45.1  
2  $\mu$ L PerCP/Cy5.5 anti-mouse CD45.2  
11  $\mu$ L Pacific Blue Lin<sup>-</sup> cocktail MIX2  
1  $\mu$ L FITC anti-mouse TER119  
1  $\mu$ L APC anti-mouse CD44

### **Murine B cells mix**

1  $\mu$ L FITCH anti-mouse CD45.1  
1  $\mu$ L Pacific Blue anti-mouse CD45.2  
2  $\mu$ L Streptavidin-Biotin anti-mouseCD45R/B220  
1  $\mu$ L APC-Cy7 anti-mouse CD19

### **Murine T cells mix**

1  $\mu$ L FITCH anti-mouse CD45.1  
1  $\mu$ L Pacific Blue anti-mouse CD45.2  
1  $\mu$ L Streptavidin-Biotin anti-mouseCD8a  
1  $\mu$ L PE anti-mouse CD4

## **2.7.1 FACs staining procedure**

Following collection and washing using PBS, cells were stained with specific antibody mix (Table 2-7) for 30 min in the dark. Cells were then washed twice using 2 mL PBS and resuspended in 200  $\mu$ L of PBS and analysed by FACs.

## **2.7.2 Cell Trace Violet staining**

### **2.7.2.1 Background**

Cell Trace Violet is a kit used to monitor cell proliferation. It's a fluorescent dye that labels cells by covalent binding of amino acids residue intra-cellularly. Based on that, it is used to monitor over-time cell division by FACs.

### **2.7.2.2 Method**

CD34<sup>+</sup> CML cells were stained at day 0 using 1  $\mu$ M of Cell Trace Violet dye for 30 min at 37°C. Cells were then washed and suspended in SFM. Cell division was assessed by FACS at day 3 and day 6.

### **2.7.3 Apoptosis staining**

Apoptosis is a programmed cell death mechanism that proceeds through several stages, characterized by distinct changes in cell morphology. During early stages of apoptosis, phospholipid phosphatidylserine is exposed to outer membrane surface which can be recognised using Annexin V. Staining using Annexin V in presence of Ca is therefore used as a measurement of early apoptosis. Late stages of apoptosis can be detected by binding of GC regions of DNA with 7-Aminoactinomycin D (7AAD).

### **2.7.4 MitoSOX staining**

MitoSOX is a fluorescent dye that can be used to monitor mitochondrial reactive oxygen species in live cells.

Cells were seeded at a concentration of  $2 \times 10^5$ / mL and treated for 72h. Cells were harvested and washed in PBS and stained using 1 mL (10  $\mu$ M) of MitoSOX and incubated for 30 min at 37°C. 1 h treatment with 100 nM NAC and H<sub>2</sub>O<sub>2</sub> were used as negative and positive control, respectively. Cells were then washed twice in 2 mL of PBS and analysed by FACS.

## **2.8 NADPH measurements**

Cells were seeded at a concentration of  $2 \times 10^5$ /mL and treated for 72h. Cells were harvested and washed in PBS and NADPH was measured and analysed as indicated by the manufacturer (*Abcam#ab65349*).

## Chapter 2 Materials and methods

Target	Species	Dye	Supplier	Cat. Number#	Usage $\mu$ L
Annexin-V	-	FITCH	BD	640906	3
Annexin-V	-	APC	BD	550475	3
7-AAD	-	-	BD	559925	3
CD45	Human	APC	BD	559864	1
CD34	Human	APC	BD	558224	1
CD38	Human	PerCP	Biologend	303519	2
CD133	Human	PE	Miltenyi	130-080-801	2
CD45.1	Mouse	PE	Biologend	110708	2
CD45.1	Mouse	FITCH	Biologend	110706	2
CD45.2	Mouse	PerCP-CY5.5	Biologend	552950	1
CD45.2	Mouse	Pacific blue	Biologend	109820	1
CD45.2	Mouse	APC	Biologend	109814	1
CD11b (Mac-1)	Mouse	PE	Biologend	101216	2
CD150	Mouse	APC	Biologend	115910	2
CD235a	Human	PerCP-CY5.5	Biologend	349110	5
TER119	Mouse	FITCH	Biologend	116206	3
CD71	Human	PE	BD	555537	5
CD71	Mouse	PE	Biologend	113808	3
CD44	Human	FITCH	Biologend	338804	1
CD44	Mouse	APC	Biologend	103012	1
Sca	Mouse	PE-CY7	Biologend	122514	2
c-kit	Mouse	APC-CY7	Biologend	105826	2
Gr-1	Mouse	APC	Biologend	108412	2
CD4	Mouse	PE	Biologend	100408	2
CD8a	Mouse	PE	Biologend	100707	2
Gr-1	Mouse	APC	Biologend	108412	2
Mac-1	Mouse	PE-CY7	Biologend	101216	2
CD48	Mouse	PE	Biologend	103412	2
CD45R	Human	FITCH	BD	347723	3
CD123	Human	PE-CY7	Biologend	306010	3
CD36	Human	PE-CY7	Biologend	336222	3
CD34	Mouse	FITCH	Bioscience	11-0341-82	2
CD16/32	Mouse	APC	BD	553142	2
Biotin-TER119	Mouse	-	BD	553672	-
Biotin-Gr-1	Mouse	-	BD	553125	-
Biotin-CD11b (Mac-1)	Mouse	-	BD	553309	-
Biotin-CD45R/B220	Mouse	-	BD	553086	-
Biotin-CD4	Mouse	-	BD	553649	-
Biotin-CD5	Mouse	-	BD	553019	-
Biotin-CD8a	Mouse	-	BD	553029	-

**Table 2-7: List of FACS antibodies**

## 2.9 Immunohistochemistry

At day 0, coverslips were incubated for 5 min in poly-lysine (*Sigma# P4707*) and then washed twice with deionized water. At day 1, coverslips were allocated in a 25 mm dish covered with parafilm.  $5 \times 10^5$  cells were resuspended in 300  $\mu\text{L}$  of RPMI and placed on coverslips coated with poly-lysine for 2 h. Parafilm was used for his hydrophobic capacity, making cells stay on top of the coverslips. Media was aspirated, and cells were fixed for 10 min using 300  $\mu\text{L}$  of 4% freshly prepared PFA. PFA was then removed and coverslips were washed using PBS and mounted on slides. Mounting media containing DAPI was used (*Vectashield#H1200*). Slides were sealed and stored at 4°C prior to confocal microscopy analysis.

## 2.10 RNA isolation and qPCR

### 2.10.1 RNA extraction

*Primary cells:* Cells were harvested in a 1.5 mL tube, spun down at 3000 g/10min and resuspended in 0.9 mL of PBS/10% BSA. Cell suspension was centrifuged at 3000 g/5 min and supernatant discarded. For RNA extraction, PicoPure™ RNA Isolation Kit (*Thermo#KIT0204*) was used. In brief, pellet was gently resuspended in 100  $\mu\text{L}$  Extraction Buffer and incubated at 42°C for 30 min. Sample was centrifuged at 3000 g/2min. Supernatant was then pipetted into a new tube and proceeded for RNA isolation, or sample stored at -80°C.

### 2.10.2 RNA isolation

Prior to RNA isolation, RNA isolation columns were pre-conditioned as follows.

250  $\mu\text{L}$  of Conditioning Buffer was added to the purification column and incubated for 5 min at RT. Column was then centrifuged at 16000 g/1min. Sample was mixed with 50  $\mu\text{L}$  of 70% ethanol. The mix was then transferred into RNA isolation column and centrifuged at 100g/2min followed by a centrifugation of 16000g/30 sec. Supernatant was discarded and column washed with 100  $\mu\text{L}$  of Wash Buffer and centrifuged at 8000g/1min. Sample was then treated with 40  $\mu\text{L}$  of DNase treatment (5  $\mu\text{L}$  DNase + 35  $\mu\text{L}$  Buffer RDD; *Qiagen#79254*) and incubated at room temperature for 15 min. 40  $\mu\text{L}$  of the Wash Buffer 1 were then added to the column and sample was centrifuged at 8000 g/15sec. Sample was washed twice with 100

## Chapter 2 Materials and methods

$\mu\text{L}$  of Wash Buffer 2, centrifuged at 8000 g/1min, washed again and then centrifuged at 16000 g/1min. Column was then transferred into a new 0.5 mL tube and 11  $\mu\text{L}$  of Elution Buffer added. Following 1 min incubation at RT, sample was centrifuged at 1000 g/1min to distribute the buffer and finally the sample was eluted by centrifuging sample at 16000g/1min. Sample was then stored at  $-80^{\circ}\text{C}$ .

### 2.10.3 RNA quantification and cDNA synthesis

Sample stored at  $-80^{\circ}\text{C}$  was defrosted in ice and RNA content was quantified using NanoDrop spectrophotometer, followed by cDNA synthesis. For cDNA reaction 2x RT master mix was prepared as indicated in **Table 2-8**.

Kit components were allowed to thaw in ice:

2X RT MASTER MIX	
Component (LifeTech#00716543)	Volume ( $\mu\text{L}$ )
10X RT Buffer	2
25x dNTP mix (100nM)	0.8
10x Random Primers	2
Reverse Transcriptase	1
RNAse inhibitor ( <i>LifeTech#00725733</i> )	1
Nuclease Free water	3.2
<b>Total Volume</b>	<b>10</b>

**Table 2-8: 2X RT MASTER MIX**

10  $\mu\text{L}$  of 2xRT master mix was pipetted into tubes containing equal concentration of RNA. Nuclease free water was added to reach final volume of 20  $\mu\text{L}$ . Tubes were centrifuged and loaded in the thermal cyclers.

cDNA was then frozen at  $-20^{\circ}\text{C}$ .

### 2.10.4 qPCR reaction

TaqMan® Array Fast Plates (10  $\mu\text{L}$  reaction) were designed as followed (*Thermo#4413255-57*).

## Chapter 2 Materials and methods

4413255												
	1	2	3	4	5	6	7	8	9	10	11	12
A	18S	AKT1	AMBRA1	ATG10	ATG12	ATG16L1	ATG16L2	ATG2A	ATG2B	ATG3	ATG4A	ATG4B
B	ATG4C	ATG4D	ATG5	ATG7	ATG9A	ATG9B	BECN1	BNIP3	DRAM1	GABARA P	GABARA P	GABARA P
C	MAP1LC3 A	MAP1LC3 B	MTOR	PIK3C3	PIK3R4	RHEB	SQSTM1	ULK1	ULK2	UVRAG	WDFY3A S	WIPI1
D	WIPI2	RB1CC1	ATG13	BCL2	BN1P3L	RPS6KB1	C12orf44	TP53	PRKAA1	ATG14	PTEN	GAPDH
E	18S	AKT1	AMBRA1	ATG10	ATG12	ATG16L1	ATG16L2	ATG2A	ATG2B	ATG3	ATG4A	ATG4B
F	ATG4C	ATG4D	ATG5	ATG7	ATG9A	ATG9B	BECN1	BNIP3	DRAM1	GABARA P	GABARA P	GABARA P
G	MAP1LC3 A	MAP1LC3 B	MTOR	PIK3C3	PIK3R4	RHEB	SQSTM1	ULK1	ULK2	UVRAG	WDFY3A S	WIPI1
H	WIPI2	RB1CC1	ATG13	BCL2	BN1P3L	RPS6KB1	C12orf44	TP53	PRKAA1	ATG14	PTEN	GAPDH

4413257												
	1	2	3	4	5	6	7	8	9	10	11	12
A	18S	AKT1	AMBRA1	ATG10	ATG12	ATG16L1	18S	AKT1	AMBRA1	ATG10	ATG12	ATG16L1
B	ATG16L2	ATG2A	ATG2B	ATG3	ATG4A	ATG4B	ATG16L2	ATG2A	ATG2B	ATG3	ATG4A	ATG4B
C	ATG4C	ATG4D	ATG5	ATG7	ATG9A	ATG9B	ATG4C	ATG4D	ATG5	ATG7	ATG9A	ATG9B
D	BECN1	BNIP3	DRAM1	GABARA P	GABARA P	GABARA P	BECN1	BNIP3	DRAM1	GABARA P	GABARA P	GABARA P
E	MAP1LC3 A	MAP1LC3 B	MTOR	PIK3C3	PIK3R4	RHEB	MAP1LC3 A	MAP1LC3 B	MTOR	PIK3C3	PIK3R4	RHEB
F	SQSTM1	ULK1	ULK2	UVRAG	WDFY3-AS	WIPI1	SQSTM1	ULK1	ULK2	UVRAG	WDFY3-AS	WIPI1
G	WIPI2	RB1CC1	ATG13	BCL2	BN1P3L	RPS6KB1	WIPI2	RB1CC1	ATG13	BCL2	BN1P3L	RPS6KB1
H	C12orf44	TP53	PRKAA1	ATG14	PTEN	GAPDH	C12orf44	TP53	PRKAA1	ATG14	PTEN	GAPDH

cDNA was de-frosted, and the mix was prepared as indicated in **Table 2-9**.

Plates were sealed and spin to collect sample at the bottom and qPCR reaction was started.

Component	Volume $\mu$ L)
cDNA	5ng (X $\mu$ L)
TaqMan® Fast Advanced Master Mix (2X) (LifeTech#1804162)	5
Nuclease Free water	X
<b>Total volume</b>	<b>10</b>

**Table 2-9: TaqMan qPCR mix**

## 2.11 Viral particles production and transfection

### 2.11.1 Viral particles production

Prior to viral particles production, following solutions were prepared as indicated

**HBS2X pH 7.0**

**2.5M CaCl<sub>2</sub>**

#### **DMEM**

For 500 mL:

5 mL of Pen/Strep (10000 U/mL<sup>-1</sup>/10000 µg/mL<sup>-1</sup>)

5 mL of Glutamine (200 mM)

50 mL of FBS

440 mL of DMEM (*Thermo# 11965-084*)

At *Day 0*  $5 \times 10^5$  HEK 293 FT (lentivirus) or Phoenix-Ampho HEK cells (retrovirus) were seeded in cell culture plate (100cm<sup>3</sup>) with 10mL DMEM.  $6 \times 10^6$  can be plated if virus production starts the day after. At *Day 4* cells will be 70-80% confluent and well adherent to cell plat and media was refreshed on each plate. Into a sterile tube were added respectively lenti/retro-viral mix as indicated in **Table 2-10**.

	Lentivirus mix	Retrovirus mix
Packaging PSPAX	12.45µg	-
Envelope VSVG	4.5µg	-
Plasmid	14.2µg	14.2µg
ddH <sub>2</sub> O	1.3 mL	1.3 mL
2.5M CaCl <sub>2</sub>	183µL	183µL
2xHBS Ph 7.0	1.5mL	1.5mL

**Table 2-10: Virus mix**

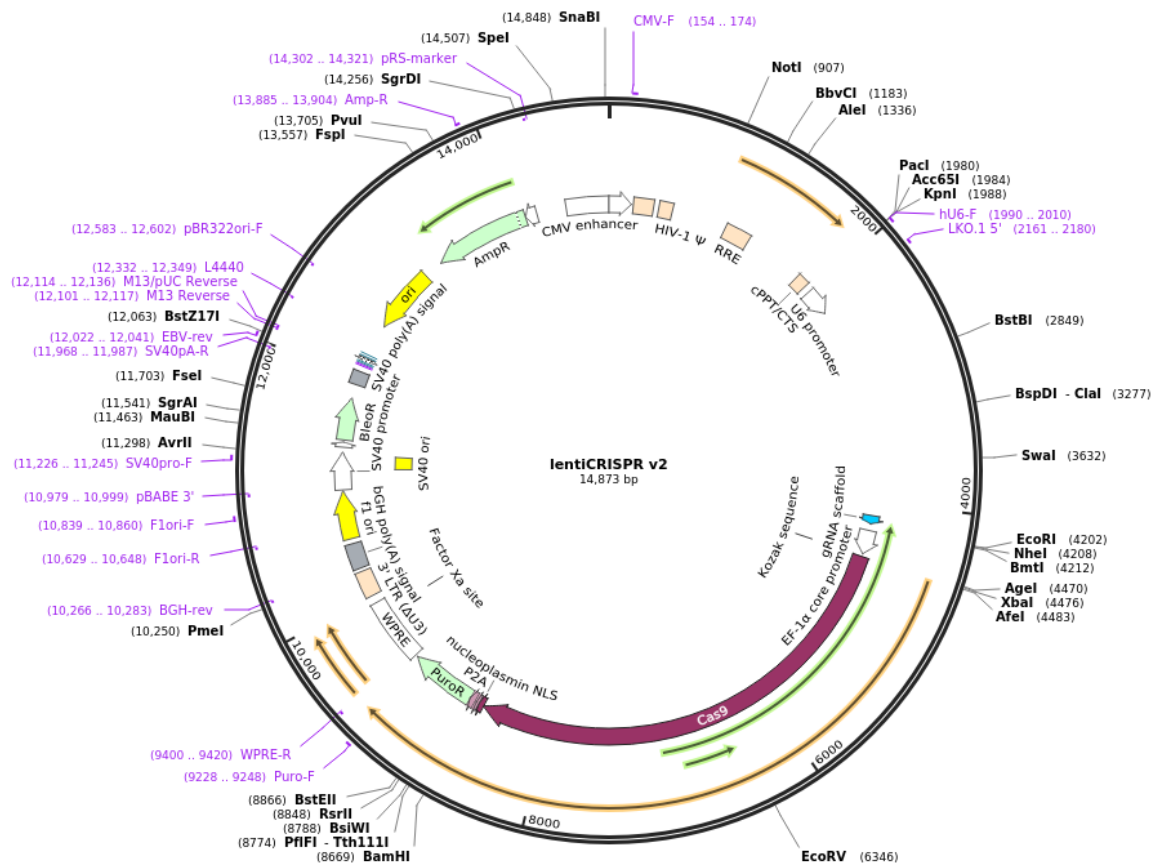
Mix were incubated for 30 min. at RT after what mix was added to cells. HEK cells were incubated with lenti- or retro- viral mix for 6-7h following which media was changed adding 10mL fresh DMEM. At *Day 5* media was refreshed adding 5 mL DMEM. At *Day 7* media was harvested and filtered using 0.45µm filter. Virus particles were freshly added to  $5 \times 10^5$  cells or frozen. At *Day 8* following 24h

## Chapter 2 Materials and methods

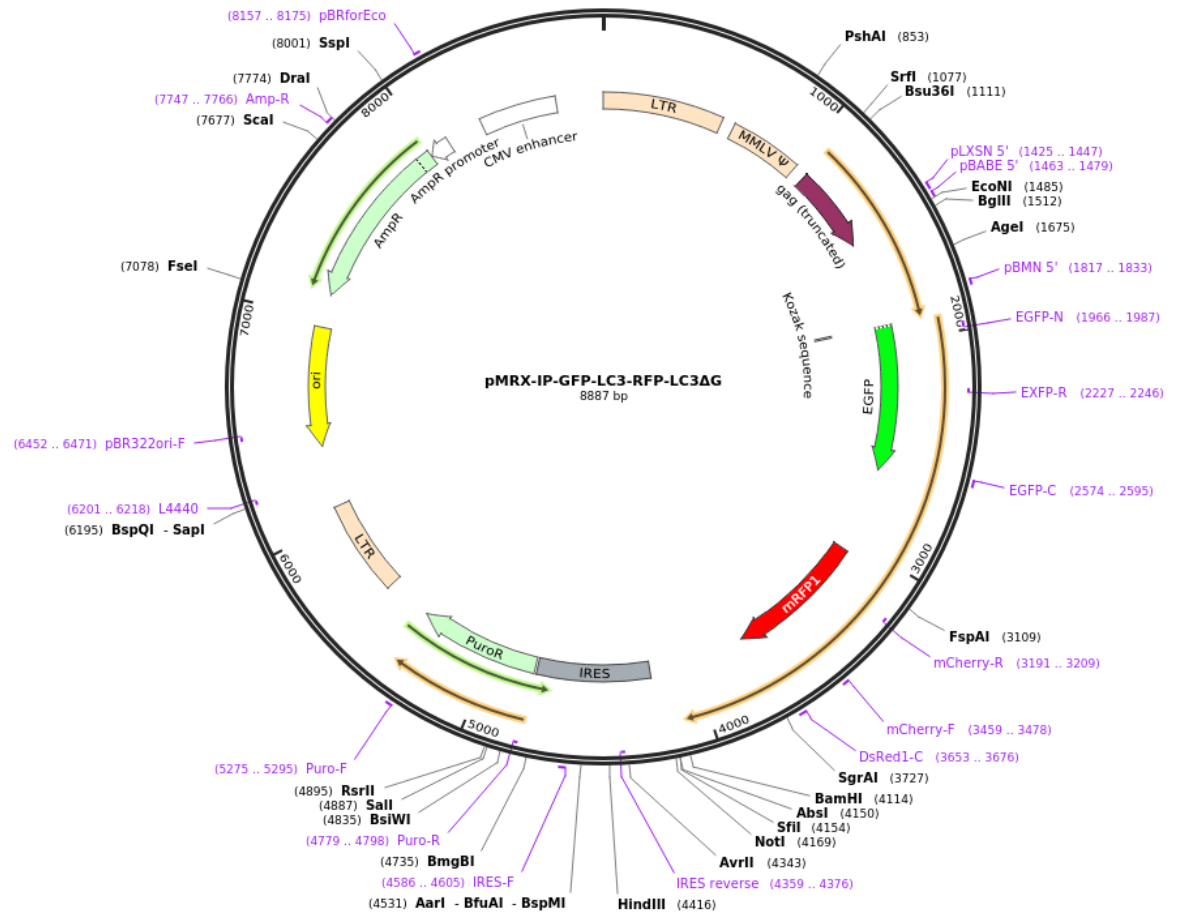
incubation with virus particles, media was re-freshened, and cells were left to recover for 48h. At Day 10 specific selection was started.

## 2.12 Plasmid vectors

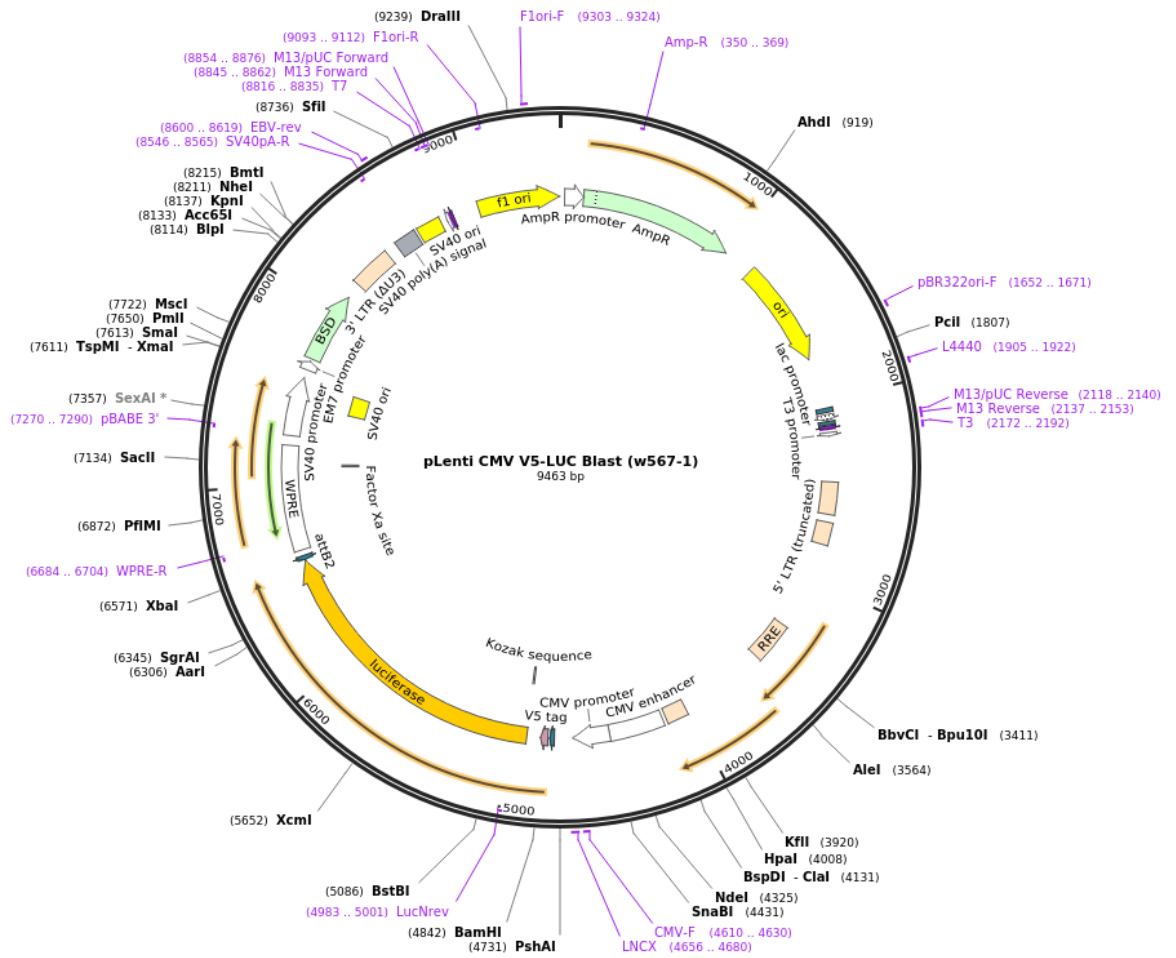
### 2.12.1 LentiCRISPR V2 vector Plasmid #52961 addgene



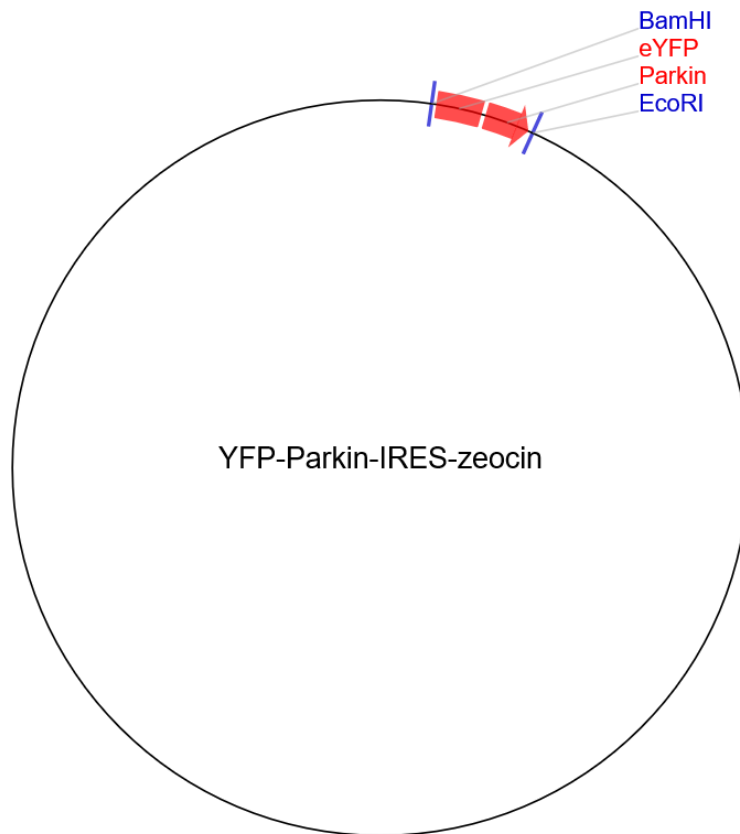
## 2.12.2 RFP-GFP LC3 puromycin vector Plasmid #84572 addgene



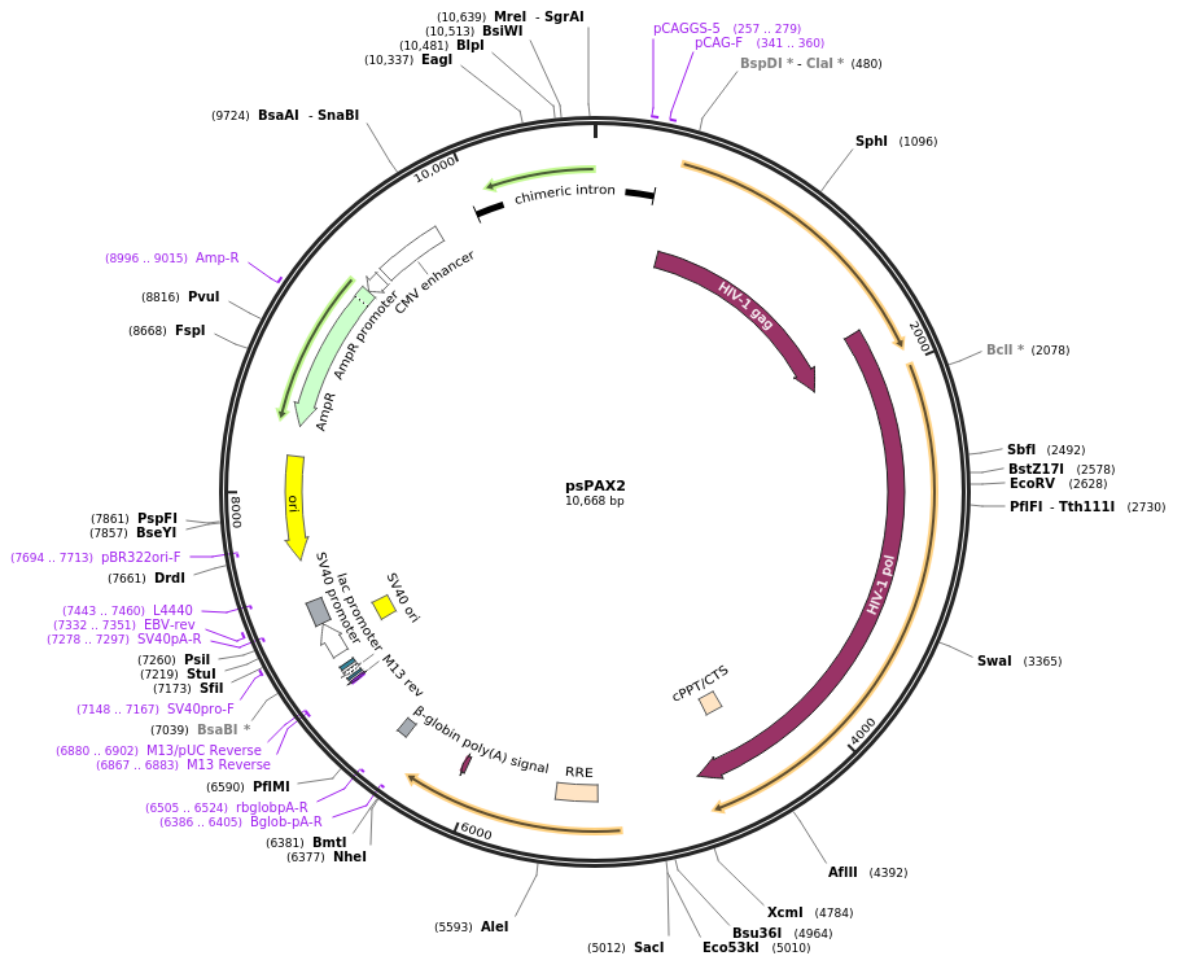
### 2.12.3 pLenti CMV V5-LUC blasticidin vector Plasmid #21474 addgene



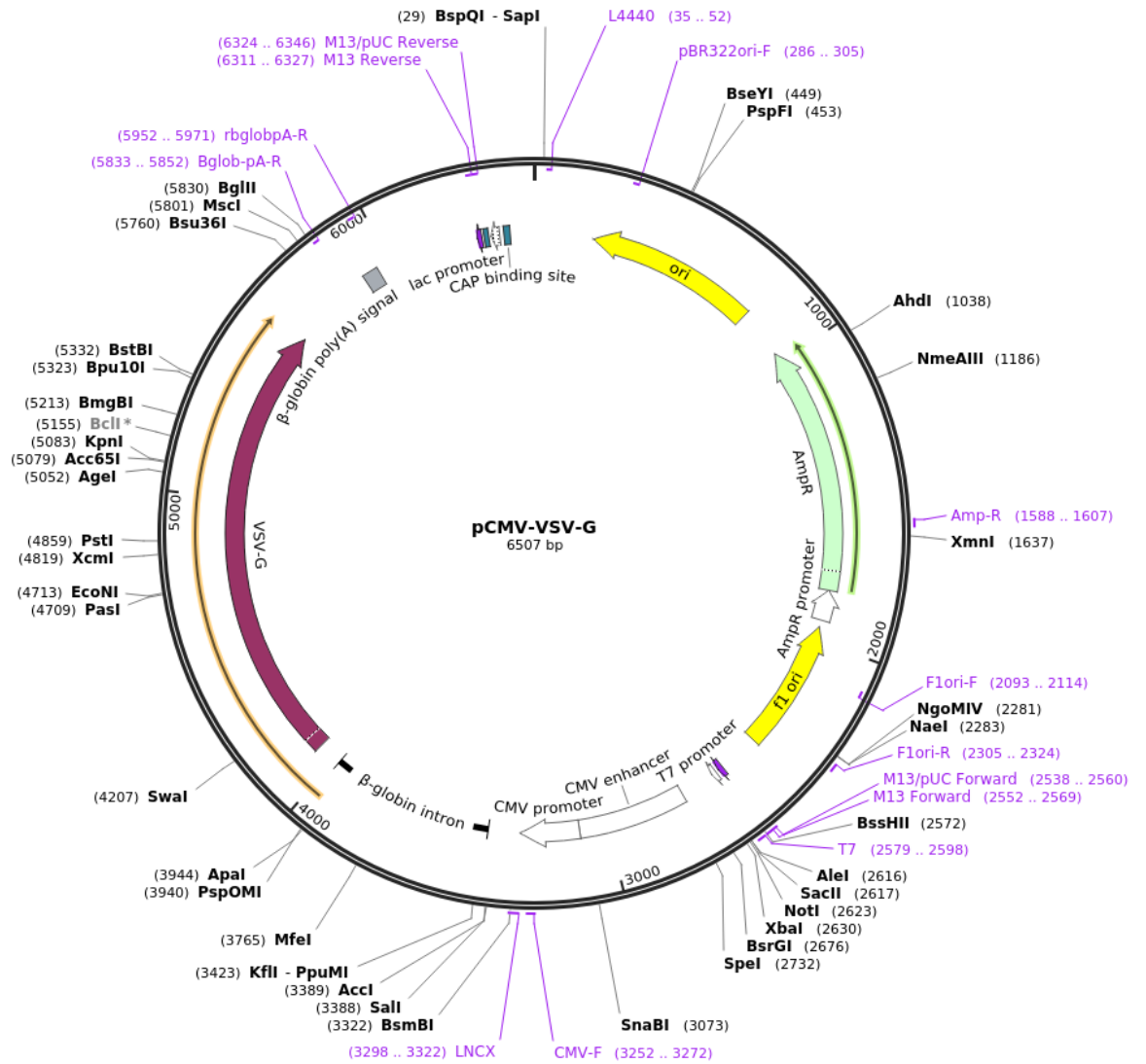
## 2.12.4 YFP-Parkin-IRES-zeocin Plasmid #61728 addgene



## 2.12.5 psPAX2 Plasmid #12260 addgene



## 2.12.6 pCMV-VSV-G Plasmid #8454 addgene



## 2.13 CRISPR cas9-mediated knock-out

### 2.13.1 Background

In 2012 Professor Emmanuelle Charpentier and Dr. Jennifer Doudna translated the molecular mechanism of the bacterial Class 2 Clustered Regularly Interspaced Short Palindromic Repeat (CRISPR)-cas9 immune system into a tool for genome editing. Microbes use the nuclease CRISPR to defend themselves from phages and plasmids raids. CRISPR loci also contains a CRISPR associated (cas) genes and non-coding RNA fragments which specify the cleavage of the CRISPR. Based on that principle, engineered CRISPR-cas9 systems, containing a CRISPR-cas9 and a guide RNA, can be used to specifically edit DNA and RNA (**Figure 2.3**).

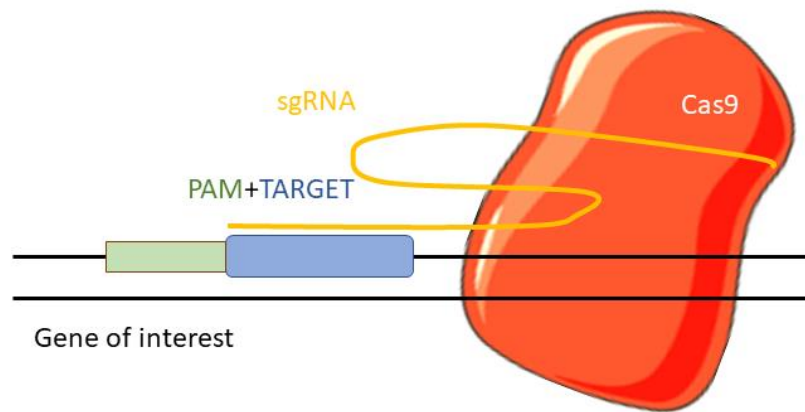


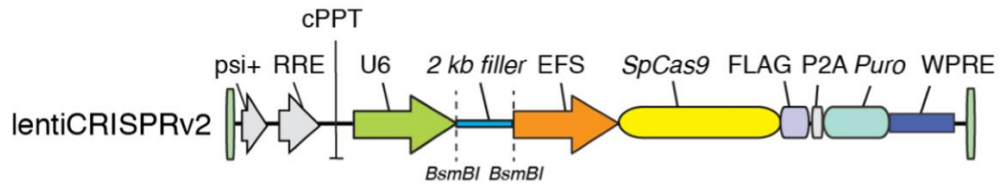
**Figure 2.3: Genome engineering using CRISPR cas9**

To generate CRISPR-cas9 mediated knock-out models, we used the one vector system using the plasmid lentiCRISPRv2.

### 2.13.2 How to design Target Guide Sequence to generate knock-out

LentiCRISPRv2 contains two expression cassettes, hSpCas9 and the chimeric guide RNA. This plasmid can be digested using BsmBI (**Figure 2.4**), and a pair of annealed oligos can be cloned into the single guide RNA scaffold.

## Chapter 2 Materials and methods



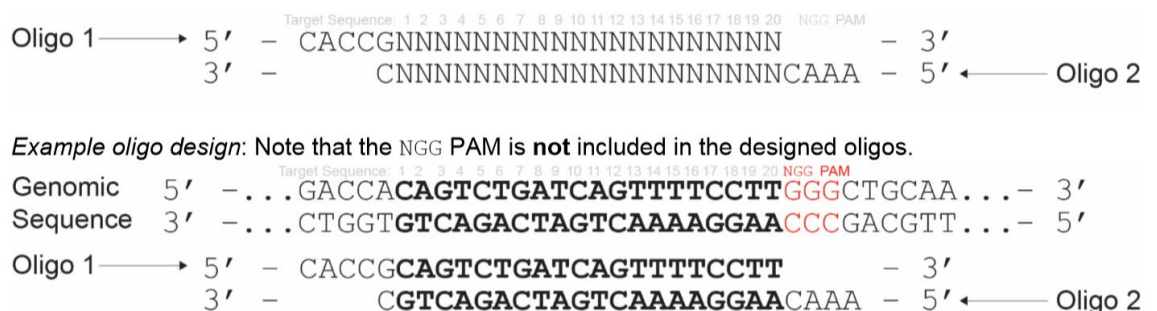
**Figure 2.4: BsmBI digestion restriction fragment on lentiCRISPRv2.**

Figure adapted from

[https://media.addgene.org/data/plasmids/52/52961/52961attachment\\_B3xTwa0bkYD.pdf](https://media.addgene.org/data/plasmids/52/52961/52961attachment_B3xTwa0bkYD.pdf)

To clone the target sequence into the lentiCRISPRv2 or backbone, a 20bp forward and reverse oligo were synthesized based on the sequence of firsts exons of gene of interest. Sequence were than scanned using (BLAST), <https://blast.ncbi.nlm.nih.gov/Blast.cgi>, to find regions of similarities between biological samples. The follow website was also used for oligos design, <https://www.genscript.com/gRNA-database.html>.

Following scheme shows how to design oligos (Figure 2.5).



**Figure 2.5: Example of oligos design.**

Figure adapted from

[https://media.addgene.org/data/plasmids/52/52961/52961attachment\\_B3xTwa0bkYD.pdf](https://media.addgene.org/data/plasmids/52/52961/52961attachment_B3xTwa0bkYD.pdf)

Name	Sequence	Exon	Quality score (%)
ULK1#1	CACCGCGAAGGCGCCGTGGCCGATC AAAC GATCGGCCACGGCGCCTTCGC	1	92
ULK1#2	CACCGGCAGCGTCTGAGACTTGGCG AAACCGCCAAGTCTCAGACGCTGCC	2	87
ULK1#3	CACCGAGCAGATCGCGGGCGCCATG AAACCATGGCGCCCGGATCTGCTC	6	88
ATG7	CACCGAACTCCAATGTTAAGCGAGC AAACGCTCGCTTAACATTGGAGTTC	3	91

Table 2-11: ULK1 and ATG7 oligo sequences

### 2.13.3 Lentiviral vector digestion, oligo annealing and cloning

LentiCRISPR-cas9 was digested ON using BsmBI at 37°C, as indicated below.

5 µg lentiCRISPRv2  
 3 µL FastDigest BsmBI (Fermentas)  
 3 µL FastAP (Fermentas)  
 6 µL FastDigest buffer (Fermentas)  
 0.6 µL 100 mM (freshly prepared)  
 X µL of deionized water to reach 60 µL total volume

Digested plasmid was isolated using 2% Agarose gel plus 10 µL DNA syber-safe.

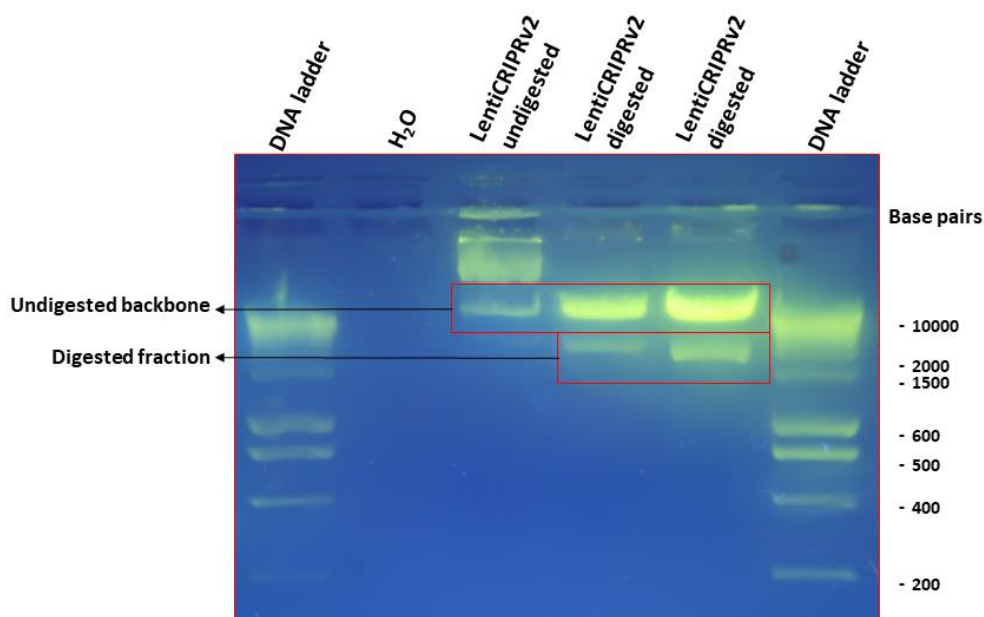


Figure 2.6: lentiCRISPRv2 following BsmBI digestion

Digested fractions were cut from gel and gel purified using QIAquick Gel Extraction Kit and elute in EB buffer (**Figure 2.6**).

Each pair of oligos designed were phosphorylated and annealed as indicated below.

1  $\mu$ L Oligo1 (forward)  
1  $\mu$ L Oligo2 (reverse)  
1  $\mu$ L 10X T4 Ligation Buffer (NEB)  
6.5  $\mu$ L deionized H<sub>2</sub>O  
0.5  $\mu$ L T4 PNK (*NEB#M0201S*)

#### **Annealing reaction**

37°C 30 min  
95°C 5min  
Ramp down to 25°C at 5°C/min

Annealed oligos were diluted in deionized water at 1:200.

Digested lentiCRISPRv2 was then ligated with annealed oligos at room temperature for 10min as indicated below.

50 ng BsmBI digested lentiCRISPRv2 Oligo1  
1  $\mu$ L diluted duplex oligos  
5  $\mu$ L 2X Quick Ligase Buffer (NEB)  
X  $\mu$ L deionized H<sub>2</sub>O to reach 10  $\mu$ L total volume  
1  $\mu$ L Quick Ligase (*NEB#M2200S*)

A negative control ligation (vector-only with water in place of oligos) and transformation was performed.

#### **2.13.4 Transformation into Stbl3 bacteria**

Ligated product was transformed into Stbl3 bacteria (*Invitrogen C7373-03*). Stbl3 were thaw on ice and 5  $\mu$ L of the DNA was added into the vial containing the Stbl3 and gently mixed. 1  $\mu$ L of pUC19 and 5  $\mu$ L of digested and not ligated lentiCRISPRv2

were used respectively as positive and negative control. Vials were incubated on ice for 30 minutes. Bacteria were then heat-shocked for 45 sec at 42 °C followed by 2 minutes on ice. 250 µL of pre-warmed S.O.C. medium (*Sigma#S1797*) was added to each vial. Vials were then shaken at 37 °C for 1 h at 225 rpm in a shaking incubator. 100 µL of each vial were then spread in pre-warmed ampicillin selective plates and incubated ON at 37 °C. Following day 3 colonies each plate was collected and a pre-inoculum was performed using 5 mL LB medium plus ampicillin. Pre-inoculum was incubated at 37 °C for 8 h at 225 rpm in a shaking incubator. Pre-inoculum was then added to 200 mL of LB medium supplemented with ampicillin and incubated ON at 37 °C ON at 225 rpm in a shaking incubator. Next day cells were collected and centrifuged at 12000 g x 30 min. Supernatant was then discarded and pellet was maxi-prepared for DNA extraction.

### **2.14 Parkin-enhanced mitophagy assay**

YFP-Parkin was established in K562 cells following retroviral transfection of YFP-Parkin-IRES-zeocin Plasmid. Cells were selected using 150µg/mL of zeocin (*Invivogen# ant-zn-1*). Following selection cells were treated using 1nM of oligomycin and 1nM of antimycinA for 24 h. Oligomycin and antimycinA were refreshed every 12 h. Cells were then lysed and mitophagy was assessed by western blot.

### **2.15 Single cell cloning**

Cells were harvested and adequately diluted to ensure accurate cell count.  $1.6 \times 10^5$  cells were collected in a 1.5 mL tube and 1:5 serial dilutions were performed to reach 50 cells in the final dilution (**Figure 2.7**). 50 cells were resuspended in a final volume of 12 mL of media and 200 µL/well were distributed in a 96 well plate. Cells were incubated at 37 °C till confluency was reached. Cells were then collected from each well and plated in 24 well plate using media enriched with specific resistant selection. Following growth in specific selection, cells were harvested and lysed, and KO was ensured by *western blot* analysis.

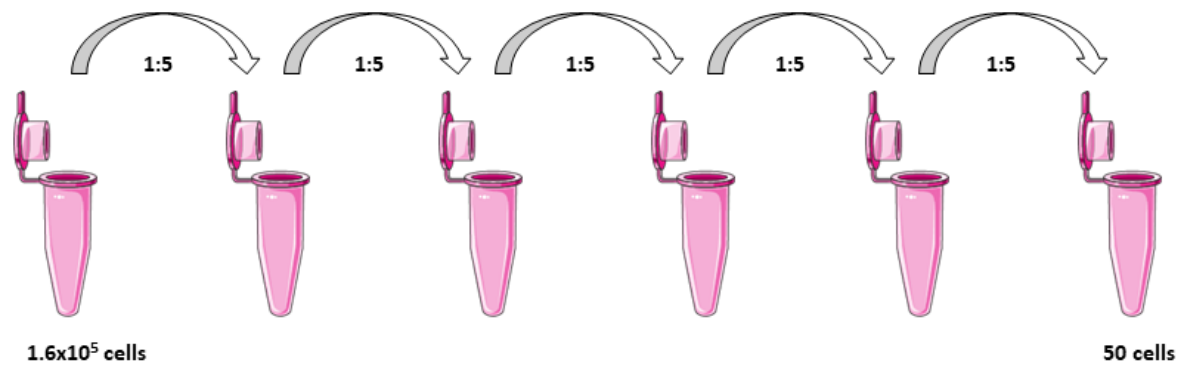


Figure 2.7: Serial dilution scheme for single cell cloning

## 2.16 Animal work

### 2.16.1 Ethical approval

All animal studies were conducted in accordance with the Animals Scientific Procedures Act 1986 and UK Home Office regulations. Animals were housed at the Beatson Institute for Cancer Research. All studies were carried out under Dr. Alison Michie's project licence (PD6C67A47) and my personal licence (IA68AFD03) and Statistical power analysis was conducted to evaluate number of animals used. Number and gender for each experiment is provided in each figure legend.

### 2.16.2 Mouse models and in vivo studies

#### 2.16.2.1 NSG mice background

*NOD.Cg-Prkdc<sup>scid</sup>Il2rg<sup>tm1Wjl</sup>/SzJ* is an immunocompromised mouse model and the most widely used for PDX studies. NSG mice have defects in multiple cytokines, as IL2 receptor gamma chain, disabling signalling pathways. They also deficient in innate immunity lacking mature T cells, B cells and functional NK cells.

#### 2.16.2.2 NRGW<sup>41</sup> mice background

*NOD.Cg-Rag1<sup>tm1Mom</sup> Kit<sup>W-41J</sup> Il2rg<sup>tm1Wjl</sup>/EavJ*<sup>214</sup> is an immunocompromised mouse model lately established in Dr. Connie Eaves lab. These mice don't carry the *Prkdc<sup>scid</sup>* allele which increases sensitivity to ionizing radiation, supporting engraftment of human cells for PDX studies with or without sub-lethal irradiation. This model, in addition to the IL2 receptor gamma chain lack, are also defective

## Chapter 2 Materials and methods

of Rag1, a protein involved in activation of immunoglobulin, impairing T and B cells maturation. They also lack the stem cell growth factor receptor KIT, resulting in higher levels of human chimerism to be obtained by impairing the competitiveness of the primitive hematopoietic cells of the recipient. This latter genetic alteration also enhances the output of human erythroid precursors selectively due to the important role of KIT in sustaining erythropoiesis in both mice and humans<sup>215,216</sup>.

### **2.16.2.3 Layout of *in vivo* PDX experiment using NSG or NRGW<sup>41</sup> mice**

8 weeks old NSG or NRGW<sup>41</sup> females and males' mice were irradiated (2.5 Gy for NSG and 2 x 100 cGy for NRGW<sup>41</sup>). Following 24 h mice were transplanted with 200  $\mu$ L of PBs 2% BSA containing  $1 \times 10^6$  human CD34<sup>+</sup> CML cells via tail vein. 4 weeks post-transplant, 20  $\mu$ L of tail vein blood was collected from each mouse and red cells were lysed to allow measurement of human cells engraftment. Between week 8 and 12, mice were divided into 4 arms (vehicle, Imatinib, MRT403 and combination of MRT403 plus Imatinib) and mice were treated for 4 weeks using a concentration of 40mg/Kg of MRT403 daily and 50mg/Kg twice per day for Imatinib. At the end of the treatment mice were sacrificed and spleen, blood, tibia, femurs and hips were harvested to allow analysis in the human compartment.

### **2.16.2.4 Double transgenic (DTG) mice**

CD45.2 SCLtTA/BCR-ABL (DTG) mice were generated crossing male SCLtTA Tet-O-cre trans-responder mice female TRE-BCR-ABL mice. BCR-ABL transcription in TRE-BCR-ABL mice is controlled by a tetracycline-responsive element (TRE; Tet-O) fused to a minimal cytomegalovirus (hCMV) promoter<sup>104</sup>. Removing tetracycline from the drinking water of the mice, the tetracycline transactivator protein (tTa) binds TRE, inducing expression of BCR-ABL. Moreover, due a 3' region of the SCL gene the tTa expression is restricted to HSPCs and megakaryocytes.

### **2.16.2.5 Layout of *in vivo* experiment using CD45.2 SCLtTA/BCR-ABL (DTG) mice**

At day0 Frozen CD45.2 SCLtTA/BCR-ABL BM cells were defrosted and left recover ON in DMEM 20% FBS, 1% P/S, 1% Glut. Same day, CD45.1 wild type (WT) C57BL/6

## Chapter 2 Materials and methods

mice sub-lethally irradiated. Following day, 200  $\mu$ L of PBS 2% BSA containing  $1 \times 10^6$  murine BM cells were injected via tail vein. 2 weeks recovery from irradiation were allowed prior of induction of the disease at the end of what engraftment was measured in the blood. Following recovery, tetracycline was removed from the drinking water inducing BCR-ABL expression. 1-week post BCR-ABL induction, mice were divided into 4 arms (vehicle, Imatinib, MRT403 and combination of MRT403 plus Imatinib) and mice were treated for 4 weeks using a concentration of 40mg/Kg of MRT403 daily and 50mg/Kg twice per day for Imatinib. At the end of the treatment mice were sacrificed and spleen, blood, tibia, femurs and hips were harvested to allow analysis.

### **2.16.3 Plasma extraction from fresh blood**

Blood was harvested from each mouse performing cardiac puncture and was immediately poured in appropriate tubes containing EDTA. Tubes was inverted 3 times to avoid blood cloth. Samples were centrifuged at 2000 g/20 min at RT to separate plasma from each sample. Plasma was then collected into a fresh tube and stored at  $-80^{\circ}\text{C}$ .

### **2.16.4 *In vivo* imaging of tumour-initiating CML cells**

KCL22 control and ULK1 deficient cells were labelled with lentiviral firefly luciferase using retroviral transfection and selected based on antibiotic resistance, blasticidine. Luciferase activity was measured in vitro using luminescent plate reader.  $4 \times 10^6$  cells were resuspended in 200  $\mu$ L of PBS/0.5% FBS and transplanted via tail vein into an 8-12-week-old male NRGW<sup>41</sup> mice. 30 minutes after the transplantation of the cells the mice were injected subcutaneously with D-luciferin and analysed by luciferase bioimaging via an IVIS Spectrum *In Vivo* Imaging System to measure the efficiency of transplantation. A dose of 3mg (200  $\mu$ L) of the substrate D-Luciferin (*Perkin Elmer*#122799) was subcutaneously injected in the mice. The luciferin oxidises under catalytic effects of the firefly luciferase and ATP and emits light, which is captured by the IVIS spectral range between 550 nm and 620 nm. Tumour growth was weekly monitored using the *in vivo* imaging until tumour burden reached the threshold and the animals were sacrificed using appropriate schedule 1 methods.

## 2.17 Live-cell Metabolic Assay using Seahorse Analyser

Seahorse XF Analyzer is an instrument developed from Agilent able to estimate repeated measurements of oxygen consumption rate (OCR) and extracellular acidification rate (ECAR), examining key cellular metabolic processes such as mitochondrial respiration and glycolysis in real time.

Prior to assay following reagents were prepared.

### Cell Tak mix

38  $\mu$ L of Corning cell Tak (*Sigma#354240*)

2.5 mL Sodium bicarbonate 0.1 M pH8

### Myto-stress XF Assay Media<sup>+</sup> for primary cells

For 50 mL:

200  $\mu$ L low density lipo-protein (10mg/mL) (*Sigma#L4646*)

2 Mercapto-ethanol (50nM) (*Invitrogen 31350-010*)

25  $\mu$ L LIF (0.05ng/mL) (*PeptoTech#300-05*)

34  $\mu$ L PGF cocktail\*

377  $\mu$ L Glucose (1.66 M)

49 mL XF Base Media

Drug	Activity	Stock conc. $\mu$ M	Required conc. $\mu$ M	Volume x 4 mL XF media ( $\mu$ L)	Chamber in the XF96 Sensor cartridges to load	Volumeto load in each well of in the XF96 Sensor cartridges ( $\mu$ L)
FCCP	ATP synthase inhibitor	10	1.6	6	A	25
Oligomycin	Mitochondrial uncloper	5	0.7	6.4	B	25
Antimycin	Inhibitor of complex I	10	1	4	C	25
Rotenone	Inhibitor of complex III	10	1	4	C	25

### Myto-stress XF Assay Media<sup>+</sup> for cell lines

For 25 mL:

167  $\mu$ L Glucose (1.66 M)

250  $\mu$ L Glutamine (200 mM)

24.3 mL XF Base Media

## Chapter 2 Materials and methods

Drug	Activity	Stock conc. $\mu\text{M}$	Required conc. $\mu\text{M}$	Volume x 4 mL XF media ( $\mu\text{L}$ )	Chamber in the XF96 Sensor cartridge	Volume to load in the XF96 Sensor cartridges ( $\mu\text{L}$ )
FCCP	ATP synthase inhibitor	10	1.6	4	A	25
Oligomycin	Mitochondrial uncloper	5	0.7	6.4	B	25
Antimycin	Inhibitor of complex I	10	1	4	C	25
Rotenone	Inhibitor of complex III	10	1	4	C	25

### Glycolytic-stress XF Assay Media<sup>+</sup> for primary cells

For 50 mL:

200  $\mu\text{L}$  low density lipo-protein (10mg/mL) (*Sigma#L4646*)

2 Mercapto-ethanol (50nM) (*Invitrogen 31350-010*)

25  $\mu\text{L}$  LIF (0.05ng/mL) (*PeptoTech#300-05*)

34  $\mu\text{L}$  PGF cocktail\*

49 mL XF Base Media

### Glycolytic-stress XF Assay Media<sup>+</sup> for cell lines

For 25 mL:

Drug	Stock conc. mM	Required conc. $\mu\text{M}$	Volume x 4 mL XF media	Chamber in the XF96 Sensor cartridges	Volume to load in each well of in the XF96 Sensor cartridges ( $\mu\text{L}$ )
Glucose	1.66	$1 \times 10^6$	221	A	25
Oligomycin	5	0.7	6.4	B	25
2-Deoxy-glucose	-	$1 \times 10^6$	-	C	25

250  $\mu\text{L}$  Glutamine (200 mM)

24.3 mL XF Base Media

Drug	Stock conc. mM	Required conc. $\mu\text{M}$	Volume x 4 mL XF media	Chamber in the XF96 Sensor cartridges	Volume to load in each well of in the XF96 Sensor cartridges ( $\mu\text{L}$ )
Glucose	1.66	$1 \times 10^6$	221	A	25
Oligomycin	5	0.7	6.4	B	25
2-Deoxy-glucose	-	$5 \times 10^5$	-	C	25

## Chapter 2 Materials and methods

Procedure: At *Day 0* Seahorse XF96 Cell Culture Microplate was coated with 25  $\mu$ l of Cell-Tak mix/well and incubated at RT for 30 min. following what microplate was washed using deionized H<sub>2</sub>O. The XF96 Sensor cartridges was hydrated using 200  $\mu$ L/well of Seahorse Bioscience XF96 Calibrant solution pH 7.6 and placed at ON at 37 °C and 0% CO<sub>2</sub>.

The XF96 Sensor cartridges were hydrated overnight by adding 200  $\mu$ l Seahorse Bioscience XF96 Calibrant solution pH 7.6 to each well of a Seahorse-96 utility plate. The sensor cartridge was then placed on the top of the utility plate, sealed with paraffin film to prevent evaporation overnight, and stored in a CO<sub>2</sub>-free incubator overnight at 37 °C. At *Day 1* prepare as indicated above XF Assay Media and place them at 37 °C. Cells were counted and resuspended in warm XF Assay Media at a concentration of  $2.9 \times 10^6$  for primary CML cells and  $1.7 \times 10^6$  for CML cell lines and 175  $\mu$ L of which were distributed to each well of the Seahorse XF96 Cell Culture Microplate. Microplate was centrifuged at 60 x g for 10 sec with no break following what microplate was placed at 37 °C and 0% CO<sub>2</sub>. To measure Myto-stress and Glycolytic-stress specific drugs were prepared and loaded in the XF96 Sensor cartridge. XF96 Sensor cartridges were placed for 10 minutes at 37 °C and 0% CO<sub>2</sub> for 10 min. following what was loaded in the Seahorse Analyser for calibration. Following XF96 Sensor cartridges calibration, microplate containing cells was loaded in the Seahorse Analyser and proceeded with measurements.

### **2.17.1 Basal respiration, maximal respiration and ATP linked analysis**

Basal respiration relative to UT was calculated as average of last rate measurements before oligomycin injection minus average of non-mitochondrial respiration rate. Maximal respiration relative to UT was calculated as average of maximum rate measurements after FCCP injection minus average of non-mitochondrial respiration. ATP linked relative to UT was calculated as average of maximum rate measurements before oligomycin injection minus average of minimum rate measurements after oligomycin injection (**Figure 2.8**).

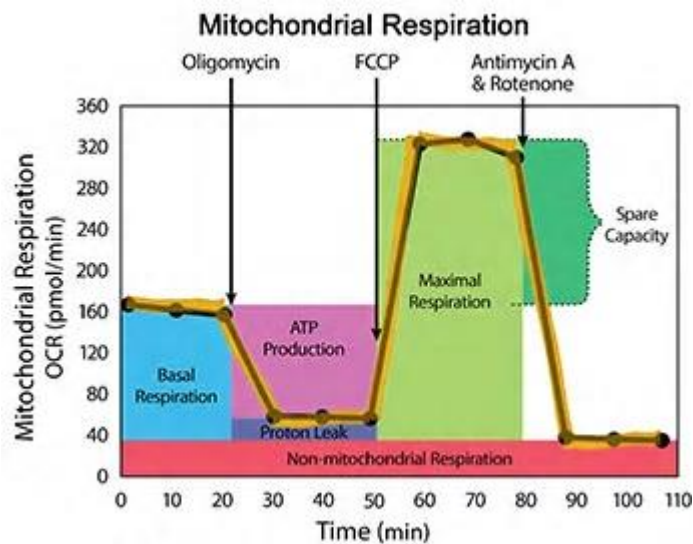


Figure 2.8: Mitochondrial respiration profile

### 2.17.2 Glycolytic function analysis

Glycolysis relative to UT calculated as average of maximum measurements before oligomycin injection minus average of last rate measurements before glucose injections. Glycolytic capacity relative to UT calculated as average of maximum measurements after oligomycin injection minus average of last rate measurements before glucose injections (Figure 2.9).

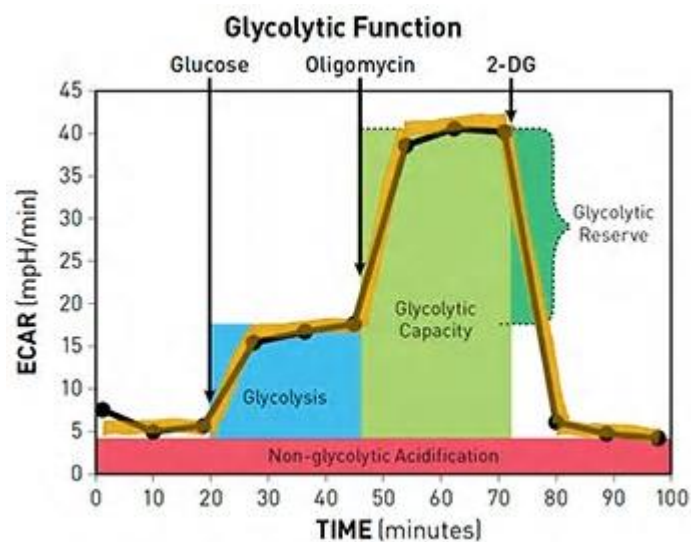


Figure 2.9: Glycolytic function profile

## 2.18 Cell viability assays

### 2.18.1 XTT assay

#### 2.18.1.1 Background

XTT assay is a colorimetric assay that uses 2,3-bis-(2-methoxy-4-nitro-5-sulphenyl)-(2H)-tetrazolium-5-carboxanilide (XTT) dye first described in 1988 by *Scudiero et al.*<sup>217</sup> and it's used as a technique to measure cell growth and drug sensitivity in tumour cells. Oxidoreductase enzymes reduce XTT into the coloured derivative formazan that absorbs between 450-500 nm. The formazan product of XTT reduction is soluble and can be used in real-time assays. XTT is combined to an intermediate electron acceptor, such as N-methyl dibenzo pyrazine methyl sulphate (PMS). PMS mediates XTT reduction by picking up electrons at the cell surface, or at a site in the plasma membrane that is readily accessible and forms a reactive intermediate that then reduces XTT to its highly pigmented formazan product.

#### 2.18.1.2 Method

At day0 2 x highest desired drug concentration was prepared in RPMI and 100  $\mu$ l were distributed in each well 12 (to have 8 replicates of each drug concentration) of a 96 well plate (**Figure 2.10**). 50  $\mu$ l of media was distributed in the remaining wells. Using a multichannel pipette, 50  $\mu$ l were aspirated from each well 12 and resuspended in well 11 assessing a 1:2 dilution. Same was performed till well 3 (**Figure 2.10**). Cells were accurately counted and  $1 \times 10^6$  cells/well were resuspend in 50  $\mu$ l of RPMI/well (concentration of  $2 \times 10^5$  cells/mL) and 50  $\mu$ l were distributed in the 96 well plate previously prepared with appropriate drug from each well 12 till each well 2 (**Figure 2.10**). Each well 1 was topped with 50  $\mu$ l RPMI only. Plate was incubated for 72 h at 37°C. At day3, 3 mg of XTT salt was added in 3 mL of RPMI and placed at 37°C for 20 minutes. After dissolution of the salt, 15  $\mu$ L of PMS stock solution (7 mg of PMS in 5 mL of PBS; aliquots kept at 20°C in the dark) were added to the XTT solution. 25  $\mu$ L of the resulting solution was added to each well and plate was incubated at 37°C for 4 h. Absorbance was then read at 492 nm using Tecan plate reader (**Figure 2.10**).

## 2.18.2 Resazurin assay

### 2.18.2.1 Background

Similarly to XTT assay, resazurin is used to assess cell growth and drug sensitivity in tumour cells. It's a non-fluorescent dye that can be reduced to resorufin, pink and highly fluorescent, in live cells<sup>218</sup>. In presence of NADPH dehydrogenase or NADH dehydrogenase, NADPH or NADH is the reductant converts resazurin to resorufin.

### 2.18.2.2 Method

At day0 2 x highest desired drug concentration was prepared in RPMI and 100  $\mu$ l were distributed in each well 12 (to have 8 replicates of each drug concentration) of a 96 well plate (**Figure 2.10**). 50  $\mu$ l of media was distributed in the remaining wells. Using a multichannel pipette, 50  $\mu$ l were aspirated from each well12 and resuspended in well 11 assessing a 1:2 dilution. Same was performed till well 3 (**Figure 2.10**). Cells were accurately counted and  $1 \times 10^6$  cells/well were resuspend in 50  $\mu$ l of RPMI/well (concentration of  $2 \times 10^5$  cells/mL) and 50  $\mu$ l were distributed in the 96 well plate previously prepared with appropriate drug from each well 12 till each well 2 (**Figure 2.10**). Each well 1 was topped with 50  $\mu$ l RPMI only. Plate was incubated for 72 h at 37°C. At day3, resazurin stock solution (25 mM, 0.313g in 50 mL of distilled water) was dilute to 500  $\mu$ M in prewarmed serum free media (1:50 dilution) and 10  $\mu$ L were added to each well. and plate was incubated at 37°C for 4 h. Absorbance was then read at 590 nm using Tecan plate reader (**Figure 2.10**).

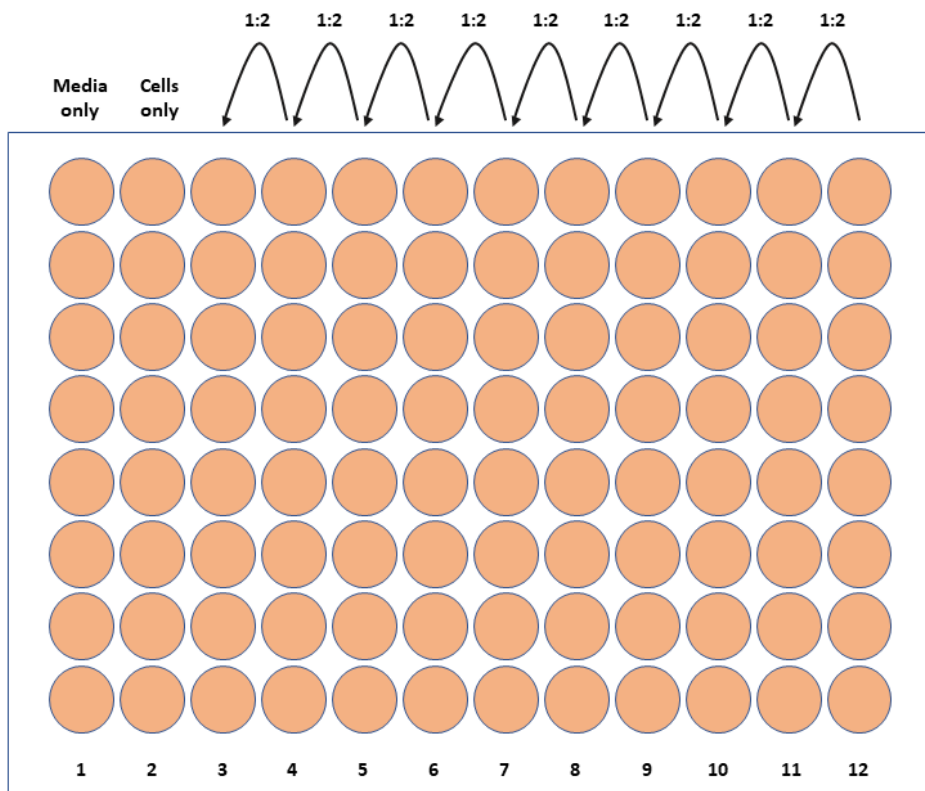


Figure 2.10: 1:2 serial dilution of compounds used for cell viability assay

## **Chapter 3    Autophagy as a survival mechanism sustain LSPCs persistence**

### 3.1 Introduction

Our first aim was to study the role of autophagy in primitive normal and CML cells. To assess levels of autophagy in cells enriched for HSPCs and LSPCs, we initially measured the basal level of autophagy in the CD34<sup>+</sup> compartment. One approach to this is to measure autophagy gene expression in normal and CD34<sup>+</sup> CML patient-derived cells. Since measuring autophagy flux is a direct measure of autophagic degradation activity, autophagy flux was also assessed in CD34<sup>+</sup> normal and CML cells. These data were consistent with previous published data indicating autophagy as a survival mechanism following TKIs treatment for CML patients<sup>112,198</sup>. Specifically, we aimed to investigate the mechanism and identify the key players of autophagy following TKIs treatment in CD34<sup>+</sup> CML cells, which indicated ULK1 as potential key player to target in CML. ULK1, in fact, not only represents one of the first step to activate autophagy, but is also one of the few autophagy proteins that has led companies in developing small molecules to specifically and pharmacologically target autophagy. In this context we aim to validate our preliminary data indicating ULK1 as a potential autophagy protein to target in CML.

To study the role of ULK1 in regulating autophagy in CML, we generated ULK1 deficient cell lines using the frontier genome engineering CRISPR-cas9 system established in 2012<sup>219,220</sup>. Using ULK1 deficient cells, we first aimed to investigate whether absence of ULK1 lead to a reduction of autophagy level in CML cells. We then studied if TKIs were able to induce autophagy in ULK1 deficient cells and whether ULK1 shortage would sensitise CML cells to TKIs treatment *in vitro* and *in vivo*.

## 3.2 Results

### 3.2.1 Second generation TKIs are not able to eradicate CML LSPCs

The introduction of TKIs in the late nineties as a front-line therapy for CML patients has revolutionised the history of cancer treatment. However, TKIs fail to eliminate LSPCs.

To determine the effect of nilotinib, a second generation TKIs, we optimised techniques to process leukapheresis product from patients diagnosed with CML from which primitive cells were enriched by positive selection of the surface marker CD34 (2.1.2). CML cells were cultured for 3 or 6 days with 2  $\mu$ M nilotinib. We established that 38% of the cells were positive for both CD34 and CD133 stem cell markers at day 0. While only 8% of the UT cells remained positive for both primitive markers following 3 days in culture, 17% of the cells were positive for CD34 and CD133 when treated with nilotinib (**Figure 3.1a**). Furthermore, following 3 days in culture, 42% of cells became CD34<sup>-</sup>, while only 12% of the cells lost CD34 marker when treated with nilotinib. Using a fluorescent dye, Cell Trace Violet, we also tracked cell division, showing that only a small fraction of the untreated cells remained un-divided with most of them being in division 2 and division 3 (**Figure 3.1b**). Instead, around 50% of nilotinib treated cells remained un-divided or in division 1 (**Figure 3.1b**). Measurements of apoptosis revealed that nilotinib targeted CML cells by increasing apoptosis to 40% at day 3 and 50% at day 6 of treatment (**Figure 3.1c, d**). More detailed analysis revealed that nilotinib-induced apoptosis was higher in the CD34<sup>-</sup> fraction, respectively 13% at day 3 and 17% at day 6, compared to apoptosis measured in the CD34<sup>+</sup> fraction (respectively 7% at day 3 and 5% at day 6 (**Figure 3.1e**)). Performing a CFC assay after 3 days treatment with nilotinib, we show that nilotinib targeted progenitor cells by reducing CFC by 40% (**Figure 3.1f**).

In line with previous published data, these results indicate that TKI treatment does not target LSPCs, while CD34<sup>-</sup> cells are more sensitive to TKI treatment.

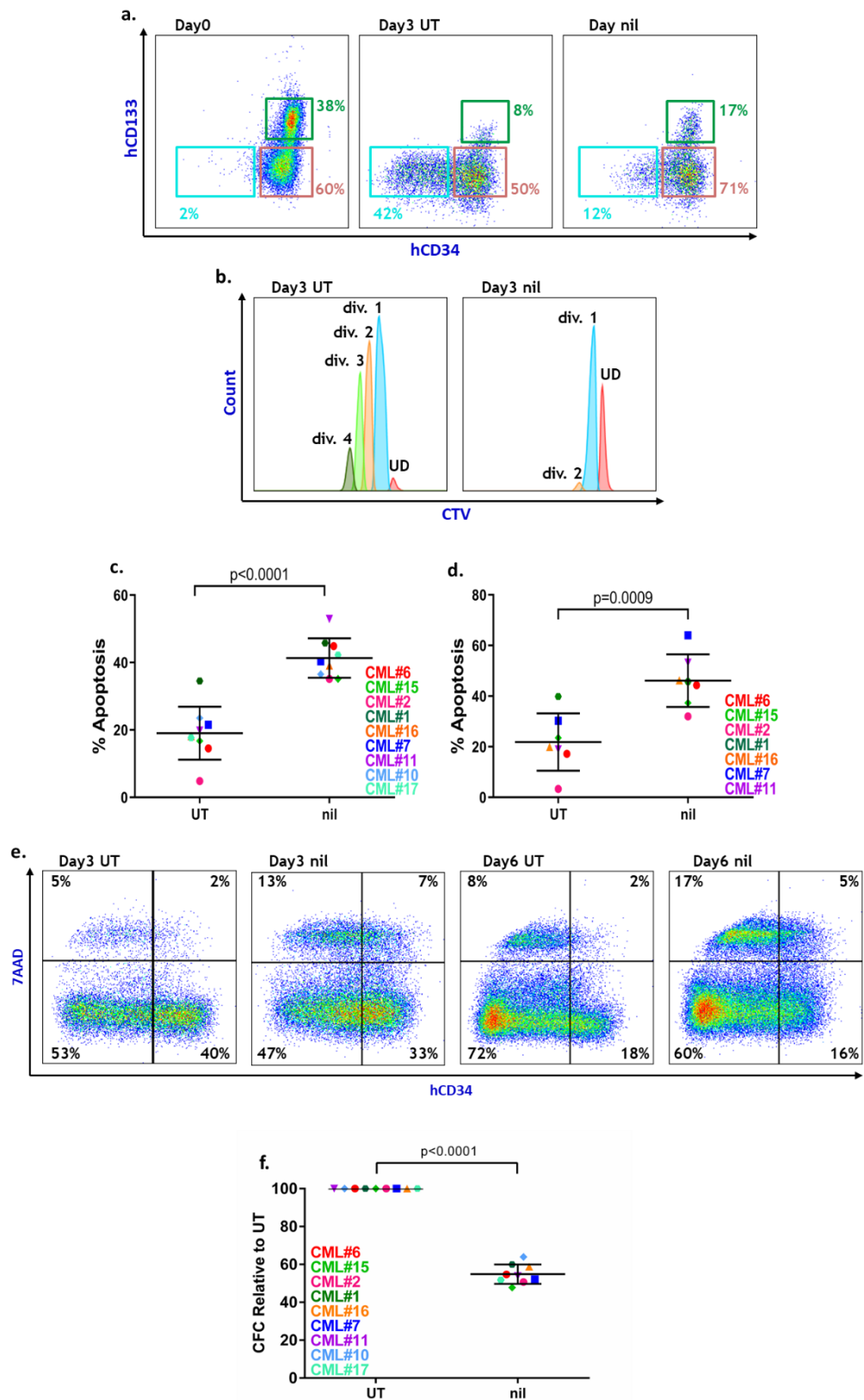


**Figure 3.1: Nilotinib only targets differentiate CML cells and enriches for CML LSPCs**

FACs plots showing expression levels of CD34/CD133 stem cell markers following 3 days treatment with nilotinib (a). FACs plots obtained from CD34<sup>+</sup> CML cells stained with Cell Trace Violet following 72 h treatment (b). Graphs showing % of apoptosis following 3-(c) or 6-days (d) treatment with nilotinib. Mean ± S.E.M. n=9 CML samples (c), n=7 CML samples (d). FACs plot showing positivity to late stage cell death marker, 7AAD, and CD34 following 3- or 6-day treatments (e). Relative number of colonies measured by CFC assay following 3 days treatment. Mean ± S.E.M. n=9 CML samples (f). p values were calculated using paired Student T test.

### 3.2.2 Autophagy level in normal and leukaemic stem cells

Several studies have identified autophagy with a protective role in HSPCs, sheltering them from metabolic stress and expansion stimuli in the BM<sup>16,19,163,164</sup>. In the case of CML, it is well established that BCR-ABL oncogene drives expansion and accumulation in the blood of the myeloid compartment. It has recently been shown that primitive CML cells have higher oxidative metabolism compared to normal cells<sup>114</sup>. Furthermore, among the multiple pathways regulated by BCR-ABL onco-protein, it is indicated that the mTOR signalling pathway is activated by BCR-ABL<sup>221-223</sup>. mTOR is a negative regulator of autophagy, whose inhibitory phosphorylation of ULK1 decreased autophagy<sup>126</sup> (**Figure 3.2**). Based on that, we hypothesised that BCR-ABL, through its activity on mTOR, controls and regulates autophagy.

To measure autophagy levels in primitive normal cells, we optimised a technique to isolate viable cells from BM of individuals undergoing hip replacement and to process leukapheresis products from patients diagnosed with CML. In both cases, primitive cells were enriched by positive selection of the surface marker CD34 (2.1.3) (**Figure 3.3a**). Following 24 h culture with PGF, RNA was extracted from normal and CD34<sup>+</sup> CML cells and autophagy gene expression was evaluated in both populations. Gene expression analysis revealed that CD34<sup>+</sup> CML cells have lower expression of autophagy genes compared to normal CD34<sup>+</sup> cells (**Figure 3.3b**), (Table 3-1). Specifically, results comparing  $\Delta\Delta\text{CT}$  values versus the average of the normal indicate that genes such as ULK1, a component of the autophagy initiation machinery<sup>123</sup>, UVRAG, which interacts with Beclin1 promoting autophagosomal maturation<sup>224</sup>, ATG4 which is involved in the ATG8 conjugation system important in the autophagosome formation<sup>225,226</sup>, and ATG7 and ATG5, involved in the ATG12 conjugation system important for ensuring LC3 lipidation<sup>227,228</sup>, are significantly upregulated in normal CD34<sup>+</sup> cells.

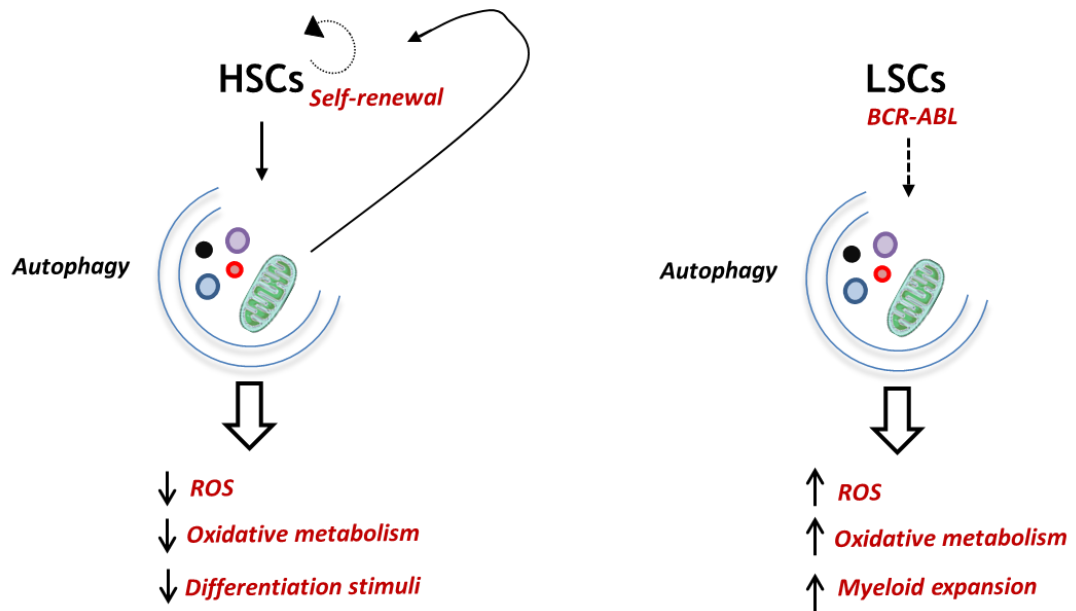


**Figure 3.2: Autophagic function in HSCs and LSCs**

Schematic diagram indicating that HSCs maintain high levels of autophagy to reduce loss of quiescent cells and reducing oxidative stress which can drive differentiation of primitive HSCs. On the other hand, BCR-ABL has a negative effect on autophagy in LSCs, showing elevated mitochondrial metabolism. One of the main characteristics of LSCs is the myeloid expansion.

we have decided that there is no accurate statistical test to compare expression of a single gene between normal and CML cells. In this regard, lab bio-informatician (Dr Brabcova) recommended to use Unpaired Student's T test which is still the most appropriate for this type of analysis. To validate the data and further test my hypothesis that BCR-ABL oncogene negatively regulates autophagy, we performed autophagic flux measurement in both normal and CML CD34<sup>+</sup> cells. LC3B-II and p62 represent the most widely used markers to monitor autophagic activity. LC3B-I is the cytoplasmic form or LC3; lipidation of LC3B-I with a PE generates LC3B-II, which is recruited to the autophagosomal membrane upon autophagic activation<sup>155,229,230</sup>. To measure autophagy flux, it is necessary to determine the amount of LC3B-II or p62 turnover in a lysosomal dependent manner. To achieve autophagic flux measurement, it is necessary to inhibit the latest stages of autophagy, suppressing maturation of autophagic vesicles, to prevent degradation of the autophagosomal content. Treatment with HCQ, a lysosomotropic agent that increases lysosomal pH, inhibiting enzyme activity, or Bafilomycin A1, an inhibitor of H<sup>+</sup> ATPase activity and an inhibitor of the fusion between autophagosomes and lysosomes, are generally used to ensure accumulation of the autophagosomal content. CD34<sup>+</sup> normal and CML cells were lysed following 12 h treatment with 10 μM HCQ or 100 nM Bafilomycin. Western blot analysis was performed indicating that while in normal CD34<sup>+</sup> cells Bafilomycin and HCQ induce LC3B-II levels, in the leukaemic counterpart, levels of LC3B-II following treatment were similar to UT cells (**Figure 3.4a, b, c**).

The increase in LC3B-II following treatment with HCQ or Bafilomycin in CD34<sup>+</sup> normal cells, indicates that primitive normal cells have a greater turnover of macromolecules via autophagy. However, even though protein content had been quantified to load same amount of proteins in each condition, the loading control GAPDH and beta-tubulin showed lower levels and, in many cases, undetectable in normal cells. This might be due to the fact that normal cells are generally smaller than LSPCs and might have a lower content in β-tubulin, which is usually considered as a loading control for western blotting analysis (**Figure 3.4b, c**).

### Chapter 3 Autophagy as a survival mechanism sustain LSPCs persistence

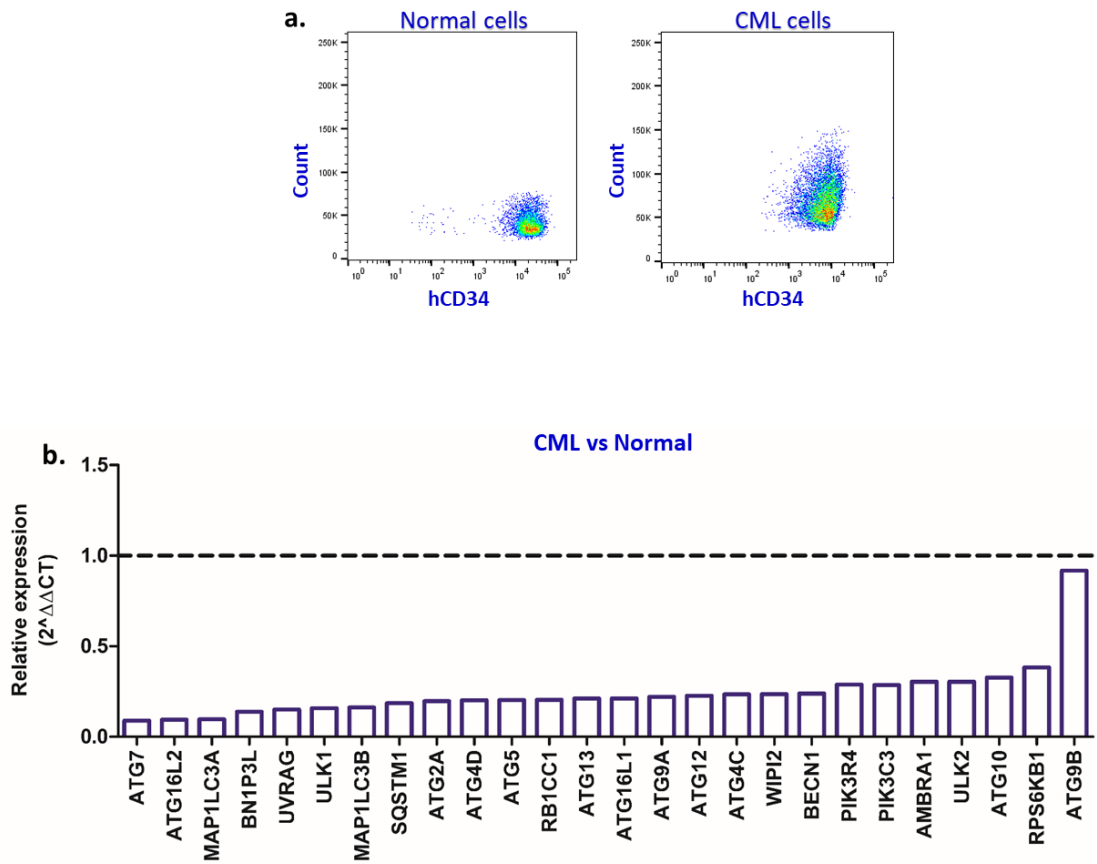


**Figure 3.3: Primitive CML cells show a decrease in autophagy genes expression compared to normal cells.**

Representative FACS plot showing normal and CML patient-derived cells positivity for the primitive marker CD34 (a). Comparative gene-expression analysis of CD34<sup>+</sup> CML and normal cells. Mean n=3 normal patient samples and n=3 CML samples (b).

### Chapter 3 Autophagy as a survival mechanism sustain LSPCs persistence

Gene	CD34 <sup>+</sup> CML1 RELATIVE TO CD34 <sup>+</sup> NORMAL	CD34 <sup>+</sup> CML2 RELATIVE TO CD34 <sup>+</sup> NORMAL	CD34 <sup>+</sup> CML3 RELATIVE TO CD34 <sup>+</sup> NORMAL	AVERAGE	Unpaired t Test	Adjusted p value
ATG7	0.05769292	0.04277324	0.16833348	0.08959988	<0.0001	<0.0004
ATG16L2	0.1177844	0.04344115	0.121421751	0.094215767	<0.0001	<0.0004
MAP1LC3A	0.1195116	0.02301983	0.148391567	0.096974332	<0.0001	<0.0004
BN1P3L	0.1394924	0.09546337	0.177931167	0.137628979	<0.0001	<0.0004
UVRAG	0.1226149	0.07182296	0.257207885	0.150548582	0.0001	0.0004
ULK1	0.10914	0.08296555	0.282861993	0.158322514	0.0002	0.0005
MAP1LC3B	0.1193209	0.09361995	0.273246684	0.162062511	0.0001	0.0004
SQSTM1	0.2115194	0.08081058	0.26583193	0.18605397	0.0001	0.0004
ATG2A	0.1288713	0.07443234	0.388736801	0.197346814	0.0012	0.0018
ATG4D	0.2026356	0.09447014	0.3084018	0.201835847	0.0002	0.0005
ATG5	0.1889133	0.09093208	0.328024222	0.202623201	0.0003	0.0007
RB1CC1	0.1746489	0.120702	0.318632839	0.204661246	0.0002	0.0005
ATG13	0.1030126	0.07174455	0.45901673	0.21125796	0.0032	0.0040
ATG16L1	0.1635243	0.1167967	0.354232607	0.211517869	0.0004	0.0008
ATG9A	0.1518258	0.1058021	0.404000768	0.220542889	0.0011	0.0018
ATG12	0.1993152	0.1302523	0.35280453	0.227457343	0.0003	0.0007
ATG4C	0.165717	0.1084674	0.430206706	0.234797035	0.0015	0.0022
WIPI2	0.1672234	0.1316241	0.408942421	0.235929974	0.0009	0.0016
BECN1	0.1608202	0.0938333	0.465319351	0.23999095	0.0027	0.0037
PIK3R4	0.1938243	0.1603193	0.511246208	0.288463269	0.0031	0.0040
PIK3C3	0.326752	0.1360534	0.395460092	0.286088497	0.0008	0.0015
AMBRA1	0.1838676	0.1171224	0.61341356	0.304801187	0.0111	0.0125
ULK2	0.1537685	0.139015	0.61859706	0.30379352	0.0115	0.0125
ATG10	0.2336886	0.141476	0.60709071	0.327418437	0.0091	0.0108
RPS6KB1	0.1069644	0.1020631	0.940405636	0.383144379	0.0912	0.0948
ATG9B	0.1640392	0.8323584	1.753546401	0.916648	0.8652	0.8652

**Table 3-1: Autophagy gene expression in CD34<sup>+</sup> CML and normal cells measured by qPCR.**

$\Delta\Delta CT$  of transcript levels in CD34<sup>+</sup> CML cells relative to average of three CD34<sup>+</sup> normal cells. n=3 normal samples and n=3 CML patient samples. P values were calculated using unpaired Student's T test with significance below p=0.05. Sometimes small p-values (less than 0.05) happen to lead by chance to incorrectly reject the true null hypotheses. To correct for multiple testing, p-values were adjusted using Benjamin-Hochberg method. It controls the false discovery rate (FalseDiscoveryRate (FDR)=Expected (FalsePositive/ (FalsePositive +TruePositive))). FDR is the expected proportion of false positives among all positives which rejected the null hypothesis and not among all the tests undertaken. The most preferable approach is controlling FDR as it not only reduces false positives, but also minimises false negatives.

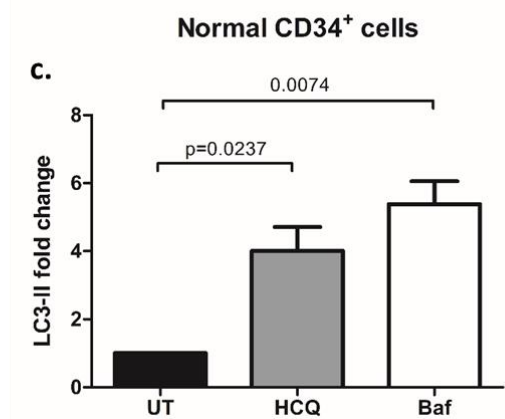
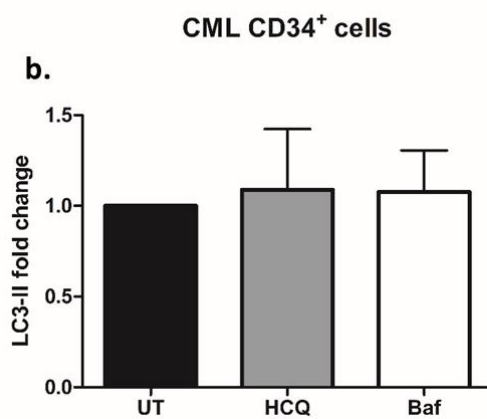
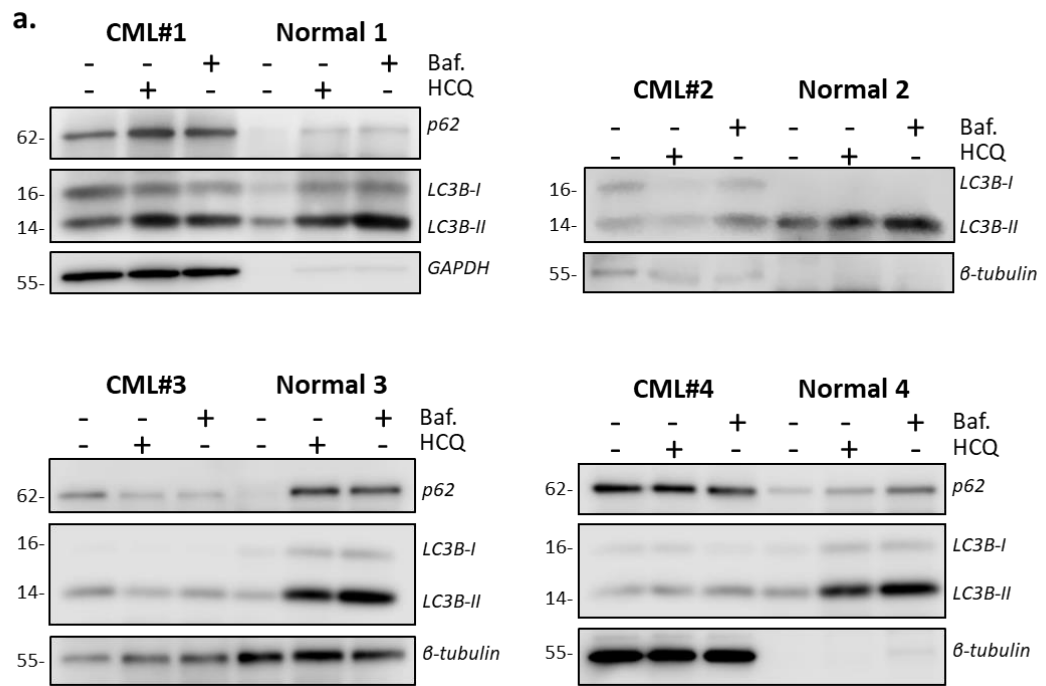


**Figure 3.4: CD34<sup>+</sup> CML cells show lower level of autophagy flux than normal CD34<sup>+</sup> cells.**

Western blot showing p62, LC3B-I and LC3B-II protein expression following 12h treatment with 100 nM Baf. and 10 $\mu$ M HCQ in CD34<sup>+</sup> CML and normal cells (a). LC3B-II-fold change relative to UT Mean  $\pm$  S.E.M. n=3 normal samples (b). LC3B-II-fold change relative to UT Mean  $\pm$  S.E.M. n=3 CML samples. p values were calculated using non-parametrical one-way Anova multiple comparison analysis (c).

### 3.2.3 Nilotinib treatment induces protective autophagy in LSPCs

We next aimed to confirm previously published data demonstrating that CD34<sup>+</sup> cells exhibit increased autophagic levels following TKIs treatment<sup>112,198</sup>. In addition, our hypothesis is that inhibition of BCR-ABL using TKIs induces AMPK activation. AMPK is a cytoplasmic energy sensor, which is a positive regulator of autophagy activating its signalling by phosphorylation of ULK1 at serine 555 (ser555). In the case of CML, autophagy sustains survival of LSPCs during TKI treatment providing building blocks and reducing intracellular stress (**Figure 3.5**). To achieve this, we first generated K562 cell line expressing RFP-GFP-LC3 by retroviral transfection (2.11). K562 cells are challenging to transfect with retroviral particles and positivity to RFP and GFP was assessed by FACS. Since only 40% efficiency was achieved followed transfection, we sorted K562 mRFP<sup>high</sup> and GFP<sup>high</sup> (**Figure 3.6**) to obtain stable cell line expressing RFP-GFP-LC3.

mRFP-GFP-LC3 is a widely used technique to monitor the different stages of autophagy. RFP-GFP-LC3 puncta are detectable when LC3 binds to the autophagosomes in which, a yellow signal can be visualised resulting from the RFP and GFP merged signals. Following autophagic induction, LC3 is internalised in the autophagosomes that will then fuse with lysosomes. Low lysosomal pH quenches the GFP signal, making only the RFP detectable. Based on this, increased level of RFP reflects higher levels of autophagy flux (**Figure 3.7a**). K562 expressing RFP-GFP-LC3 were treated for 4 h using 2  $\mu$ M nilotinib. Following fixation and nuclear staining, autophagy induction was measured using confocal microscopy. As expected, nilotinib increased levels of red LC3 puncta compared to UT cells suggesting enhanced autophagy in the treated cells (**Figure 3.7b**). In order to validate and further prove these findings, we treated CD34<sup>+</sup> CML cells for 24 h with 2  $\mu$ M nilotinib and RNA was extracted. Autophagic gene expression analysis showed that treated CD34<sup>+</sup> CML cells exhibit greater levels of autophagy gene expression compared to UT cells (**Figure 3.8**). In particular, we established that “drug-able” autophagy genes such as ULK1 and VPS34 are expressed significantly higher after nilotinib treatment (**Figure 3.8**), (**Table 3-2**).

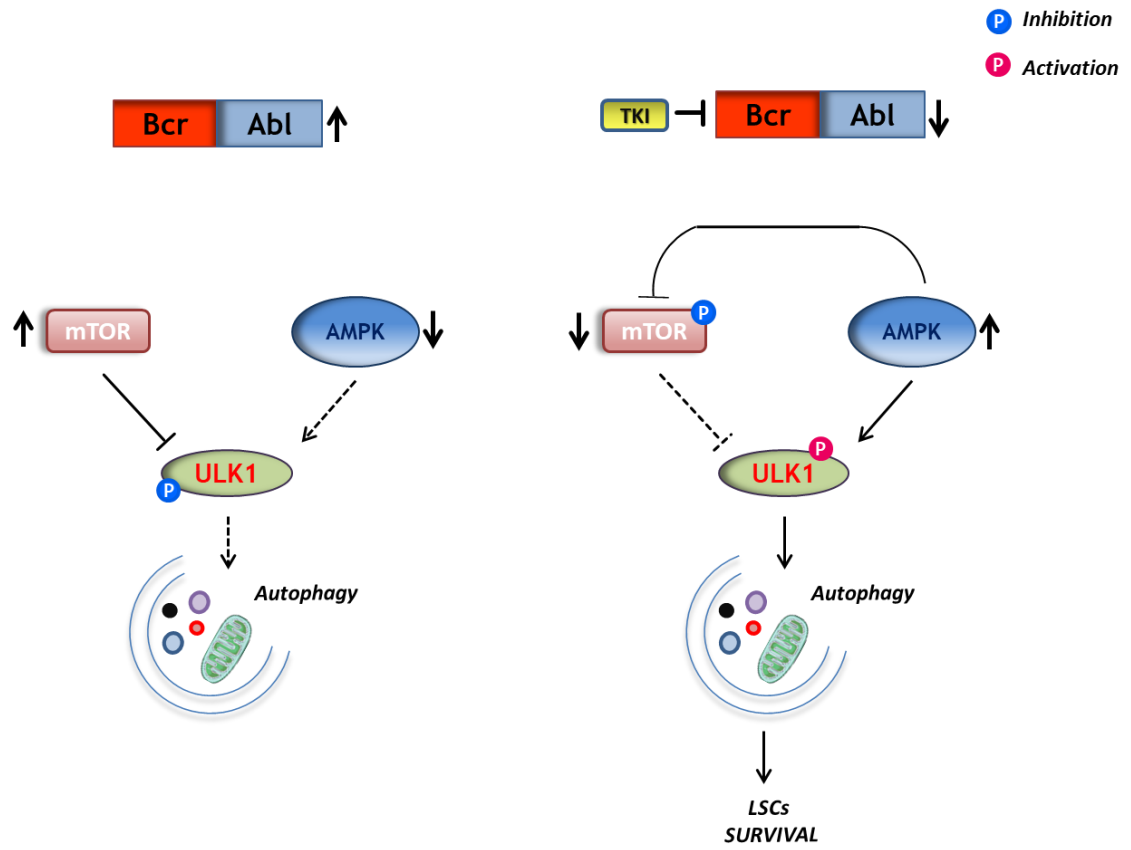
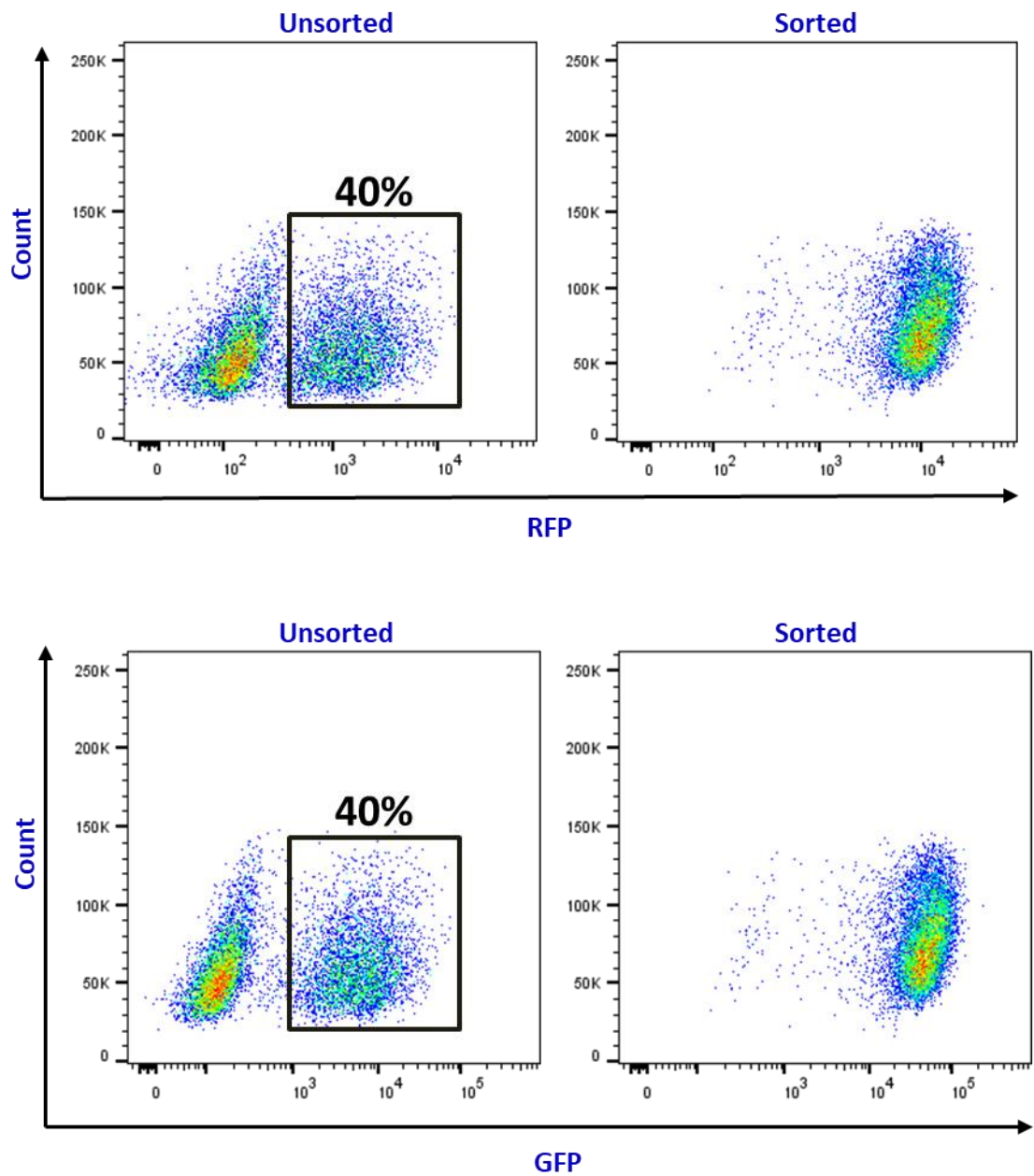


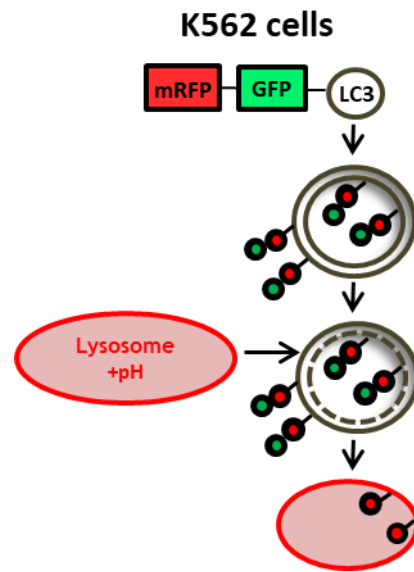
Figure 3.5: Mechanistic hypothesis of TKIs-induced autophagy in CML cells.



**Figure 3.6: Efficiency of retroviral transfection in K562 cells.**

FACS plots showing K562 expressing RFP-GFP-LC3 following retroviral transfection. Cells were FACS selected to enrich for double positive cells.

a.



b.

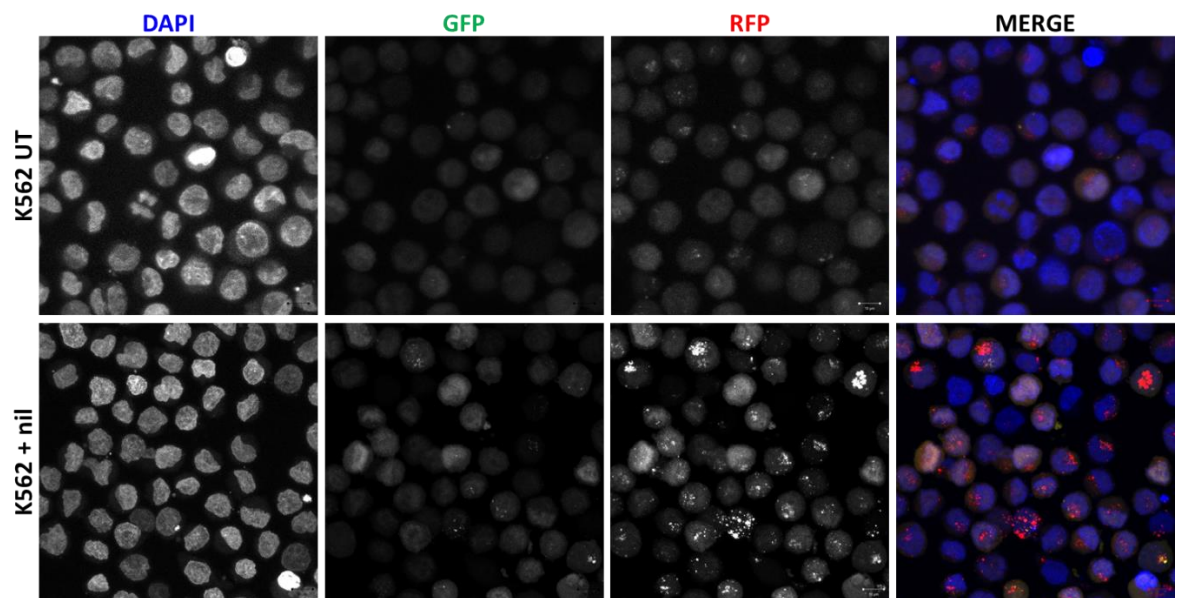


**Figure 3.7: Autophagy is induced in K562 following TKI treatment.**

Schematic representation of the RFP-GFP-LC3 assessment of autophagy at different stages (a). Representative confocal microscopy images of K562 RFP-GFP-LC3 showing LC3 puncta following 4 h UT and treatment with nilotinib (b).

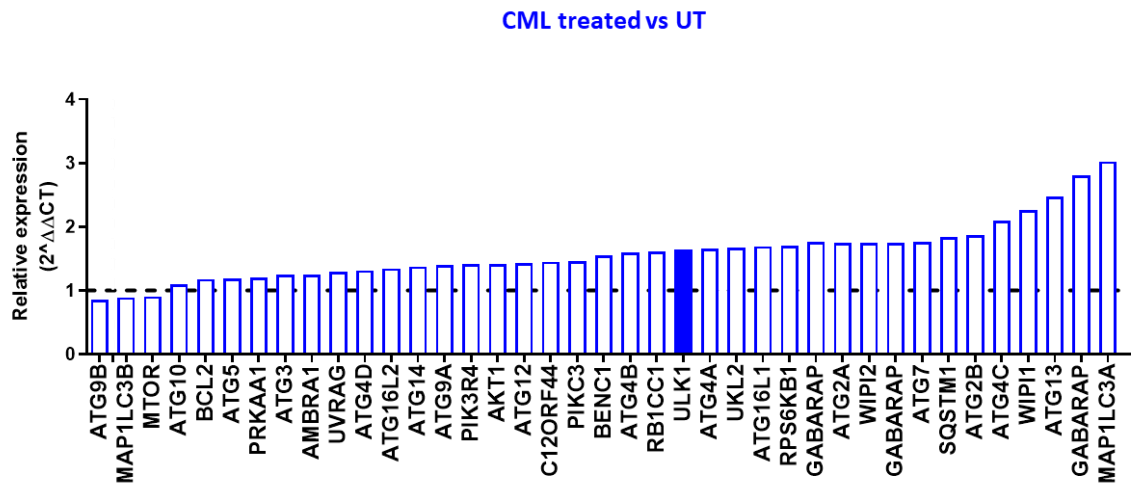


**Figure 3.8: Primitive CML cells show an increase in autophagy genes expression following nilotinib treatment.**

Comparative gene-expression analysis of CD34<sup>+</sup> CML cells treated and untreated with nilotinib. Mean n=3 CML patient samples.

### Chapter 3 Autophagy as a survival mechanism sustain LSPCs persistence

Gene	CD34 <sup>+</sup> CML1 Treated RELATIVE to UT	CD34 <sup>+</sup> CML2 Treated RELATIVE to UT	CD34 <sup>+</sup> CML3 Treated RELATIVE to UT	AVERAGE $\Delta\Delta$ CT	Paired t Test
ATG9B	0.574832	0.583487	1.413658	0.857325667	0.6591
MAP1LC3B	1.068377	0.758863	0.850125	0.892455	0.3622
<b>MTOR</b>	0.898662	0.893863	0.926974	0.906499667	0.012
ATG10	1.146673	1.052759	1.090839	1.096757	0.0711
BCL2	1.082673	0.890633	1.56325	1.178852	0.4656
ATG5	1.044352	1.045331	1.459988	1.183223667	0.3165
PRKAA1	1.097728	1.124783	1.375464	1.199325	0.1529
ATG3	1.53504	1.005975	1.179245	1.240086667	0.2631
AMBRA1	0.953061	1.633454	1.157911	1.248142	0.3433
UVRAG	1.620704	0.850357	1.393223	1.288094667	0.3346
ATG4D	1.205903	1.176494	1.565438	1.315945	0.1274
ATG16L2	0.713774	0.893309	2.422279	1.343120667	0.5915
ATG14	1.252954	1.163214	1.707912	1.374693333	0.1563
ATG9A	1.081816	1.69755	1.412845	1.397403667	0.1551
PIK3R4	1.494453	1.208116	1.54651	1.416359667	0.0583
AKT1	1.827744	1.161022	1.264851	1.417872333	0.1811
<b>ATG12</b>	1.402006	1.511688	1.368715	1.427469667	0.0101
C12ORF44	2.149368	1.063536	1.146364	1.453089333	0.3237
PIKC3	1.605403	1.115817	1.650135	1.457118333	0.1162
BENC1	0.921206	1.212615	2.501167	1.544996	0.3782
ATG4B	1.663405	1.998279	1.128201	1.596628333	0.1427
RB1CC1	1.706374	1.227347	1.88638	1.606700333	0.091
<b>ULK1</b>	1.681503	1.480533	1.764971	1.642335667	0.0168
ATG4A	1.562957	2.005334	1.391247	1.653179333	0.0703
UKL2	1.503639	2.075382	1.431403	1.670141333	0.0813
ATG16L1	1.825873	1.961868	1.291954	1.693231667	0.0771
RPS6KB1	2.321874	1.812199	0.957187	1.697086667	0.2221
<b>GABARAP</b>	1.687799	1.705054	1.886615	1.759822667	0.0069
ATG2A	1.648386	2.122347	1.460927	1.743886667	0.0634
<b>WIPI2</b>	1.579628	1.947965	1.710839	1.746144	0.0202
GABARAP	1.704017	2.340589	1.18612	1.743575333	0.1558
ATG7	2.146376	1.819546	1.317981	1.761301	0.0872
<b>SQSTM1</b>	1.999978	1.690912	1.822505	1.837798333	0.0112
<b>ATG2B</b>	1.916333	1.961288	1.730101	1.869240667	0.0066
ATG4C	1.469413	2.569676	2.260277	2.099788667	0.0784
WIPI1	2.093694	3.398827	1.282779	2.258433333	0.178
ATG13	3.37515	2.487777	1.553163	2.47203	0.1075
GABARAP	1.934784	4.374382	2.098886	2.802684	0.1492
<b>MAP1LC3A</b>	2.793409	3.787997	2.490457	3.023954333	0.0355

**Table 3-2: Autophagy gene expression in CD34<sup>+</sup> CML treated and untreated with nilotinib for 24h measured by qPCR.**

$\Delta\Delta$ CT of genes levels in CD34<sup>+</sup> CML cells treated with nilotinib relative to untreated. n=3 CML samples. Significant differences in gene expression between CML treated and untreated cells are highlighted in red.

To validate our hypothesis that AMPK and mTOR play a role in regulating autophagy upon BCR-ABL inhibition we performed time point treatment of CD34<sup>+</sup> CML cells using 2  $\mu$ M nilotinib. Western blot analysis demonstrated that nilotinib treatment reduced BCR-ABL signalling measured by reduced phosphorylation of Crkl (**Figure 3.9a, b**). As hypothesised, this resulted in activation of AMPK assessed by phosphorylation of AMPK on Thr-172 (**Figure 3.9a**). To assess the effect of BCR-ABL inhibition on mTOR activity, we measured levels of p-mTOR and its downstream S6 protein-kinase that was dephosphorylated following nilotinib treatment, demonstrating that mTOR signalling was inhibited, which correlated with autophagy activation, indicated by reduced levels of p62 (**Figure 3.9b**). Since both AMPK and mTOR regulate autophagy through ULK1, phosphorylation of ATG13 was measured as a direct indicator of ULK1 activity. As expected, ATG13 phosphorylation was induced following nilotinib treatment demonstrating that ULK1 represents one of the main features in the activation of autophagy following nilotinib treatment (**Figure 3.9a, b**).

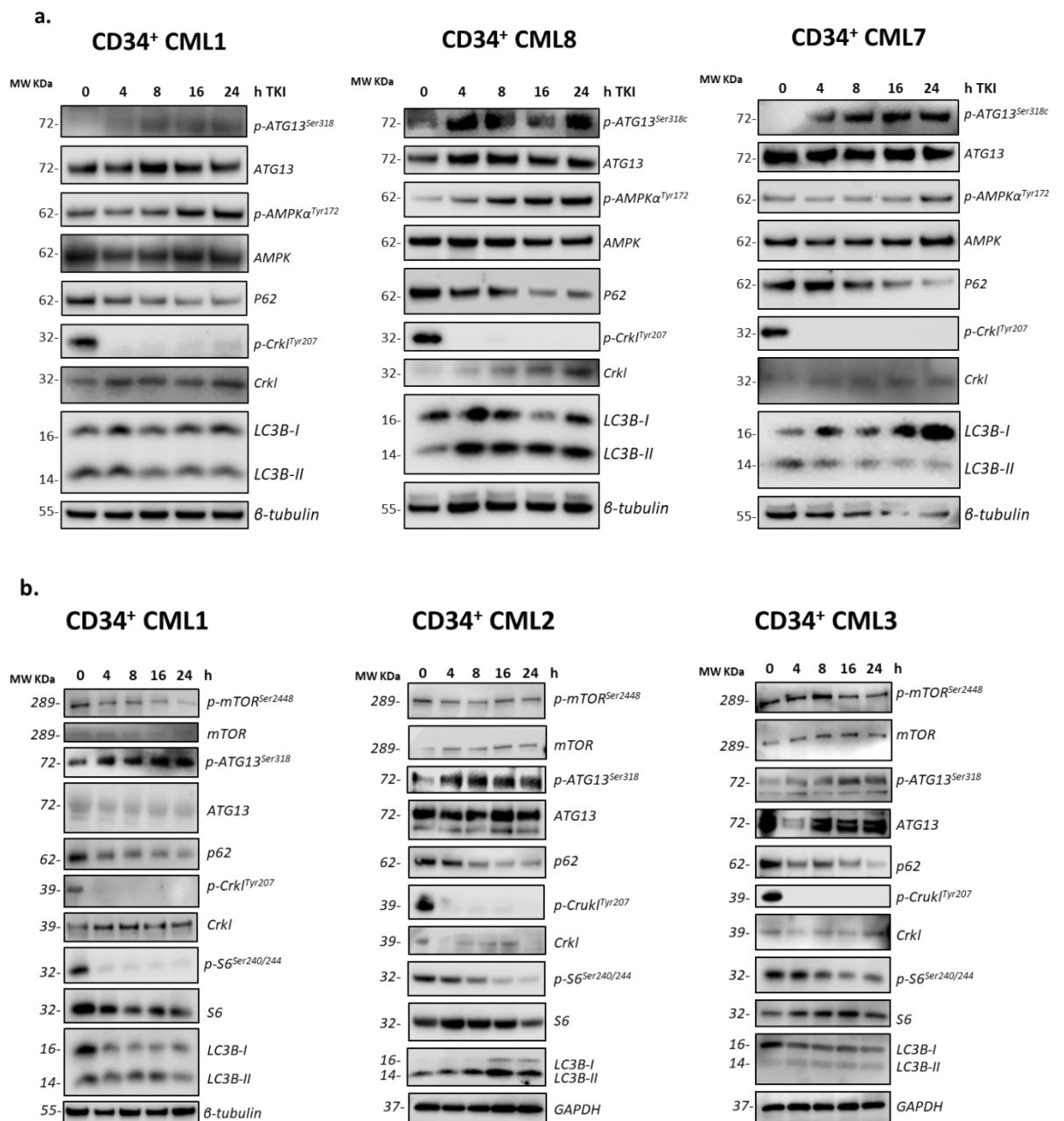


**Figure 3.9: AMPK and mTOR regulates autophagy in CD34<sup>+</sup> cells following nilotinib treatment.** Western blot analysis using CD34<sup>+</sup> cells exposed to 2  $\mu$ M nilotinib from 4 to 24 h using 5 independent patient samples (a, b).

### 3.2.4 Deletion of ULK1 using CRISPR-Cas9 technology reduces autophagy levels in CML cells

To study the role of ULK1 in CML we generated ULK1 deficient cells using a CRISPR-CAS9-mediated gene editing. Three different guide-RNAs were designed as described in material and methods to specifically target ULK1. Each of these sequences were cloned into Lenti-CRISPR-V2 plasmid previously digested with BsmBI restriction enzyme. Lentiviral infection was used to independently transduce each sequence in KCL22 or K562 CML cell lines. Following selection with 3µg/mL puromycin, cells were lysed, and western blot performed to confirm absence of ULK1 protein. Results indicate that sequence #3 and #2 significantly reduced levels of ULK1 in both KCL22 or K562 cells compared to control cells (a, b). Furthermore, increased levels of p62 were detected in ULK1 deficient cells, indicating that depletion of ULK1 results in inhibition of basal level of autophagy in CML cells (Figure 3.10a, b). However, both KCL22 and K562 showed increased levels of ULK1 if cells were not kept under puromycin selection. This was probably due to resistant puromycin clones in the bulk cells that have a growth advantage compared to ULK1 deficient cells in the absence of puromycin. Single cell cloning was therefore performed revealing presence of resistance clones still expressing ULK1 confirming the hypothesis (Figure 3.10c). Based on LC3B-II accumulation and increased levels of p62, Clone#5 and Clone#8 were chosen for further studies (from this point forward referred to as Clone#1 and Clone#2, respectively). As expected, had no phosphorylation on ULK1 was visible in KCL22 ULK1 deficient cells (Figure 3.10d). Furthermore, we also show that ULK1 deficient cells have reduced phosphorylation of ATG13 compared to control cells resulting in inhibition of autophagy (Figure 3.10d).

### 3.2.5 ULK1 deficiency sensitises CML cells to TKIs treatment *in vitro*

Next, we wanted to address if nilotinib would have had an enhanced effect on autophagy deficient cells. We treated control and ULK1 deficient cells for 72 h with 2 µM nilotinib and measured the effect of nilotinib treatment on apoptosis colony formation in

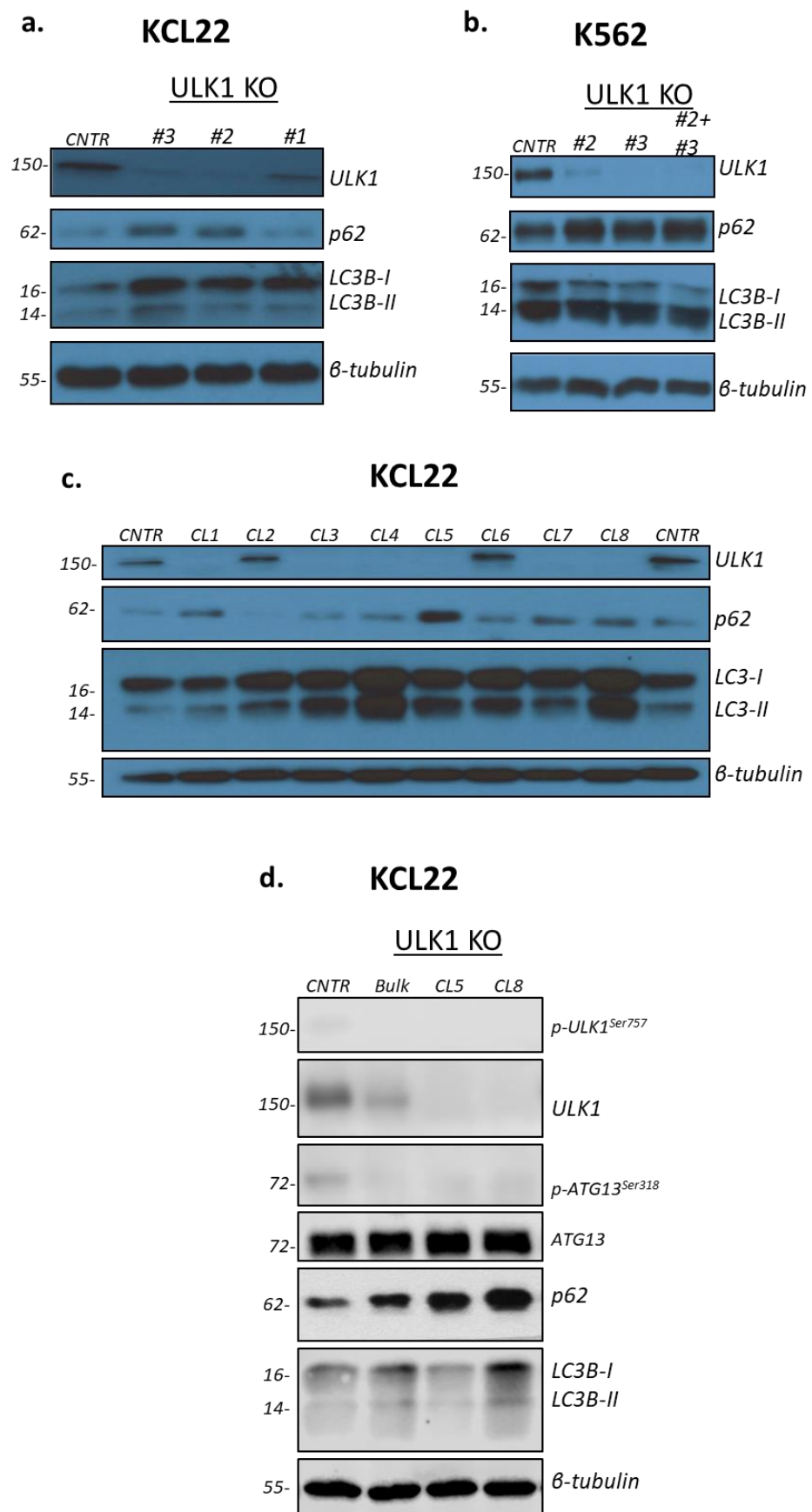


**Figure 3.10: Using CRISPR cas9 to knock-out ULK1 in CML cells**

Western blot analysis showing deletion of ULK1 using 3 different guides in KCL22 cells (a) and K562 cells (b). Western blot analysis showing deletion of ULK1 following single cells cloning in KCL22 cells (c). Western blot analysis of autophagic markers in KCL22 ULK1 deficient (d).

both cell lines. Results show that apoptosis was increased by almost 20% in ULK1 KO when treated with nilotinib (**Figure 3.11a**). As well, colony forming ability was reduced by 20% in ULK1 deficient cells in the presence of nilotinib (**Figure 3.11b**). From these results we conclude that ULK1 deficient cells are more sensitive to nilotinib treatment compared to autophagy competent cells.

### **3.2.6 Nilotinib fails to induce autophagy in ULK1 deficient cells**

As discussed in the previous paragraph, ULK1 deficient cells exhibit lower basal level of autophagy compared to control cells. Furthermore, ULK1 KO cells show enhanced sensitivity to nilotinib treatment compared to cells expressing ULK1. Encouraged by these results we tested if nilotinib induced autophagy in ULK1 KO cells. Western blot analysis performed in control and ULK1 KO cells show that treatment with 2  $\mu$ M nilotinib for 24 h reduced inhibitory phosphorylation of ULK1 on serine757 in control cells (**Figure 3.12**). Control cells increased phosphorylation of ATG13 while this was undetectable in ULK1 null cells (**Figure 3.12**). Furthermore, while nilotinib reduced levels of p62 in control cells, this was not detectable in ULK1 deficient cells (**Figure 3.12**).

All together these results highlighted that removal of ULK1 in CML cells inhibited nilotinib-induced autophagy and sensitised CML cells to nilotinib treatment.

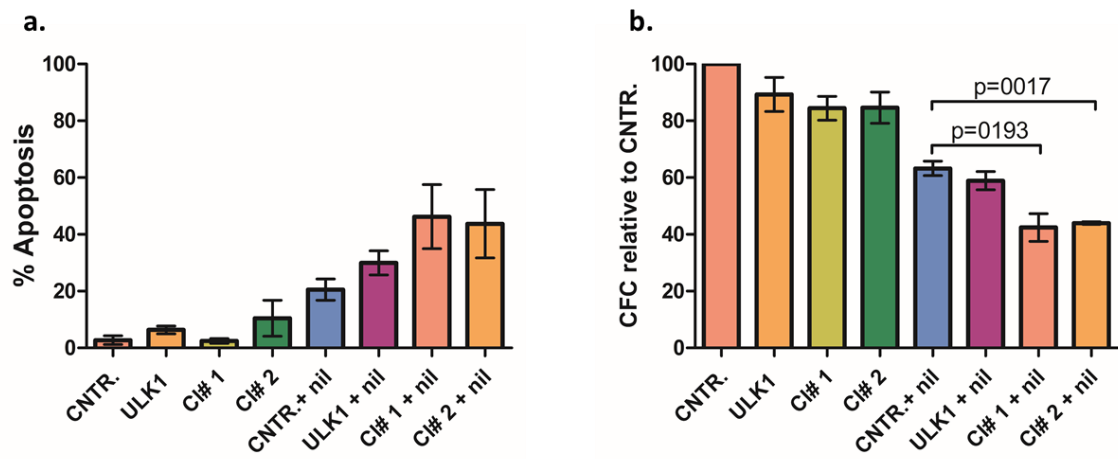


**Figure 3.11: ULK1 deficient cells are more sensitive to TKIs treatment.**

Graphs showing % of apoptosis following 3 days treatment with nilotinib (a). Number of colonies measured by CFC assay following a 3 days treatment with 2  $\mu$ M nilotinib (b). ULK1 represents bulk cells following KO of ULK1 and selection with puromycin; Cl#1 and Cl#2 represent the 2 ULK1 KO clones chosen following single cell cloning. Mean  $\pm$  S.E.M. P values were evaluated using unpaired Student T test.

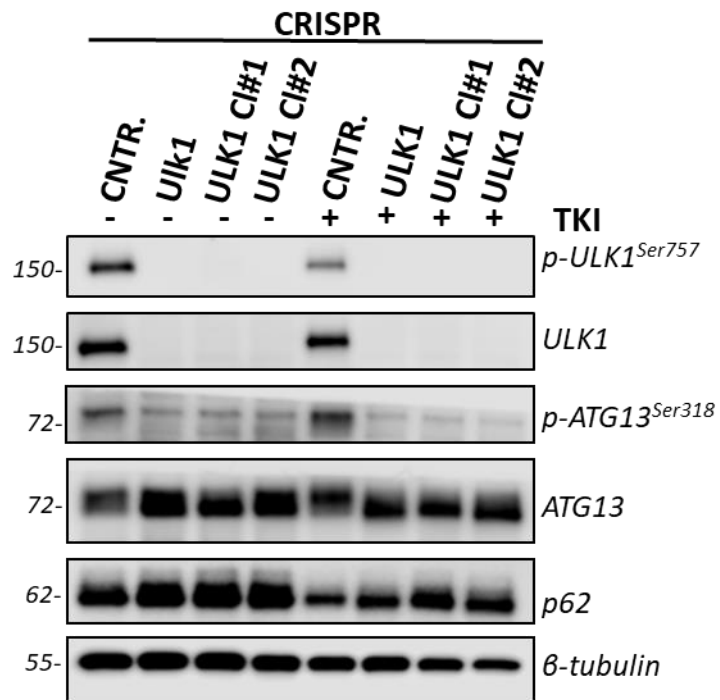


**Figure 3.12: Nilotinib fails to induce autophagy in ULK1 deficient cells**

Representative western blot analysis showing autophagic markers in KCL22 control or ULK1 deficient cells following 24 h treatment with nilotinib. n=3 independent experiments.

### **3.2.7 ULK1 deficiency sensitises CML cells to TKIs treatment *in vivo***

To further study the effect of TKIs in targeting ULK1 deficient cells, a bioluminescent xenograft mouse model for CML using KCL22 cells was established. KCL22 were transfected with pLenti-CMV-V5 luciferase-expressing plasmid. After transfection, luciferase activity was measured in KCL22 control and ULK1 KO cells using a luminescence plate reader. Following lysis and injection of luciferin, we established emission of luminescence from both control and ULK1 KO clones (**Figure 3.13**). Since control and ULK1 KO Clone#1 expressed the same intensity of fluorescence, Clone#1 was chosen for downstream studies. Four million control and ULK1 KO Clone#1 cells were transplanted via tail vein injection into NRGW<sup>41</sup> recipient mice (**Figure 3.14a**). 30 minutes following transplant mice were subcutaneously injected with 200  $\mu$ L of luciferin and imaged using a bioluminescent imager, IVIS, to determine success of equal transplant of both control and ULK1 KO cells. 13 days post-transplant, mice receiving control or ULK1 deficient cells were respectively allocated in 2 arms each. Mice were treated twice per day with vehicle or imatinib, front-line treatment for CML patients, and imaged weekly to monitor tumour growth. By week 4, mice receiving ULK1 deficient cells and treatment with imatinib had significantly reduced tumour growth compared to mice receiving control cells (**Figure 3.14b**). Combining ULK1 deficiency and imatinib treatment significantly extended survival of mice compared to control cells treated with imatinib (**Figure 3.15**). In fact, mice receiving ULK1 KO cells and treatment with imatinib survived 23 days longer than mice receiving control cells (**Figure 3.15**).

Furthermore, number of tumours in each mouse was counted upon mouse sacrifice. As expected, a statistically significant reduction in number of tumours was observed in mice receiving ULK1 KO cells compared to control cells (**Figure 3.16a, b**). This reduction was further enhanced when ULK1 KO was combined with imatinib treatment (**Figure 3.16a, b**).

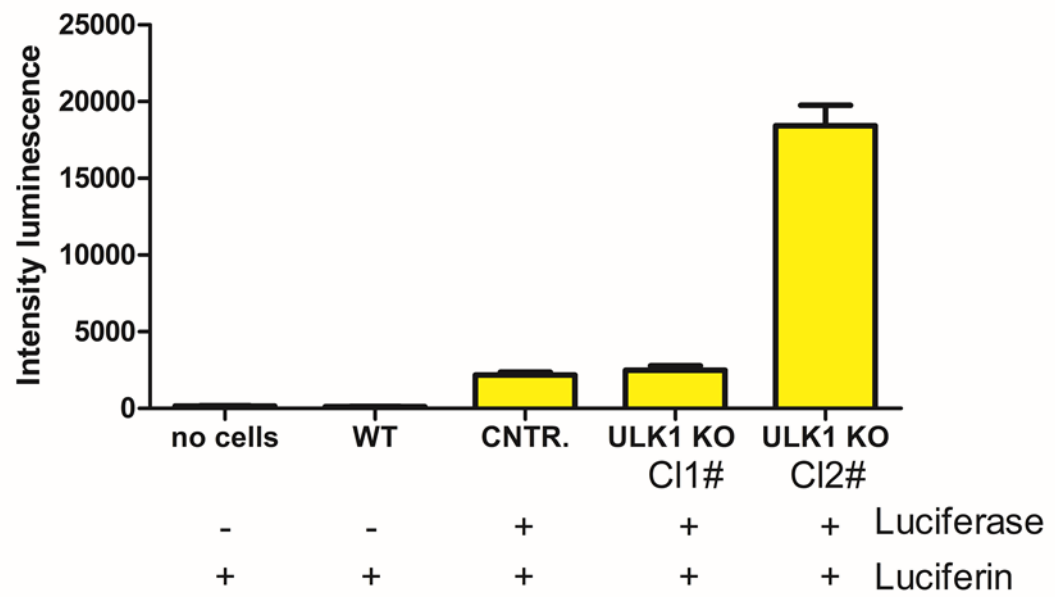


**Figure 3.13: Luminescence of CNTR. and ULK1 KO cells following transfection with luciferase expressing plasmid.**

Assessment of luciferase activity in control and ULK1 KO cells after transfection of luciferase expressing plasmid with and without luciferin.

## Chapter 3 Autophagy as a survival mechanism sustain LSPCs persistence

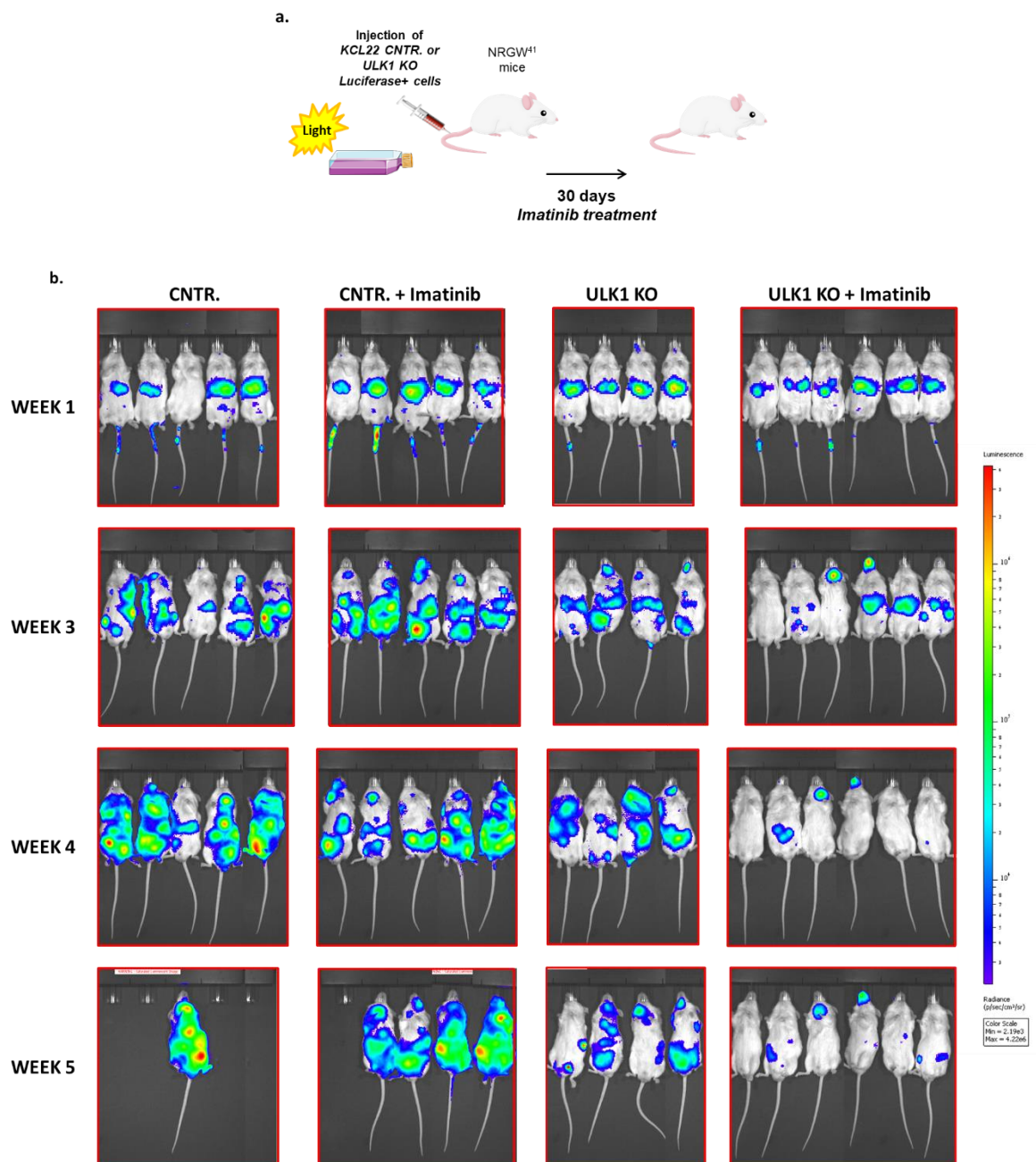


**Figure 3.14: Xenografted NRGW41 mice with ULK1 deficient cells are more sensitive to imatinib treatment compared to mice receiving control cells.**

Control and ULK1 KO cells Luciferase+ were transplanted via tail vein into recipient NRGW<sup>41</sup> male mice, followed by 30 days *in vivo* treatment (a). Weekly luciferase bio-imaging of mice receiving control or ULK1 deficient cells, treated or untreated with imatinib (b).

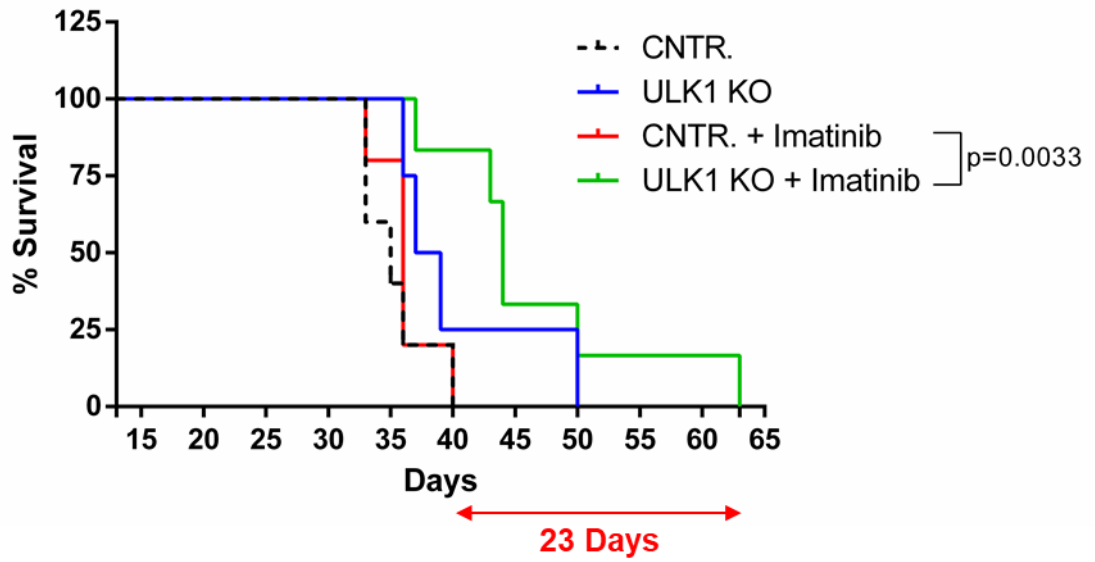


**Figure 3.15: Imatinib extend survival of NRGW<sup>41</sup> mice receiving ULK1 KO cells.**

Overall survival measured by Kaplan-Meier analysis. P values were evaluated using unpaired Student T test.

### Chapter 3 Autophagy as a survival mechanism sustain LSPCs persistence

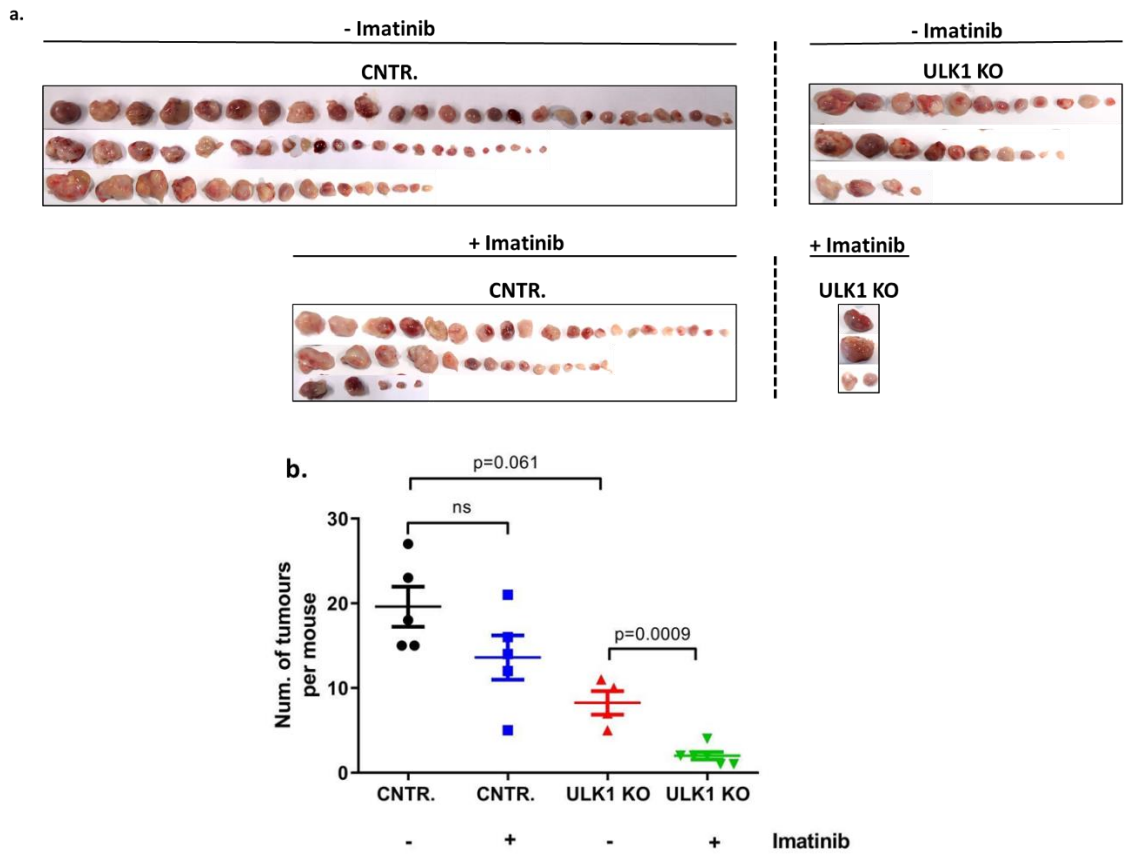


**Figure 3.16: ULK1 KO cells significantly reduce number of tumours following imatinib treatment.**

Image showing number of tumours in each mouse at the time of cull (a). Graph showing number of tumours in each mouse at time of death (b). Mean  $\pm$  S.E.M. P values were evaluated using unpaired Student T test.

### Chapter 3 Autophagy as a survival mechanism sustain LSPCs persistence

Furthermore, we also wanted to address if the observed reduction in number of tumours, leading to an extension of mice survival, was due to reduced autophagy levels in ULK1 deficient cells.

We firstly confirmed absence of mouse cells in the tumours, which totally constituted of human cells (**Figure 3.17a**). Secondly, we confirmed absence of ULK1 in ULK1 deficient tumour, and showed that tumours derived from ULK1 deficient cells had reduced levels of autophagy, measured by increased level of p62. Interestingly, p62 levels were enhanced in some of the control and ULK1 KO tumours following treatment with imatinib (**Figure 3.17b**), which could be explained by increased gene transcription in line with **Figure 3.8**.

All together these results show that mice receiving ULK1 deficient cells are insensitive to imatinib-induced autophagy, leading to a higher sensitivity to imatinib treatment *in vivo*.

### Chapter 3 Autophagy as a survival mechanism sustain LSPCs persistence

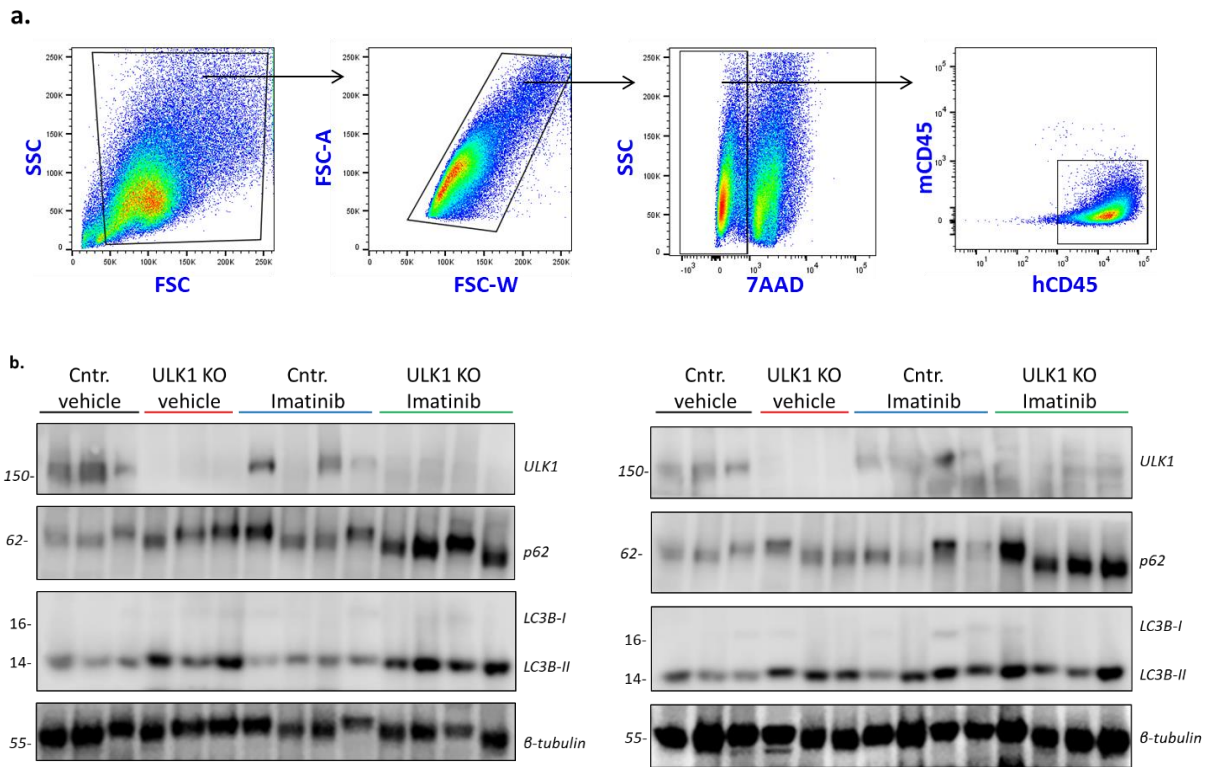


**Figure 3.17: ULK1 deficient tumours show reduced level of autophagy following imatinib treatment.**

FACs plot showing positivity of tumours to human CD45 (a). Western blot analysis for autophagic markers of tumours derived from control or ULK1 KO cells (b).

### 3.3 Discussion

In this chapter we first investigated the dependency of HSPCs and LSPCs on autophagy. As per previously published data, we show that CD34<sup>+</sup> normal cells possess an elevated turnover of cytoplasmic organelles and compartments using autophagy as a recycling and cleaning process. This results in minimising/controlling intracellular stress that represents a major obstacle to HSPCs maintenance. It's in fact known that HSPCs enhance fatty acid oxidation and glycolysis to sustain their metabolic rates, avoiding oxidative metabolism that might increase ROS levels and induce differentiation with loss of the most primitive population<sup>30,31</sup>. In the CML counterpart, cells exhibit high proliferative rates and BCR-ABL drives expansion of the myeloid compartment resulting in cell accumulation in peripheral blood of CML patients. BCR-ABL is also responsible for the de-regulation of intracellular survival and metabolic sensors such as AMPK and mTOR. We demonstrate that CD34<sup>+</sup> CML cells show a reduced autophagic transcript signature compared to normal cells and CML cells exhibit lower autophagic flux than their normal counterpart.

Following BCR-ABL inhibition using nilotinib, autophagy gene expression was increased. Previously published data indicate that autophagy represented a survival mechanism for LSPCs following TKI treatment, balancing intracellular stress and cell survival. AMPK and mTOR are the main proteins in regulating energy metabolism and autophagy in these cells. AMPK behaves as a regulator of cellular growth in conditions where nutrients are limited. AMPK controls cell growth by suppressing mTOR, a negative regulator of autophagy. Suppression of mTOR not only results in cellular growth inhibition but also in activation of autophagy. In the case of CML, where BCR-ABL activates growth factor signalling and TKI treatment can mimic a situation where nutrients are limited and the ratio between AMP and ATP can reach elevated levels. In this environment elevated levels of AMP or ADP will promote AMPK activation, which can suppress mTOR and activate autophagy to enhance building block recycling. We show that upon TKIs treatment, AMPK is active, driving autophagic flow via activation of ULK1 measured by increased phosphorylation of its down-stream effector protein ATG13 (**Figure 3.5**).

### Chapter 3 Autophagy as a survival mechanism sustain LSPCs persistence

Furthermore, deletion of ULK1 confirmed our hypothesis. In fact, inhibiting BCR-ABL with TKIs does not lead to autophagic induction in ULK1 deficient cells. As a result, ULK1 deficient cells show increased sensitivity to TKIs *in vitro* and *in vivo*.

Despite the promising results showed in this section, we also want to highlight the limitations of using K562 and KCL22 cell lines. These have in fact been isolated from BC phase patient and not from CP, a more advanced and aggressive stage of the disease. To properly study CP-CML it would be ideal to use cell lines derived from this stage of the malignancy. However, this has not yet been achieved. Furthermore, performing CRISPR cas9-mediated knock-out also has its own limitations. Even though in our case sequence to target ULK1 where accurately checked on the BLAST platform for off-targets effect, the use of multiple clones higher than 2 would have been ideal to increase the confidence of the results. As well, rescue experiments re-introducing the ULK1 would have allowed us to confirm the specificity of our results in a ULK1-dependent manner. However, these experiments still remain very challenging.

In summary we demonstrate that on one hand CML cells exhibit lower turnover of autophagic flow compared to normal cells, and on the other hand, following nilotinib treatment CML cells upregulate autophagy to sustain survival. Our results indicate that ULK1 represents one of the main features in the activation of autophagy and might represent a strategic target to suppress autophagy during TKI treatment and to eradicate CML cells. ULK1 is also one of few druggable proteins of the autophagic process.

# Chapter 4 Using MRT921 to target CML LSPCs

## 4.1 Introduction

Thus far, we have shown that treatment with TKIs induce protective autophagy in CD34<sup>+</sup> CML cells and promotes cell survival and persistence of CML LSPCs. Our preliminary data suggest that the link between autophagy activation during TKIs treatment is due to BCR-ABL modulation of mTOR and AMPK, which represent two of the main regulators of autophagy and cellular energy homeostasis. We show that following TKIs treatment, inactivation of mTOR and enhancement of AMPK activity positively regulates ULK1, an essential stem feature during autophagy initiation, measured by phosphorylation of ATG13 on ser318. We also show that removal of ULK1 using CRISPR-cas9 inhibited TKI-induced autophagy *in vitro*, sensitising CML cells to death.

Combining current standard-of-care (TKI treatment) with autophagy inhibition in CML is of clinical relevance. CHOICES (CHlOroquine and Imatinib Combination to Eliminate Stem cells), a recently completed phase II clinical trial, combined front line treatment for CML patients (imatinib) with HCQ. However, HCQ is a non-specific autophagy inhibitor that targets lysosomes and requires high doses to inhibit autophagy *in vivo* that might not be achievable in patients. This underlines the need to develop more specific autophagy inhibitors to target autophagy in cancer patients. Thus far, pre-clinical ULK1/2 and VPS34 inhibitors have been developed, with *in vitro* results suggesting that these compounds are promising candidates to target autophagy in CML patients<sup>138,193,199,200</sup>.

Based on our findings showing a potential role of ULK1 in regulating autophagy in CML, we have established a purposeful collaboration with LifeArc, an independent medical research company that has recently developed pre-clinical ULK1/2 inhibitors, including MRT68921<sup>200</sup>. *Petherick et al.* demonstrated that MRT921 targets ULK1, enabling autophagy initiation and leading to accumulation of immature autophagosomes.

In this chapter we show the effect of MRT921 in the context of leukaemia in combination with TKIs. We indicate that MRT921 targets autophagy as a single agent in CML cells measured by inhibition of Parkin-dependent mitophagy. Furthermore, we found that the MRT921-mediated effect on inhibition of

mitophagy correlates with increased mitochondrial content, increased mitochondrial respiration and increased levels of ROS.

According to recent publication indicating that ULK1 regulates glycolysis by direct phosphorylation of glycolytic enzymes<sup>145</sup>, we show that following inhibition of ULK1 using MRT921, glycolysis and glycolytic capacity is diminished CML cells.

We also showed that MRT921 significantly inhibited TKI-induced autophagy, resulting in increased nilotinib-induced death in CML cells. However, we demonstrated that MRT921 treatment, at a 1  $\mu$ M concentration induced cell death and reduced CFC in ULK1 KO cells, probably due to off-target effect. As well, undesirable toxic effects were detected following MRT921 treatment of normal CD34<sup>+</sup> cells. As suggested by Petherick *et al.*, this might correlate with the fact that 1  $\mu$ M of MRT921 affects the activity of a wide range of kinases and its cytotoxic effect may be independent from inhibition of ULK1/2.

## 4.2 Results

### 4.2.1 MRT921 treatment inhibits CML cells proliferation in a concentration dependent manner

Given the role ULK1 plays in inducing autophagy following TKIs treatment in CML, we hypothesise that restraining autophagy by pharmacological inhibition of ULK1 may enhance the TKIs effect in targeting CML cells.

As previously mentioned, pharmacological inhibition of ULK1 has been studied using MRT921. *Petherick et al.* demonstrated that 1  $\mu\text{M}$  of MRT921 effectively targets mTOR dependent-autophagy<sup>200</sup>. Before assessing autophagy inhibition, we first aimed to determine the concentration of MRT921 that giving half-maximal cell growth response (EC50) in our CML model. CML cells were treated for 72 h with increased concentration of MRT921 and inhibition of growth measured by colorimetric XTT assay. Using a concentration range between 0 and 10  $\mu\text{M}$  we established that MRT921 EC50 was  $\sim 5 \mu\text{M}$  in KCL22 CML cell line (**Figure 4.1a**). Similar results were obtained using TKI-resistant KCL22 cells (KCL22<sup>T315I</sup>), with EC50 value remaining  $\approx 5 \mu\text{M}$  (**Figure 4.1b**). This suggest that both TKI-sensitive and TKI-resistant KCL22 cells are sensitive to MRT921 treatment with EC50  $\approx 5 \mu\text{M}$ .

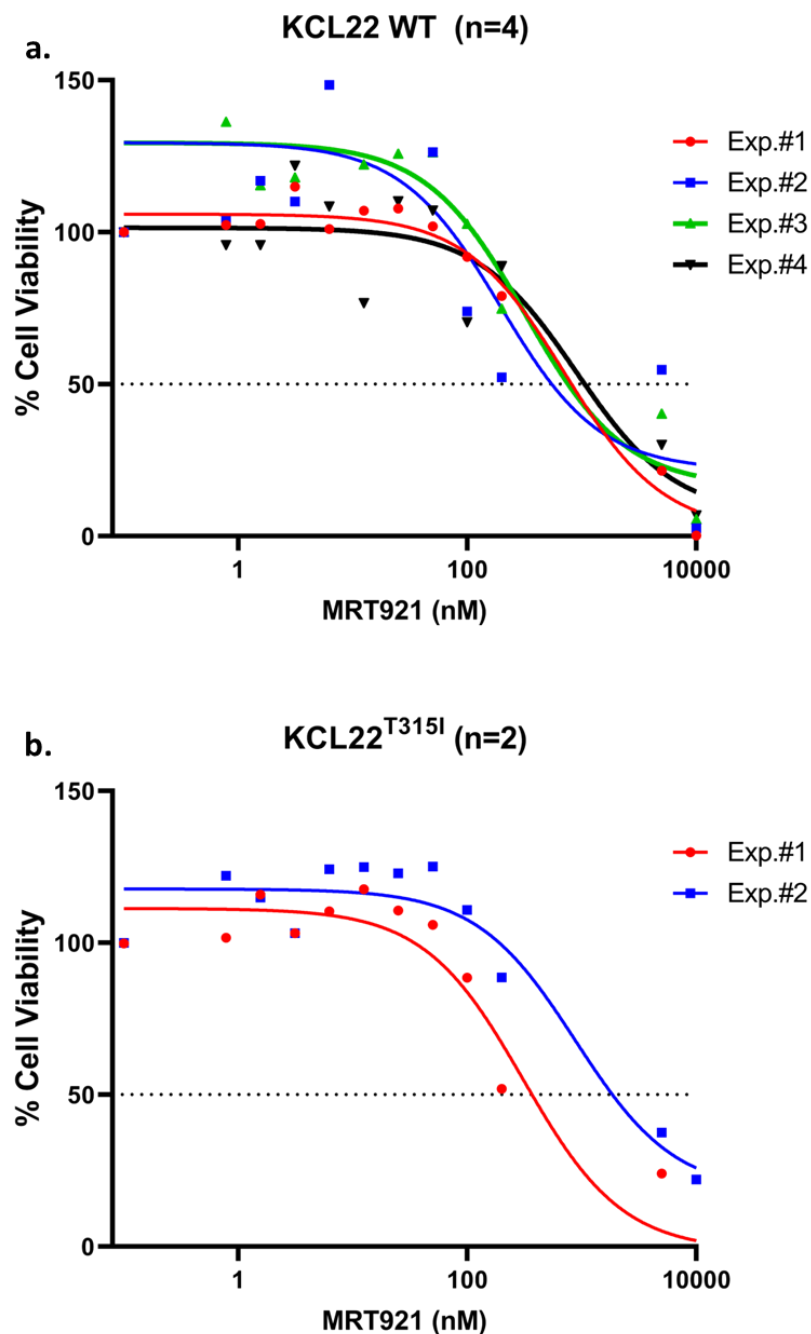


**Figure 4.1: MRT921 inhibits growth of TKI-sensitive and TKI-resistant CML cell lines**

Measurements of proliferation in KCL22 TKI-sensitive upon exposure to increased concentrations of MRT921. n=4 independent experiments (a). Measurements of proliferation in KCL22 TKI-resistant (KCL22<sup>T315I</sup>) cells upon exposure to increased concentrations of MRT921. n=2 independent experiments (b).

### 4.2.2 MRT921 induces cell death in WT and ULK1 deficient cells

To study whether the cytotoxic effects of MRT921 were selectively mediated through ULK1 inhibition, we measured apoptosis and colony forming ability following treatment with increased concentration of MRT921 in WT and ULK1 deficient KCL22 cells.

We treated KCL22 cells using 1, 3 and 5  $\mu\text{M}$  of MRT921. Results show that while 1  $\mu\text{M}$  of MRT921 did not induce apoptosis in KCL22 WT cells, a 10% increase in apoptosis was obtained in KCL22 ULK1 KO using 1  $\mu\text{M}$  of MRT921 (**Figure 4.2a, b**). Furthermore, concentrations higher than 1  $\mu\text{M}$  induced 80% increase in apoptosis in both KCL22 WT and ULK1 deficient cells (**Figure 4.2a, b**). Treatment using 1  $\mu\text{M}$  MRT921 resulted in a 10% decrease of CFC in KCL22 WT and a 20% decrease in KCL22 ULK1 deficient cells (**Figure 4.2a, b**). However, increasing MRT921 concentration resulted in reduction of CFC of 80% in both KCL22 WT and ULK1 deficient cells.

These results demonstrate that ULK1 activity is not required for MRT921-induced cell death, indicating that either inhibition of ULK2 is critical, or the cytotoxic effect of MRT921 is mediated through off target effect on other proteins/kinases.

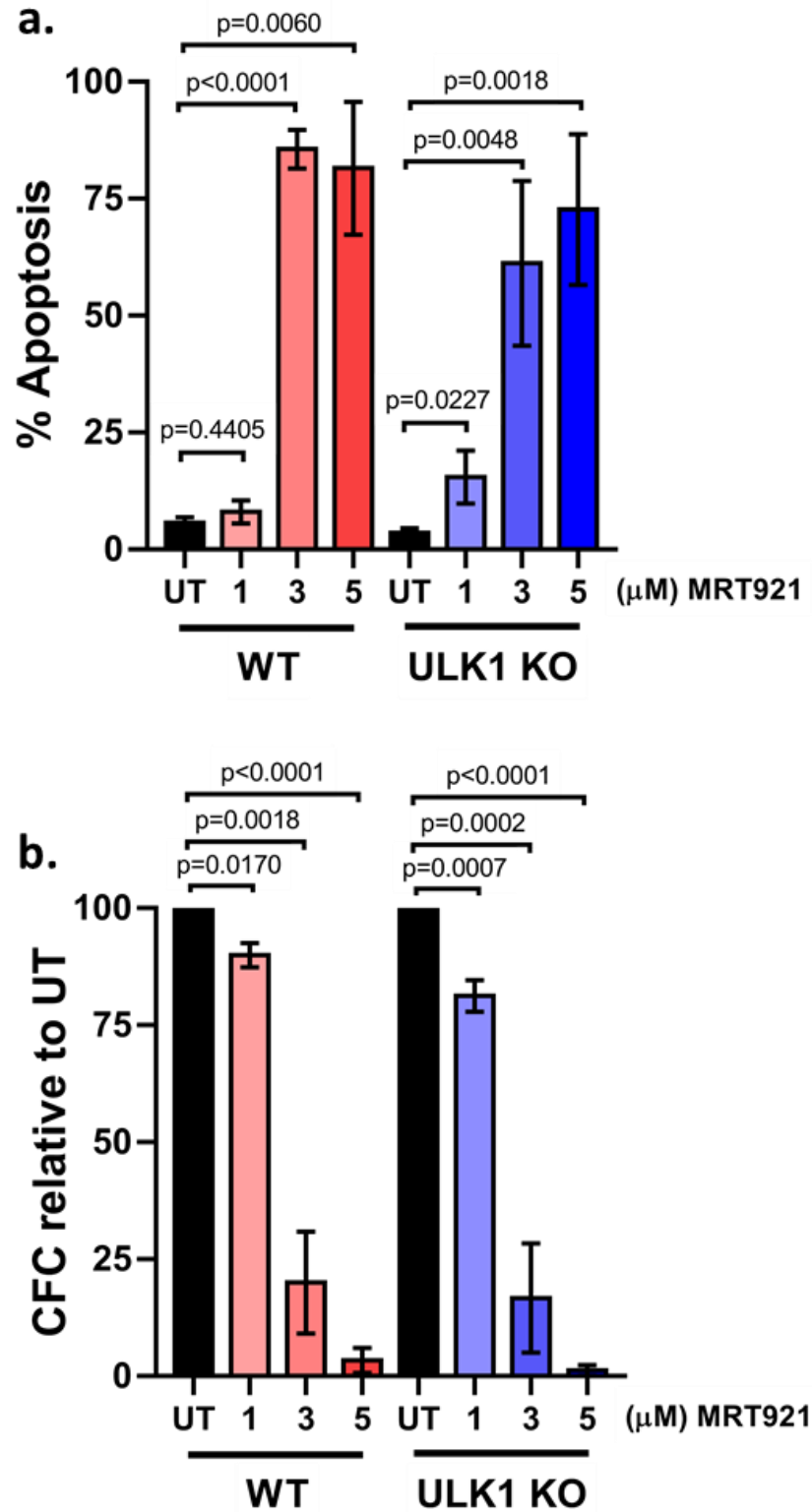


**Figure 4.2: ULK1/2 inhibitor affects apoptosis and CFC in WT and ULK1 deficient CML cells**

Measurements of apoptosis following 72 h treatment using 1, 3 e 5 μM of MRT921 in KCL22 WT (a) and ULK1 KO cells (b). Measurements of CFC following 72 h treatment using 1, 3 e 5 μM of MRT921 in KCL22 WT (c) and ULK1 KO cells (d). Mean ± S.E.M. P values were calculated using unpaired Student T-test. n=3 independent experiment in each case.

### 4.2.3 ULK1 and ATG7 deficient CML cells exhibit lower level of basal and stressed-induced Parkin-dependent mitophagy

Since accurate measurements of basal autophagic flux is challenging, we monitored the autophagic degradation of mitochondria to determine the efficacy of MRT921 treatment on the autophagic cargo digestion.

Using retroviral system, we infected K562 CML cells, resulting in stable over-expression of Parkin conjugated to YFP. We tested whether exogenous Parkin expression could be used to measure autophagic degradation of mitochondria<sup>178</sup> in CML cells. We treated control and YFP-Parkin expressing K562 cells for 24 h with antimycinA, an inhibitor of complex III of the electron transport chain, and oligomycin, an inhibitor of the ATP synthase. Since both compounds are unstable in culture, drugs were refreshed every 12 h. Western blot analysis revealed that following treatment with antimycinA and oligomycin, depletion of mitochondrial protein in K562 control cells was barely detectable, whereas expression of exogenous Parkin dramatically increased removal of mitochondria complexes including YFP-Parkin (**Figure 4.3**). Reduction was visible for mitochondrial complexes II-V (CII, CIII, CIV and CV), demonstrating suitability of this assay to assess autophagy flux.

We then used ULK1 and ATG7 deficient K562 cells over-expressing Parkin to measure levels of basal and stressed induced Parkin-dependent mitophagy in autophagy deficient cells. ULK1 and ATG7 KO cells were treated for 12 h using antimycinA and oligomycin following what cells lysates were prepared. Western blot analysis revealed that both ULK1 and ATG7 deficient cells exhibit increased levels of mitochondrial complexes even following treatment with antimycinA and oligomycin (**Figure 4.4**). Moreover, using ULK1 KO lines, it resulted in decreased mitophagy (**Figure 4.4**). Furthermore, while ATG7 cells completely inhibited mitophagy, ULK1 KO cells still exhibited partial Parkin-dependent mitophagy which might be due to incomplete removal of ULK1. In fact, even using guide #3, K562 cells still show residual expression of ULK1 (**Figure 4.4**). However, it is also possible that the clearance of specific complex might occur in a ULK1 or ATG7 dependent manner. In fact, accumulation of complex IV was more robust in ULK1 deficient cells, while complex I and complex II was higher in ATG7 deficient cells (**Figure 4.4**).

## Chapter 4 Using MRT921 to target CML LSPCs

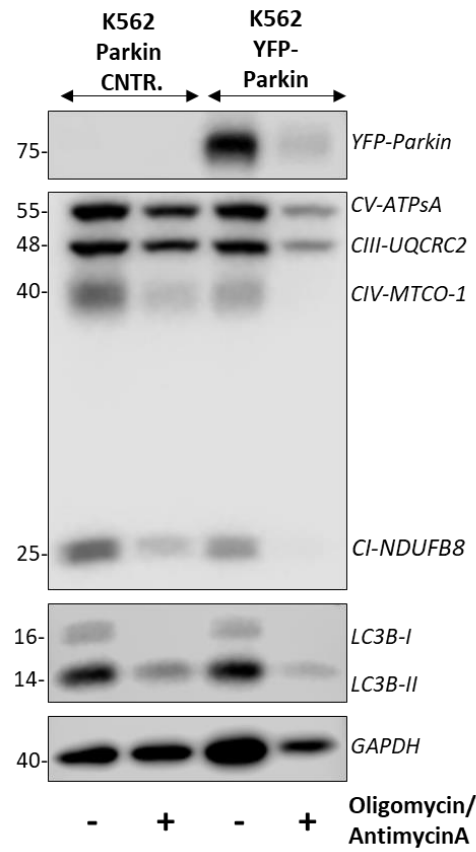


**Figure 4.3: Over-expression of Parkin enhances mitophagy in CML cells**

Western blot analysis showing mitochondrial complexes levels following 24 h treatment with 1 nM of antimycin A and 1 nM of oligomycin in K562 control and YFP-Parkin overexpressing cells.

## Chapter 4 Using MRT921 to target CML LSPCs

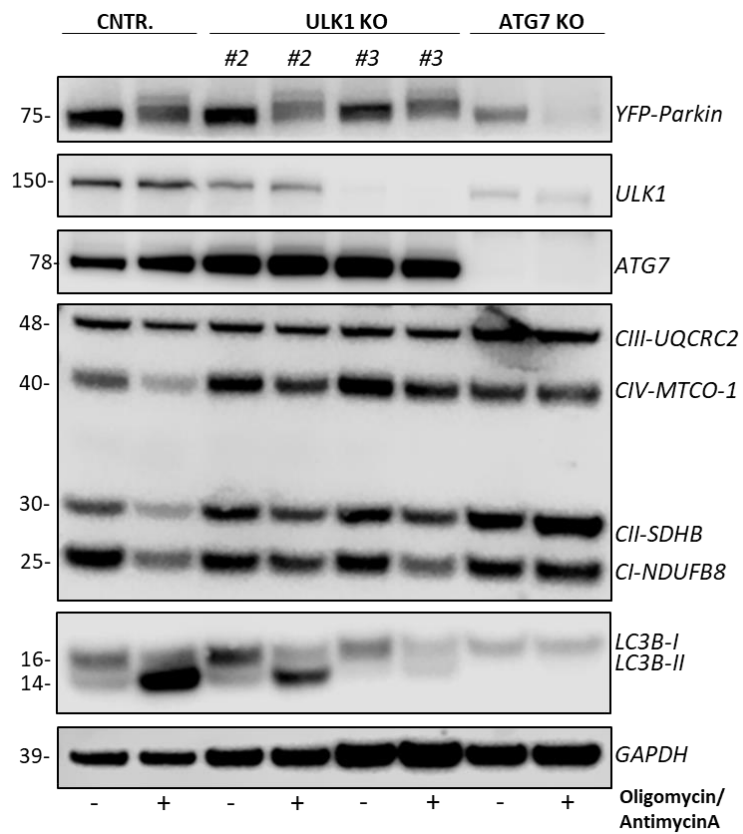


**Figure 4.4: ULK1 and ATG7 deficient cells exhibit decreased Parkin-dependent mitophagy**

Representative western blot analysis showing mitochondrial complexes levels following 12 h treatment with 1 nM of antimycin A, 1 nM of oligomycin in control, ULK1 and ATG7 deficient cells; n=2 independent experiment.

Even though a more efficient KO of ULK1 is required, we established reduced Parkin-dependent mitophagy in both ULK1 and ATG7 deficient CML cells.

#### **4.2.4 MRT921 treatment inhibits stressed-induced Parkin-dependent autophagy**

To understand if the effect of MRT921 in inhibiting cell growth and CFC in CML cells was due to inhibition of autophagy, we measured autophagy flux following treatment with MRT921.

Established that overexpression of Parkin can be used to measure autophagic flux and mitochondrial degradation, we used this approach as a measure of autophagy inhibition following MRT921 treatment. We treated K562 control and YFP-Parkin cells with a range of concentrations of MRT921 between 0 and 3  $\mu$ M for 24 h and in combination with antimycin A and oligomycin. As shown in (**Figure 4.4**), removal of mitochondria is minimum in K562 control cells when treated with antimycin A and oligomycin (**Figure 4.5a**), (lane 1 and lane 7). Likewise, inhibition of mitophagy is undetectable in K562 control cells when treatment with antimycinA and oligomycin is combined with increased concentration of MRT921 (**Figure 4.5a**). Instead, enhancing mitophagy using YFP-Parkin and mitochondrial stressors, we show that MRT921 significantly inhibited autophagic flux (**Figure 4.5b, c**). Furthermore, we established that complex II, III, IV and V levels were restored following treatment with increasing concentration of MRT921 (**Figure 4.5b**). Since complex V was the more abundant protein, complex V was used for quantification analysis (**Figure 4.5c**).

Thus far, our results indicated that MRT921 inhibited autophagy-mediated degradation of stressed mitochondria (mitophagy).

## Chapter 4 Using MRT921 to target CML LSPCs

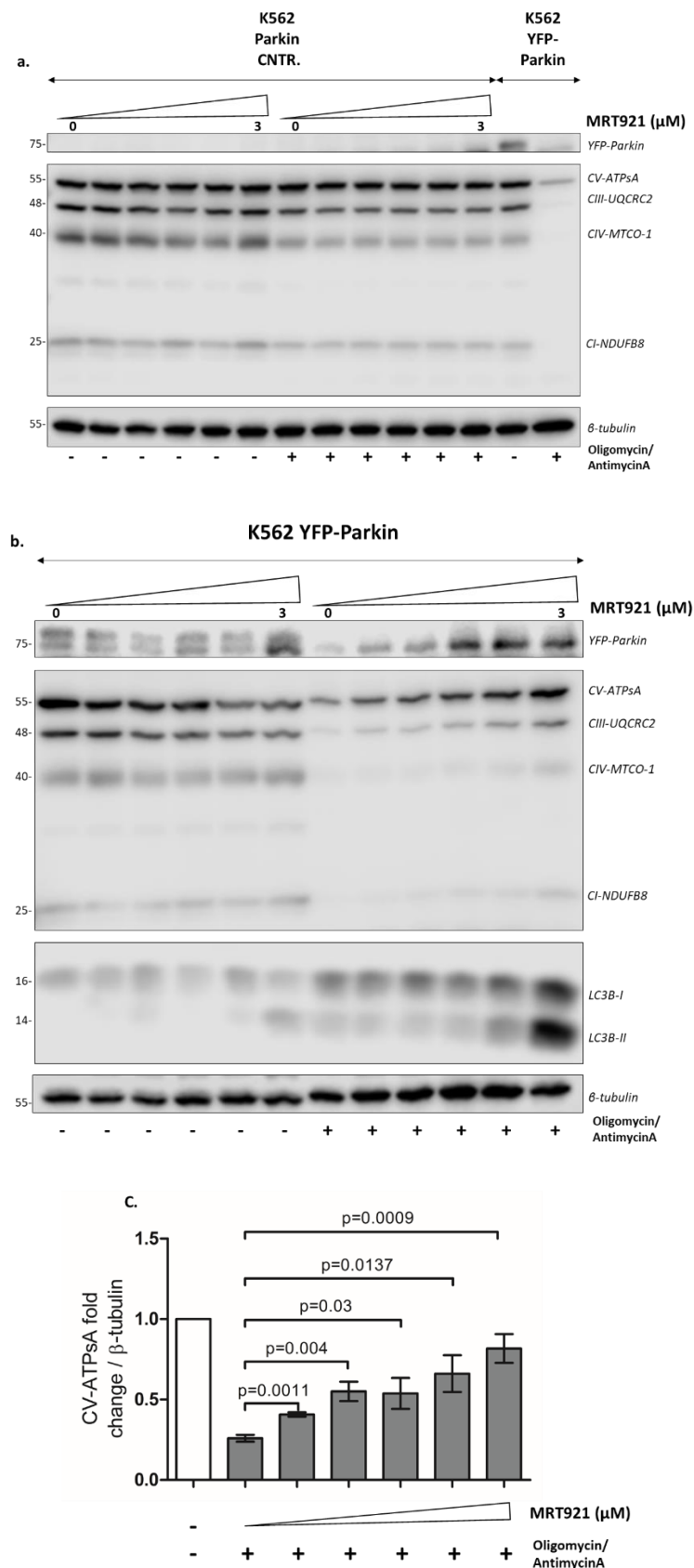


**Figure 4.5: MRT921 inhibits Parkin-dependent mitophagy**

Representative western blot analysis showing mitochondrial complexes levels following 24 h treatment with 1 nM of antimycin A, 1 nM of oligomycin and increasing concentration (0-3  $\mu\text{M}$ ) of MRT921 in K562 control (a) and YFP-Parkin cells (b). CV-ATPsA fold change relative to UT Mean  $\pm$  S.E.M. P values were calculated using unpaired Student T-test. n=3 independent experiment (a) and n=4 independent experiments (b).

#### **4.2.5 MRT921 treatment increases accumulation of mitochondria and increases oxidative metabolism in CML cells**

Here we aim to assess if MRT921-mediated mitophagy inhibition correlates with changes in mitochondrial quantity and function.

Based on our previous findings, we performed these studies using 1  $\mu\text{M}$  MRT921 to reduce undesired off target effects. Following 72 h treatment using 1  $\mu\text{M}$  MRT921, mitochondrial mass was measured using the fluorescent dye MitoTrackerGreen (MTG). As reflected by the representative histograms (**Figure 4.6a**), the mitochondrial content in CML cells was increased following treatment with MRT921 compared to untreated cells suggesting impairment in mitochondrial degradation. Furthermore, to assess if inhibition of mitophagy leads to changes in mitochondrial respiration following pharmacological ULK1/2 inhibition, we measured cellular OCR in real time in live cells following 72 h treatment with 1  $\mu\text{M}$  MRT921 (**Figure 4.6b**). Results show a significant increase in basal and maximal OCR following ULK1/2 inhibition, correlating with increased mitochondrial content (**Figure 4.6c, d**). ATP-linked OCR was also increased following inhibition of ULK1/2, although this did not reach statistical significance (**Figure 4.6e**).

Incompletely reduced oxygen in the mitochondrial electron transport chain can result in electron leakage that can give rise to superoxide anion, the most abundant ROS produced in mitochondria. An increase in basal mitochondrial respiration can lead to an increase in ROS<sup>231</sup>. We treated CML cells for 72 h with 1  $\mu\text{M}$  MRT921 and ROS levels were measured using MitoSOX, a fluorescent dye that specifically measures mitochondrial ROS. Results show that treatment with MRT921 significantly increased ROS (from 5 to 40%). Treatment with 3.7% H<sub>2</sub>O<sub>2</sub> for 1 h was used as a positive control, which results in 80% increase in ROS. NAC is an aminothiols and a precursor of cysteine and glutathione (GSH) and is considered as an important antioxidant<sup>232</sup>. Treatment with 100 nM NAC for 1 h reverted increased ROS to basal levels.

All together, these results showed that MRT921 treatment increased mitochondrial content, mitochondrial respiration and ROS levels, possibly through impairment of mitophagy.

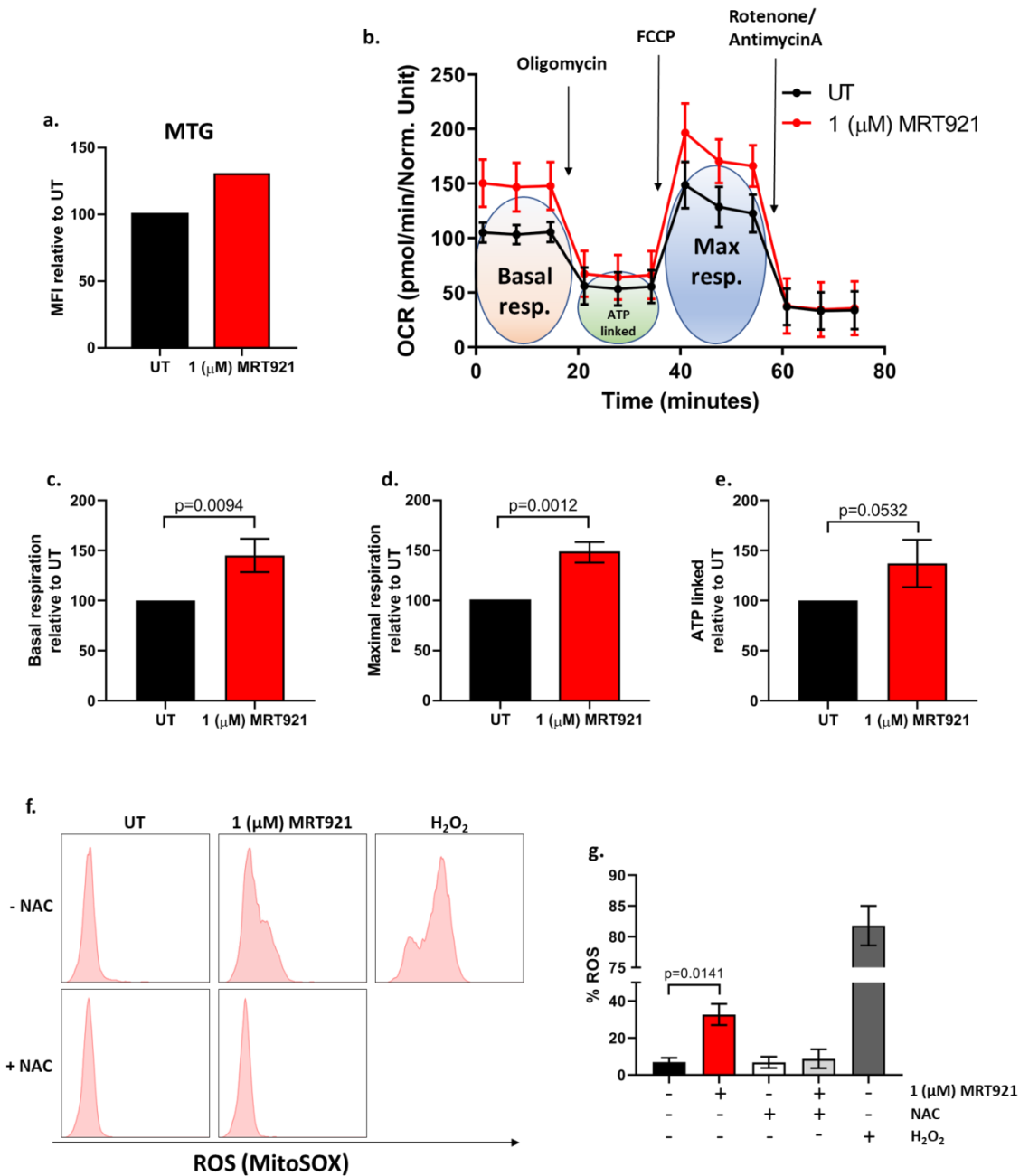


**Figure 4.6: MRT921 induces accumulation of mitochondria and affects mitochondrial metabolism**

Graph showing mean fluorescence intensity (MFI) of MTG stained cells following 72 h treatment with 1  $\mu$ M MRT921 (a). Representative OCR profile measured using Seahorse Mitostress Analyser following 72 h treatment with 1  $\mu$ M MRT921 (b). Graphs showing basal respiration relative to UT (c). Maximal respiration relative to UT (d). ATP linked relative to UT (e). Representative FACS plots showing measurements of ROS following 72 h treatment with 1  $\mu$ M MRT921 (f). Measurements of ROS following 72 h treatment with 1  $\mu$ M MRT921 (g) Mean  $\pm$  S.D. n=2 independent experiments for MTG measurements. n=3 independent experiments each. P values were calculated using unpaired Student T-test.

#### 4.2.6 MRT921 treatment reduces glycolytic rate in CML cells

Recent study highlights ULK1 as a regulator of glycolysis by directly activating or inhibiting glycolytic enzymes and by balancing glycolysis and pentose phosphate pathway (PPP) for NADPH production, preventing accumulation of ROS during stressful condition (such as amino acids starvation)<sup>145</sup>.

To further understand the metabolic changes in CML cells following inhibition of ULK1/2 using MRT921 we measured glycolysis using Seahorse Extracellular Flux analyser. Following 72 h treatment with 1  $\mu$ M MRT921, KCL22 exhibit a significant 30% decrease in basal glycolysis and glycolytic capacity (measured by extracellular acidification rate; ECAR) (Figure 4.7b, c).

#### 4.2.7 MRT921 treatment inhibits TKI-induced autophagy in CML

Inhibition of Parkin-dependent mitophagy using MRT921 suggested that it might represent a good candidate for inhibition of TKI-induced autophagy in CML cells.

To test this hypothesis, K562 and KCL22 cell lines were treated for 24 h with 1, 3 and 5  $\mu$ M of MRT921 and in combination with 2  $\mu$ M nilotinib. Western blot analysis on KCL22 indicated that nilotinib repressed phosphorylation of ULK1 on ser757 (activating ULK1) (Figure 4.8a). Accordingly, nilotinib treatment increased phosphorylation of ATG13 on ser318 and induced autophagy measured by reduction of p62 and increased conversion of LC3B-I to LC3B-II (Figure 4.8a). MRT921 treatment inhibited phosphorylation of ATG13 on ser318 and increased levels of p62 even at the lowest concentration, resulting in inhibition on TKI-induced autophagy (Figure 4.8a). Western blot analysis performed on K562 confirmed these data showing that treatment with MRT921 was inhibiting TKI-induced autophagy measured as accumulation of p62 (Figure 4.8b). Furthermore, accumulation of LC3B-II was observed when cells were treated with MRT921 alone

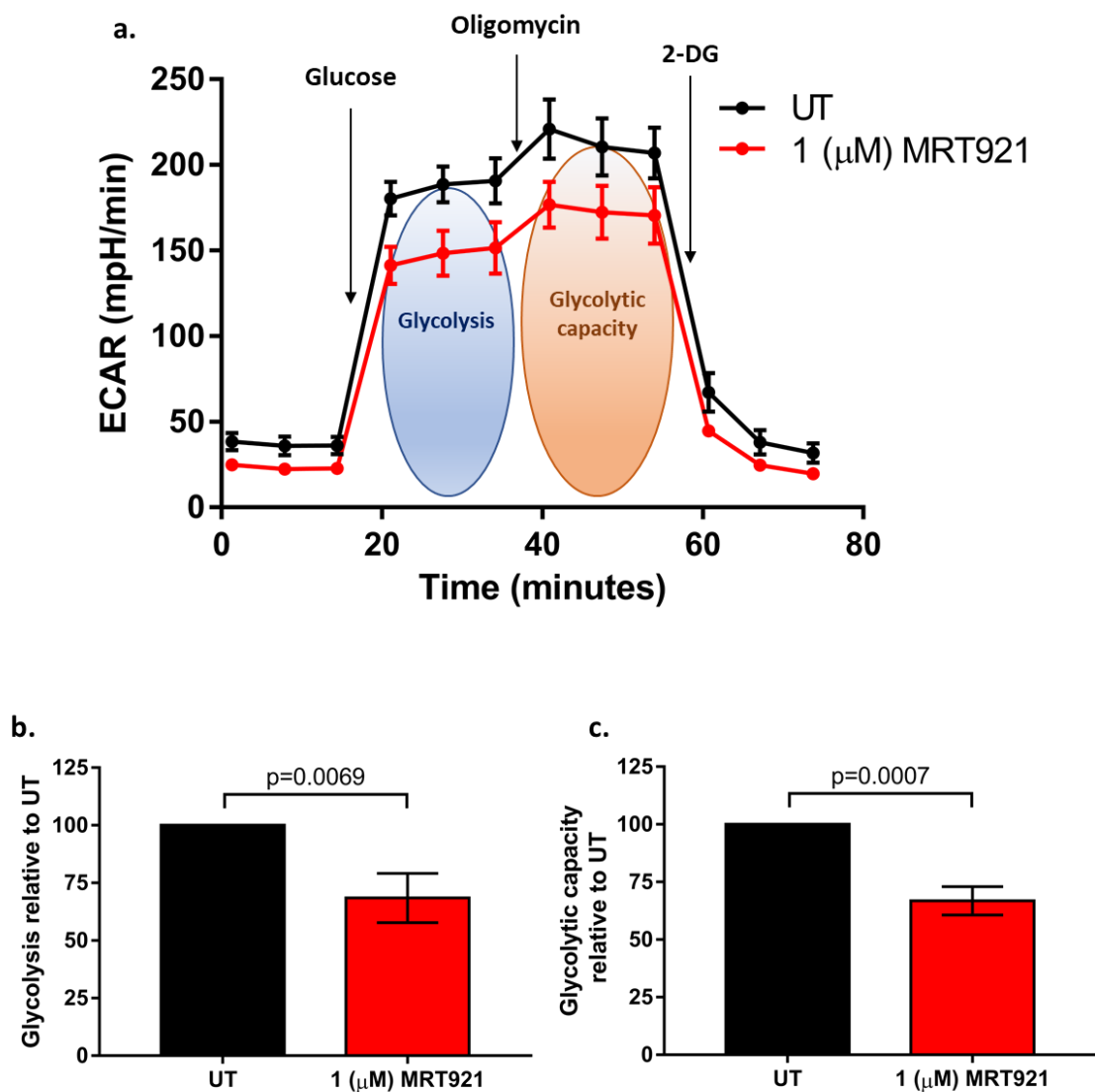


**Figure 4.7: MRT921 impairs glycolytic capacity in CML cells**

Representative ECAR profile measured using Seahorse Extracellular Flux Analyser following treatment with 1  $\mu$ M MRT921 for 72 h (a). Graphs showing glycolysis relative to UT (b). Glycolytic capacity relative to UT (c). Mean  $\pm$  S.D. n=3 independent experiments. P values were calculated using unpaired Student T-test.

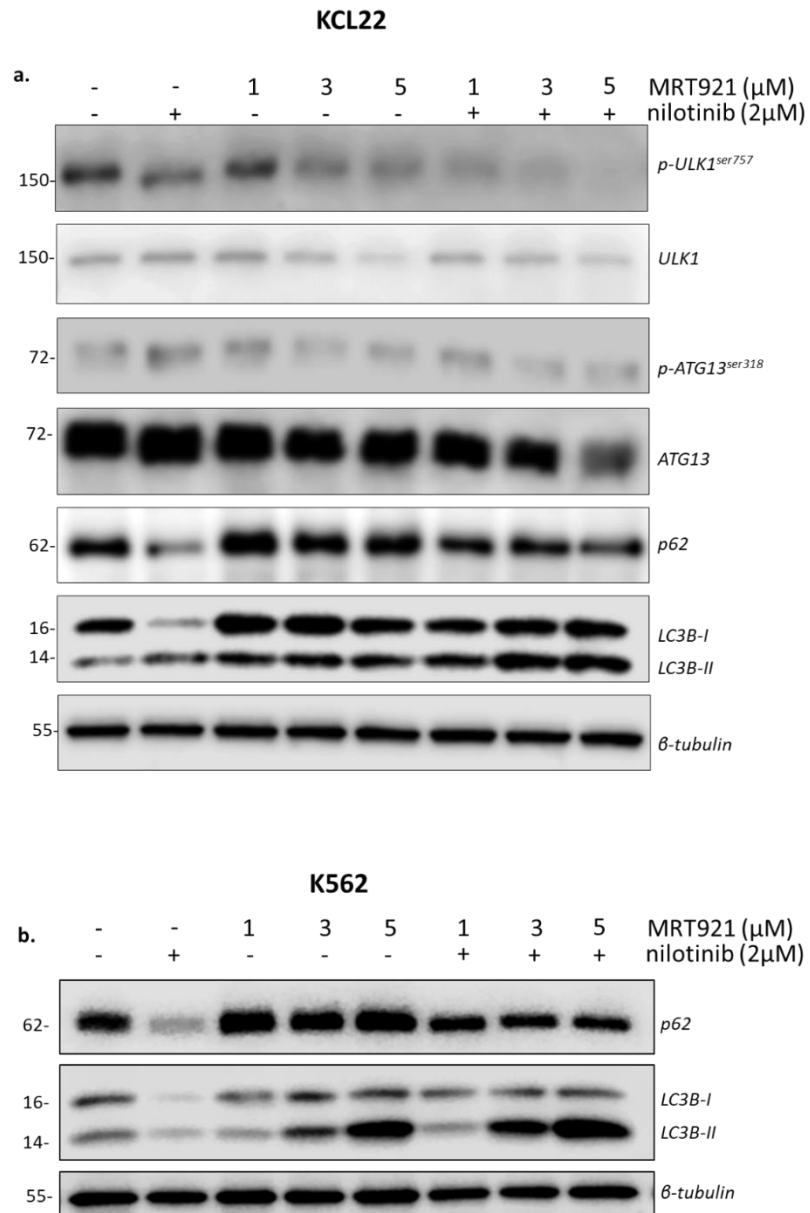


**Figure 4.8: MRT921 inhibits TKI-induced autophagy in CML cells**

Representative western blot analysis showing autophagy related protein expression following 24 h treatment using increased concentration of MRT921 alone and in combination with nilotinib in KCL22 (a) and K562 (b). n=2 independent experiments in KCL22 and n=1 in K562.

or in combination with nilotinib indicating accumulation of autophagosomes in botK562 and KCL22 (**Figure 4.8a, b**).

All together those results indicated that MRT921 inhibited TKI-induced autophagy at a concentration of 1  $\mu$ M in both K562 and KCL22 cells.

#### **4.2.8 MRT921 treatment enhances TKIs effect in targeting CML cells**

In the previous paragraph, we showed that MRT921 inhibited TKI-induced autophagy. Here we aim to investigate if inhibition of autophagy using MRT921 in combination with TKI potentiates TKI-induced death in targeting CML cells.

KCL22 cells were treated for 72 h with 1, 3 and 5  $\mu$ M of MRT921 and in combination with 300 nM nilotinib. As previously indicated, measurements of apoptosis show 80% increase with concentration of MRT921 above than 1  $\mu$ M (**Figure 4.9a**). While treatment with 300 nM nilotinib induced 30% apoptosis, combining nilotinib treatment with 1  $\mu$ M MRT921 induced 15% cell death compared to nilotinib alone (**Figure 4.9a**). No additive affect was measured with concentration above than 1  $\mu$ M in combination with nilotinib compared to single dose MRT921 treatment (**Figure 4.9a**). CFC assay show that 1  $\mu$ M MRT921 treatment reduces the number of colonies by 10%, compared to UT cells, while using 3 and 5  $\mu$ M concentration, a 25 and 90% reduction in number of colonies is seen, respectively (**Figure 4.9b**). Treatment with nilotinib results in 25% reduction in CFC ability, while combining nilotinib with 1  $\mu$ M MRT921 it further reduces CFC output by 20% (**Figure 4.9b**). In line with high levels of apoptosis following 3 and 5  $\mu$ M MRT921 treatment, the combination does not enhances nilotinib effect on CFC potential, which may be explained by the dramatic effect when used as a single agent (**Figure 4.9b**).

These results indicate that using 1  $\mu$ M MRT921 in combination with nilotinib enhances nilotinib effect in targeting CML cells.

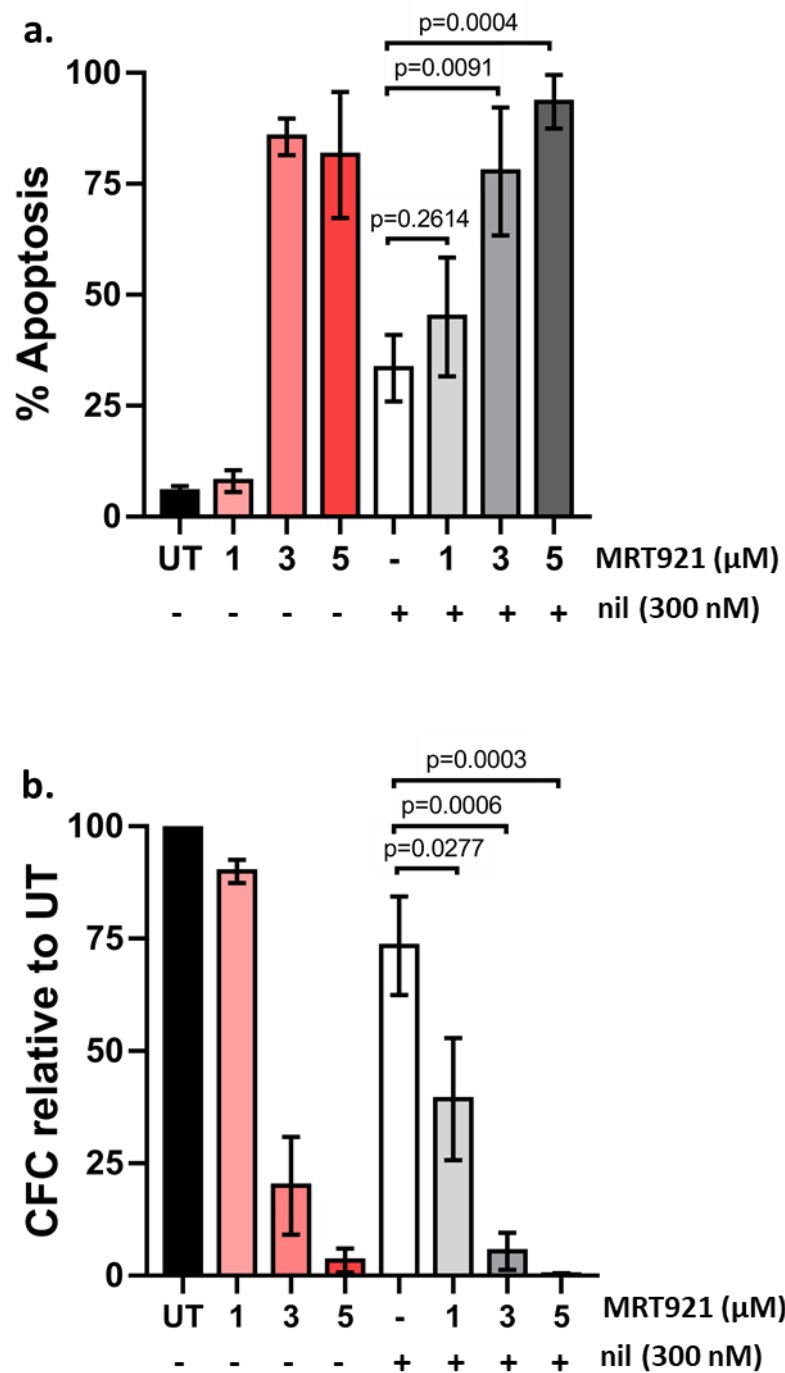


**Figure 4.9: Combination treatment using nilotinib and MRT921 targets CML cells**

Measurement of apoptosis following 72 h treatment using 1, 3 and 5 μM MRT921 in combination with 300 nM nilotinib (a). Measurement of CFC following 72 h treatment using 1, 3 5 μM MRT921 in combination with 300 nM nilotinib (b). Mean ± S.E.M. n=3 independent experiments. P values were calculated using unpaired Student T-test.

#### 4.2.9 MRT921 treatment affects cell viability of CD34<sup>+</sup> CML cells in a concentration dependent manner

To move to more clinically relevant *in vitro* model, we tested the effect of MRT921 on patient-derived CML cells.

We first aimed to establish EC<sub>50</sub> in mononuclear cells (MNCs) and stem cell-enriched (CD34<sup>+</sup>) CML cells. Following 72 h treatment using concentrations range between 0 and 10  $\mu$ M of MRT921, the calculated EC<sub>50</sub> was  $\approx$  100 nM (using MNCs from 3 independent patient samples) (**Figure 4.10a**). Using same patient samples, we also isolated more primitive CD34<sup>+</sup> cells. As for MNC, variability in responses of individual CD34<sup>+</sup> patient samples to MRT921 was evident with 50% growth inhibition of CD34<sup>+</sup> cells ranging between 4 and 300 nM when treated with MRT921 (**Figure 4.10b**). Interestingly, primitive patient-derived CML cells had increased sensitivity to MRT921 compared to CML cell lines.

To confirm cell viability data derived from treatment of CD34<sup>+</sup> CML cells and previous data using CML cell lines, we measured apoptosis and CFC following 72 h treatment using 5 different concentration of MRT921, specifically from 0.5 to 10  $\mu$ M. We used 10 nM omacetaxine, a cytotoxic protein translation inhibitor (used in some TKI-resistant CML patients), as a positive control to assess enhanced toxicity. Measurements of apoptosis, using CD34<sup>+</sup> cells derived from 3 CML patients, show that concentrations above 1  $\mu$ M of MRT921 enhanced apoptosis to almost 60% (similar to omacetaxine treatment) (**Figure 4.11a**). Likewise, concentration between 2.5 and 10  $\mu$ M of MRT921 inhibited ability of colony forming by almost 100% (**Figure 4.11b**). Similar results were obtained with treatment of omacetaxine.

Here we establish that MRT921 reduced cell viability in a concentration dependent manner in CD34<sup>+</sup> CML cells. Furthermore, concentrations above 1  $\mu$ M dramatically increased apoptosis and reduced CFC in CML cells, which may result from unspecific inhibitory effects when using elevated concentrations of MRT921.

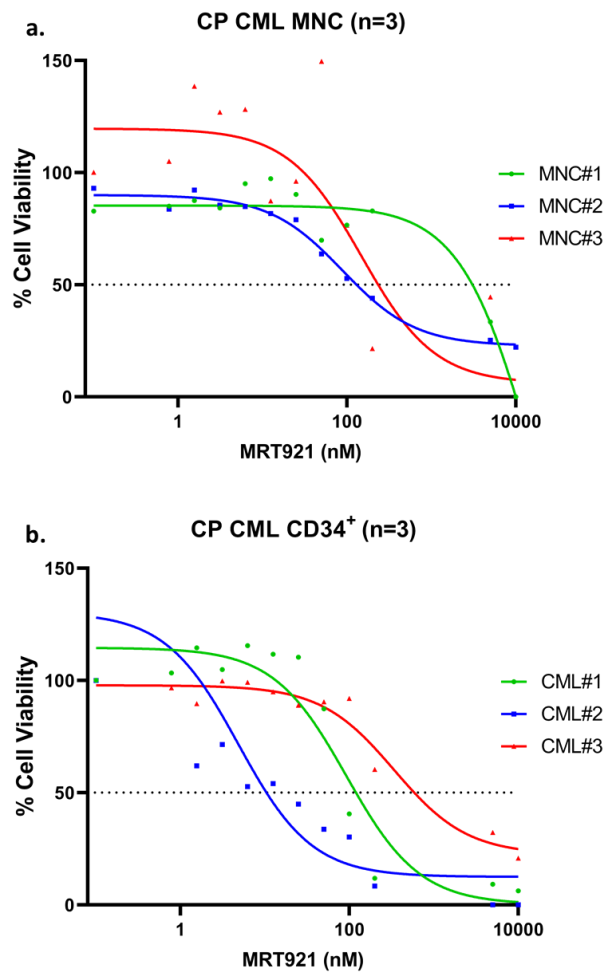


**Figure 4.10: MRT921 effect on inhibition of growth of CML CD34<sup>+</sup> cells**

Measurements of proliferation in patient-derived CD34<sup>+</sup> cells upon exposure to increased concentrations of MRT921. n=3 CD34<sup>+</sup> CML samples (a). Measurements of proliferation in patient-derived MNC cells (b) upon exposure to increased concentrations of MRT921. n=3 MNC CML samples.

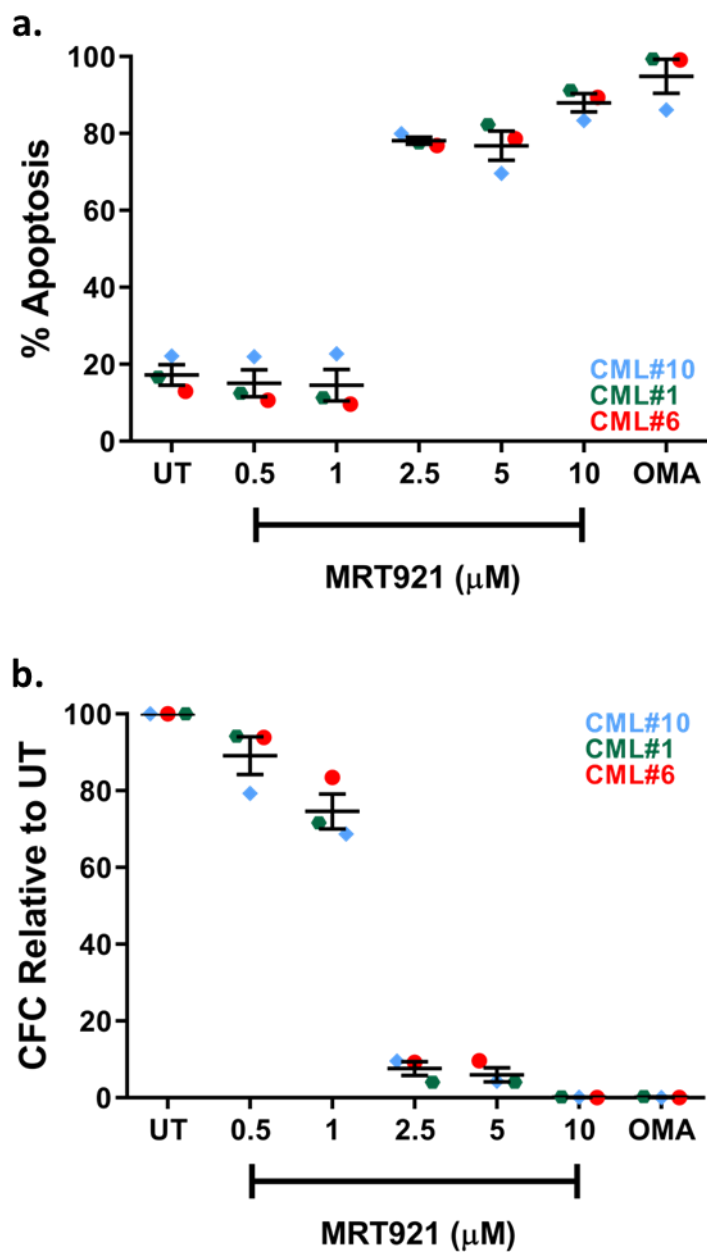


**Figure 4.11: MRT921 induces apoptosis and inhibits CFC in a concentration dependent manner in CML cells**

Measurements of cell death upon 72 h treatment with increased concentration of MRT921 using Annexin V and 7AAD staining (a). Colony number following 72 h drug treatment using increased concentration of MRT921 (b). n=3 CML samples. All data are presented as Mean ± S.E.M.

#### 4.2.10 MRT921 inhibits TKI-induced autophagy in CD34<sup>+</sup> CML cells

Encouraged by our results in cell lines, we tested the effect of MRT921 on TKI-induced autophagy in CD34<sup>+</sup> CML cells at 1 and 2.5  $\mu$ M. CD34<sup>+</sup> CML cells were treated for 24 h with 1 and 2.5  $\mu$ M of MRT921 and in combination with 2  $\mu$ M nilotinib. Analysis of p62 in 4 individual CML patient samples shows that treatment with nilotinib reduces p62 levels (**Figure 4.12a, b**). However, treatment with MRT921 significantly inhibited the nilotinib effect on p62 levels (**Figure 4.12a, b**). Furthermore, measurements of additional autophagy substrates as NBR1<sup>233</sup>, an autophagy receptor that contains LC3 and ubiquitin (Ub)-binding domains, ARA70<sup>234</sup>, androgen receptor associated protein 70, was decreased following treatment with nilotinib (**Figure 4.12a**). As well, we revealed in 1 of the 4 samples an increase in phosphorylation of ATG13 on ser318 following treatment with nilotinib (**Figure 4.12a**). However, combining nilotinib with MRT921 rescued TKI-induced autophagy, measured by increasing levels of previously mentioned autophagic markers (**Figure 4.12a**).

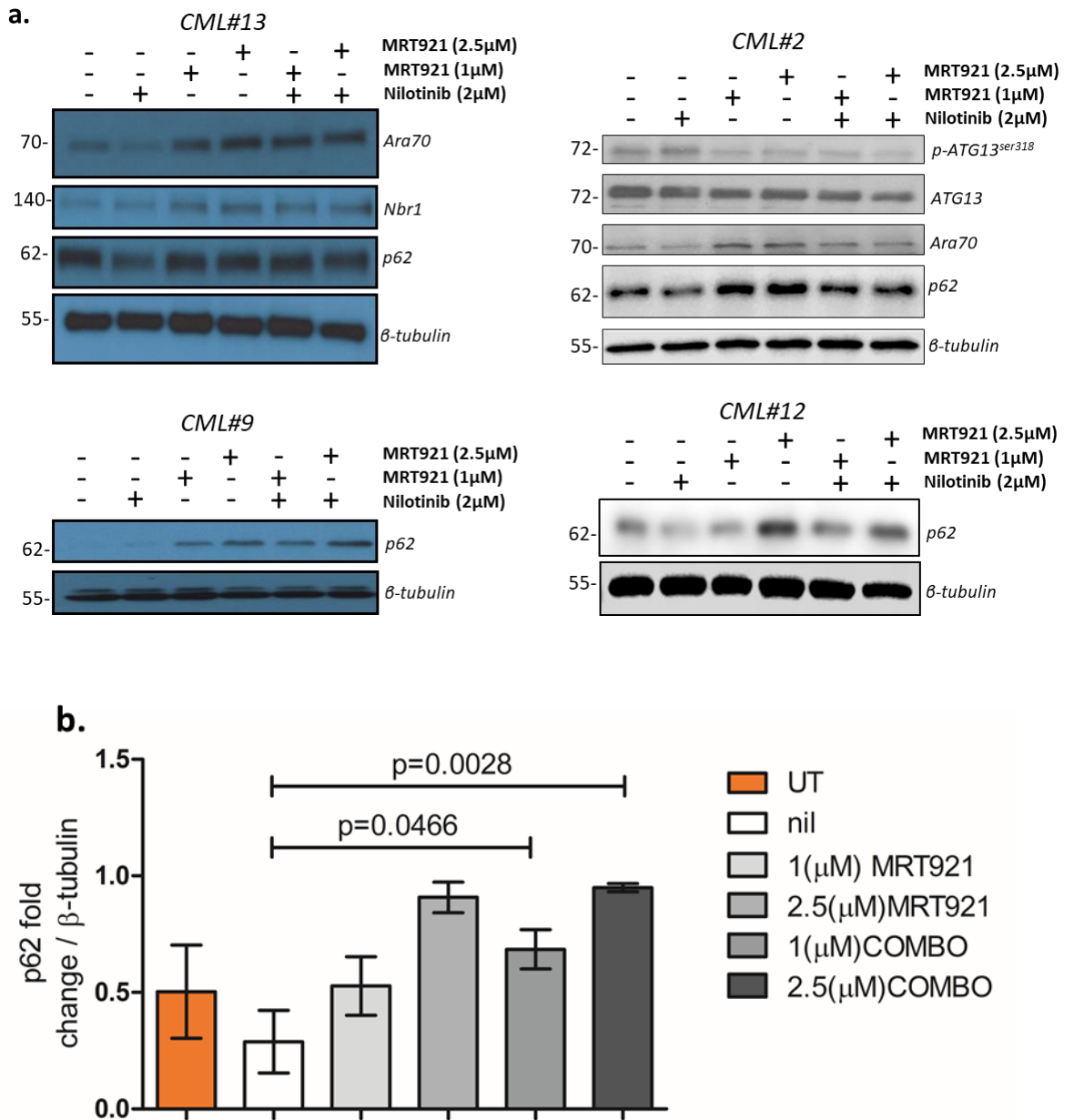


**Figure 4.12: MRT921 inhibits TKI-induced autophagy in patient-derived CD34<sup>+</sup> CML cells**

Western blot analysis of autophagic markers following 24 h treatment with 1 and 2 µM of MRT921 and combination with 2 µM nilotinib (a). p62 fold change Mean  $\pm$  S.E.M. n=4 CML samples. P values were calculated using unpaired Student T-test (b).

#### 4.2.11 MRT921 enhances nilotinib-induced cell death in CD34<sup>+</sup> cells

We next aimed to assess if MRT921-mediated of autophagy inhibition would lead to enhancement in TKI-induced LSPCs eradication. CD34<sup>+</sup> CML cells were plated for 72 and 96 h in presence of MRT921, nilotinib or the combination, and the percentage of Annexin V/ 7AAD positive cells evaluated by flow cytometry at day 3 and day 6. Analysis at day 3 indicated that using 1  $\mu$ M MRT921 as a single agent did not show any increase in apoptosis (**Figure 4.13a, b**). As expected, 3  $\mu$ M MRT921 induced 60% cell death (**Figure 4.13a, b**). Nilotinib treatment induced 45% apoptosis which increased to 60% when combined with 1  $\mu$ M MRT921 (**Figure 4.13a, b**). Similar results were obtained at day 6 with no further increase in apoptosis compared to day 3 (**Figure 4.13c**). The effect of the combination of nilotinib with ULK1/2 inhibition was assessed performing CFC assay. As for measurements of apoptosis, treatment with 1  $\mu$ M MRT921 did not significantly reduce the number of CFC (**Figure 4.14a, b**). Toxicity effect was evaluated when MRT921 was used at 3  $\mu$ M with almost 100% reduction in CFC (**Figure 4.14a, b**). Treatment with nilotinib reduced CFC of 50% which was enhanced in combination with 1  $\mu$ M MRT921 (**Figure 4.14a, b**).

To complement these results and further characterise the effect of inhibition of ULK1 in primitive stem cells, we performed an LTC-IC assay. CD34<sup>+</sup> CML cells were treated for 6 days using MRT921 alone and in combination with nilotinib, followed by co-culture with feeder cells and CFC assay. Analysis in primitive LSPCs indicates that 1  $\mu$ M MRT921 treatment significantly reduces CFC derived from primitive cells (**Figure 4.14c**). Strikingly, the effect of nilotinib, which reduces CFC following LTC-IC assay by 60%, was further reduced by 90% when combined with MRT921 (**Figure 4.14c**).

Taken all together, these results indicate that inhibition of ULK1/2 using MRT921 enhances nilotinib effect in targeting CD34<sup>+</sup> CML cells. Furthermore, we show

## Chapter 4 Using MRT921 to target CML LSPCs

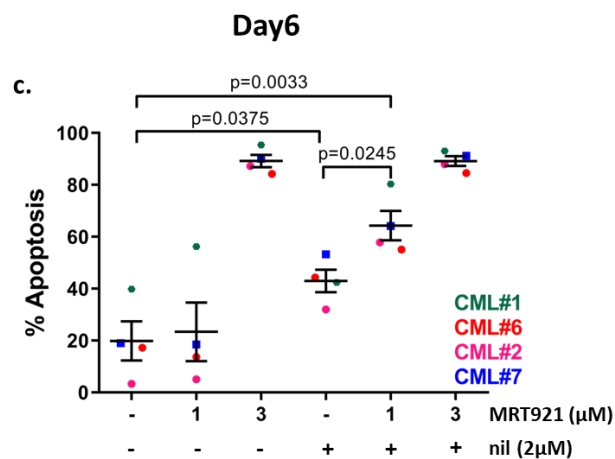
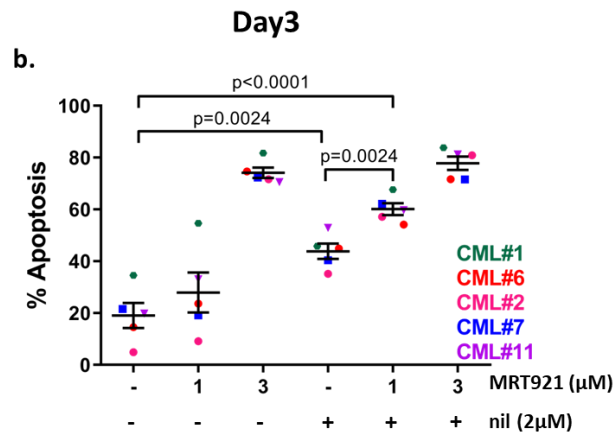
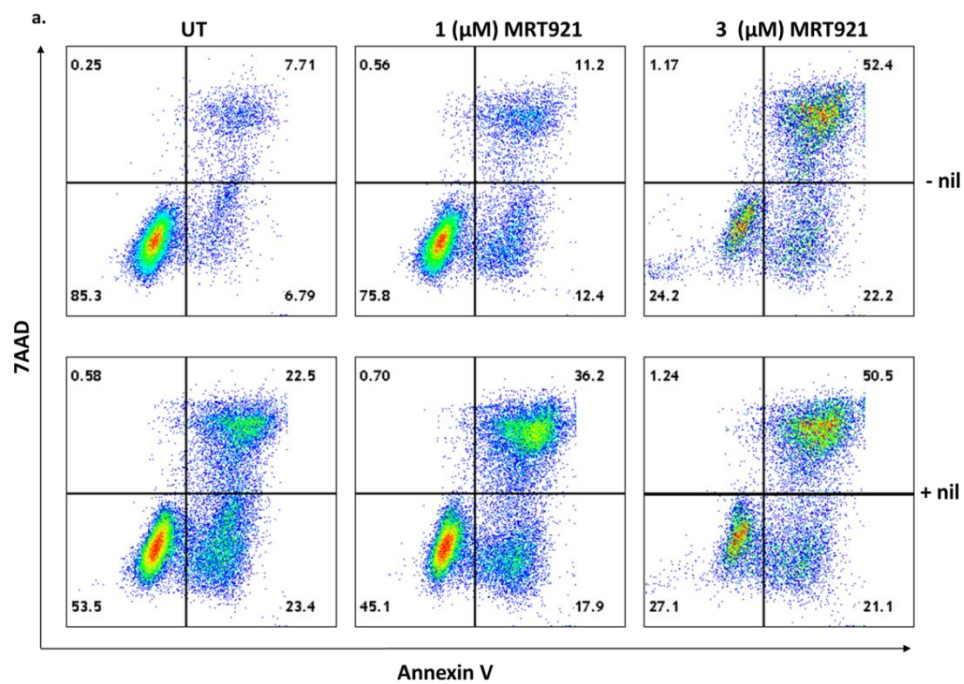


**Figure 4.13: MRT921 targets CD34<sup>+</sup> CML cells in combination with nilotinib**

Representative FACS plots showing measurements of apoptosis following 72 h treatment using MRT921 alone and in combination with nilotinib (a). Measurements of apoptosis following MRT921 treatment alone or in combination with nilotinib after 3 (b) or 6 (c) days. Mean ± S.E.M. n=5 CML samples. P values were calculated using unpaired Student T-test.

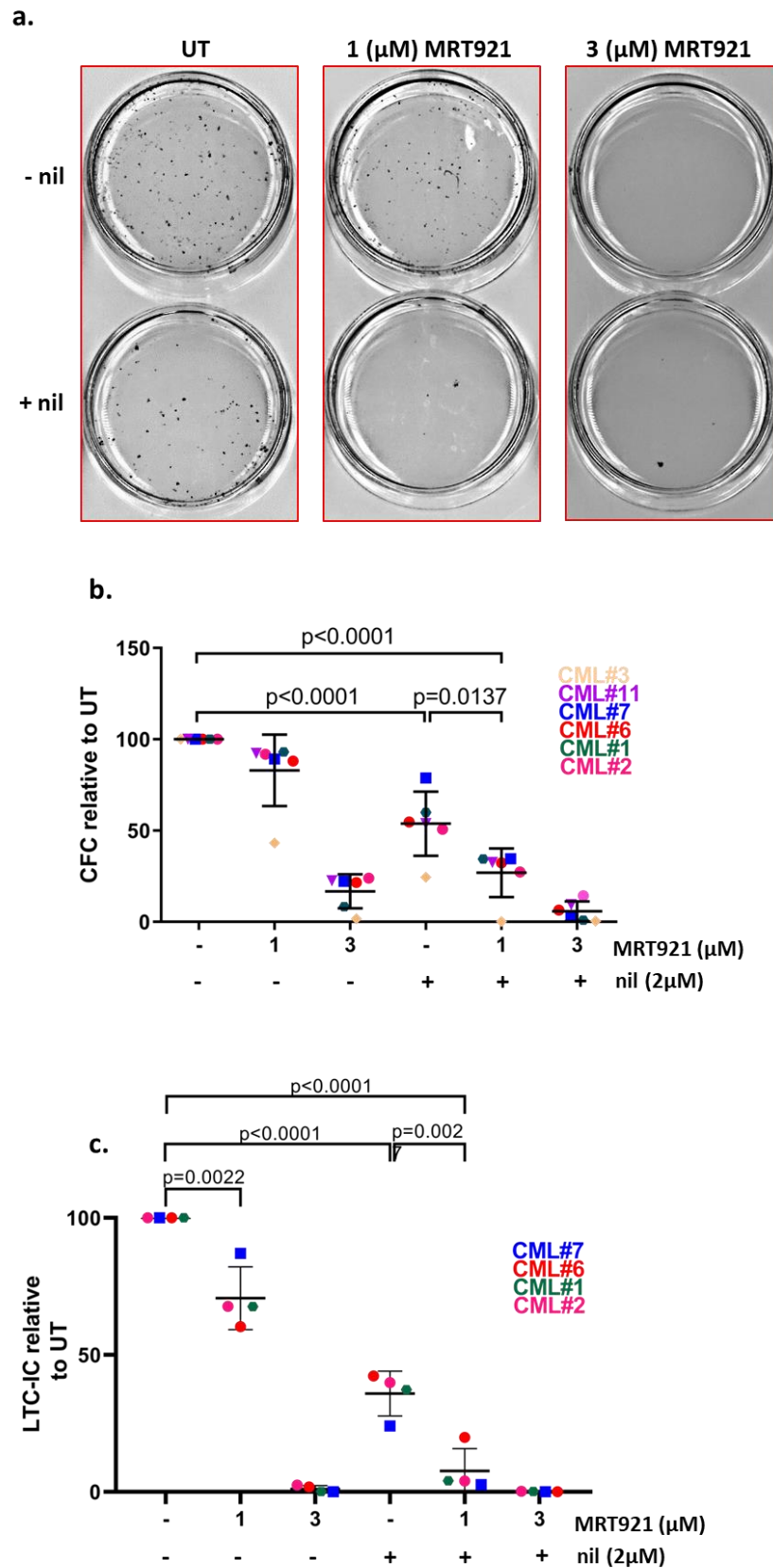


**Figure 4.14: MRT921 targets LSPCs**

Representative CFC pictures following 72 h treatment using MRT921 alone and in combination with nilotinib (a). CFC relative to UT following MRT921 treatment alone or in combination with nilotinib (b). CFC relative to UT following LTC-IC using MRT921 treatment alone or in combination with nilotinib for 6 days (c). Mean  $\pm$  S.E.M. n=6 CML samples for CFC and n=4 CML samples for LTC-IC. P values were calculated using unpaired Student T-test.

that combination treatment significantly enhances nilotinib effect in reducing LSPCs survival.

#### **4.2.12 MRT921 at 1 $\mu$ M has minimal effect on normal CD34<sup>+</sup> CML cells**

To investigate the selectivity of MRT921 against CML cells, (**Figure 4.13**), (**Figure 4.14**), we measured the effect of targeting ULK1 in normal HSPCs performing measurements of apoptosis and analysis on LT- and ST- HSPCs.

Following 72 h treatment using MRT921 as a single agent and in combination with nilotinib, measurements of Annexin V/7AAD positive cells show that 1  $\mu$ M MRT921 induces a 10% cell death (**Figure 4.15a**). As expected, nilotinib doesn't induce apoptosis in normal CD34<sup>+</sup> cells, however combination treatment with 1  $\mu$ M MRT921 has minimal residual effect (**Figure 4.15a**). Toxicity effect of 3  $\mu$ M was measured as a single agent or in combination with nilotinib, showing levels of apoptosis close to those induced by omacetaxine (OMA) used as a positive control (**Figure 4.15a**). To further confirm our data, we measured effects in progenitor and HSPCs. CFC assay confirmed cytotoxic effect of 3  $\mu$ M MRT921 alone or in combination of nilotinib (**Figure 4.15b, c**). Furthermore, 10% decrease in progenitors and 25% decrease in HSPCs was assessed following treatment with 1  $\mu$ M MRT921 (**Figure 4.15b, c**). Minimal effect was seen in both progenitor and HSCs when treated with nilotinib, with no additional effect when combined with 1  $\mu$ M MRT921 (**Figure 4.15b, c**).

Taken together, these results revealed that MRT921 has minimal effect on normal HSPCs alone or in combination with nilotinib when used at 1  $\mu$ M concentrations. However, 3  $\mu$ M concentrations are cytotoxic to normal progenitor and stem cells.

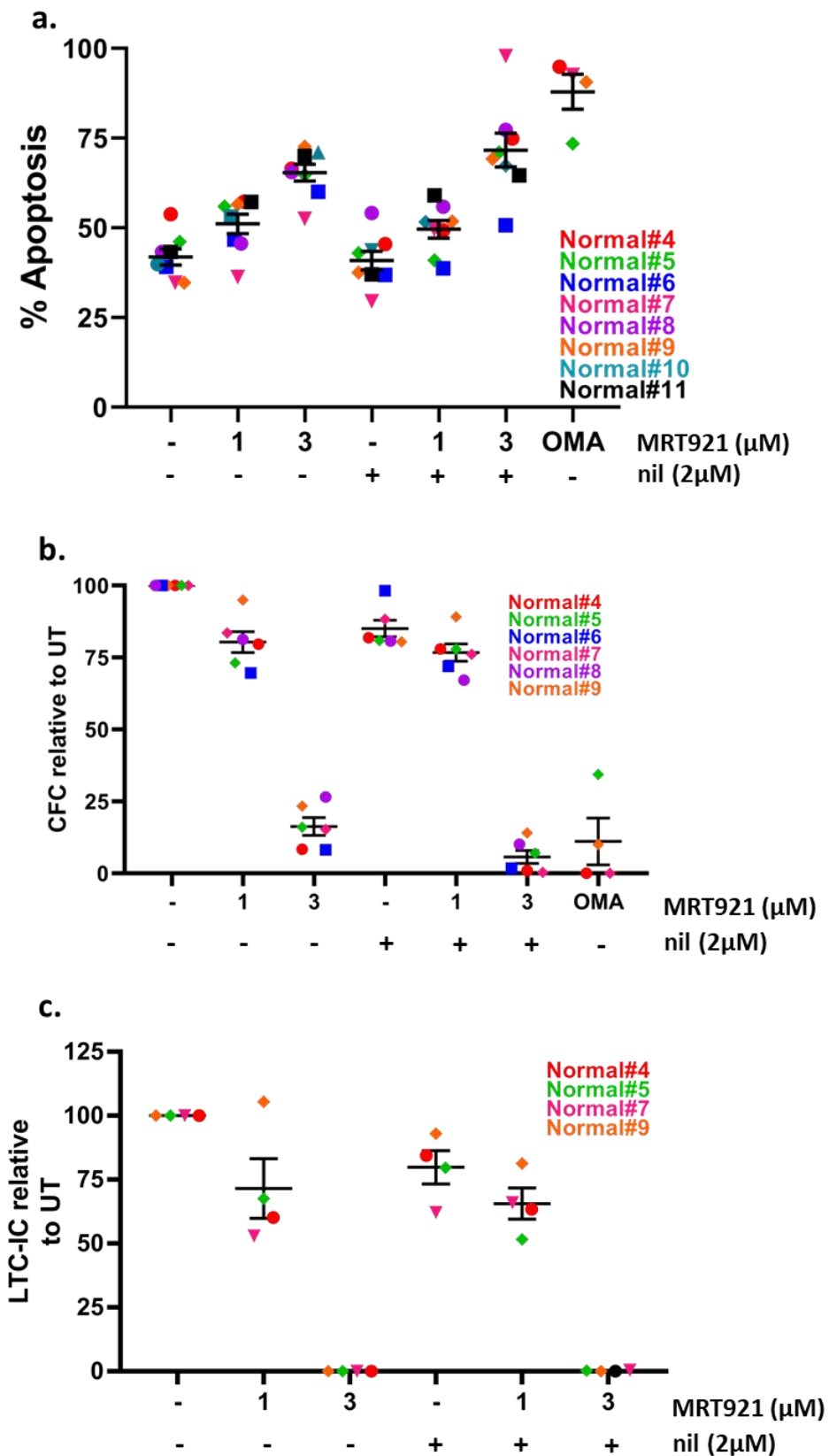


**Figure 4.15: Effect of MRT921 alone and in combination with nilotinib in CD34<sup>+</sup> normal cells**

Measurement of apoptosis following 72 h treatment using MRT921 alone and in combination with nilotinib (a). CFC relative to UT following MRT921 treatment alone or in combination with nilotinib (b). CFC relative to UT following LTC-IC using MRT921 treatment alone or in combination with nilotinib for 6 days (c). Mean  $\pm$  S.E.M. n=8 normal samples for apoptosis, n=6 normal samples for CFC and n=4 normal patients for LTC-IC. P values were calculated using unpaired Student-test.

### 4.3 Discussion

In this chapter we assessed the effect of MRT921, a ULK1/2 inhibitor, on survival of CML and normal cells, including HSPCs and LSPCs.

We first identified concentration that would induce cytotoxic effect in CML cell line and showed that 3 - 5  $\mu$ M concentrations of MRT921 almost targeted 100% of cells, measured by induction of apoptosis and reduction CFC potential. Using Parkin-enhanced mitophagy assay, we showed that MRT921 reduced mitochondrial clearance resulting an increase in numbers of mitochondria and an increase on OCR. However, even though basal and maximal respiration was significantly increased, no statistically significant changes measured in ATP-linked. Since we have previously shown that inhibition of ULK1/2 reduces clearance of mitochondria, the increase in OCR might be due to increase in uncleared mitochondria. However, since those mitochondria were addressed to mitophagy they might be damaged and even though they seem to consume oxygen, this might only result in proton leak through the electron transport chain and production of ROS within the complex IV, which does not translate in ATP production. However, further analysis is required to confirm this hypothesis.

In agreement with previous published data we observed a decrease in glycolysis following pharmacological inhibition of ULK1/2. We hypothesise that to sustain CML cells metabolism, the increase in mitochondrial respiration might be due to a reduced consumption of glucose. Furthermore, we also show that inhibition of ULK1/2 leads to an increase in mitochondrial respiration and increased ROS.

Furthermore, we show that MRT921 significantly impairs nilotinib-induced autophagy in CML cell lines and patient-derived CD34<sup>+</sup> cells, which enhanced nilotinib effect in targeting LSPCs. However, using ULK1 deficient cell lines we show that MRT921 still targets CML cells that don't express ULK1. This may be due to unspecific effect of MRT921. We hypothesized that since ULK1 deficient cells are still ULK2 competent, this might compensate ULK1 withdrawal. In this case, since MRT921 targets both ULK1 and ULK2, the effect we established in ULK1 deficient cells might be mediated by inhibition of ULK2. However, further studies are necessary to investigate the role of ULK2 in ULK1 competent and deficient cells and to clarify if the effects seen are ULK1 dependent or independent. In fact,

## Chapter 4 Using MRT921 to target CML LSPCs

MRT921 hits a wide range of kinases. Furthermore, to clarify the specificity of the results in a ULK1-dependent manner and of relevance on the LSPCs, it would have been interesting to perform ULK1 KO in CD34<sup>+</sup> cells. However, these experiments are still challenging due to limitation of patient-derived cells. Also, ULK2 has similar functions to ULK1 and could compensate the loss of ULK1. To assess no compensation effects due to ULK2 it would have been interesting to perform ULK2 KO and ULK1/ULK2 KO to address this question.

## Chapter 5 Using MRT403 to target CML LSPCs

## 5.1 Introduction

Thus far we have highlighted ULK1 as an important feature for autophagy activation during TKIs treatment in CD34<sup>+</sup> CML cells. In the previous chapter we investigated treatment using MRT921, a pre-clinical inhibitor of ULK1/2, in combination with nilotinib, a second generation TKI. Our results indicate that MRT921 prevents TKI-induced autophagy, enhancing nilotinib effect towards LSPCs eradication. However, unspecific effects and cyto-toxic effect were established using MRT921 treatment on ULK1 deficient cells and normal CD34<sup>+</sup> cells. We therefore tested the effect of derivatives of MRT921, with increased ULK selectivity, kindly provided by LifeArc.

In this chapter we investigate the effect of additional ULK1/2 inhibitors, MRT993, MRT016 and MRT403, in terms of cytotoxicity and unspecific targets, to identify the most suitable candidate to inhibit TKI-induced autophagy and target CML LSPCs in combination with TKIs.

Using Parkin-enhanced mitophagy we investigated the effect of new generation ULK1/2 inhibitors in inhibiting basal and stress-induced mitophagy, and then measured their ability in targeting TKI-induced autophagy. Based on our results, we proposed MRT403 as our candidate compound to combine with TKI and measure combination effect in targeting LSPCs *in vitro* and *in vivo*.

Furthermore, exploiting *in vitro* and *in vivo* assays, we investigated the effect of MRT403 in inducing differentiation of LSPCs. Previous published data indicate an increase in erythropoiesis in CML cells following pharmacological inhibition of autophagy and genetical removal of key autophagic markers such as ATG7<sup>189</sup>. Based on that, we investigated the role of ULK1 in inducing erythroid maturation and its potential in rescuing anaemia, a major undesirable effect occurring in CML patients.

## 5.2 Results

### 5.2.1 Validating new ULK1/2 inhibitors in CML

We previously used a pre-clinical ULK1/2 inhibitor that inhibits ULK1/2 kinases activity when used at a concentration of 1  $\mu\text{M}$ . In this paragraph we aim to test the effect of more specific ULK1/2 inhibitors to target CML cells. We treated KCL22 cell line for 72 h using a concentration range between 1 and 10  $\mu\text{M}$  of MRT921, MRT993, MRT403 and MRT016.

#### 5.2.1.1 Using new generation ULK1/2 inhibitors to target CML cells

Differently from (4.2.1), we measured cell viability exploiting the more widely used colorimetry Resazurin assay. We used MRT921 to measure accuracy and reproducibility of the data moving from XTT to Resazurin assay. Results show similar effects regarding inhibition of growth between the two assays with cells treated with MRT921 resulting in  $\text{EC}_{50} \approx 1 \mu\text{M}$  (Figure 5.1a). Instead, using MRT993 we established that  $\text{EC}_{50}$  was  $\approx 10 \mu\text{M}$  in KCL22 cells (Figure 5.1b) while using MRT403 or MRT016 we could not evaluate EC using a concentration range between 0 and 10  $\mu\text{M}$  because of no effect of the inhibitor on CML cells (Figure 5.1c, d).

To further investigate the effect of new ULK1/2 inhibitors in targeting CML cells and to assess if the effect was specifically through ULK1 inhibition, we measured apoptosis and CFC ability following treatment with increased concentration of MRT993, MRT403 and MRT016 in KCL22 WT and ULK1 deficient cells. Specifically, we treated KCL22 cells using 1, 3 and 5  $\mu\text{M}$  of the 3 inhibitors. Importantly, none of the drugs resulted in a significant increase in apoptosis except for MRT993, inducing 10% increase in cell death in WT cells (Figure 5.2a). Furthermore, no increase in cell death was seen using MRT403 or MRT016 in KCL22 ULK1 KO cells (Figure 5.2b). However, a 25% increase was measured following treatment with 5  $\mu\text{M}$  MRT993 (Figure 5.2b). Similar results were obtained measuring CFC ability. A 25% decrease in number of CFC was measured following treatment with 5  $\mu\text{M}$  MRT993, while only moderate decrease was seen following MRT403 or MRT016 treatment (Figure 5.2c). As well, ULK1 KO cells showed reduced number of CFC following treatment with 5  $\mu\text{M}$  MRT993, while marginal effect was seen using MRT403 or MRT016 (Figure 5.2b).

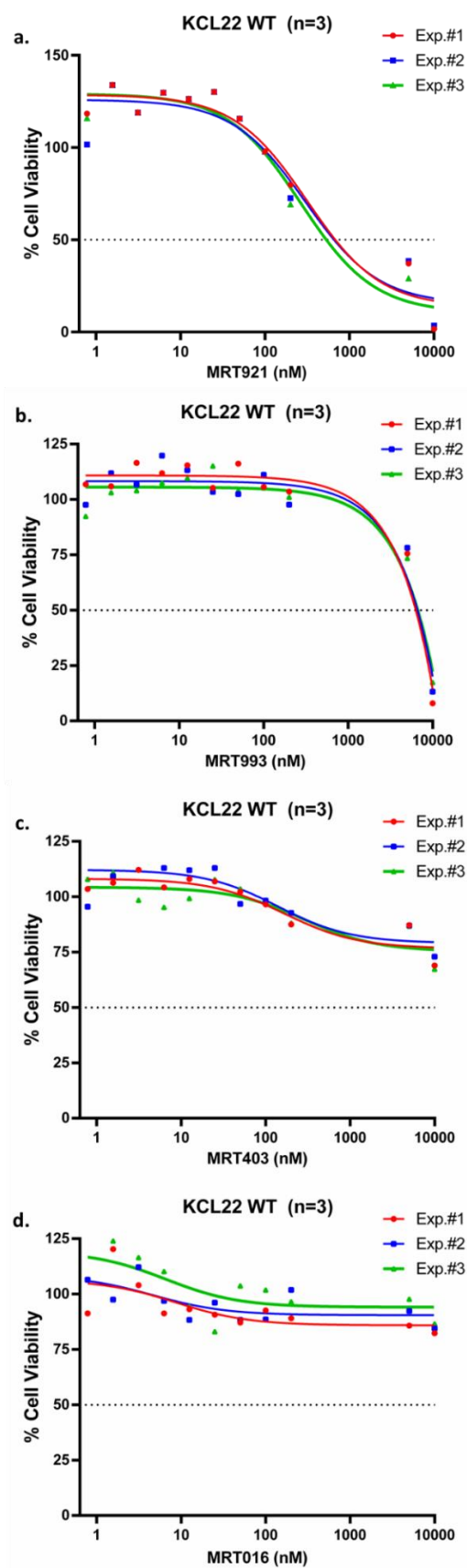


**Figure 5.1: New ULK1/2 inhibitor effect on viability of CML cells**

Measurements of proliferation in KCL22 TKI-sensitive upon exposure of increased concentrations of MRT993 (a), MRT403 (b) and MRT016 (c). n=3 independent experiments in each case.

## Chapter 5 Using MRT403 to target CML LSPCs

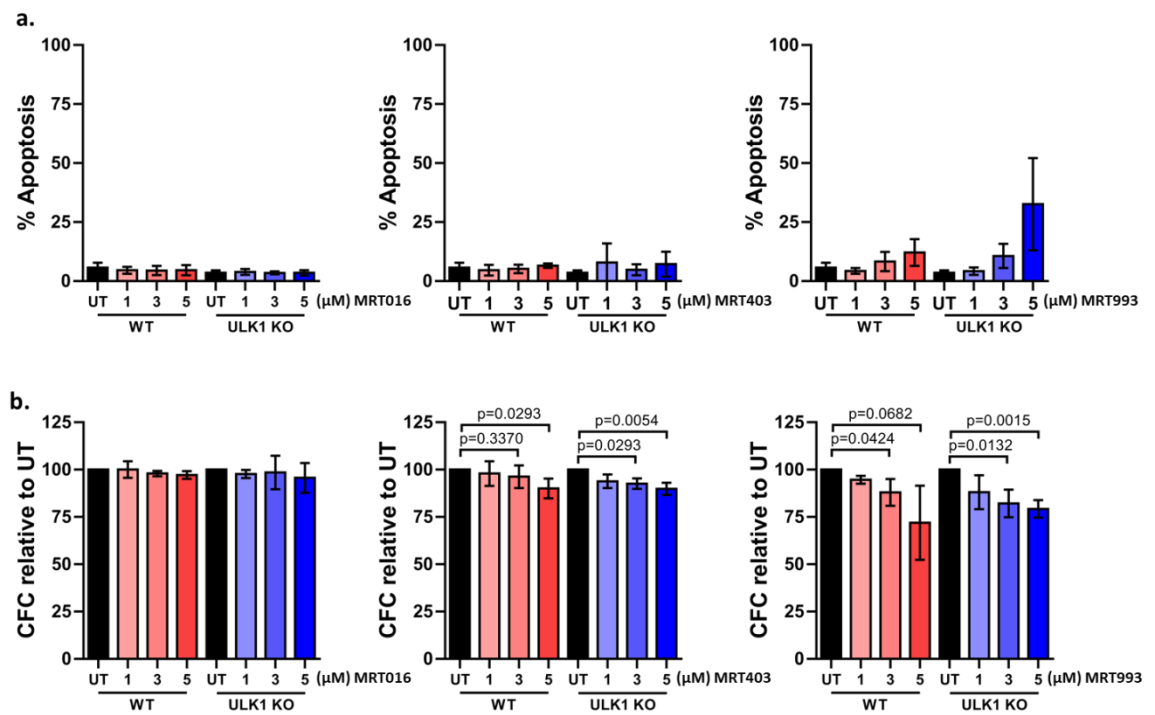


**Figure 5.2: Effect of ULK1/2 inhibition in KCL22 ULK1-deficient and ULK1-competent cells**

Measurements of apoptosis following 72 h treatment using 1, 3 e 5  $\mu$ M of MRT016, MRT403 and MRT016 in KCL22 WT (a). Measurements of apoptosis following 72 h treatment using 1, 3 e 5  $\mu$ M of MRT016, MRT403 and MRT993. in KCL22 ULK1 KO (b). Measurements of CFC following 72 h treatment using 1, 3 and 5  $\mu$ M of MRT016, MRT403 and MRT993 in KCL22 WT (c) and ULK1 KO cells (d). n=3 independent experiment in both cases.

Taken all together, these results indicate that KCL22 cell lines show reduced off-target effects in response to new ULK1/2 inhibitors compared to MRT921. However, increased apoptosis and reduced number of colonies was assessed at a concentration of 5  $\mu$ M MRT993 in both KCL22 WT and ULK1 deficient cells probably due to unspecific target or effect on ULK2.

### **5.2.1.2 Using Parkin-dependent mitophagy to measure autophagy flux following treatment with new generation ULK1/2 inhibitors**

We now aim, using parkin-dependent mitophagy assay to test the effect of MRT993, MRT016 and MRT403 in targeting basal and stressed induced clearance of mitochondria.

K562 YFP-Parkin cells were treated with a range of concentrations of MRT016, MRT993 and MRT403 between 0 and 3  $\mu$ M for 24 h, alone and in combination with antimycinA and oligomycin. In each case we show that treatment with antimycinA and oligomycin induces mitophagy measured by decreased levels of mitochondrial complexes (**Figure 5.3a, b**) and (**Figure 5.4a, b**). However, using MRT016 doesn't increase levels of mitochondrial complexes as a single agent or in combination with antimycinA and oligomycin, even at the highest concentration (**Figure 5.3a**). Using MRT993 has an effect as a single agent and in combination with antimycin A and oligomycin in inhibiting basal and stressed induced mitophagy, although only at the highest concentration (**Figure 5.3b**). However, a significantly change in basal and stress-induced mitophagy was observed using MRT403 at concentrations higher than 0.25  $\mu$ M (**Figure 5.4a, b**).

These results indicate that mitophagy is not inhibited using MRT016. Instead, MRT993 inhibited basal and stressed induced mitophagy at the highest concentration. Strikingly, MRT403 significantly inhibited basal mitophagy when used at 3  $\mu$ M and even at the lowest concentration of 0.5  $\mu$ M.

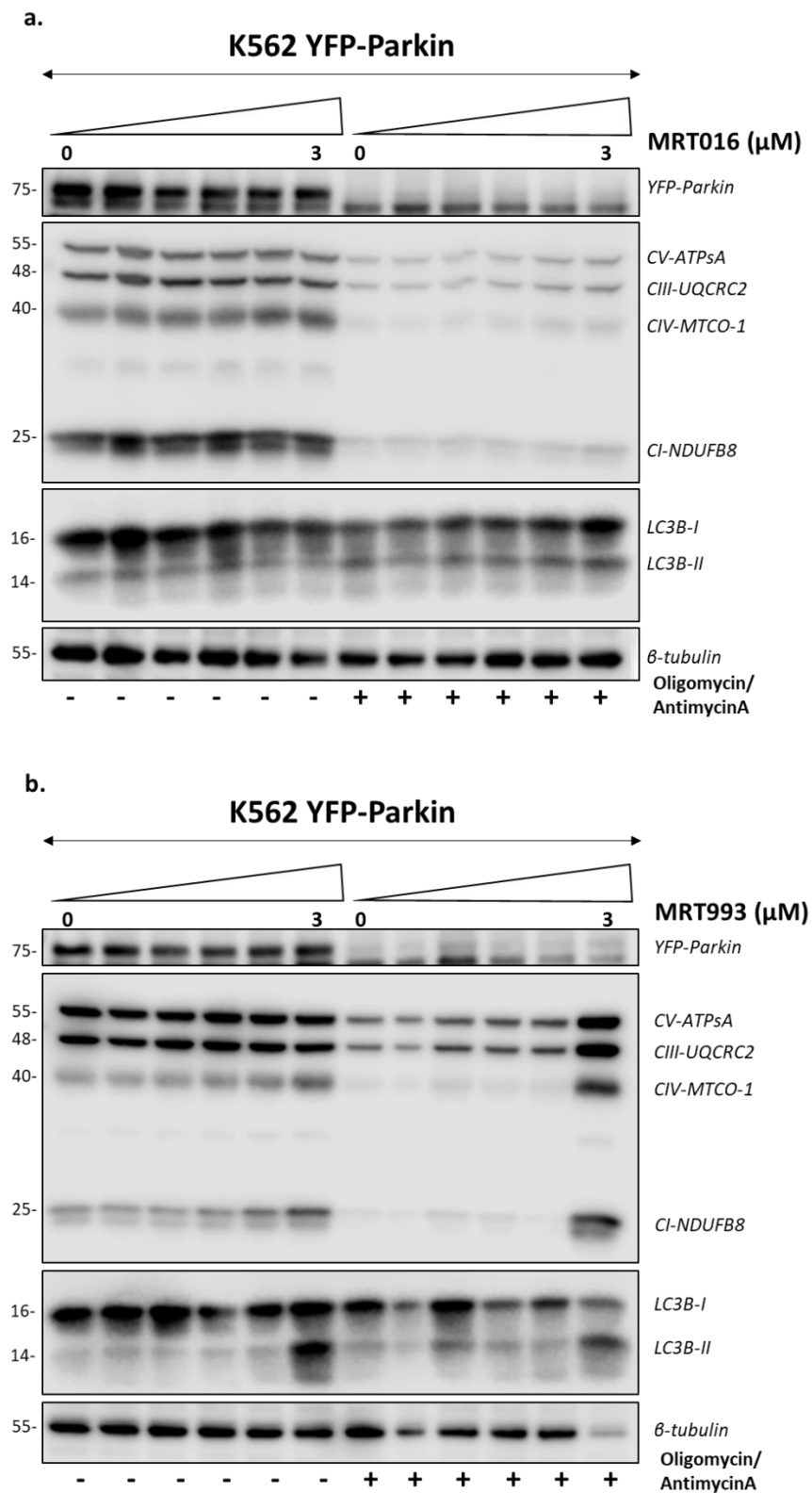


**Figure 5.3: Measurements of mitophagy inhibition using MRT993 and MRT016**

Representative western blot analysis showing mitochondrial complexes levels following 24 h treatment with 1 nM antimycinA and 1 nM oligomycin, alone or in combination with a range of concentration (0-3  $\mu\text{M}$ ) of MRT016 (a) and MRT993 (b) in K562 YFP-Parkin cells (b). n=2 independent experiment in each case

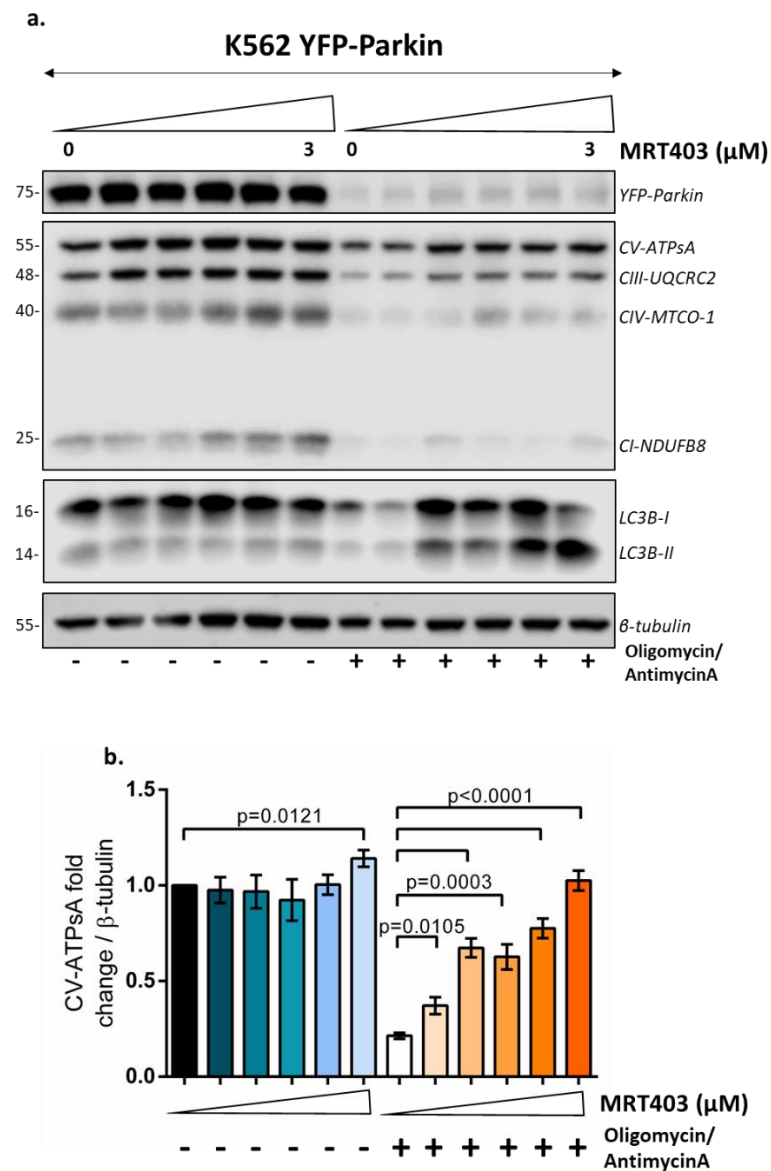


**Figure 5.4: Using MRT403 to inhibit Parkin-dependent mitophagy**

Representative western blot analysis showing mitochondrial complexes levels following 24 h treatment with 1 nM antimycinA and 1 nM oligomycin, alone and in combination with a range of concentration (0-3 μM) of MRT403 in K562 YFP-Parkin cells (a). CV-ATPsA fold change relative to UT Mean ± S.E.M. n=5 independent experiment. P values were calculated using unpaired Student T-test.

### 5.2.1.3 Using new generation ULK1/2 inhibitors to target TKI-induced autophagy

We have previously shown the efficacy of new generation of ULK1/2 inhibitors in targeting basal and stressed induced mitophagy. In this paragraph we aim to address our hypothesis that ULK1/2 inhibitors target TKI-induced autophagy.

To test this hypothesis, KCL22 cells were treated for 24 h with 1, 3 and 5  $\mu\text{M}$  of MRT993, MRT403 and MRT016 as single agents and in combination with 2  $\mu\text{M}$  nilotinib. Following cell lysates preparation, western blot analysis indicated that nilotinib repressed phosphorylation of ULK1 on ser757, activating ULK1 (**Figure 5.5a, b lane 2**). Furthermore, nilotinib increased phosphorylation of ATG13 on ser318 (**Figure 5.5a, b**) and induced autophagy measured by reduction of p62 and increased conversion of LC3B-I to LC3B-II (**Figure 5.5a, b and c**). Treatment using MRT993, even at the lowest concentration, reduced TKI-induced phosphorylation of ATG13 on ser318 and increased levels of p62 and LC3B-II (**Figure 5.5a**).

Treatment with MRT403 in combination with nilotinib, rescued reduction of phosphorylation of ULK1 on ser757, resulting in inhibition of ULK1 (**Figure 5.5a, b**). Furthermore, this revealed that MRT403 inhibited TKI-induced phosphorylation of ATG13 and increased levels of p62 and LC3B-II, even at 1  $\mu\text{M}$  concentration (**Figure 5.5b**).

However, MRT016 treatment increased phosphorylation on ULK1 on ser757 as a single agent and in combination with nilotinib but did not induce levels of p62 and LC3B-II when combined with nilotinib (**Figure 5.5c**).

All together these results indicated that MRT993 and MRT403 inhibit TKI-induced autophagy even at a concentration of 1  $\mu\text{M}$ . However, minimum effect is shown in targeting TKI-induced autophagy with MRT016.

## Chapter 5 Using MRT403 to target CML LSPCs

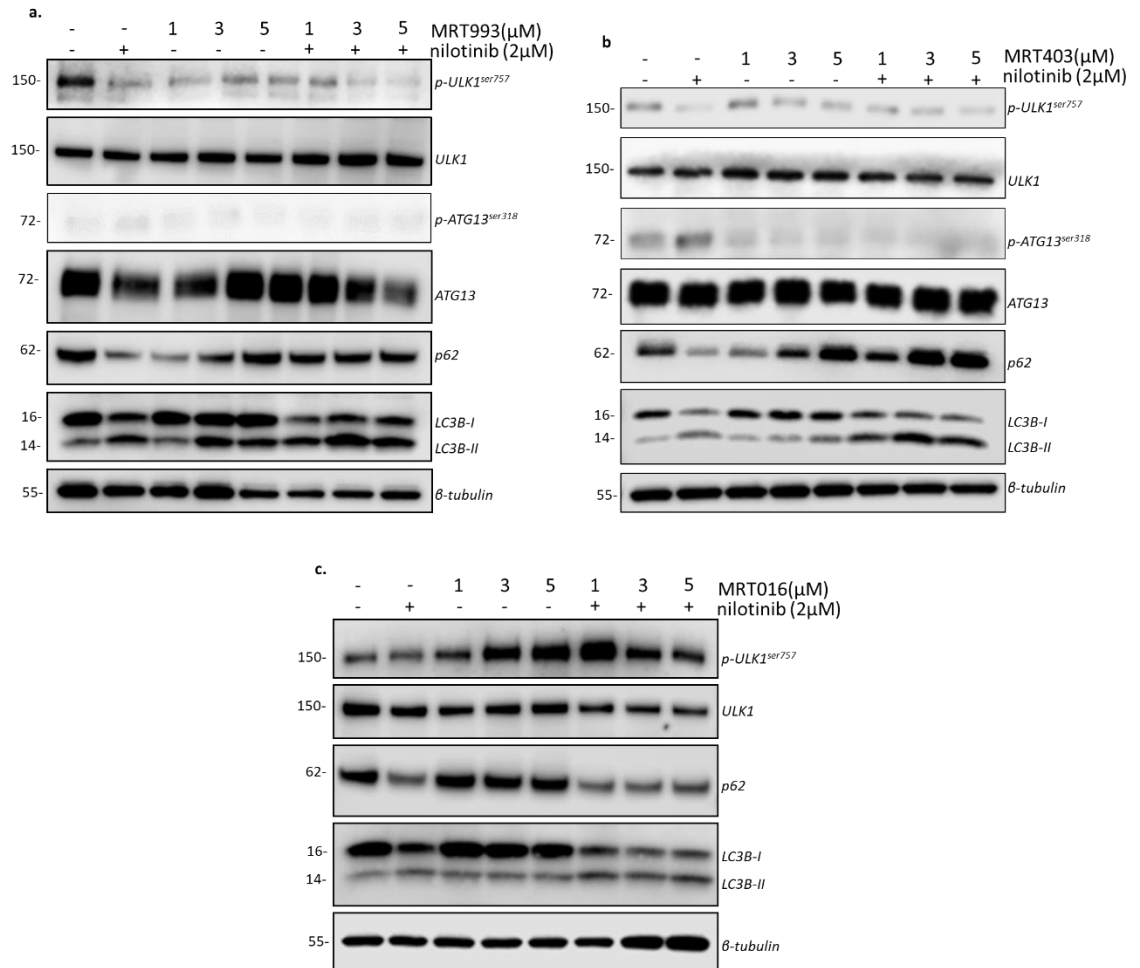


**Figure 5.5: Using new generation ULK1/2 inhibitors to target TKI-induced autophagy**

Representative western blot analysis showing autophagy related protein expression following 24 h treatment using increased concentration of MRT993 (a), MRT403 (b) and MRT016 (c) as single agents and in combination with nilotinib in KCL22 WT cells. n=2 independent experiments in each case.

#### **5.2.1.4 New generation of ULK1/2 inhibitors as a potential treatment to target CML cells**

In the previous paragraph we measured the effect of new generation ULK1/2 inhibitors in targeting TKI-induced autophagy. We now aim to investigate if inhibition of TKI-induced autophagy will increase TKI effect in targeting CML cells.

KCL22 cells were treated for 72 h with 1, 3 and 5  $\mu\text{M}$  of MRT016, MRT403 and MRT993 as single agents or in combination with 300 nM nilotinib. Treatment with nilotinib induced 30% increase in apoptosis (**Figure 5.6a**). Treatment with new ULK1/2 inhibitors as a single agent did not induce apoptosis except a 10% increase using 5  $\mu\text{M}$  MRT993 (**Figure 5.6a**). Combining nilotinib with new ULK1/2 inhibitors did not enhance apoptosis levels compared to nilotinib alone, except using 5  $\mu\text{M}$  MRT993 (**Figure 5.6a**). To further investigate combination treatment effect on longer-term cell death, we performed CFC assay, which revealed that nilotinib reduces CFC ability by 25% compared to untreated cells (**Figure 5.6b**). Combining nilotinib with 5  $\mu\text{M}$  MRT016 reduced CFC by further 10% (**Figure 5.6b**), although this was not statistically significant. Instead, 20% reduction in CFC was induced combining nilotinib with 3 and 5  $\mu\text{M}$  of MRT403 (**Figure 5.6b**). Using MRT993 in combination with nilotinib enhanced nilotinib effect in targeting CML cells even at the lowest concentration, resulting in 20% reduction at 1  $\mu\text{M}$  and 50% reduction at 3 and 5  $\mu\text{M}$  compared to nilotinib alone (**Figure 5.6b**).

#### **5.2.2 MRT403 further inhibits TKI-induced autophagy in ULK1 KO cells**

We have previously shown that MRT403 treatment in ULK1 deficient cells induces less death compared to MRT921. To investigate if MRT403 treatment further inhibited TKI-induced autophagy in ULK1 deficient cells, we treated KCL22 control and ULK1 KO cells with 3  $\mu\text{M}$  MRT403 alone and in combination with 2  $\mu\text{M}$  nilotinib. While treatment with MRT403 inhibited TKI-induced autophagy, measured as accumulation of p62 and LC3B-II in control cells, ULK1 deficient cells showed minimum signs of TKI-induced autophagy when compared to control cells (**Figure 5.7**).

## Chapter 5 Using MRT403 to target CML LSPCs

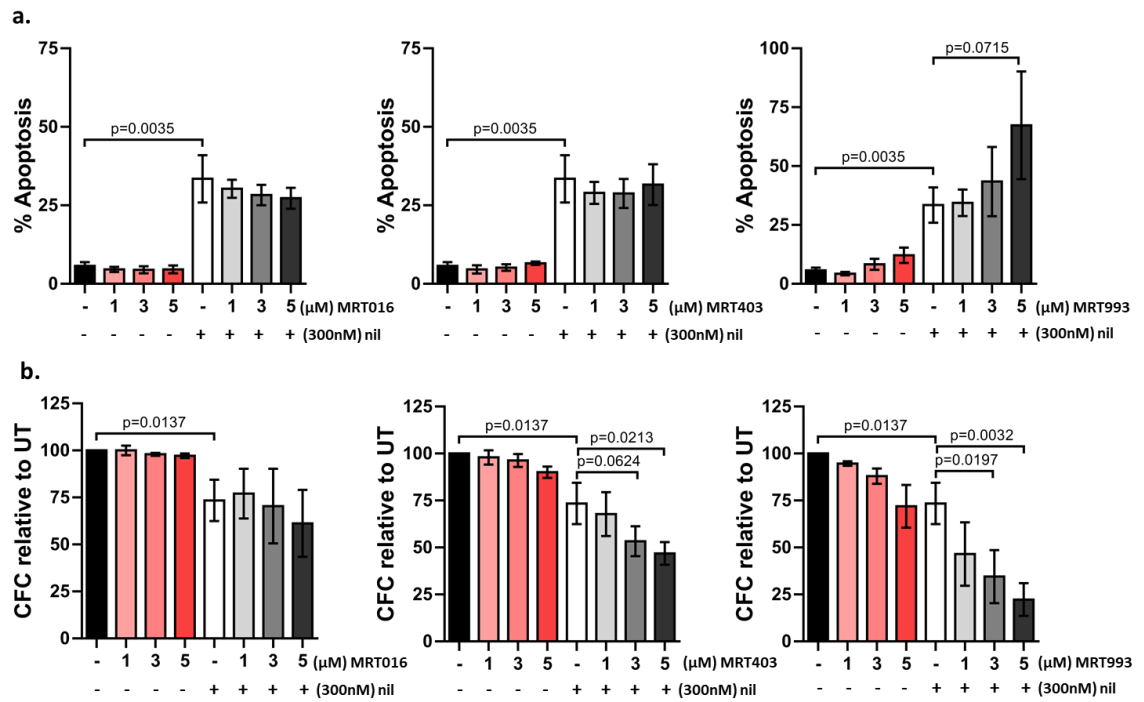


**Figure 5.6: Validating new ULK1/2 inhibitors in combination with nilotinib to target CML cells**

Measurement of apoptosis following 72 h treatment using 1, 3 and 5 μM MRT016, MRT403, MRT993 in combination with 300 nM nilotinib (a). Measurement of CFC following 72 h treatment using 1, 3 5 μM MRT016, MRT403 and MRT993 in combination with 300 nM nilotinib (b). Mean ± S.E.M. n=3 independent experiments.

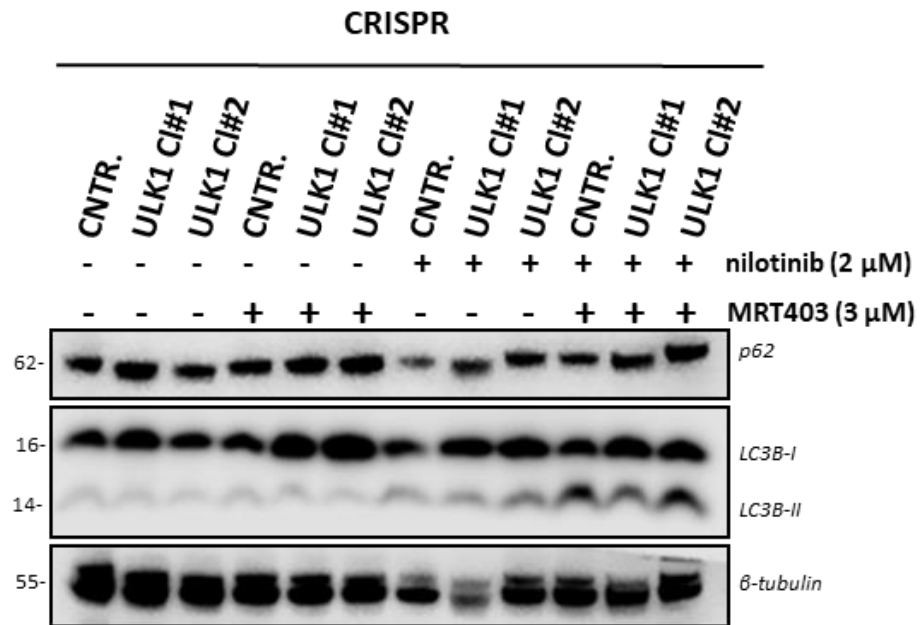


**Figure 5.7: Effect of MRT403 treatment is dependent on ULK1**

Representative western blot analysis of autophagy markers following treatment using 3  $\mu$ M MRT403 alone and in combination with 2  $\mu$ M nilotinib in KCL22 control and ULK1 deficient cells.

### 5.2.3 Discussion

Thus far we indicate that validating MRT993 in combination with nilotinib inhibited TKI-induced autophagy and potentiates nilotinib in targeting CML cells. However, inhibition of mitophagy was measured only when tested at 3  $\mu$ M with some unspecific effect shown on ULK1 deficient cells. Using MRT016 did not show inhibition of basal or stress-induced mitophagy or inhibition of TKI-induced autophagy. As well, no enhancement in targeting CML cells was measured. Instead, using MRT403 we show inhibition of basal and stress-induced mitophagy as well as increasing TKI-induced autophagy. Furthermore, we show that using MRT403 at 3  $\mu$ M enhances nilotinib effect in reducing CFC without affecting ULK1 deficient cells. We conclude that MRT016 is not a preferred candidate for combination studies to eradicate CML cells and that effect of MRT993 might be due to unspecific targets since cytotoxic effect are also measured in ULK1 KO cells. We indicate that MRT403 is the most suitable candidate to test in combination with TKI for further studies. Since our data don't show any cytotoxic effect on ULK1 KO cells even at 3  $\mu$ M of MRT403 and since 3  $\mu$ M significantly inhibited basal and stressed-induced mitophagy we decided to validate the concentration of 3  $\mu$ M MRT403 for further studies. Furthermore, LifeArc also indicated that MRT403 at a concentration of 3  $\mu$ M showed less nonspecific kinase inhibition compared to MRT921.

## 5.2.4 Using MRT403 to inhibit TKI-induced autophagy and targeting of LSPCs using

Prior to studying the effect of MRT403 in combination with TKI, we have investigated the role of ULK1 in CML conducting studies using CD34<sup>+</sup> CML cells and ULK1 deficient cells treated with MRT403 as a single agent.

### 5.2.4.1 MRT403 treatment inhibits basal mitophagy in CD34<sup>+</sup> CML cells

In this paragraph we aimed to study the effect of MRT403 treatment on basal mitophagy in CD34<sup>+</sup> patient-derived cells as a single agent and in combination with nilotinib.

Following treatment with 3  $\mu$ M MRT403 for 24 h, accumulation of mitochondrial complexes in CD34<sup>+</sup> CML samples (n=6) was assessed performing western blot analysis (**Figure 5.8**). MRT403 treatment consistently induced accumulation of complex II, or succinate dehydrogenase, located in the mitochondrial inner membrane, and complex IV, a transmembrane complex also known as cytochrome c oxidase (**Figure 5.8**). Accumulation of complex V, a transmembrane complex also known as ATP synthase, was detected in sample#15, #18, #1 and #6 following treatment with MRT403 (**Figure 5.8**). However, no increase in complex V is detected in sample#9 and a decrease is detected in sample#16 (**Figure 5.8**). Accumulation of complex III, a transmembrane complex also known as cytochrome c reductase, was detected in sample#18, #1, #9 and #6 (**Figure 5.8**).

Treatment with nilotinib showed more variable results. In some cases, nilotinib treatment induced mitophagy (i.e. sample#1) with visible reduction of mitochondrial complexes, while in other cases treatment had the opposite effect on mitochondrial protein levels (**Figure 5.8**). Combination treatment however, increased mitochondrial complex levels in all samples (**Figure 5.8**).

Thus far we have shown that pharmacological inhibition of ULK1/2 using MRT403, inhibited basal mitophagy in CD34<sup>+</sup> CML cells. However, the role of nilotinib in the context of mitophagy still remains unknown and further investigations are required to elucidate its effect, which might be more patient sample specific.

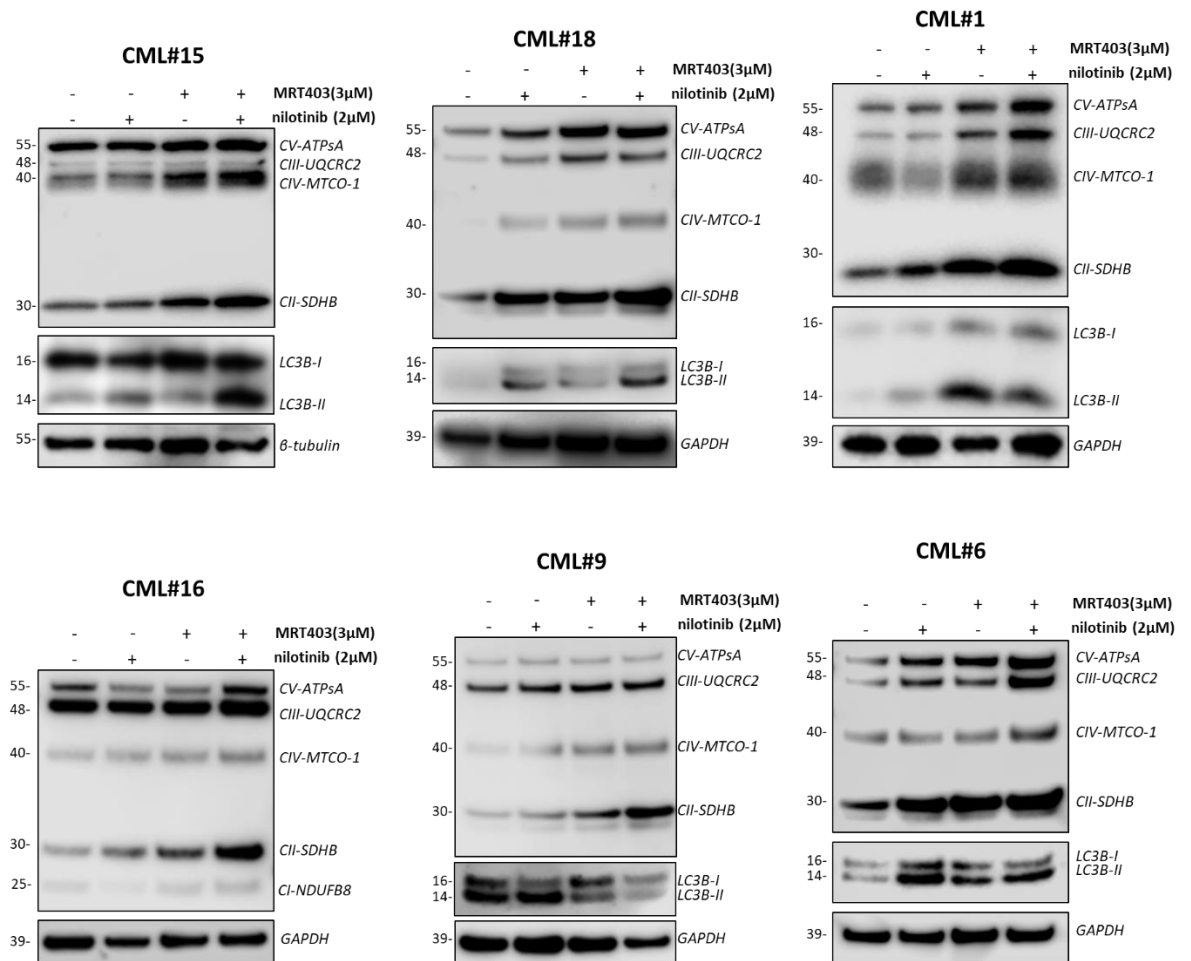


**Figure 5.8: MRT403 inhibits basal mitophagy in CD34<sup>+</sup> CML cells**

Western blot analysis showing mitochondrial complexes levels following 24 h treatment with 3 μM of MRT403, 2 μM of nilotinib and the combination of MRT403 and nilotinib.

### 5.2.4.2 MRT403 increases ROS and mitochondrial respiration in CD34<sup>+</sup> CML cells

In this section, we aim to assess if MRT403-mediated mitophagy inhibition correlates with changes in mitochondrial function.

To assess if inhibition of mitophagy leads to potential mitochondrial dysfunction and/or electron leakage following pharmacological inhibition of ULK1/2, we initially measured levels of ROS following 72 h treatment with 3  $\mu$ M MRT403 (

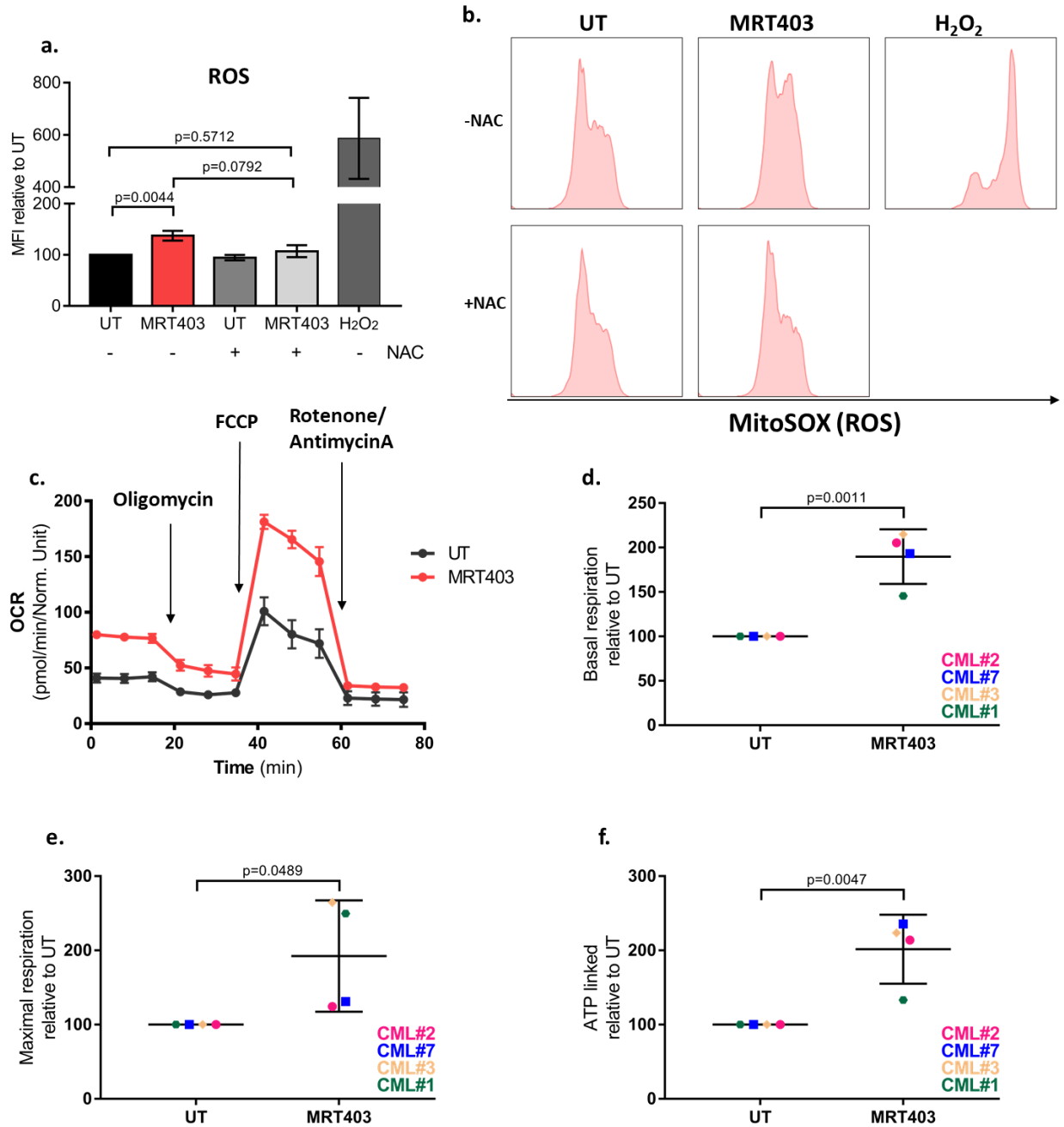


**Figure 5.9a, b).** Treatment with MRT403 significantly increased ROS levels compared to untreated cells (

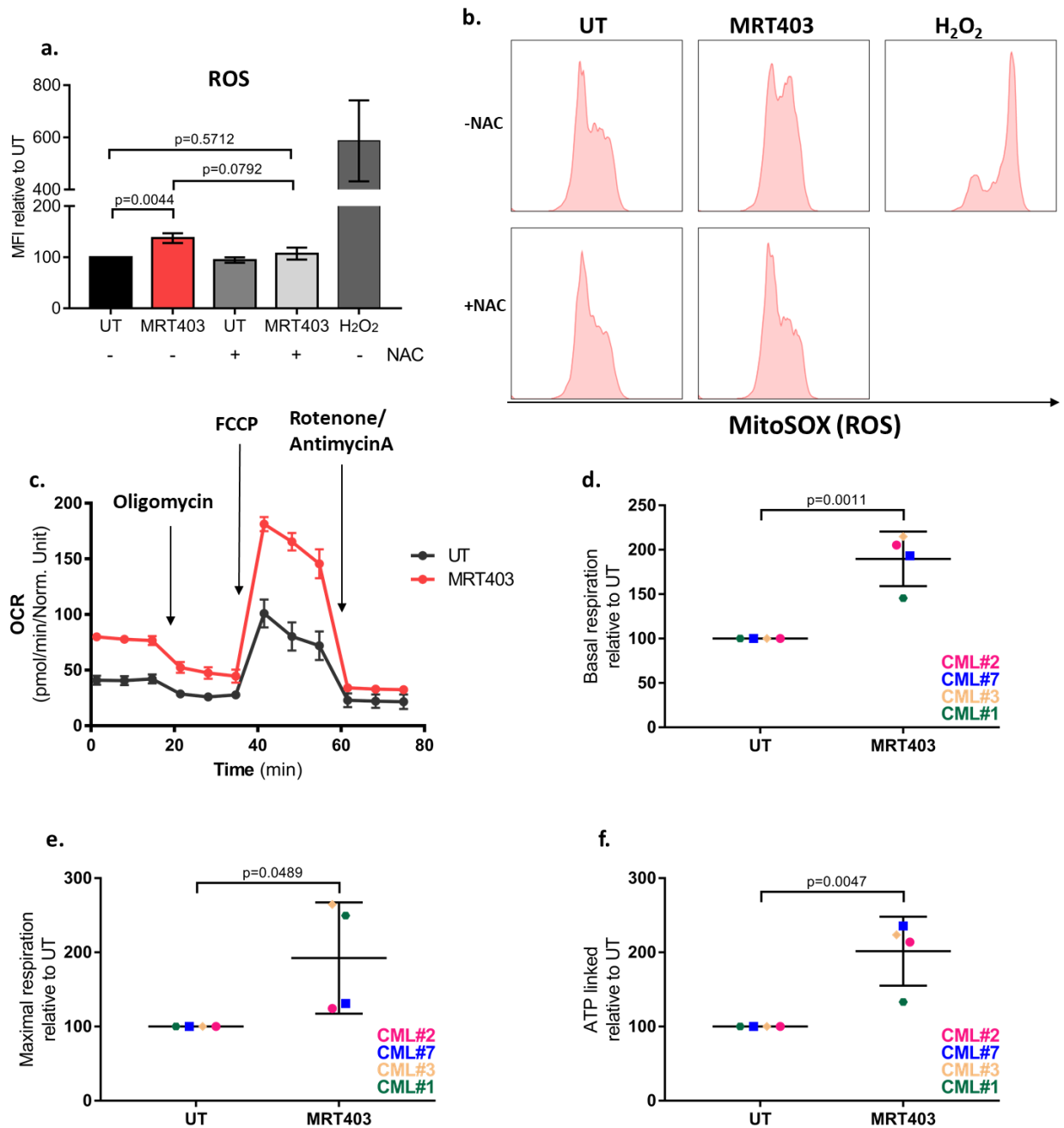


**Figure 5.9a, b).** As previously described in 4.2.5, treatment with 3.7% H<sub>2</sub>O<sub>2</sub> for 1 h was used as a positive control and treatment with 100 nM NAC for 1 h reverted ROS to basal levels (

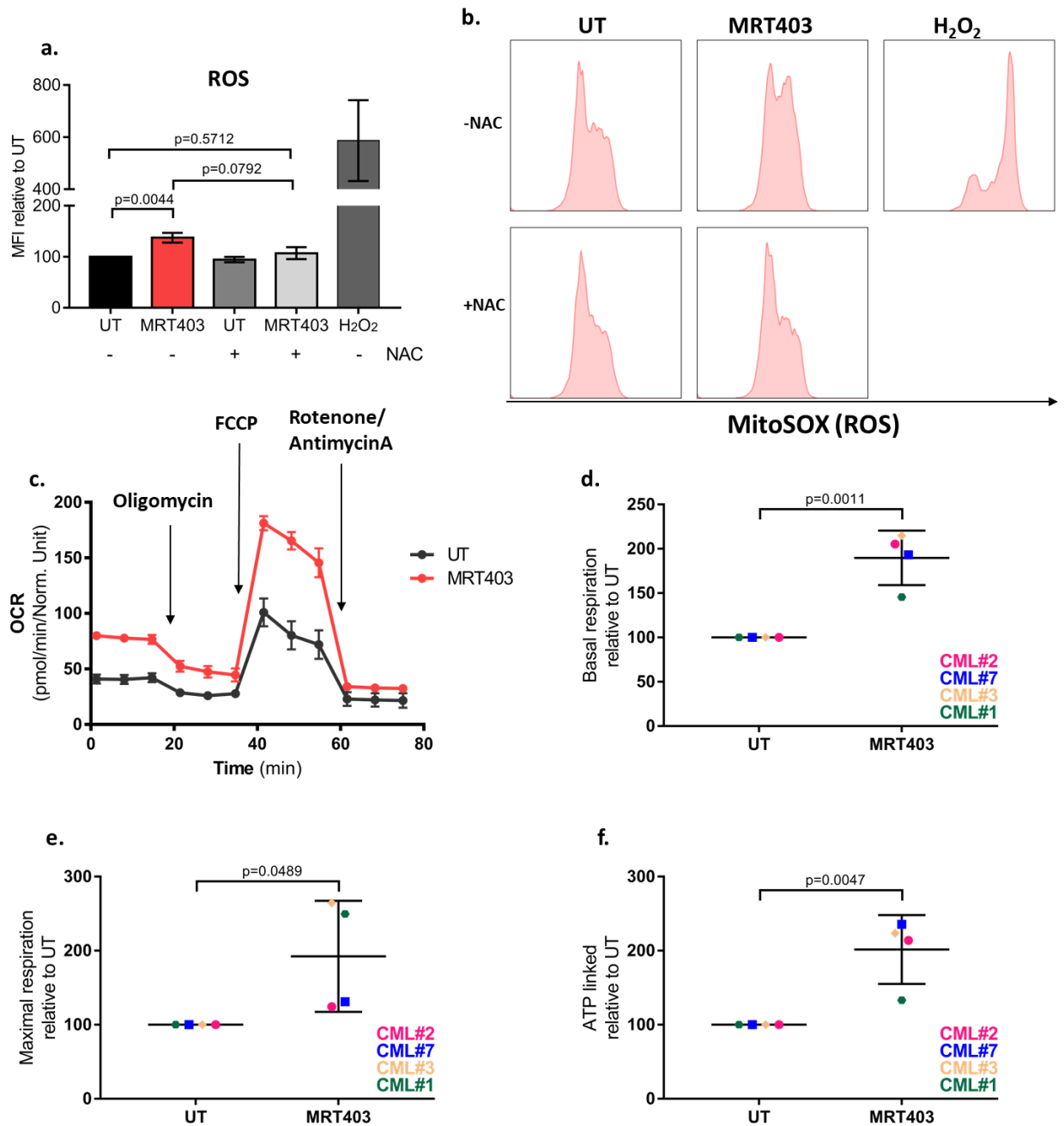


Figure 5.9a, b).

To further test our hypothesis, we measured OCR in real time in live cells following 72 h treatment with 3  $\mu$ M MRT403 (

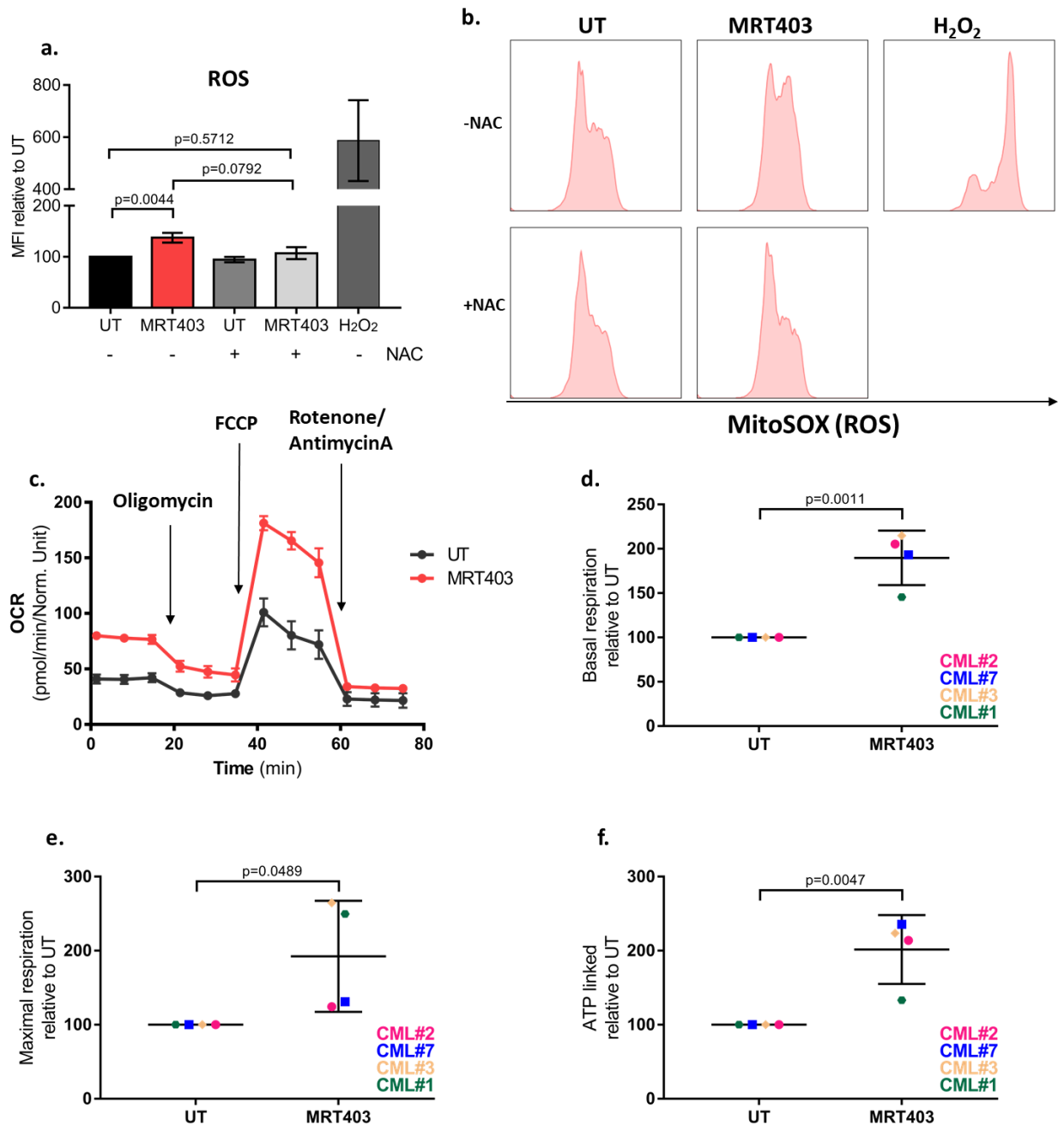
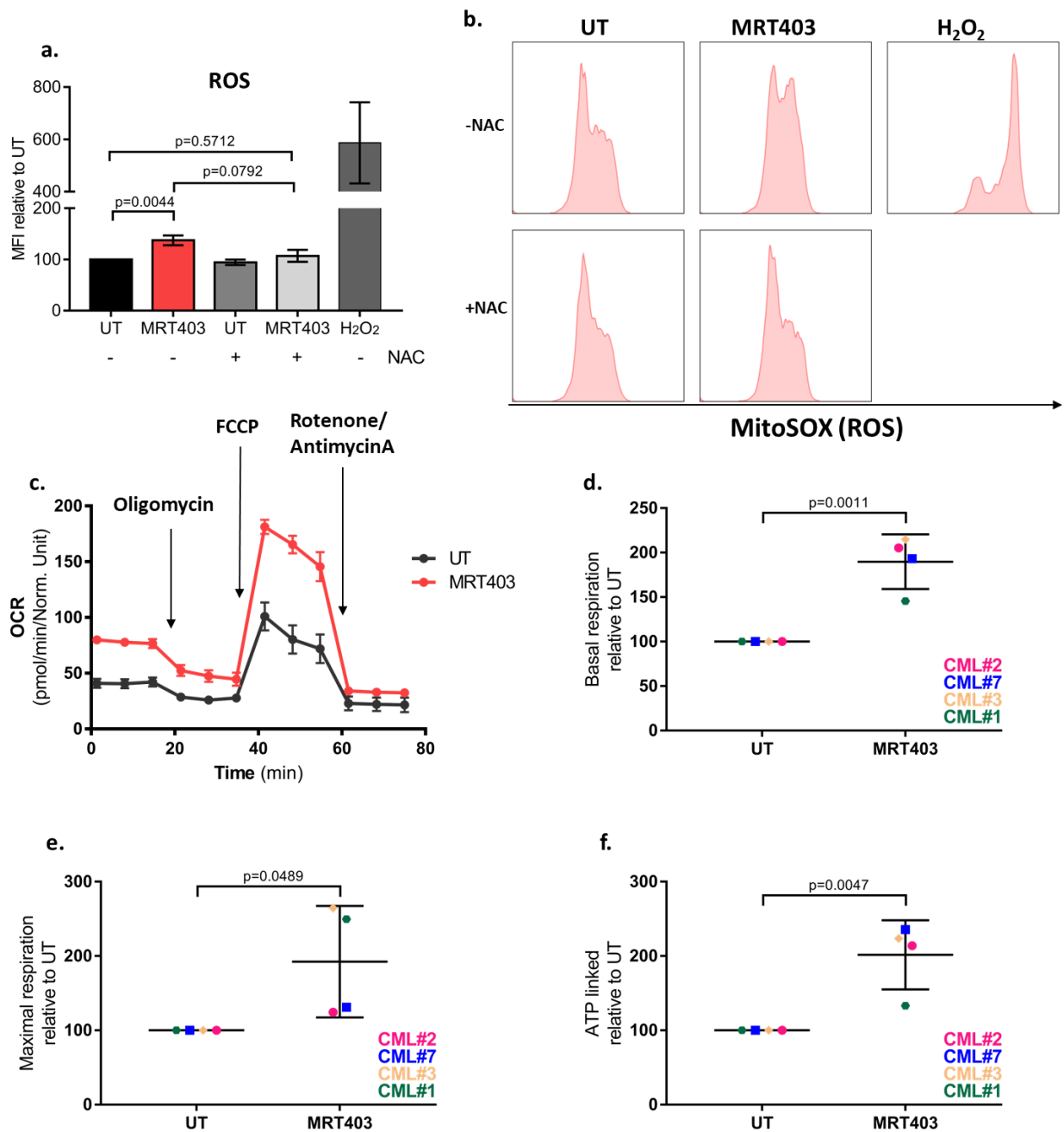


Figure 5.9c). Results show a significant increase in basal OCR following ULK1/2 inhibition



**Figure 5.9c, d).** Significant increase in maximal OCR was also assessed, however two of the samples exhibited a modest increase in maximal OCR, while the remaining two doubled maximal OCR following treatment with MRT403 (

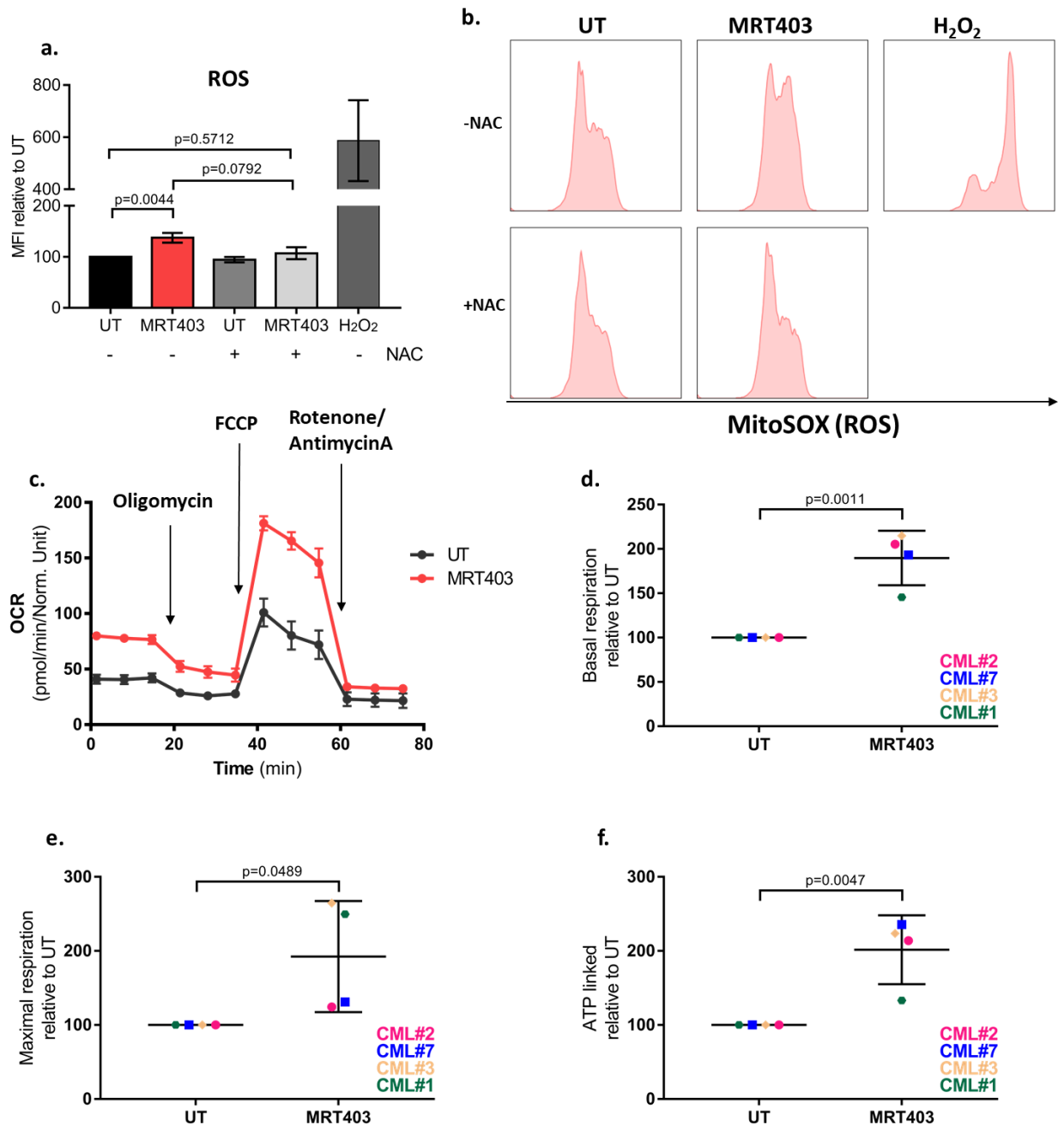


Figure 5.9e). Moreover, a significant increase was also measured in ATP-linked OCR

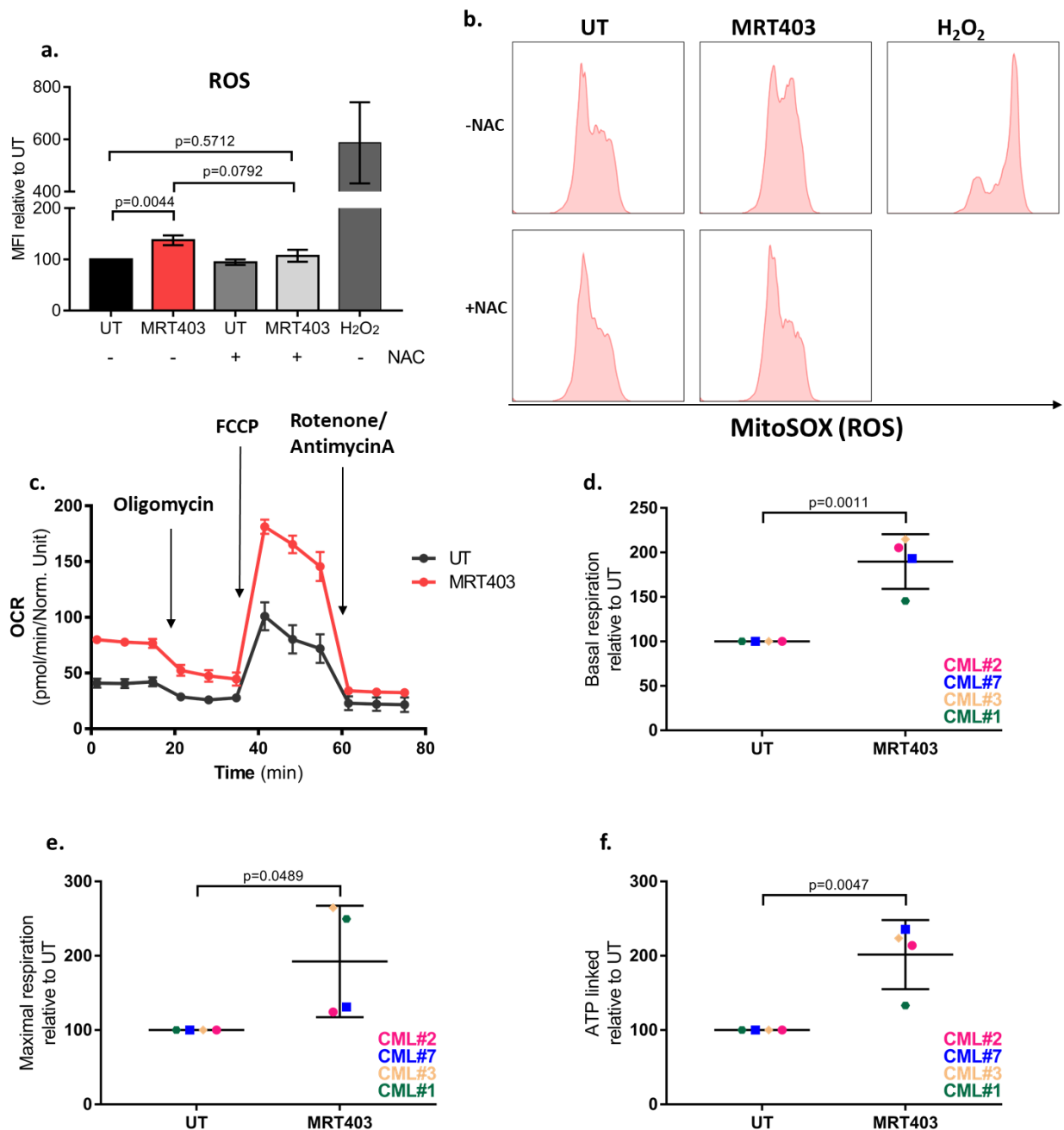
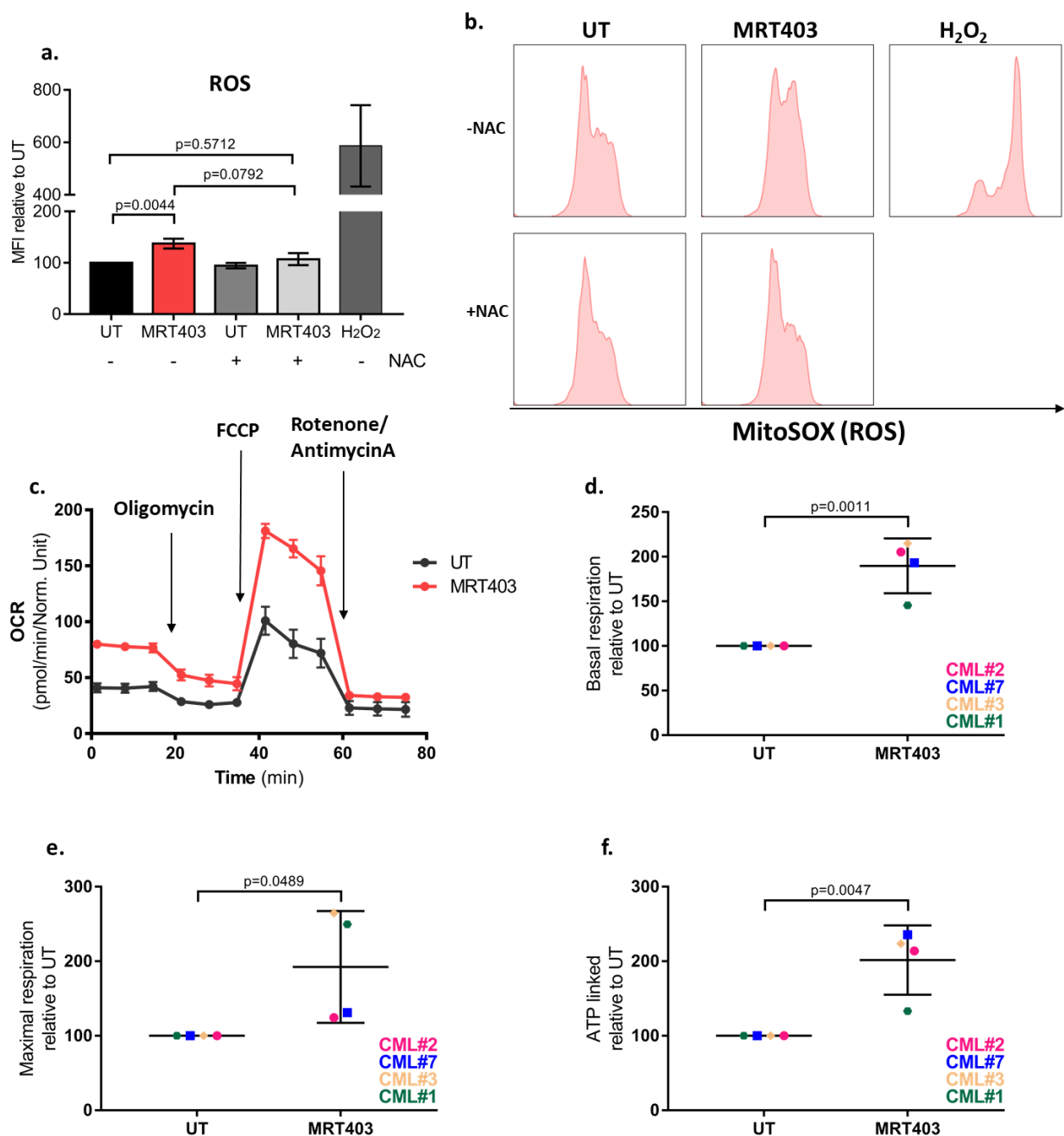


Figure 5.9f).

### 5.2.4.3 ULK1 and ATG7 KO cells show increased OCR in CML cells

To further assess if autophagy inhibition leads to increased mitochondrial function, we measured OCR in ULK1 and ATG7 deficient CML cells following 72 h treatment with 3  $\mu$ M MRT403 (Figure 5.10a). We show that both ULK1 and ATG7 deficient cells had increased basal and maximal OCR (Figure 5.10b, c). Furthermore, treatment with MRT403 did not increase further basal or maximal respiration in both ULK1 and ATG7 deficient cells (Figure 5.10b, c).



**Figure 5.9: MRT403 treatment increases ROS levels and OCR in CD34<sup>+</sup> CML cells**

Measurements of ROS following 72 h treatment with 3  $\mu$ M MRT403; n=5 CML samples (a). Representative FACS plots showing measurements of ROS following 72 h treatment with 3  $\mu$ M MRT403 (b). Representative OCR profile measured using Seahorse Mitostress Analyser following 72 h treatment with 3  $\mu$ M MRT403 (c). Graphs showing basal respiration relative to UT (d). Maximal respiration relative to UT (e). ATP linked relative to UT; n=4 CML samples (f). Mean  $\pm$  S.D. n=4 CML samples. P values were calculated using unpaired Student T-test.

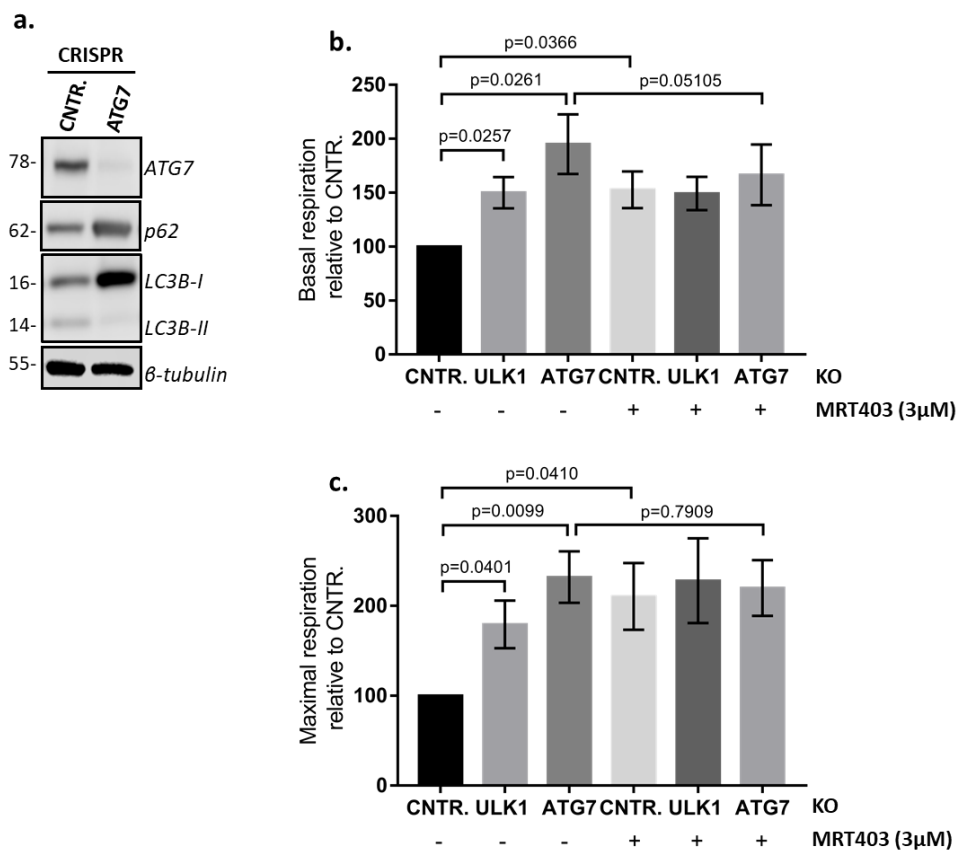


**Figure 5.10: ULK1 and ATG7 KO cells exhibit an increase in mitochondrial respiration**

Western blot analysis showing deletion of ATG7 in KCL22 cells (a). Graphs showing basal respiration relative to CNTR. following treatment using 3 µM MRT403 for 72 h (b). Maximal respiration relative to CNTR. following treatment using 3 µM MRT403 for 72 h (c) Mean ± S.E.M n=3 independent experiments. P values were calculated using unpaired Student T-test.

Thus far we showed that treatment with MRT403 increased CD34<sup>+</sup> CML mitochondrial function, correlating with impaired mitophagy. We also showed that this might occur in an autophagic dependent manner since increased OCR was exhibited in both ULK1 and ATG7 deficient cells.

#### **5.2.4.4 MRT403 reduces glycolysis in CD34<sup>+</sup> CML cell**

To further understand the metabolic changes in patient-derived CD34<sup>+</sup> CML cells following inhibition of ULK1/2 using MRT403, we measured glycolysis using Seahorse Extracellular Flux analyser. Following 72 h treatment with 3  $\mu$ M MRT403, CD34<sup>+</sup> CML samples (n=5) exhibited a significant decrease in basal glycolysis (measured by extracellular acidification rate; (ECAR) (**Figure 5.11a, b**).

Previous work demonstrates that ULK1 plays a bifurcate role, regulating glucose flux between glycolysis and PPP<sup>145</sup>. To test the hypothesis that pharmacological inhibition of ULK1/2 resulted in lower glucose flux, we measured NADPH/NADP<sup>+</sup> ratio (as NADPH being a final product of the PPP). Following 72 h treatment using 3  $\mu$ M MRT403, we measured a decrease NADPH/NADP<sup>+</sup> compared to untreated CD34<sup>+</sup> CML cells (**Figure 5.11c**).

#### **5.2.4.5 ULK1 deficient cells exhibit reduced glycolysis in an autophagy independent manner**

Using ULK1 and ATG7 deficient CML cells treated and untreated with 3  $\mu$ M MRT403 for 72 h, we show that while ULK1 deficient cells exhibit lower glycolysis and lower glycolytic capacity, no changes were observed in ATG7 deficient CML cells (**Figure 5.12a, b**). Furthermore, treatment using 3  $\mu$ M MRT403 decreased both glycolysis and glycolytic rates in both control and ATG7 deficient cells (**Figure 5.12a, b**). No further reduction in glycolysis or glycolytic capacity was observed in ULK1 deficient cells following treatment with 3  $\mu$ M MRT403 (**Figure 5.12a, b**).

Based on these results we conclude that treatment using 3  $\mu$ M MRT403 reduces glycolytic fluxes and NADPH levels in CD34<sup>+</sup> CML cells. Interestingly, while ULK1 treated cells exhibit lower glycolysis and glycolytic capacity, this wasn't observed in ATG7 deficient cells, suggesting an autophagic-independent effect but a ULK1 specific effect.

## Chapter 5 Using MRT403 to target CML LSPCs

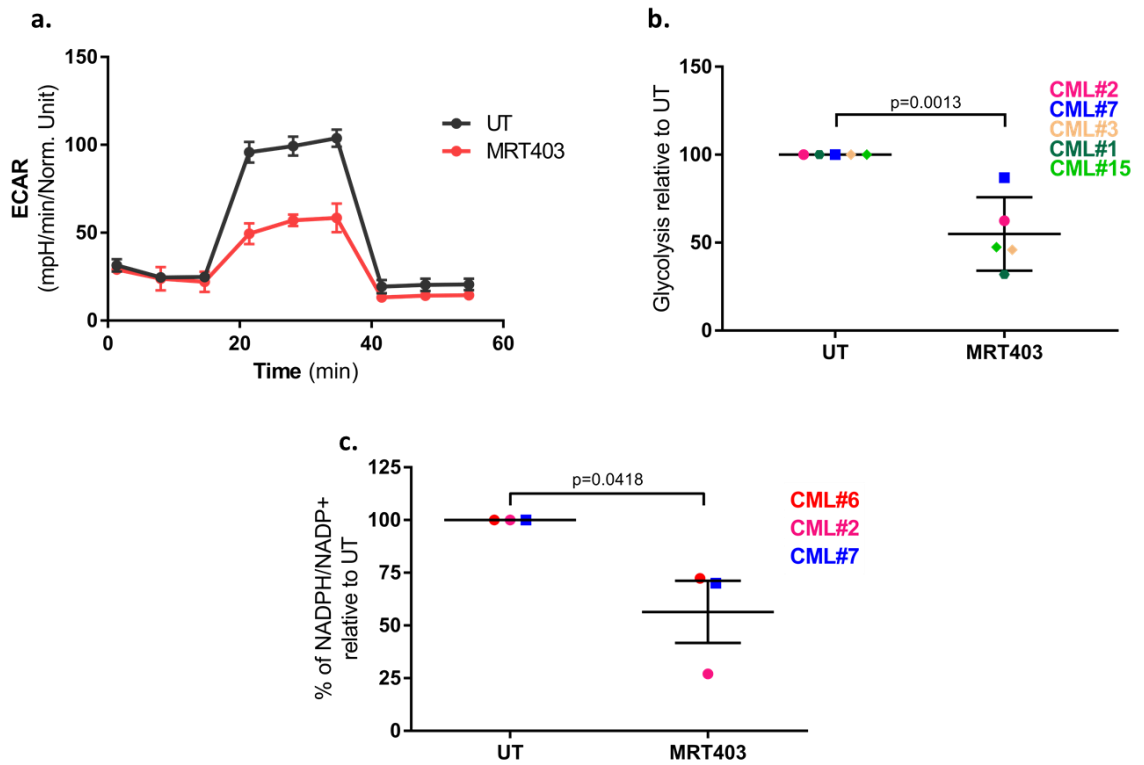


**Figure 5.11: MRT403 impairs glycolytic capacity and reduces NADPH in CD34<sup>+</sup> CML cells**

Representative ECAR profile measured using Seahorse Extracellular Flux Analyser following treatment with 3  $\mu$ M MRT403 for 72 h n=4 CML samples; n=5 CML samples (a). Graphs showing glycolysis relative to UT n=5 CML samples (b). Graphs showing NADPH/NADP<sup>+</sup> relative to UT; n=3 CML samples (c). Mean  $\pm$  S.D. P values were calculated using unpaired Student T-test.

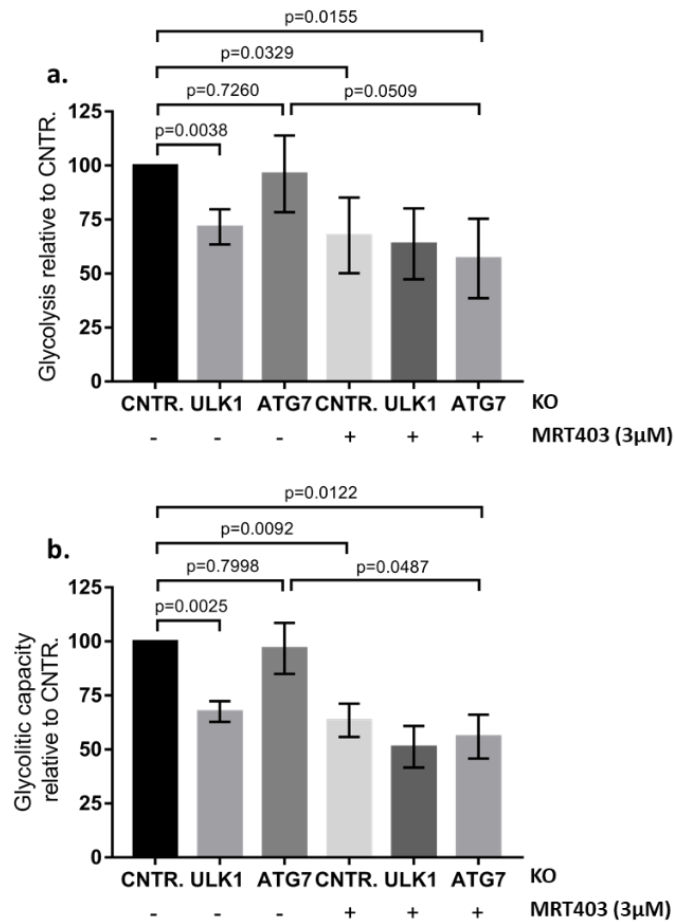


**Figure 5.12: Pharmacological or genetical inhibition of ULK1 impairs glycolysis independently from autophagy inhibition.**

Graphs showing glycolysis relative to CNTR. following treatment using 3 µM MRT403 for 72 h (a). Graphs showing glycolytic capacity relative to CNTR. following treatment using 3 µM MRT403 for 72 h (b). n=3 independent experiments. Mean ± S.E.M. P values were calculated using unpaired Student T-test.

#### 5.2.4.6 MRT403 induces loss of CD34<sup>+</sup>CD133<sup>+</sup> levels in patient-derived CML cells and enhanced erythroid maturation following exposure to low units of erythropoietin (EPO)

In the previous part we show that following inhibition of ULK1/2 using MRT403 induces increased OCR and ROS, together with reduction in glycolysis. It has been shown previously that increased ROS and increased mitochondrial metabolism promotes differentiation<sup>189,235,236</sup>.

To test our hypothesis that inhibition of ULK1/2, causing increased ROS and OCR, might result in enhanced differentiation, we treated CD34<sup>+</sup> CML cells for 72 h using 3  $\mu$ M MRT403 and measured levels of LSPC surface markers (i.e. CD34<sup>+</sup> and CD34<sup>+</sup>CD133<sup>+</sup>). Results indicate that treatment with MRT403 induces a loss of CD34<sup>+</sup> cells by 40% compared to untreated cells (**Figure 5.13a, b**). Furthermore, inhibition of ULK1/2 using MRT403 also resulted in a 20% decrease of the more primitive CD34<sup>+</sup>CD133<sup>+</sup> cell population (**Figure 5.13c**).

Since SFM media used to culture CD34<sup>+</sup> CML cells is supplemented with physiological concentration of growth factors and cytokines to prevent rapid differentiation *in vitro*, we decided to supplement SFM media with low units of EPO<sup>237</sup>, (i.e. 3u/mL) to further address our hypothesis that loss of CD34<sup>+</sup> cells correlates with enhanced differentiation. Positive control was used to assess erythroid maturation using physiological concentration of EPO ( $\gamma$ EPO) (i.e. 25u/mL).

CD34<sup>+</sup> CML cells were treated for 3, 6 and 9 days with 3  $\mu$ M MRT403 and erythroid maturation was measured by FACs using 4 different surface markers. GlycophorinA, a sialoglycoprotein found in the erythrocytes membrane<sup>238</sup>, CD71, a protein necessary to import iron from the transferrin inside the cell<sup>239</sup>, CD36 a glycoprotein with several functions expressed on the surface of erythrocytes cells<sup>240,241</sup>, and CD44, a glycoprotein mainly involved during cell migration and cell interaction, which expression is lost on the surface of erythrocytes<sup>238</sup>.

Results indicate that following 3 days treatment with 3  $\mu$ M MRT403, cells had an increase from 100 to 150% in CD44<sup>-</sup>GlyA<sup>+</sup> cells compared to untreated cells, although this was not statistically significant (**Figure 5.14a**).

## Chapter 5 Using MRT403 to target CML LSPCs

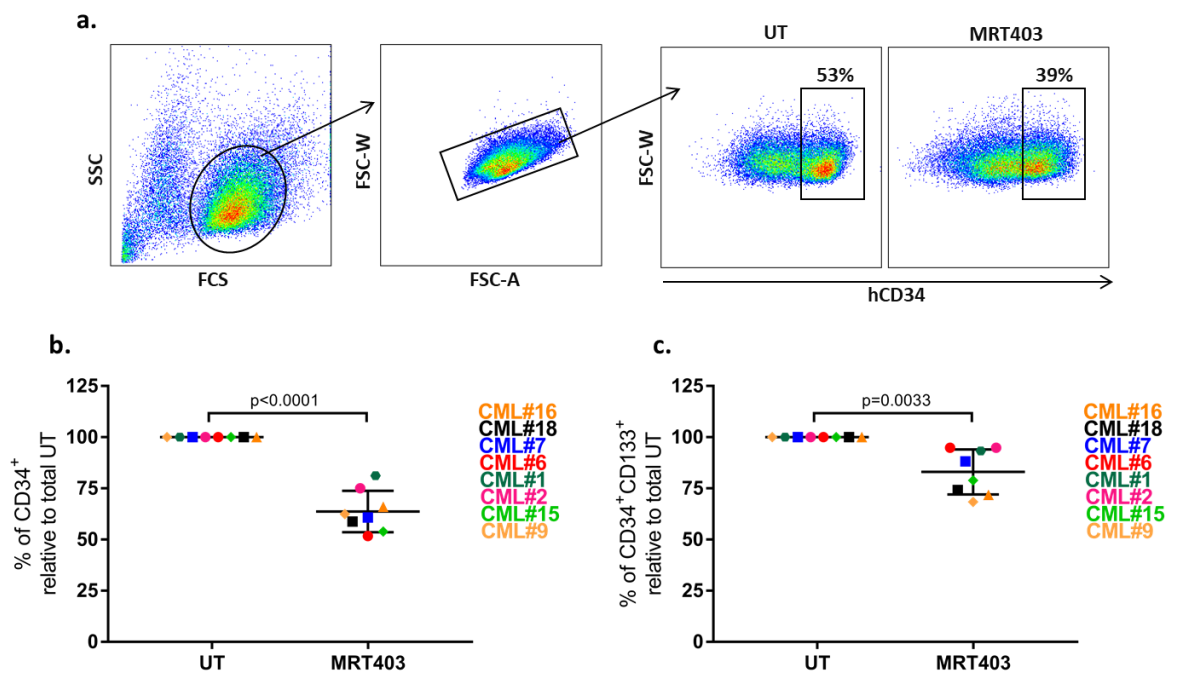


**Figure 5.13: MRT403 treatment reduces percentage of CD34<sup>+</sup> and CD34<sup>+</sup>CD133<sup>+</sup> cells**

Strategy of gating and representative graphs showing CD34 surface marker levels, following treatment with 3  $\mu$ M MRT403 for 72 h (a). % of CD34<sup>+</sup> cells relative to total number of untreated cells following treatment using 3  $\mu$ M MRT403 for 72 h (b). % of CD34<sup>+</sup>CD133<sup>+</sup> cells relative to total number of untreated cells following treatment with 3  $\mu$ M MRT403 for 72 (c). n=8 CML samples. Mean  $\pm$  S.D. P values were calculated using paired Student T-test.

A non-significant increase from 100 to 120% in CD44<sup>+</sup>GlyA<sup>+</sup> was also measured in cells treated using physiological concentration of EPO ( $\gamma$ EPO) (**Figure 5.14a**). Treatment with NAC reverted the phenotype in cells treated with either 3  $\mu$ M MRT403 or  $\gamma$ EPO (**Figure 5.14a**). A more variable expression of CD71<sup>+</sup>GlyA<sup>+</sup> was measured between individual patient samples following treatment with 3  $\mu$ M MRT403 for 3 days (**Figure 5.15a**). Sample#1 and #9 had respectively an increase from 100 to 480 and 390%, while no changes were measured in sample#18 and #6 (**Figure 5.15a**). Treatment with  $\gamma$ EPO didn't change % of CD71<sup>+</sup>GlyA<sup>+</sup> compared to untreated cells (**Figure 5.15a**). Similar to CD71<sup>+</sup>GlyA<sup>+</sup>, sample#1 and #9 had respectively an increase from 100 to 620 and 590% in positivity for CD36 and GlyA, while no changes in CD36<sup>+</sup>GlyA<sup>+</sup> cells were measured in sample#18 and #6 (**Figure 5.16a**). However, treatment with  $\gamma$ EPO for 3 days didn't change % of CD36<sup>+</sup>GlyA<sup>+</sup> compared to untreated cells (**Figure 5.16a**).

Following 6 days treatment using 3  $\mu$ M MRT403, patient-derived CML cells exhibit a significant increase from 100 to 300% in CD44<sup>+</sup>GlyA<sup>+</sup>, while using  $\gamma$ EPO, increased from 100 to 790% CD44<sup>+</sup>GlyA<sup>+</sup> (**Figure 5.14b**). As well, an increase from 100 to 300% was assessed in expression of CD71<sup>+</sup>GlyA<sup>+</sup> following treatment with 3  $\mu$ M MRT403, and a change from 100 to 690% using  $\gamma$ EPO (**Figure 5.15b**). Expression of CD36 and GlyA was shifted from 100 to 500% following treatment using 3  $\mu$ M MRT403, and from 100 to 740% using  $\gamma$ EPO (**Figure 5.16b**). Treatment with NAC inhibited expression of CD71, CD36, CD44 and GlyA in both MRT403 treated cells and with  $\gamma$ EPO<sup>242</sup> (**Figure 5.14b**), (**Figure 5.15b**), and (**Figure 5.16b**).

Treatment with 3  $\mu$ M MRT403 for 9 days induced a significant increase of 10% in CD44<sup>+</sup>GlyA<sup>+</sup> positive cells compared to untreated cells (**Figure 5.14c, d**). A 14% increase in CD44<sup>+</sup>GlyA<sup>+</sup> positive cells was measured following 9 days treatment with  $\gamma$ EPO (**Figure 5.14c, d**). Percentage of CD71<sup>+</sup>GlyA<sup>+</sup> cells significantly increased following treatment with both MRT403 and  $\gamma$ EPO compared to untreated cells, (respectively 14 and 17% increase) (**Figure 5.15c, d**). As well, a significant increase was shown in CD36<sup>+</sup>GlyA<sup>+</sup> cells following treatment with both MRT403 and  $\gamma$ EPO compared to untreated cells (respectively 14 and 17% increase) (**Figure 5.16c, d**). Treatment with NAC inhibited expression levels of CD71, CD36, and GlyA even following 9 days treatment with both MRT403 and with  $\gamma$ EPO (**Figure 5.14c, d**), (**Figure 5.15c, d**) and (**Figure 5.16c, d**). Furthermore, we could

visually assess increased erythropoiesis following 9 days treatment with both MRT403 and  $\gamma$ EPO and inhibition of erythropoiesis using NAC (**Figure 5.14a**).

#### **5.2.4.7 ULK1 deficient cells exhibit increased ROS levels and enhanced erythropoiesis in CML cells**

In the previous paragraph we show that following inhibition of ULK1/2 using MRT403, LSPCs had enhanced loss of CD34<sup>+</sup>CD133<sup>+</sup> and CD34<sup>+</sup> cell populations when cultured in the presence of low concentration of EPO. To further address induction of erythropoiesis following inhibition of ULK1/2, we tested the effect by genetical inhibition of ULK1 in K562 cells, a CML erythroid cell line.

Following inhibition of ULK1 in 3 independent experiments, we show a 50% increase in ROS levels (**Figure 5.17a**). In addition, treatment with NAC decreased levels of ROS in ULK1 deficient cells (**Figure 5.17a**). Following KO of ULK1, we observed that the cell pellets appeared to have a stronger red colour than control cells, suggesting an increase in erythroid maturation which caused a higher haemoglobin content and the appearance of a red pellet (**Figure 5.17b**). To further support erythroid maturation in ULK1 deficient cells, we measured by FACs expression of erythroid lineage such as CD71 and GlyA. Results show a significant increase in both CD71 and GlyA, respectively 70 and 30% increase, in ULK1 deficient cells compared to control cells (**Figure 5.17c, d**). Furthermore, treatment with NAC significantly reverted the erythroid phenotype (**Figure 5.17c, d**).

Thus far we show that following genetic removal of ULK1, CML cells exhibit an increased level of ROS which correlates with increased OCR (**5.2.4.3**) and reduced mitochondrial clearance (**4.2.3**). The change in oxidative metabolism might also explain the induction of differentiation measured in ULK1 deficient cells.

## Chapter 5 Using MRT403 to target CML LSPCs

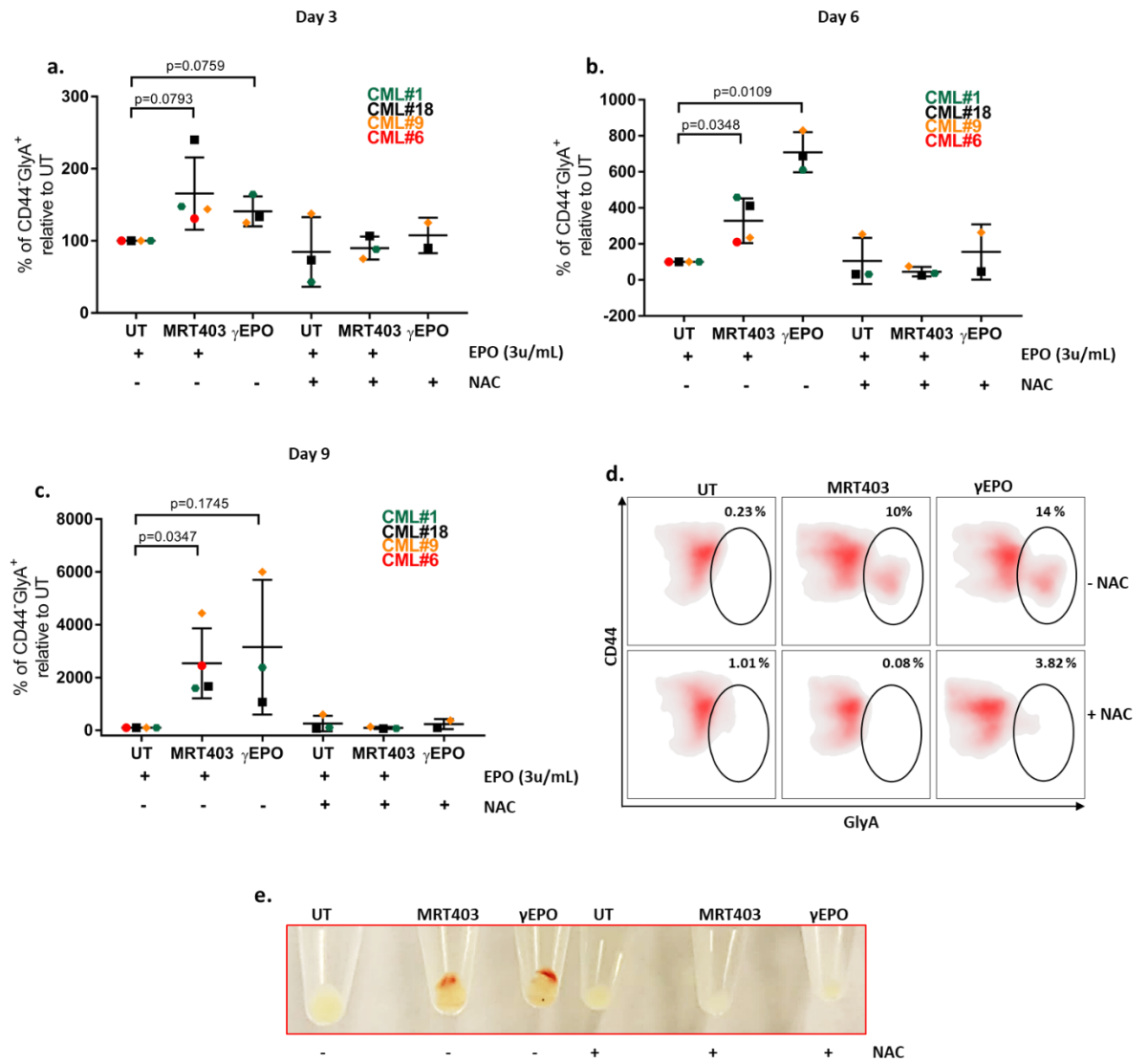


**Figure 5.14: MRT403 treatment drives an increase in CD44<sup>+</sup>GlyA<sup>+</sup> cells**

% of CD44<sup>+</sup>GlyA<sup>+</sup> cells relative to untreated following 3 days treatment using 3 μM MRT403, or γEPO and in combination with NAC (a). % of CD44<sup>+</sup>GlyA<sup>+</sup> cells relative to untreated following 6 days treatment using 3 μM MRT403, or γEPO and in combination with NAC (b). % of CD44<sup>+</sup>GlyA<sup>+</sup> cells relative to untreated following 9 days treatment using 3 μM MRT403, or γEPO and in combination with NAC (c). Graph plots showing % of CD44<sup>+</sup>GlyA<sup>+</sup> cells following 9 days treatment using 3 μM MRT403, or γEPO and in combination with NAC (d). Picture of cell pellets following 9 days treatment using 3 μM MRT403, or γEPO and in the combination with NAC (e). n=4 CML samples. Mean ± S.D. P values were calculated using paired Student T-test.

## Chapter 5 Using MRT403 to target CML LSPCs

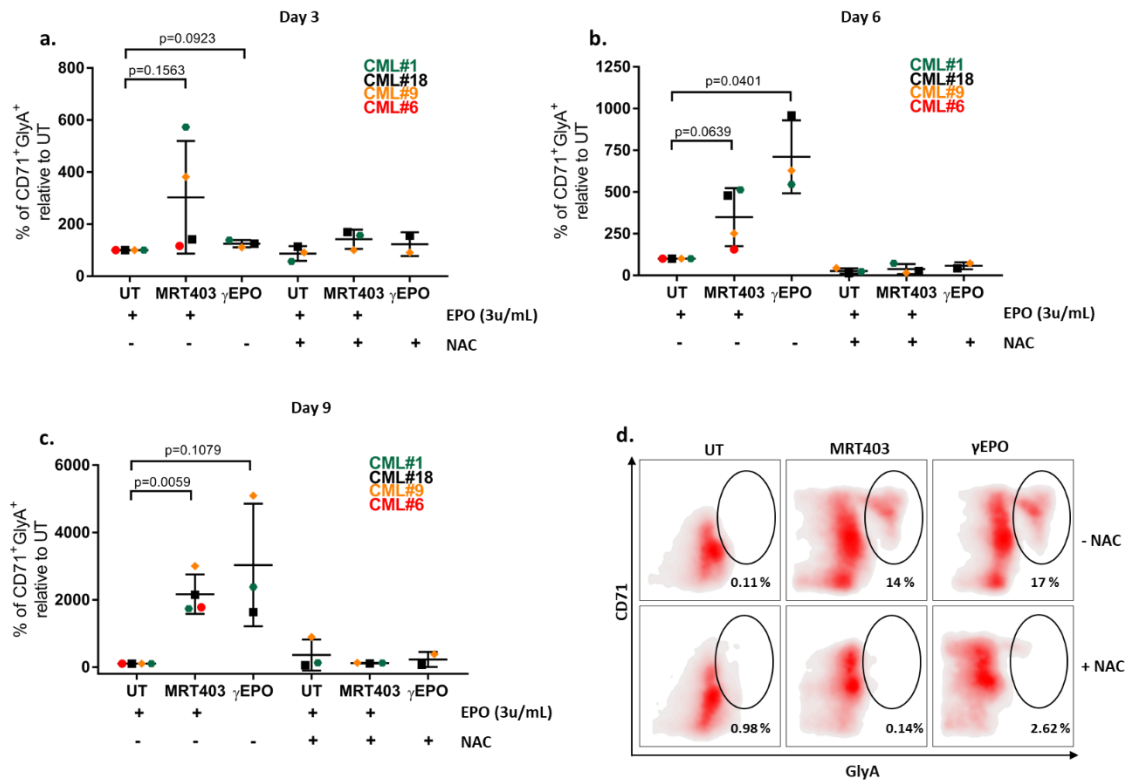


**Figure 5.15: MRT403 treatment drives an increase in CD71<sup>+</sup>GlyA<sup>+</sup> cells**

% of CD71<sup>+</sup>GlyA<sup>+</sup> cells relative to untreated following 3 days treatment using 3 μM MRT403, or γEPO and in combination with NAC (a). % of CD71<sup>+</sup>GlyA<sup>+</sup> cells relative to untreated following 6 days treatment using 3 μM MRT403, or γEPO and in combination with NAC (b). % of CD71<sup>+</sup>GlyA<sup>+</sup> cells relative to untreated following 9 days treatment using 3 μM MRT403, or γEPO and in the combination with NAC (c). Graph plots showing % of CD71<sup>+</sup>GlyA<sup>+</sup> cells following 9 days treatment using 3 μM MRT403, or γEPO and in combination with NAC (d). n=4 CML samples. Mean ± S.D. P values were calculated using paired Student T-test.

## Chapter 5 Using MRT403 to target CML LSPCs

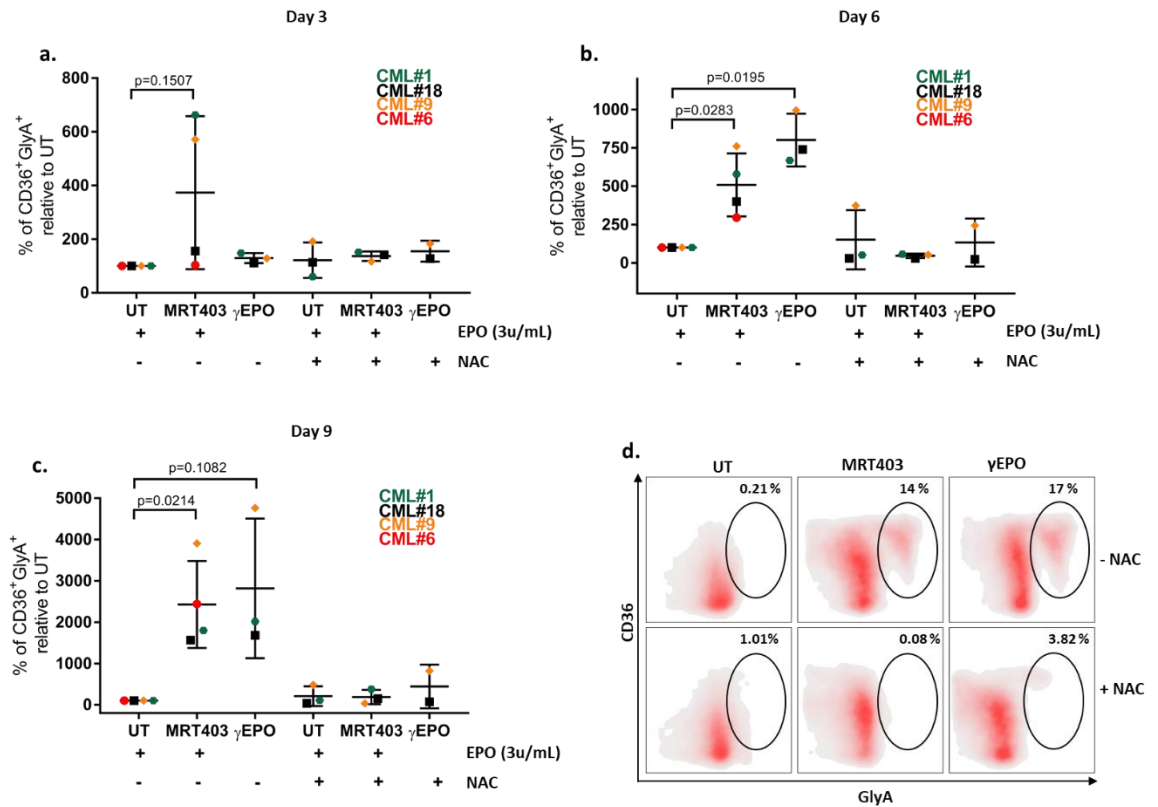


**Figure 5.16: MRT403 treatment drives an increase in CD36<sup>+</sup>GlyA<sup>+</sup> cells**

% of CD36<sup>+</sup>GlyA<sup>+</sup> cells relative to untreated following 3 days treatment using 3 μM MRT403, or γEPO and in combination with NAC (a). % of CD36<sup>+</sup>GlyA<sup>+</sup> cells relative to untreated following 6 days treatment using 3 μM MRT403, or γEPO and in combination with NAC (b). % of CD36<sup>+</sup>GlyA<sup>+</sup> cells relative to untreated following 9 days treatment using 3 μM MRT403, or γEPO and in combination with dNAC (c). Graph plots showing % of CD36<sup>+</sup>GlyA<sup>+</sup> cells following 9 days treatment using 3 μM MRT403, or γEPO and in combination with NAC (d). n=4 CML samples. Mean ± S.D. P values were calculated using paired Student T-test.

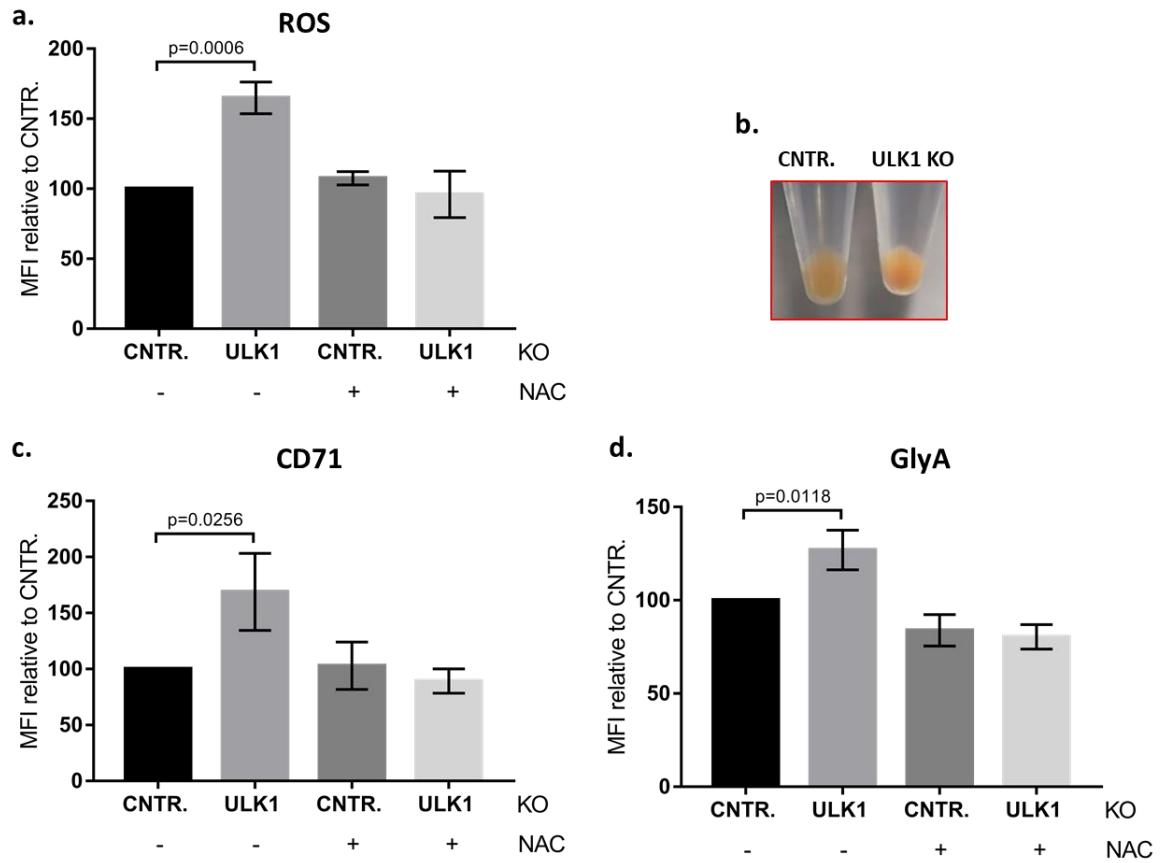


**Figure 5.17: ULK1 deficient cells exhibit an increase in ROS levels and in erythropoiesis markers such as CD71 and GlyA<sup>+</sup>**

% of ROS relative to control following ULK1 KO and/or treatment with NAC (a). Picture of cell pellets in control and ULK1 deficient cells (b). % of CD71<sup>+</sup> cells relative to control following ULK1 KO and/or treatment with NAC (c). % of GlyA<sup>+</sup> cells relative to control following ULK1 KO and/or treatment with NAC (d). n=3 independent experiments. Mean ± S.D. P values were calculated using unpaired Student T-test.

#### **5.2.4.8 NSG mice show high tolerability of MRT403 following *in vivo* drug escalating study**

To determine whether MRT403 could be applied *in vivo*, a dose escalating study was performed in NSG mice. Mice were treated daily for a length of 2 weeks with dose being doubled every 5 days (with a starting dose of 5 mg/Kg and highest dose of 40 mg/Kg) (**Figure 5.18a**). At the end of the treatment, mice were sacrificed and the spleen from each mice was collected showing no increase in spleen size (**Figure 5.18b**). Mice did not exhibit any dramatic body weight loss, indicating good tolerability of the drug and mice were looking healthy while dosed (**Figure 5.18c**). Furthermore, plasma from circulating blood was extracted after 24 h from lowest dose (i.e. 5mg/Kg), after 5 days treatment with 10mg/Kg and following 5 days treatment using 40mg/Kg (**Figure 5.18d**). Results indicate that no significant changes in MRT403 plasma concentration were achieved between lowest and highest dose.

Further investigation are required to give a more detailed tolerability of the compound *in vivo*. However preliminary data doesn't highlight any undesirable effect in terms of toxicity *in vivo* and drug accumulation in the plasma.

## Chapter 5 Using MRT403 to target CML LSPCs

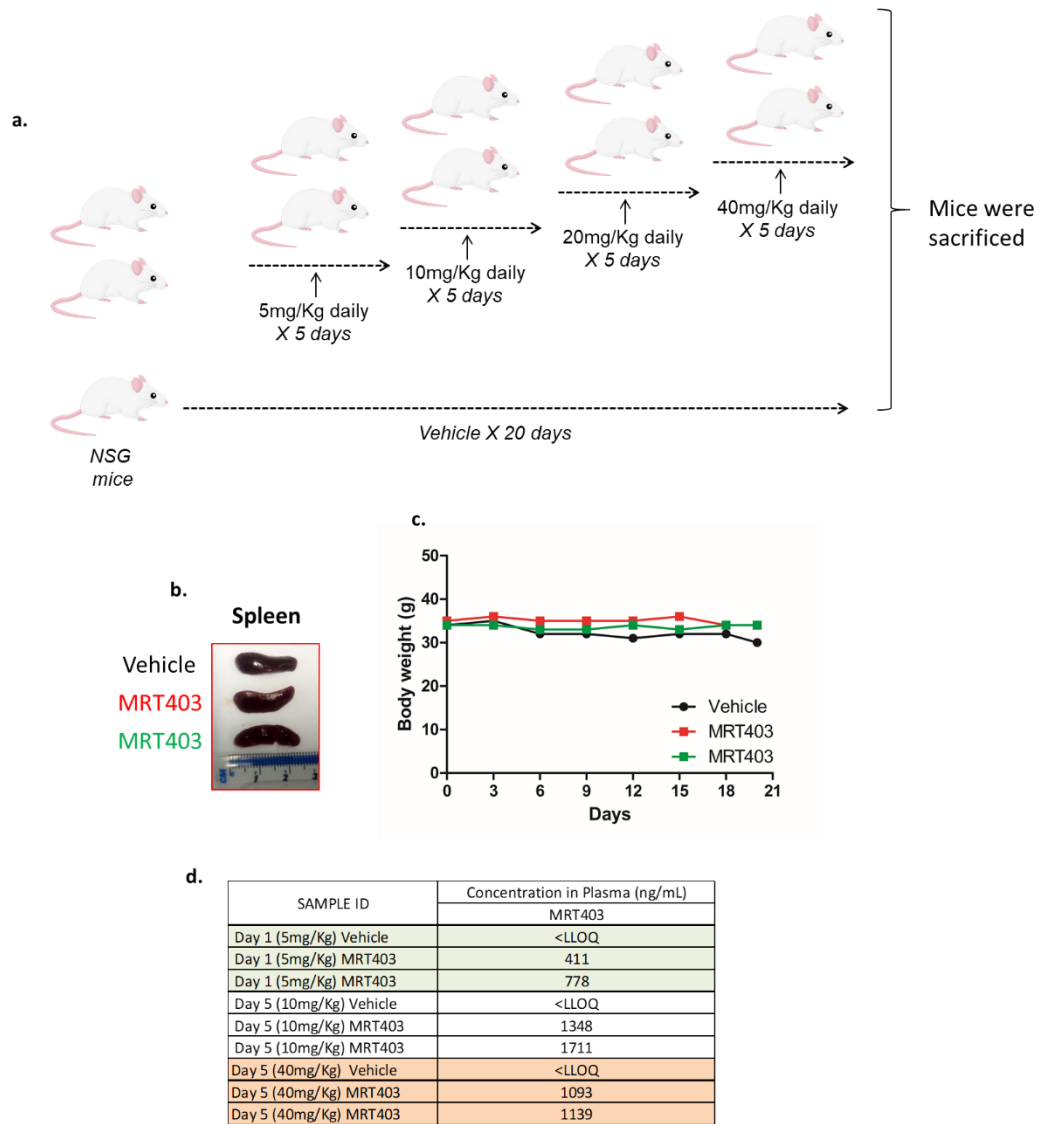


**Figure 5.18: MRT403 is well tolerated in NSG mice**

Experimental plan; MRT403 dose was doubled following 5 days *in vivo* treatment until a highest dose of 40 mg/Kg (a). Image of spleen size harvested from treated and untreated mice (b). Graph showing mice body weight during dosing using MRT403 (c). Table indicating concentration of MRT403 in plasma following 24 h and 5 days *in vivo* treatment (d).

### **5.2.4.9 Using a BCR-ABL *in vivo* model to study leukemogenesis**

As mentioned in 2.16.2.4, the CD45.2 SCLtTA/BCR-ABL DTG mouse model is suitable for studying leukemogenesis following removal of tetracycline from the drinking water. Mice develop leukaemia which highly resembles the human disease, with mice showing signs of splenomegaly, anaemia and accumulation of myeloid cells in the blood and in the spleen.

To determine whether MRT403 treatment induces differentiation of LSPCs *in vivo*, decreasing number of LSPCs, two experiments using separate BCR-ABL DTG mouse cohorts were performed.

In the first experiment, following sub-lethal irradiation a co-transplant of 50% CD45.1 cells (WT, BCR-ABL<sup>-</sup>) and 50% CD45.2 cells (BCR-ABL<sup>+</sup>) were tail vein injected into black6 mice (C57BL/6 mice) (**Figure 5.19a**). To allow transplanted cells to engraftment and recovery from the irradiation toxicity, mice were kept for 2 weeks on tetracycline (ON Tet, i.e. BCR-ABL OFF). Following that, the antibiotic was removed from the drinking water for 10 days to induce the disease (**Figure 5.19a**). Following disease induction, mice were distributed into 2 arms, vehicle and MRT403, and treated daily with a dose of 40 mg/Kg of MRT403 (**Figure 5.19a**). As a BCR-ABL negative control, 2 mice were kept ON TET for the entire length of the study.

In the second experiment, following sub-lethal irradiation, CD45.2 cells (BCR-ABL<sup>+</sup>) were tail vein injected into C57BL/6 mice (**Figure 5.19b**). To allow cell engraftment and recovery from the irradiation toxicity, mice were kept for 3 weeks on tetracycline (ON Tet, i.e. BCR-ABL OFF), following what the antibiotic was removed from the drinking water for 10 days to induce the disease (**Figure 5.19b**). Following the disease was induced, mice were distributed into 4 arms, vehicle and MRT403 and treated daily with a dose of 40 mg/Kg of MRT403 and twice/day with 50mg/Kg imatinib (**Figure 5.19b**). As well, as a BCR-ABL negative control, 2 mice were kept ON TET for the entire length of the study.

Following 4 weeks of treatment, mice were sacrificed, and bone, spleen and blood were harvested for analysis. The use of CD45.1 and CD45.2 specific antibodies allowed us to separate normal from leukaemic cells and specifically study the

effect in both normal and leukaemic cells (**Figure 5.19c**). However, even though in the first experiment normal cells were co-transplanted, the engraftment of those cells wasn't high enough to allow us to perform any further FACs analysis than measuring the percentage of CD45.1 (i.e. normal cells) (**Figure 5.19c**).

#### **5.2.4.10 Treatment using MRT403 reduced number of CD45.2 engrafted cells *in vivo* without having an effect on myeloid cells**

Since leukaemic patients develop splenomegaly, we harvested the spleen and measured size and weight following 4 weeks treatment with either vehicle or MRT403 as a measure of disease progression. Both vehicle and MRT403 treated mice had a 30% increase in spleen weight compared to BCR-ABL OFF mice, with no sign of spleen size reduction in the MRT403 arm (**Figure 5.20a, b**). Analysis of the transplanted CD45.2 in the bone marrow showed a significant reduction of 10% in CD45.2<sup>+</sup> cells compared to vehicle mice (**Figure 5.20c**). Increase in the number of myeloid cells in the BM (measure as granulocytes and macrophages, GR1-Mac1 cells), represents another sign of leukaemia burden. A 40% increase in GR1-Mac<sup>+</sup> cells was observed in the vehicle mice compared to BCR-ABL OFF mice (**Figure 5.20d**). However, treatment using MRT403 induced a further 10% increase in GR1-Mac1<sup>+</sup> cells compared to vehicle mice (**Figure 5.20d**).

#### **5.2.4.11 MRT403 treatment increases MEPs inducing BM erythropoiesis in leukaemic mice**

As mentioned before, anaemia represents a major disease adverse effect for leukaemic patient<sup>243,244</sup>. Even though treatment using EPO has represented a valuable option to ameliorate the symptoms of anaemia not every patient responds to EPO<sup>245,246</sup>. Our *in vitro* studies (**5.2.4.7**) show that treating patient-derived CML cells with 3  $\mu$ M MRT403 in the presence of low concentration of EPO, induced erythroid maturation in CD34<sup>+</sup> CML cells. Based on that, we next assessed the number of megakaryocytes/erythroid progenitors (MEPs) *in vivo* following treatment with MRT403 (**Figure 5.21a, b**).

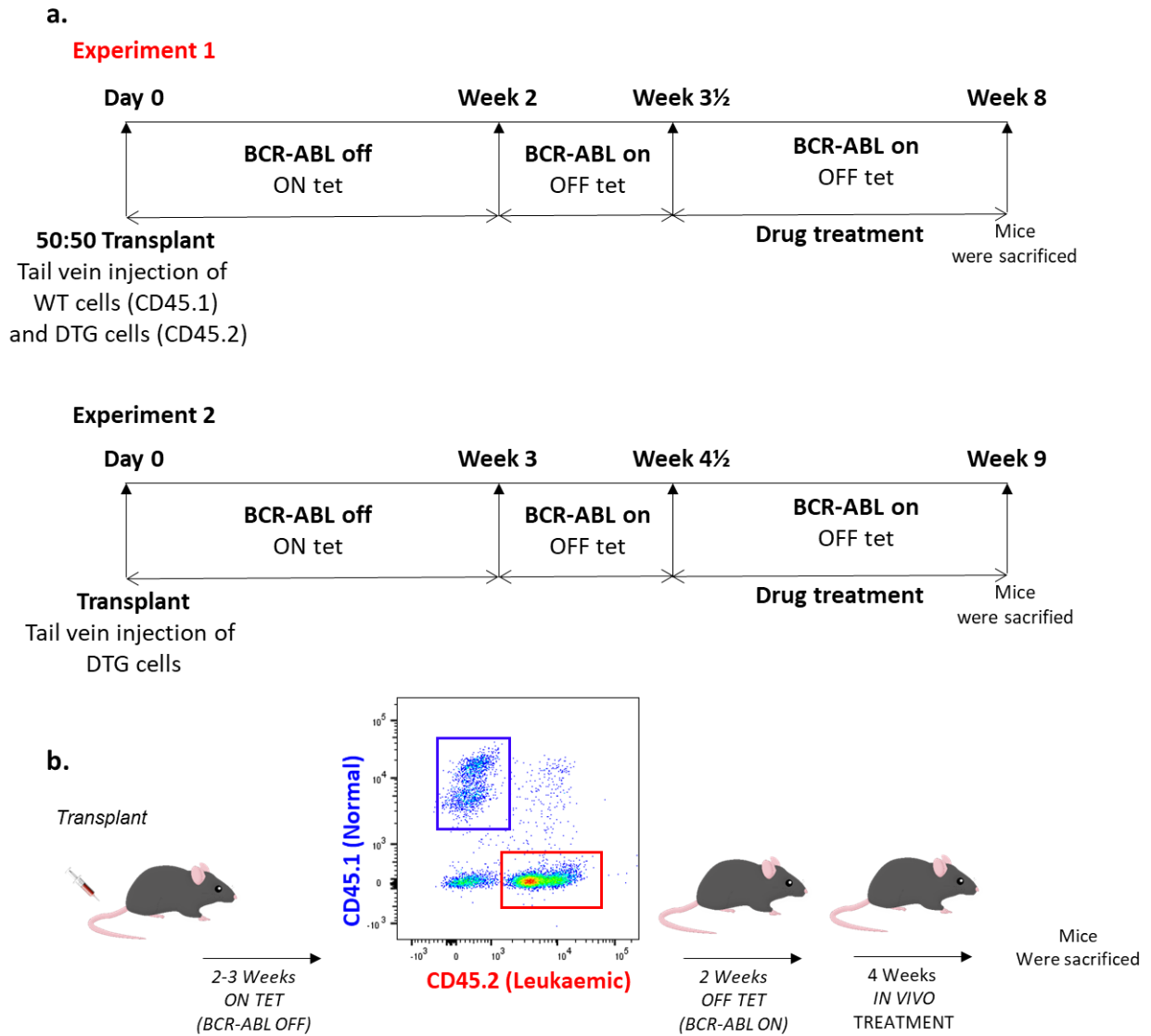


**Figure 5.19: Experimental plan of *in vivo* study treating DTG mice using MRT403**

Experimental plan: in experiment 1, black 6 mice were co-transplanted with  $1 \times 10^6$  STG cells and  $1 \times 10^6$  DTG cells; engraftment was allowed to take place for 2 weeks. Tetracycline was then removed from the drinking water to switch on BCR-ABL. In experiment 2 black 6 mice were co-transplanted with  $2 \times 10^6$  DTG cells; engraftment was allowed to take place for 2 weeks. Tetracycline was then removed from the drinking water to switch on BCR-ABL. In both experiments, mice were kept on tetracycline for 10 days and then treated for 4 weeks with vehicle or 40 mg /Kg daily of MRT403 (a). Schematic representation using BCR-ABL+ mice with strategy of gating using CD45.1 as a surface marker of normal cells and CD45.2 as a surface marker of leukaemic cells (b).

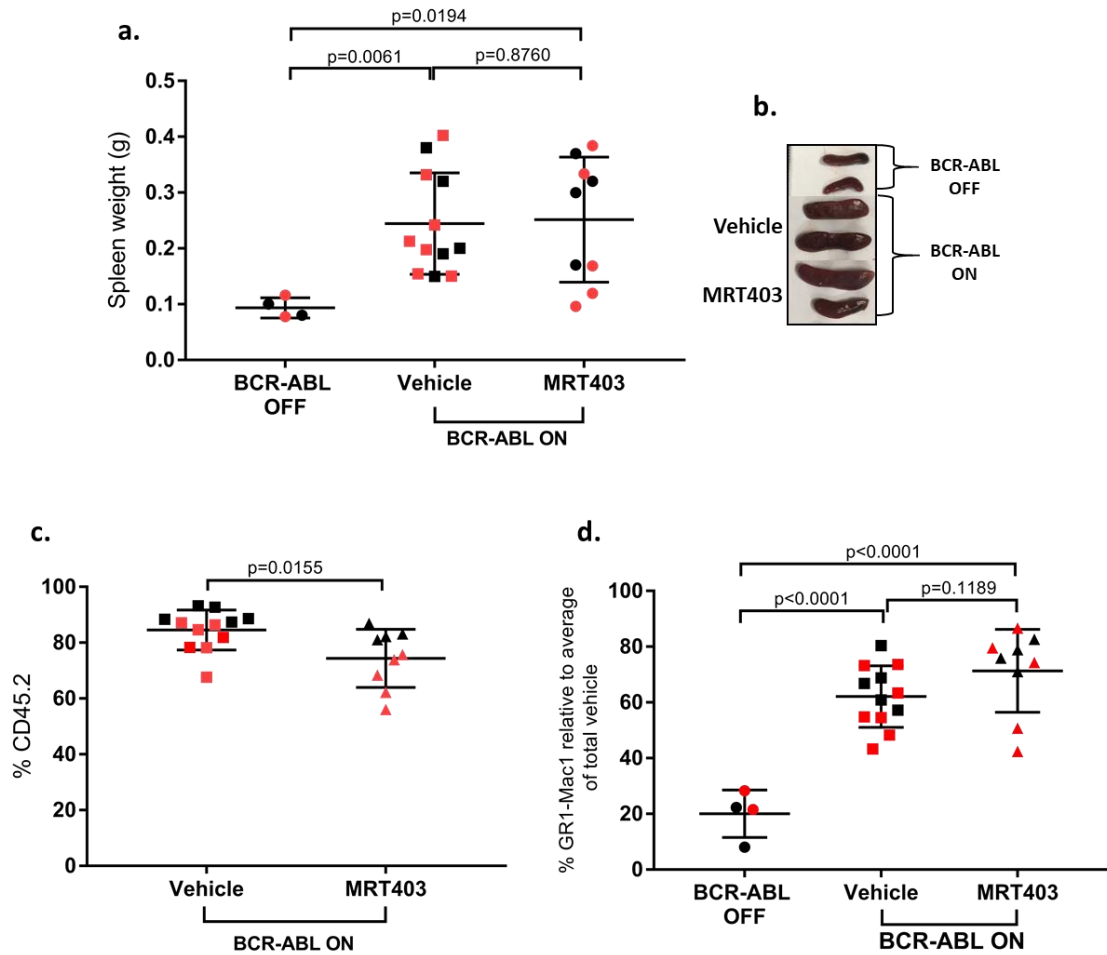


**Figure 5.20: MRT403 treatment reduces percentage of transplanted leukaemic cells without affecting myeloid cells**

Graph showing spleen weight from each mouse following *in vivo* treatment using vehicle, MRT403 and BCR-ABL OFF mice (a). Representative picture of spleen from 2 mice from each treatment arm (b). % of CD45.2 cells in the BM of mice treated with vehicle or MRT403 (c). % of BM GR1-Mac1 relative to average of absolute number of vehicle treated mice (d). Mean  $\pm$  S.D. P values were calculated using unpaired Student T-test.

Following gating on CD45.2<sup>+</sup> cells, lineage specific surface markers conjugated to streptavidin was used to exclude lineage committed cells (**Figure 5.21a**). Within the Sca1<sup>+</sup>C-KIT<sup>+</sup> cells, also known as LK cells, the use of CD16/32 and CD34 allowed us to separate CMP, GMP and MEP cells (**Figure 5.21a**).

Flow cytometry analysis indicated no changes in the number of CMP between vehicle and MRT403 treatment mice (**Figure 5.21c**). The % of MEPs was significantly increased (60%) in the BM of leukaemic mice treated with MRT403 (**Figure 5.21d**). However, no significant changes in the number of GMPs was induced in the BM of BCR-ABL expressing mice following treatment with MRT403 (**Figure 5.21e**).

To further analyse these data, we also assessed number of mature erythrocytes within the total BM, measuring the expression of the surface marker Ter119 in CD45<sup>-</sup> BM cells by FACs. Results indicate that mice treated daily with MRT403 showed a significant increase in number of erythroid cells (**Figure 5.22a**). Furthermore, we visually assessed an increased erythropoiesis as shown in the red colour appearance in the BM of the MRT403 treated mice (**Figure 5.22b**). Furthermore, we also resolved the distinct stages of the erythroid maturation by FACs combining expression of Ter119 and loss of CD44 surface markers (**Figure 5.22c**). Cells appearing in region I are positive to both CD44 and Ter119 which is an indication of primitive and less mature erythrocytes<sup>238</sup> (**Figure 5.22c**). Moving from region I to region V, cells lose expression of CD44 marker remaining positive to Ter119, which is an indication of erythroid maturation (**Figure 5.22c**). Based on that, cells in region V represents predominantly mature red cells (**Figure 5.22c**). As expected, vehicle treated mice had a decrease in BM cells belonging to region V compared to BCR-ABL OFF mice while MRT403 treated mice showed same level of population V when compared with BCR-ABL OFF mice (**Figure 5.22d**). Accurate analysis of cells belonging to each specific stage of the erythroid maturation, showed that treatment with MRT403 significantly reduced (by 50%) BM cells of region I compared to vehicle mice (**Figure 5.22e**). Furthermore, treatment using MRT403 decreased BM cells in region IV and increased BM cells in region V (**Figure 5.22f, g**), although this was not statistically significant.

## Chapter 5 Using MRT403 to target CML LSPCs

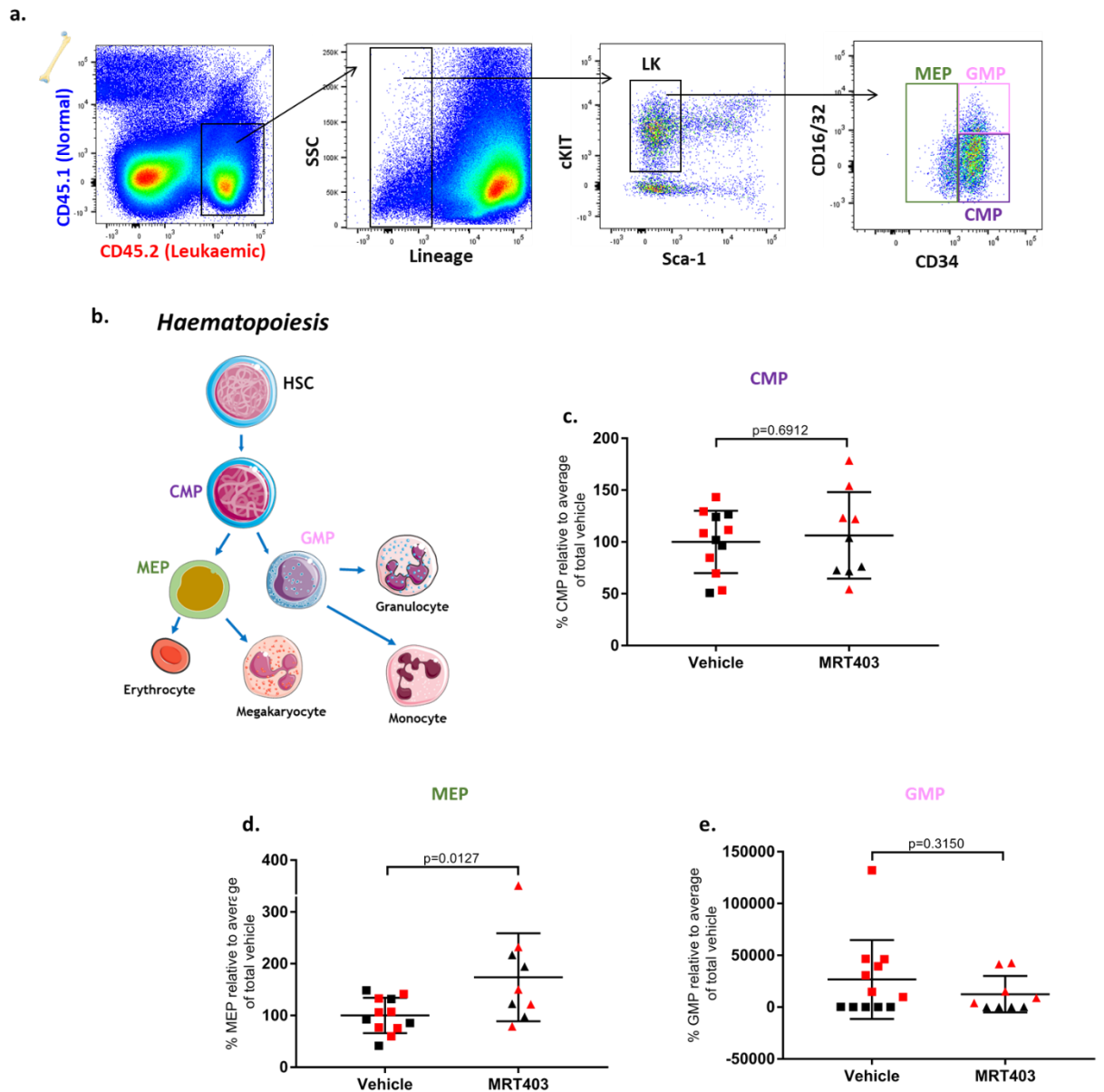


**Figure 5.21: MRT403 treatment increases percentage of leukaemic MEP**

Graph showing strategy of gating used to measure by FACS levels of CMP, GMP, MEP. Cells were first gated on CD45.2 and then using an in house made lineage cocktail, lineage<sup>+</sup> cells were excluded. From lineage<sup>-</sup> cells, LK cells were selected as C-KIT<sup>+</sup> and Sca1<sup>-</sup> cells. Within the LK cells CMP, GMP and MEP were identified based on expression of CD16/32 and CD34 surface marker (a). Schematic diagram of the different myeloid progenitor expansion during erythropoiesis (b). % of CMP (c), MEP (d), GMP (e) cells in the BM relative to average of absolute number of vehicle treated mice. Mean ± S.D. P values were calculated using unpaired Student T-test.

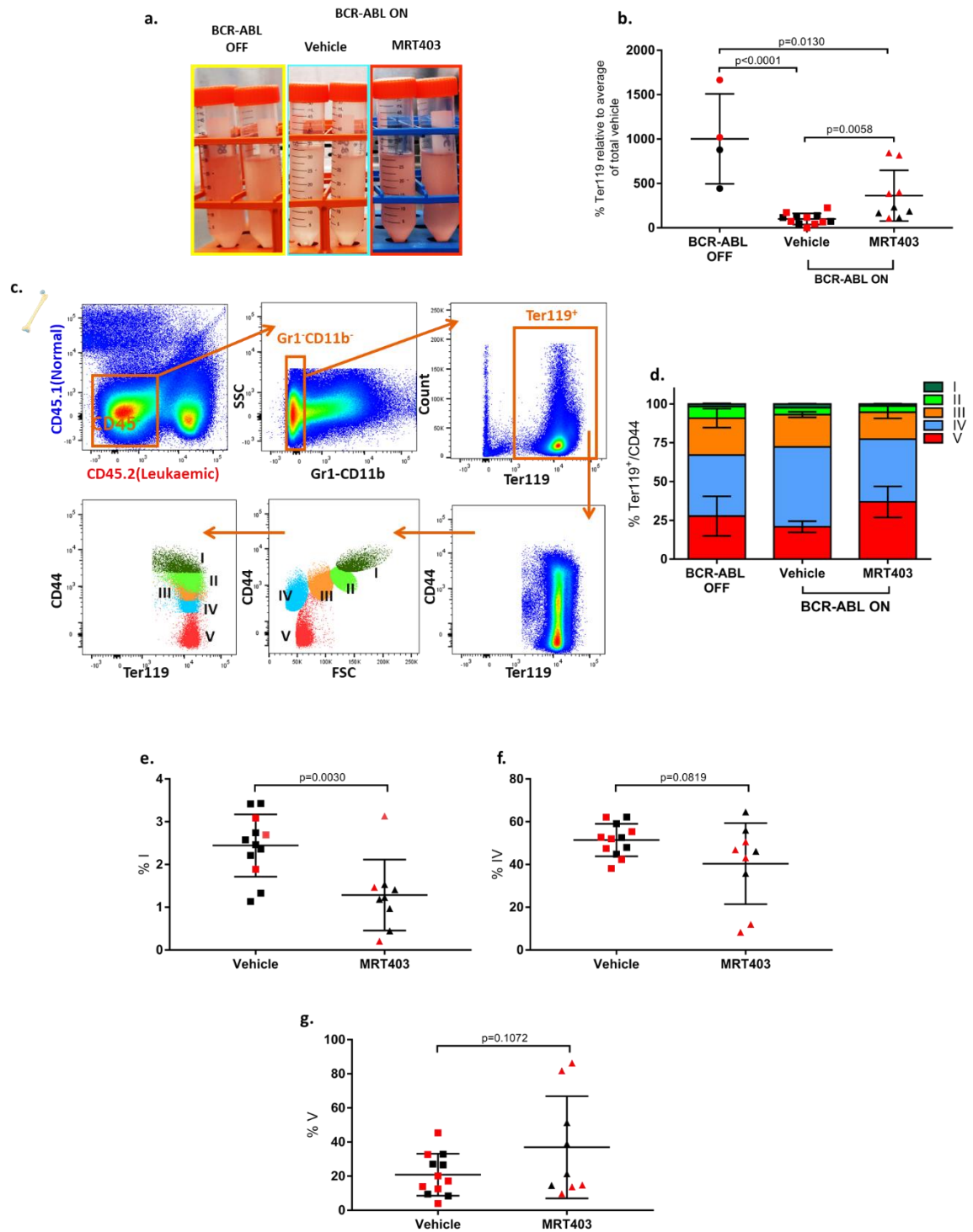


**Figure 5.22: MRT403 treatment increases number of Ter119<sup>+</sup> cells in the BM of leukaemic mice**  
 Representative picture of BM cells following 4 weeks *in vivo* treatment using vehicle or MRT403 and in BCR-ABL OFF mice (a). Graph showing strategy of gating used to measure by FACs levels of erythroid maturation. Cells were first gated on CD45<sup>+</sup> cells and then using an in house made lineage cocktail, GR1<sup>+</sup> and CD11b<sup>+</sup> cells were excluded. From lineage<sup>-</sup> cells (GR1<sup>-</sup>CD11b<sup>-</sup>) Ter119<sup>+</sup> cells were gated and using expression of CD44 surface marker, cells belonging to different stages of erythropoiesis were selected (b). % of Ter119<sup>+</sup> cells in the BM relative to average of absolute number of vehicle treated mice (c). % Ratio of different erythroid precursors following treatment with vehicle or MRT403 and in BCR-ABL OFF mice (d). % of cells within region I (e), IV (f) or V (g) of erythroid maturation Mean  $\pm$  S.D. P values were calculated using unpaired Student T-test.

Even though the analysis performed on the erythroid maturation was performed on the CD45<sup>-</sup> BM cells, which is a mix of leukaemic and normal cells, we anticipate that since the majority of the BM cells were CD45.2<sup>+</sup>, the same trend might occur within the CD45<sup>-</sup> cells. Based on that, we show that leukaemic mice express an anaemic phenotype reducing number of MEPs and most mature erythroid cells (region V). Interestingly, treatment using MRT403 rescued induced BM erythropoiesis in leukaemic mice increasing both MEPs and most mature BM red cells.

#### **5.2.4.12 MRT403 treatment has marginal effect in long-term (LT) and short-term (ST) LSCs *in vivo***

We next investigated whether treatment using MRT403 affected survival of CML LSPCs. To distinguish the different population within the BM harvested from leukaemic mice, FACs multicolour analysis was performed (**Figure 5.23a**). Following gating on live cells and CD45.2<sup>+</sup> cells, lineage specific and differentiated cells were excluded using of streptavidin conjugated antibodies against lineage<sup>-</sup> surface markers (**Figure 5.23a**). Within the lineage<sup>-</sup> BM cells, we identified primitive murine cells as the Sca<sup>+</sup> and C-KIT<sup>+</sup> cells, commonly known as LSK cells. Finally, within the LSK BM cells, LT, ST and MPP subpopulations were identified performing stainings of the surface markers CD48 and CD150, also known as SLAM family markers<sup>247,248</sup> (**Figure 5.23a**).

Results indicate that treatment using MRT403 did not have any significant effect in targeting primitive leukaemic cells such as LT, ST or MPP HSCs (**Figure 5.23b, c and d**). However, a trend of increased MPP is shown following MRT403 treatment.

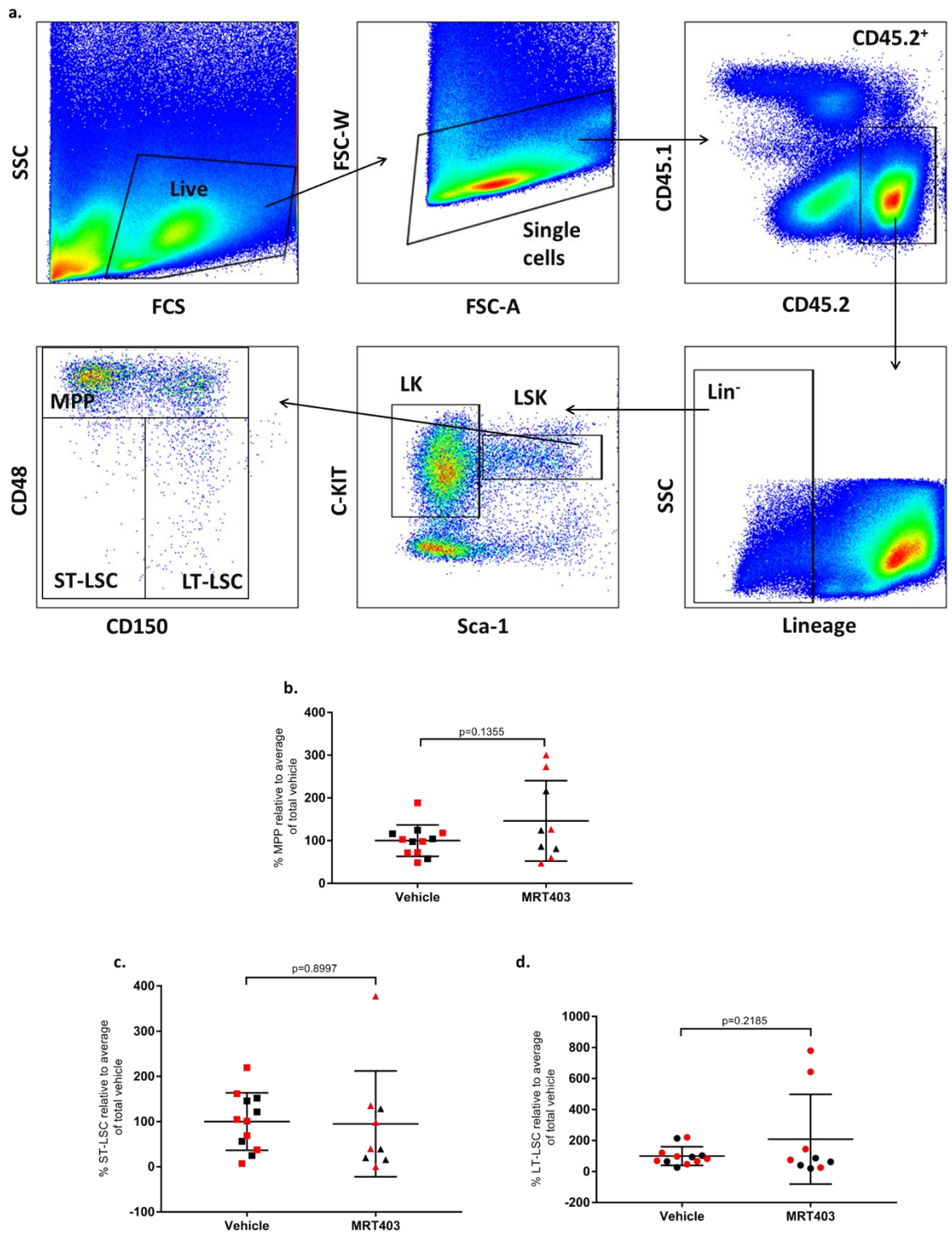


**Figure 5.23: MRT403 treatment has marginal effect on LT- and ST-LSCs and on MPP subpopulation**

Graph showing strategy of gating used to measure by FACS levels of LT-LSCs, ST-LSCs and MPP following treatment using MRT403. Cells were first gated on CD45.2 cells and then using an lineage cocktail, lineage<sup>+</sup> cells were excluded. From lineage<sup>-</sup> cells, LSK cells were selected as C-KIT<sup>+</sup> and Sca1<sup>+</sup> cells. Within the LSK cells, LT-LSCs, ST-LSCs and MPP were revealed based on expression of CD48 and CD150 surface marker (a). % of MPP (b), ST-LSCs (c) and LT-LSC (d) in the BM relative to average of absolute number of vehicle treated mice Mean  $\pm$  S.D. P values were calculated using unpaired Student T-test.

#### 5.2.4.13 MRT403 inhibits TKI-induced autophagy in CD34<sup>+</sup> CML cells

Encouraged by our results using MRT403 as a single agent in inducing differentiation both *in vitro* and *in vivo*, and its effect in inhibiting TKI-induced autophagy in cell lines, we tested the effect of MRT403 on TKI-induced autophagy in CD34<sup>+</sup> CML cells at 3  $\mu$ M.

CD34<sup>+</sup> CML cells were treated for 24 h with 3  $\mu$ M of MRT403 and in combination with 2  $\mu$ M nilotinib. Analysis of p62 in 4 individual CML patient samples shows that treatment with nilotinib reduced p62 levels and increased lipidation of LC3, converting it from LC3B-I to LC3B-II, in 4 different CML samples (**Figure 5.24**). Reduction of p62 and conversion of LC3B-I to LC3B-II confirmed our previously published work that TKI treatment induces autophagy. Depending on the level of autophagy in the individual patient-samples, treatment with MRT403 induced accumulation of p62, specifically sample#9, #6 and#15 (**Figure 5.24**). No clear accumulation of p62 was detected in sample#1, highlighting the need for using additional autophagy marker for autophagy assessment in primary cells. In addition, treatment with MRT403 induced accumulation of both LC3B-I and LC3B-II (**Figure 5.24**). Based on previously published data we expected that following inhibition of early stages of autophagy, lipidation of LC3 might still occur<sup>200</sup>. In this scenario, autophagy is inhibited following treatment with MRT403 and autophagic turn-over of proteins reduced, possible leading to stalled autophagosomes and accumulation of LC3B-II. Finally, combination treatment using MRT403 and nilotinib, inhibited nilotinib-induced autophagy, leading to accumulation of p62 and LC3B-II (**Figure 5.24**).

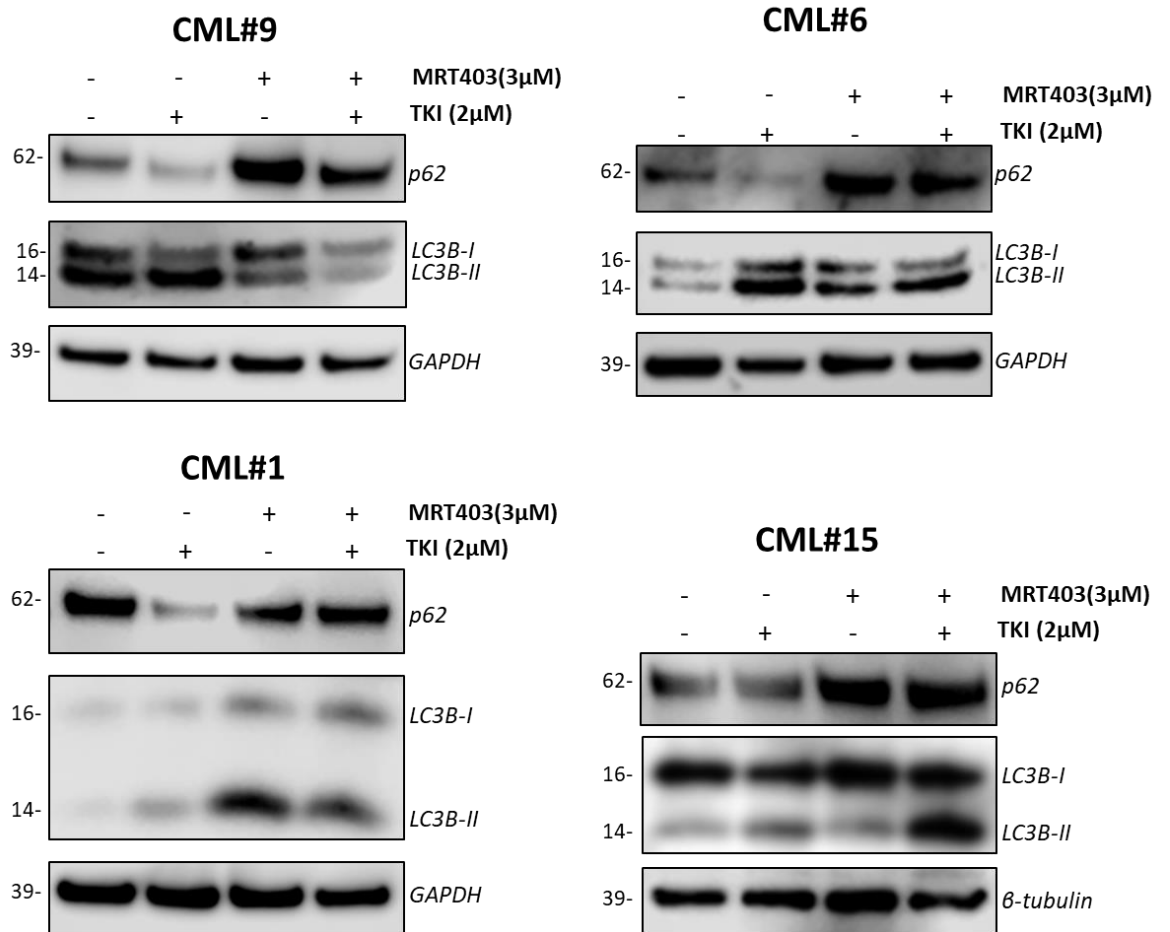


**Figure 5.24: MRT403 inhibits TKI-induced autophagy in CD34<sup>+</sup> CML cells**

Western blot analysis of autophagic markers following 24 h treatment with 3 μM of MRT403 and combination with 2 μM nilotinib. n=4 CML samples.

#### **5.2.4.14 MRT403 enhances nilotinib-induced cell death in CD34<sup>+</sup> cells**

Having demonstrated that MRT403 inhibits TKI-induced autophagy in 4 separate CML samples, we next aimed to assess if MRT403-mediated autophagy inhibition would lead to enhancement in TKI-induced LSPCs eradication. CD34<sup>+</sup> CML cells were plated for 72 and 96 h in presence of MRT403, nilotinib or the combination, and the percentage of Annexin V/7AAD positive cells evaluated by flow cytometry at day 3 and day 6. Analysis at day 3 indicated that using 3  $\mu$ M MRT403 as a single agent did not show any significant increase in apoptosis (**Figure 5.25a, b**). Nilotinib treatment induced 45 % apoptosis which increased to 55 % when combined with 3  $\mu$ M MRT403 (**Figure 5.25a, b**). Similar results were obtained at day 6 with no further increase in apoptosis compared to day 3 (**Figure 5.25c**). The longer-term effect of the combination of nilotinib with ULK1 inhibition was further assessed performing CFC assay. As for measurements of apoptosis, treatment with 3  $\mu$ M MRT403 did not significantly reduce the number of CFC (**Figure 5.26a, b**). Treatment with nilotinib reduced CFC by 50 % which was significantly enhanced in combination with 3  $\mu$ M MRT403 (**Figure 5.26a, b**). To further confirm these results, we measured the number of CD34<sup>+</sup> cells following treatment with MRT403, nilotinib or the combination. As shown in paragraph 5.2.4, treatment using 3  $\mu$ M MRT403 reduced number of CD34<sup>+</sup> cells by 40 %. As well treatment with nilotinib targeted CD34<sup>+</sup> cells with similar efficacy as MRT403, which was significantly enhanced in combination with MRT403 with a 60 % reduction in CD34<sup>+</sup> cells (**Figure 5.26c**).

Furthermore, we measured number of CD34<sup>+</sup>CD133<sup>+</sup> to complement these results. Treatment with MRT403 for 3 days, significantly reduced number of CD34<sup>+</sup>CD133<sup>+</sup> cells (**Figure 5.26d**). Treatment using nilotinib resulted in variable responses between samples in targeting most primitive LSPCs, showing overall no significant decrease. However, effect of nilotinib was significantly enhanced when combined to MRT403 (**Figure 5.26d**). To complement these results and further characterise the effect of inhibition of ULK1 in primitive stem cells, we performed an LTC-IC assay. CD34<sup>+</sup> CML cells were treated for 6 days using MRT403 alone and in combination with nilotinib, followed by co-culture with feeder cells and CFC assay. Analysis on LSCs indicates that 3  $\mu$ M MRT403 treatment significantly reduces

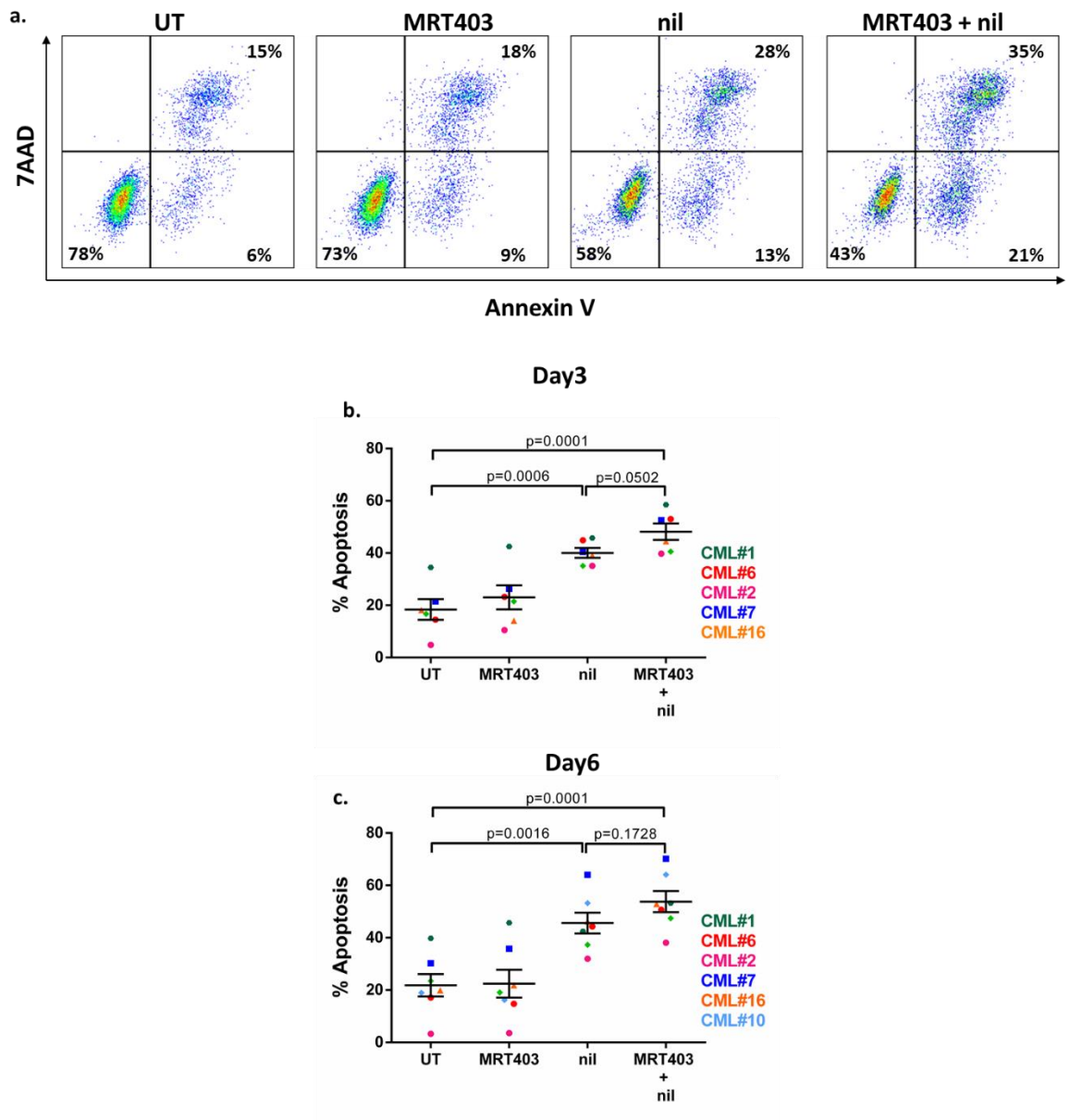


**Figure 5.25: MRT403 targets CD34<sup>+</sup> CML cells in combination with nilotinib**

Representative FACs plots showing measurements of apoptosis following 72 h treatment using MRT403 alone and in combination with nilotinib (a). Measurements of apoptosis following MRT403 treatment alone or in combination with nilotinib after 3 (b) or 6 (c) days. Mean  $\pm$  S.E.M. n=5 CML samples at day 3 and n=6 CML samples at day 6. P values were calculated using unpaired Student T-test.

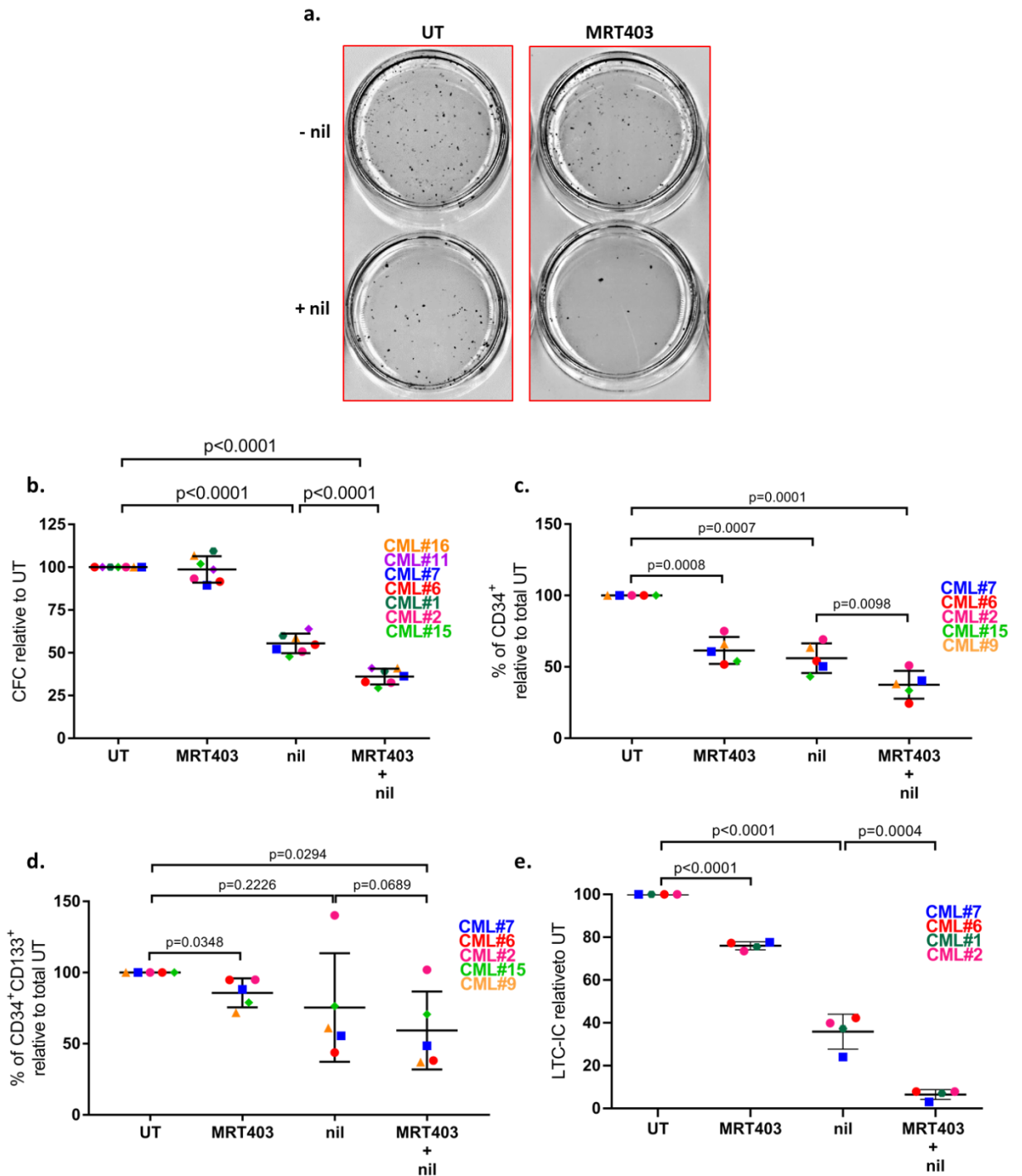


**Figure 5.26: MRT403 targets patient-derived stem and progenitor CML cells**

Representative CFC pictures following 72 h treatment using MRT403 alone and in combination with nilotinib (a). CFC relative to UT following MRT403 treatment alone or in combination with nilotinib (b). % of CD34<sup>+</sup> cells relative to total number of untreated cells following treatment using 3 μM MRT403 and in combination with nilotinib for 72 h (c). % of CD34<sup>+</sup>CD133<sup>+</sup> cells relative to total number of untreated cells following treatment using 3 μM MRT403 and in combination with nilotinib for 72 (d). CFC relative to UT following LTC-IC using MRT403 treatment alone or in combination with nilotinib for 6 days (e). Mean ± S.E.M. n=6 CML samples for CFC, n=5 CML samples and n=4 CML samples for LTC-IC. P values were calculated using unpaired Student T-test.

CFC derived from primitive cells (**Figure 5.26e**). Strikingly, the effect of nilotinib, which reduces CFC following LTC-IC assay by 60 %, was further reduced to 95 % when combined with MRT403 (**Figure 5.26e**).

Taken all together, these results indicate that inhibition of ULK1/2 using MRT403 enhances nilotinib effect in targeting CD34<sup>+</sup> and CD34<sup>+</sup>CD133<sup>+</sup> CML cells. Furthermore, we show that combination treatment significantly enhances nilotinib effect in reducing LSPC survival.

#### **5.2.4.15 Using MRT403 at 3 $\mu$ M has minimal effect on normal CD34<sup>+</sup> CML cells**

To investigate the selectivity of MRT403 against CML cells, we measured the effect of targeting ULK1/2 in normal HSPCs performing measurements of apoptosis and analysis on LSPCs.

Following 72 h treatment using MRT403 as a single agent and in combination with nilotinib, measurements of Annexin V/7AAD positive cells show that 3  $\mu$ M MRT403 induces no changes in cell death compared to untreated cells (**Figure 5.27a, b**). As expected, nilotinib doesn't induce apoptosis in normal CD34<sup>+</sup> cells (**Figure 5.27a, b**). Strikingly, combination treatment with 3  $\mu$ M MRT403 did not induce any increase in cell death either (**Figure 5.27a, b**). To further confirm our data, we measured effects in progenitor and HSCs. CFC assay confirmed no decrease in progenitors following treatment with 3  $\mu$ M MRT403 with a 20% decrease in HSPCs (**Figure 5.27c, d and e**). Minimal effect was seen in both progenitor and HSCs when treated with nilotinib, with no additional effect when combined with 3  $\mu$ M MRT403 (**Figure 5.27c, d and e**).

Taken together, these results show that MRT403 has no effect in normal progenitor cell survival and minimal effect on normal HSC survival alone or in combination with nilotinib. We used treatment with OMA as a positive control.

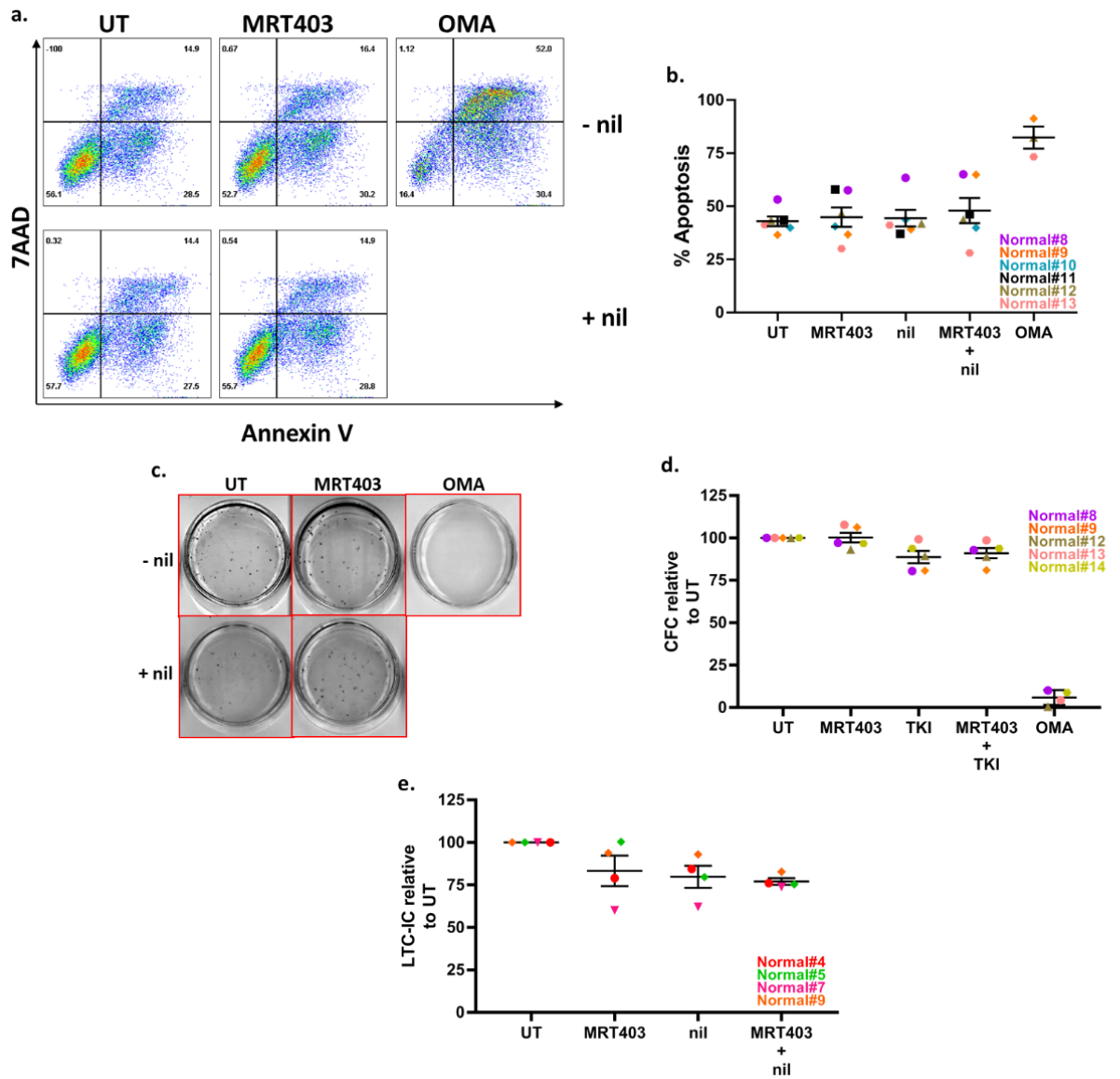


**Figure 5.27: MRT403 has minimal effect in normal stem and progenitor cells**

Measurement of apoptosis following 72 h treatment using MRT403 alone and in combination with nilotinib (a). CFC relative to UT following MRT403 treatment alone or in combination with nilotinib (b). CFC relative to UT following LTC-IC using MRT403 treatment alone or in combination with nilotinib for 6 days (c). Mean  $\pm$  S.E.M. n=8 normal patients for apoptosis, n=6 normal samples for CFC, n=5 normal samples and n=4 CML sample for LTC-IC. P values were calculated using unpaired Student-t-test.

#### **5.2.4.16 MRT403 inhibits basal autophagy in CD45<sup>+</sup> CML cells *in vivo***

Thus far our promising *in vitro* results indicate that MRT403 inhibited TKI-induced autophagy *in vitro*, enhancing TKI in targeting LSPCs.

To study the effect of MRT403 in targeting autophagy in transplanted patient-derived CML cells, we conducted a state-of-the-art patient-derived xenograft (PDX) study transplanting CD34<sup>+</sup> CML cells in immune-compromised NRGW<sup>41</sup> mice<sup>214</sup>. Following 4 weeks after transplant, mice were treated daily with 40mg/Kg for 5 days (**Figure 5.28a, b**). Mice were then sacrificed and hips, femur and tibia were harvested from each mouse (**Figure 5.28a, b**). hCD45<sup>+</sup> cells were FACs sorted and lysed (**Figure 5.28b**). Western blot analysis showed that hCD45<sup>+</sup> transplanted into NRGW<sup>41</sup> mice exhibit accumulation of p62 and measurable increase in levels of complex IV of the electron transport chain following treatment using MRT403 (**Figure 5.28c, d and e**).

Here we have shown for the first time that treatment using a ULK1/2 inhibitor targeted autophagy (and potentially mitophagy) *in vivo*.

#### **5.2.4.17 MRT403 targets LSPCs *in vivo* in combination with imatinib**

Following showing that treatment using MRT403 *in vivo* could target autophagy in hCD45 *in vivo*, we wanted to confirm that combination treatment using MRT403 and imatinib would target CML LSPCs in a PDX study.

Two separate PDX studies were performed using 2 independent patient samples (**Figure 5.29a, b**). In experiment 1, CD34<sup>+</sup> CML coming from sample#15 were transplanted in sub-lethally irradiated and immuno-deficient NOD.CgPrkdcscidll2rgtm1Wjl/SzJ (NSG) female mice (**Figure 5.29a**). Following 6 weeks post-transplant, engraftment of human cells was confirmed by FACs analysis of the human leucocyte surface marker (CD45) in the blood of the animals (**Figure 5.29a**). Based on level of engraftment, mice were then split into 4 treatment arms (i.e. vehicle, MRT403, imatinib and combination of MRT403 and imatinib) and at week 12 post-transplant, mice were treated for 4 weeks (**Figure 5.29a**). In experiment 2, CD34<sup>+</sup> CML sample#6 were transplanted in

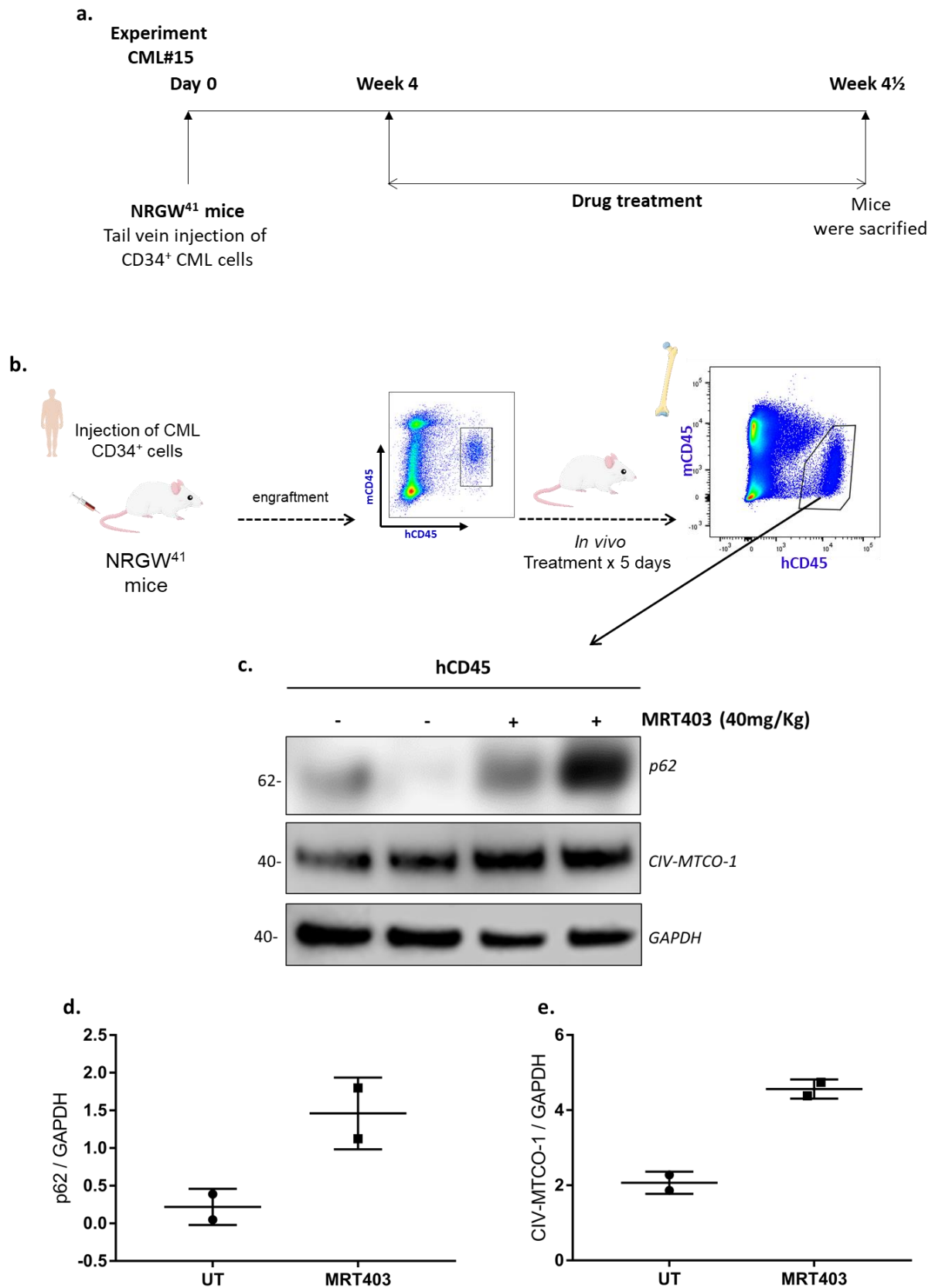


**Figure 5.28: MRT403 inhibits autophagy *in vivo* in transplanted hCD45**

Experimental plan a PDX study using MRT403 treatment (a, b). Males NRGW<sup>41</sup> mice were transplanted with hCD34<sup>+</sup> CML cells and engraftment was allowed to take place for 4 weeks. Mice were then treated *in vivo* for 5 days using MRT403 (a, b). Mice were then sacrificed and hCD45<sup>+</sup> were sorted and lysed (a, b). Western blot analysis of autophagy marker and mitochondrial complex 1 levels (c). Graph showing levels p62/GAPDH (d). Graph showing levels CIV-MTCO-1/GAPDH (e). Mean  $\pm$  S.D.



sub-lethally irradiated and immuno-deficient NRGW<sup>41</sup> female and male mice (that are more irradiation resistant compared to NSG mice and mutation of C-KIT enhances engraftment)<sup>214</sup> (**Figure 5.29b**). The use of different mouse models was in an attempt to reduce the effect of irradiation and potentially increase engraftment efficiency, which is often low using the NSG model. Following 4 weeks post-transplant, engraftment of human cells was confirmed by FACs analysis of the human leucocyte surface marker CD45 in the peripheral blood (**Figure 5.29b**). Based on level of engraftment, mice were split into 4 treatment arms (i.e. vehicle, MRT403, imatinib and combination of MRT403 and imatinib) and at week 9 post-transplant mice were treated for 4 weeks (**Figure 5.29b**). Following treatment, mice were sacrificed, and spleens, hips, femur and tibia were harvested from each mouse.

Since the difference between the experiment was marginal and showed similar trend, the results from both experiments were combined as presented.

Using a hCD45 specific antibody, human transplanted cells were identified (**Figure 5.30a**). Treatment using MRT403 did not show any significant difference in number of hCD45<sup>+</sup> cells compared to vehicle treated mice. Even though treatment with imatinib had no significant effect, variability in engrafted hCD45 was reduced and decreased to  $5 \times 10^5$  number of cells (**Figure 5.30a, b**). No significant additive effect was reached combining imatinib with MRT403 (**Figure 5.30a, b**). To investigate the effect of combination treatment using imatinib with MRT403 in human progenitor cells, hCD45 was combined with expression of the surface marker hCD34 (**Figure 5.30c**). Analysis on hCD45<sup>+</sup>CD34<sup>+</sup> showed that MRT403 had no significant effect on human progenitor cells (**Figure 5.30c, d**). Treatment with imatinib decreased number of hCD45<sup>+</sup>CD34<sup>+</sup>, which was further enhanced in combination with MRT403, significantly reducing number of hCD45<sup>+</sup>CD34<sup>+</sup> in comparison to vehicle treated mice (**Figure 5.30c, d**). Combining hCD34 with hCD133 stem cell markers, we measured the effect of primitive LSCs (**Figure 5.30e, f**). Strikingly, while imatinib had only modest effect when used alone, the combination treatment significantly reduced hCD45<sup>+</sup>CD34<sup>+</sup>CD133<sup>+</sup> cells compared to both vehicle and imatinib treated mice (**Figure 5.30f**).

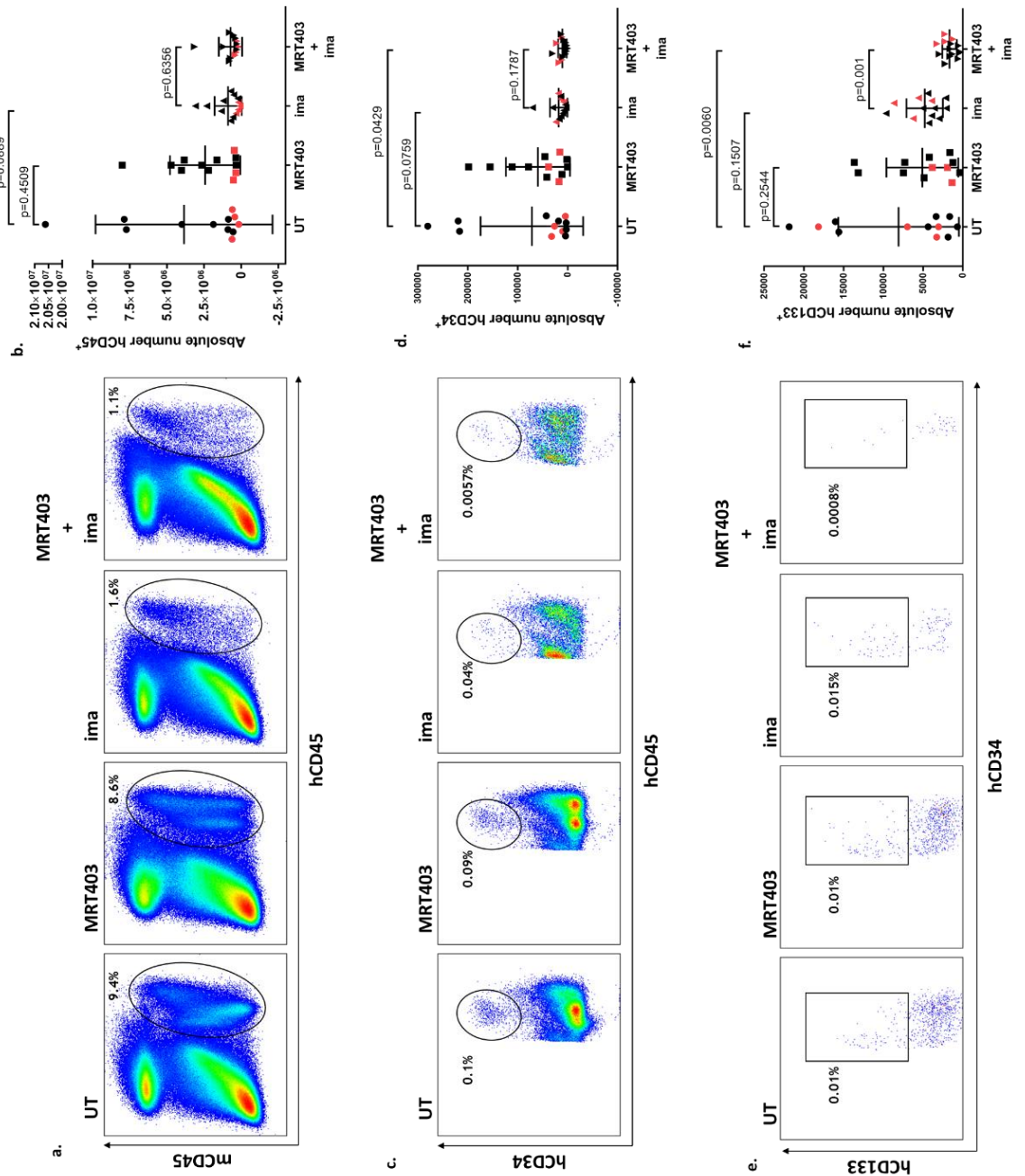


**Figure 5.30: MRT403 targets human LSPCs *in vivo* in combination with TKI**

Graphs showing % of hCD45<sup>+</sup> cells within mouse BM cells (a). % of hCD45<sup>+</sup> relative to total number of BM cells following *in vivo* treatment using vehicle, MRT403, imatinib and combination of imatinib and MRT403 (b). Graphs showing % of hCD45<sup>+</sup>CD34<sup>+</sup> cells within mouse BM cells (c). % of hCD45<sup>+</sup>CD34<sup>+</sup> relative to total number of BM cells following *in vivo* treatment using vehicle, MRT403, imatinib and combination of imatinib and MRT403 (d). Graphs showing % of hCD45<sup>+</sup>CD34<sup>+</sup>CD133<sup>+</sup> cells within mouse BM cells (e). % of hCD45<sup>+</sup>CD34<sup>+</sup>CD133<sup>+</sup> relative to total number of BM cells following *in vivo* treatment using vehicle, MRT403, imatinib and combination of imatinib and MRT403 (f). Mean ± S.D. P values were calculated using unpaired Student T-test.

Thus far we have shown that combining treatment of first and second generation TKIs with MRT403 increased TKIs effect in eradicating primitive leukaemic stem cells.

#### **5.2.4.18 MRT403 treatment reduces number of CD45.2 as a single agent and in combination with imatinib increasing the ratio of normal cells**

The study conducted in this Chapter showed that combining TKI treatment with a specific autophagy inhibitor, human LSPCs were significantly reduced both *in vitro* and *in vivo*. Since treatment using MRT403 in the human PDX model showed promising results, we next aimed to test the combination of imatinib and MRT403 using an inducible murine leukaemic model.

Experiment was conducted transplanting CD45.2<sup>+</sup> cells in sub-lethally irradiated mice. A time frame of 3 weeks was given to establish engraftment of transplanted leukemic cells (keeping BCR-ABL OFF). Tetracycline was then removed from the drinking water, inducing BCR-ABL. Following 10 days BCR-ABL induction, mice were allocated into 4 arms (i.e. vehicle, MRT403, imatinib and the combination of imatinib and MRT403) and treated for 4 weeks. At the end of the treatment, spleen, bone and blood were harvested and analysed measuring the level of the disease.

Measure of the spleen size in the vehicle mice compared to BCR-ABL OFF mice confirmed leukaemia burden in these animals (**Figure 5.31a, b**). As previously shown in **5.2.4.10**, MRT403 treatment did not decrease spleen size, which however was reduced in both imatinib and in combination with MRT403 compared to vehicle treated mice (**Figure 5.31a, b**). As in **5.2.4.10**, treatment with MRT403 significantly reduced the percentage of cells expressing the leukocyte common antigen CD45.2 (**Figure 5.31c**). While imatinib had no effect on the percentage of CD45.2 cells, the combination with MRT403 significantly reduced these cells compared to both imatinib and vehicle mice (**Figure 5.31c**). Moreover, treatment with MRT403, as a single agent or in combination with imatinib, affected the chimerism of CD45.1 and CD45.2 cells by increasing the ratio of CD45.1 normal cell (**Figure 5.31d**).

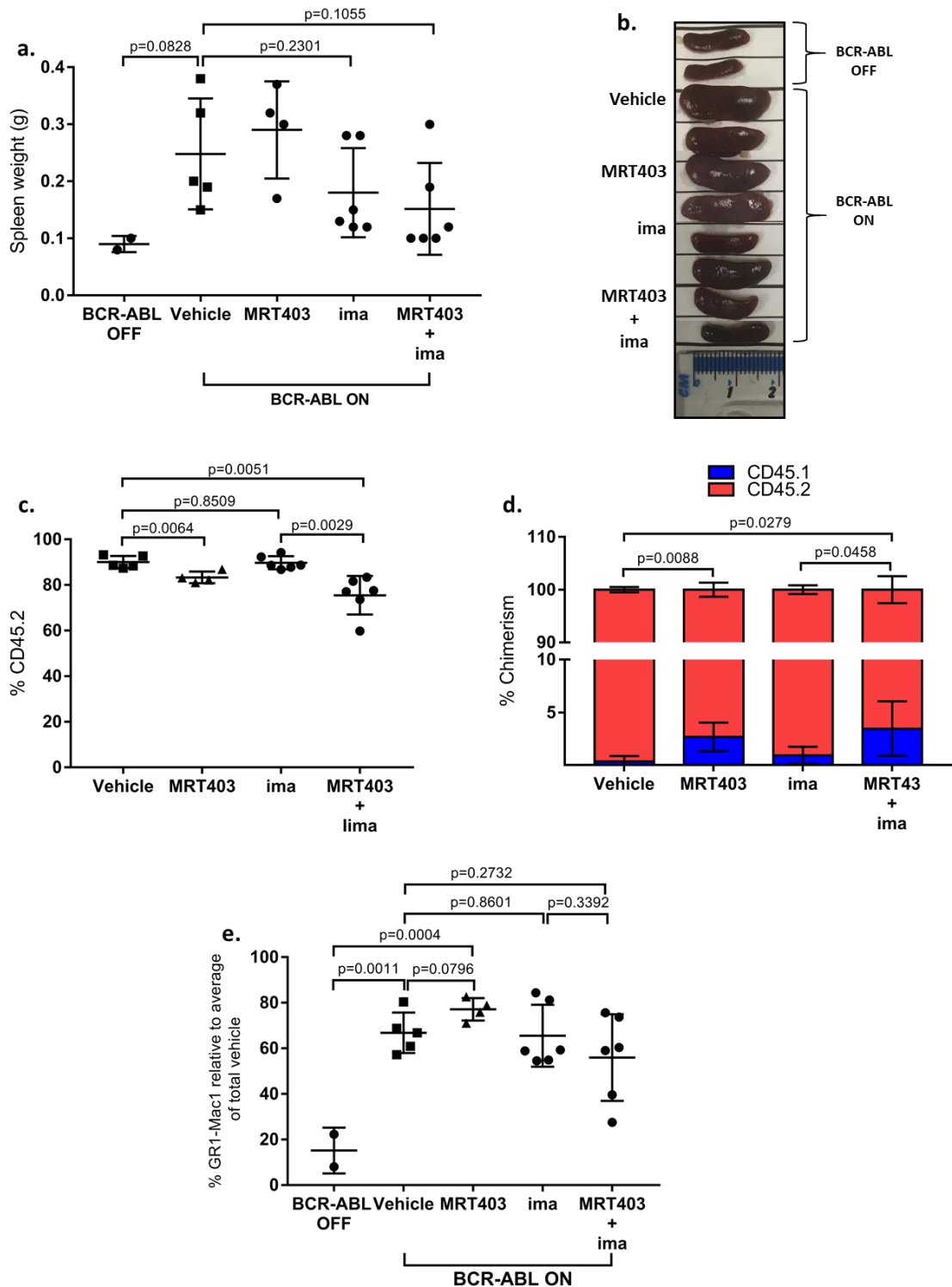


**Figure 5.31: MRT403 reduced percentage of leukaemic cells increasing ratio of normal cells as a single agent and in combination with TKI**

Graph showing spleen weight from each mouse following *in vivo* treatment using vehicle, MRT403, imatinib and the combination of imatinib and MRT403 and BCR-ABL OFF mice (a). Representative picture of spleen from 2 mice from each treatment arm (b). % of CD45.2 cells in the BM of mice treated with vehicle or MRT403 (c). % Ratio of CD45.1 and CD45.2 cells in the BM of mice treated using vehicle, MRT403, imatinib and the combination of imatinib (d) % of BM GR1-Mac1 relative to average of absolute number of vehicle treated mice (e). Mean  $\pm$  S.D. P values were calculated using unpaired Student T-test.

(**Figure 5.31d**). Measurement of myeloid cells, GR1-Mac1<sup>+</sup>, showed an increase in these cells in both vehicle and MRT403 mice, indicating leukaemia induction (**Figure 5.31e**). Neither treatment with imatinib nor the combination with MRT403 significantly reduced number of myeloid cells, although a trend of reduction is shown in the combination arm (**Figure 5.31f**).

#### **5.2.4.19 MRT403 in combination with imatinib inducing BM erythropoiesis in leukaemic mice**

To further elucidate the effect of MRT403 in combination with imatinib *in vivo*, we measured levels of the 3 different myeloid progenitor populations. Results showed no significant difference between the 4 arms in the number of CMPs (**Figure 5.32a**). Interestingly, while both MRT403 and imatinib as a single agent had only a marginal effect on MEPs, the combination of MRT403 and imatinib significantly increased MEPs compared to vehicle treated mice (**Figure 5.32b**). However, no significant effect was shown between the 4 arms in the percentage of GMPs (**Figure 5.32c**).

As described in 5.2.4.11, anaemia remains a problem for leukaemic patients. Furthermore, several studies indicate that anaemia represents one of the side effects induced by treatment with imatinib<sup>249-252</sup>. Treatment using EPO has shown to improve anaemia induced by imatinib treatment in patients however, a variable response has been shown between patients<sup>253</sup>. We now aim to investigate if increased MEPs, induced by MRT403 treatment, results in increased erythroid maturation when MRT403 is used in combination with imatinib.

FACs analysis of number of Ter119<sup>+</sup> cells confirmed our previous data indicating that MRT403 increased number of erythroid cells compared to vehicle mice (**Figure 5.33a**). While treatment with imatinib had no significant effect on the percentage of Ter119<sup>+</sup> cells, combination of imatinib and MRT403 significantly increased number of erythroid cells compared to both vehicle and imatinib treated mice (**Figure 5.33a**).

Analysis of each stage of the erythropoiesis, combining Ter119 with CD44 surface marker, showed that MRT403 as a single agent and in combination with imatinib increased the percentage of cells within region V, which represents mostly mature red cells (**Figure 5.33c**).

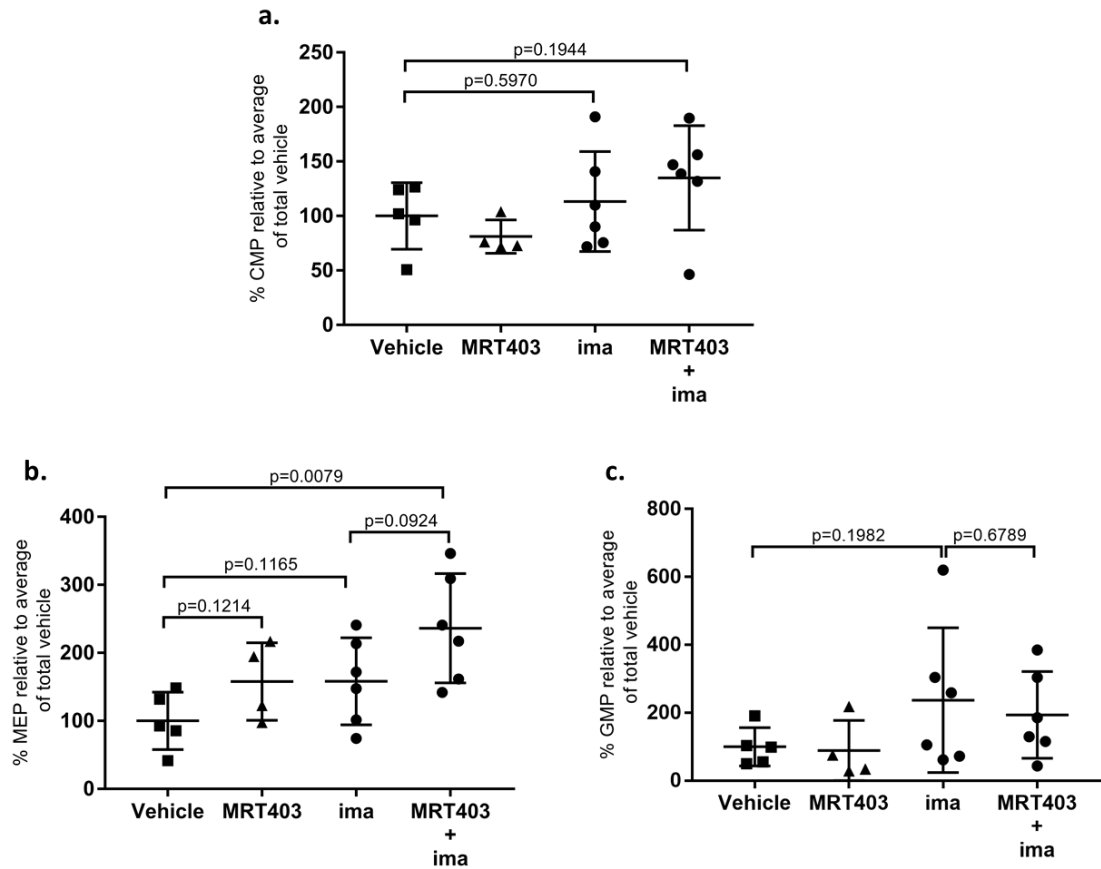


**Figure 5.32: MRT403 and imatinib combination treatment increases percentage of leukaemic MEP *in vivo***

% of CMP (a) MEP (b) and GMP (c) cells in the BM relative to average of absolute number of vehicle treated mice. Mean ± S.D. P values were calculated using unpaired Student T-test.

Analysis on the most immature population, represented by cells in region I, showed that treatment with MRT403, imatinib and the combination of MRT403 with imatinib significantly decreased this population (**Figure 5.33c**). Combination treatment significantly decreased the % of cells within region IV compared to both vehicle and imatinib treated mice (**Figure 5.33d**). Finally, MRT403 as a single agent and in combination with imatinib increased percentage of mature red cells within region V (**Figure 5.33e**).

Thus far we conclude that MRT403 has potential beneficial effect when used in combination with imatinib, by increasing the number of MEP cells. Since the majority of the cells is represented by the leukemic population (CD45.2<sup>+</sup>), we propose that the erythroid differentiation, induced by treatment of MRT403 as a single agent and in combination with imatinib, occurs within the leukaemic cells.

#### **5.2.4.20 MRT403 treatment targets LT-LSCs when used in combination with imatinib**

Finally, we investigated whether combination treatment using MRT403 and imatinib could target LCPCs using the BCR-ABL mouse model. Measurements of MPPs indicates that while imatinib treatment showed no significant effect, combination with MRT403 significantly increased number of MPPs (**Figure 5.34a**). A significant increase was also induced in number of ST-LSCs following combination treatment with MRT403 and imatinib compared to both vehicle and imatinib treated mice (**Figure 5.34b**). Strikingly, while treatment with imatinib significantly enriched for LT-LSCs, combination of imatinib with MRT403 significantly reduced LT-LSCs.

These results suggest that imatinib does not target LT-LSCs. However, combining imatinib with MRT403 significantly reduced LT-LSCs. As suggested by increased number of MPPs and ST-LSCs when imatinib is combined with MRT403, we hypothesis that treatment using MRT403 might induce differentiation of most primitive LSPCs, potentiating imatinib effect in eradicating LT-LSCs.

## Chapter 5 Using MRT403 to target CML LSPCs

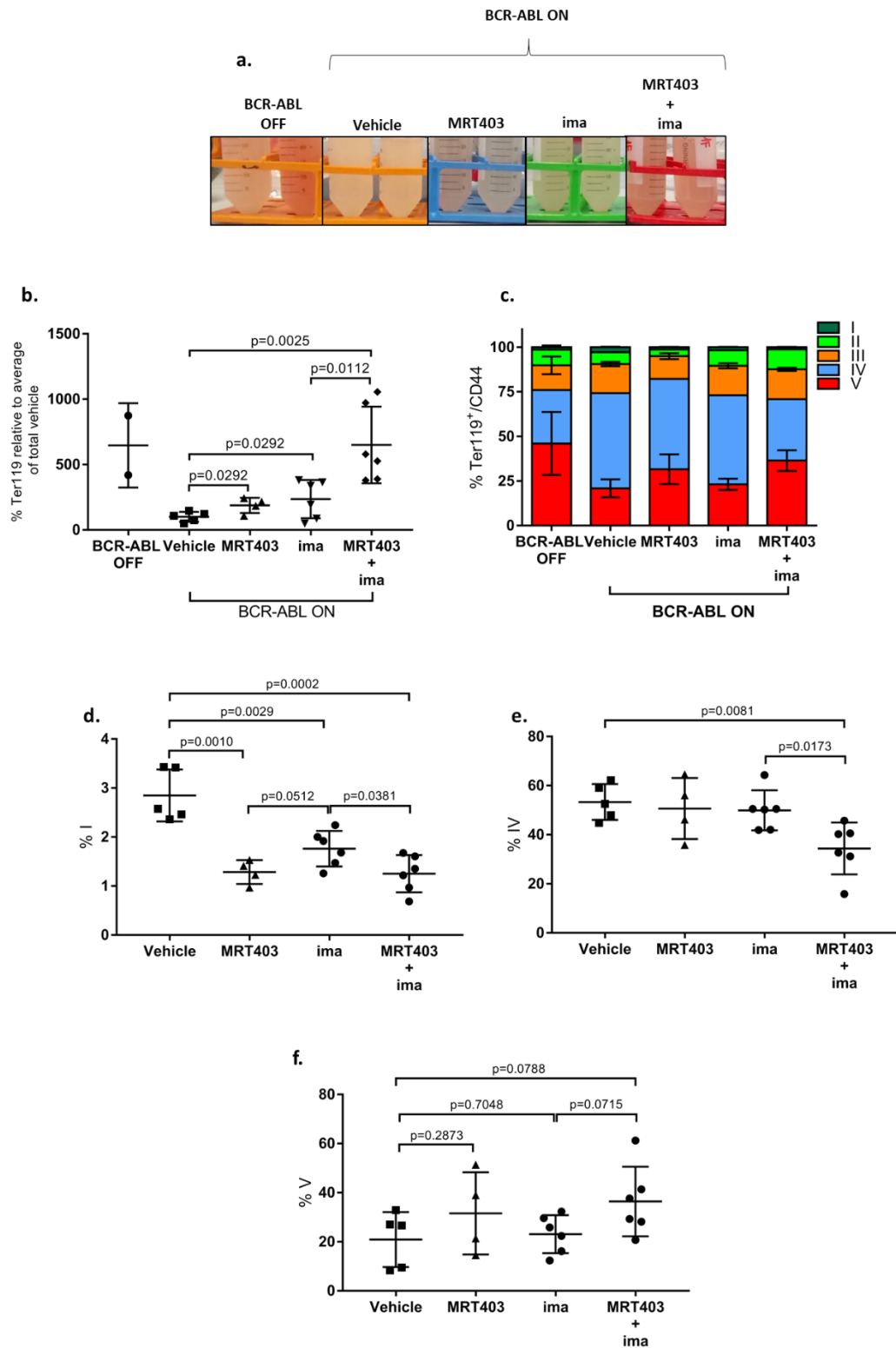


**Figure 5.33: MRT403 treatment increases number of Ter119<sup>+</sup> cells in the BM of leukaemic mice**

Representative picture of BM cells following 4 weeks *in vivo* treatment using vehicle, MRT403, imatinib and the combination of imatinib and MRT403 and in BCR-ABL OFF mice (a). % of Ter119<sup>+</sup> cells in the BM relative to average of absolute number of vehicle treated mice (b). % Ratio of different erythroid precursors following treatment with vehicle or MRT403 and in BCR-ABL OFF mice (c). % of cells within region I of erythroid maturation (d). % of cells within region IV of erythroid maturation (e). % of cells within region V of erythroid maturation (f). Mean  $\pm$  S.D. P values were calculated using unpaired Student T-test.

## Chapter 5 Using MRT403 to target CML LSPCs

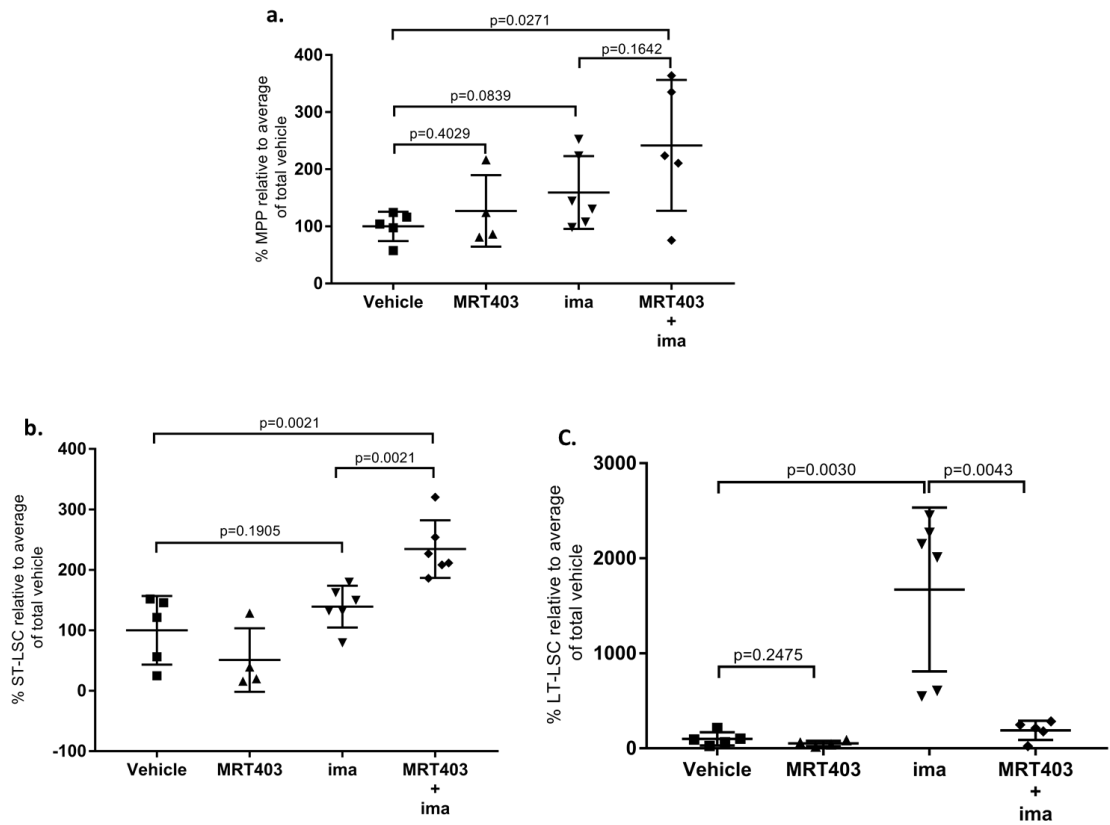


**Figure 5.34: MRT403 treatment in combination with imatinib targets imatinib-resistant LT-LSCs *in vivo***

% of MPP (a) ST-LSC (b) and LT-LSC (c) cells in the BM relative to average of absolute number of vehicle treated mice. Mean  $\pm$  S.D. P values were calculated using unpaired Student T-test.

### 5.3 Discussion

In this chapter we tested the effect of new inhibitors of ULK1/2 since previously used MRT921 had shown off-target and toxicity effects (4.2.2), (4.2.12.)

A number of 3 inhibitors provided by LifeArc were tested in WT and ULK1 deficient cells, showing reduced cytotoxicity effect. However, Parkin-dependent mitophagy assay revealed that only MRT993 at high concentration and MRT403 at concentration higher than 0.25  $\mu\text{M}$  inhibited basal and stress induced mitophagy. These results, together with measurements of TKI-induced autophagy, led us to choose our top candidate to test in combination with TKI *in vitro* and *in vivo*.

Using patient-derived CD34<sup>+</sup> CML cells we showed that MRT403 treatment used at a concentration of 3  $\mu\text{M}$  inhibited basal mitophagy, increased OCR and ROS levels, and reduced glycolysis. Using ULK1 and ATG7 deficient cells, we showed that while the increase in OCR was occurring in both autophagy deficient cells, reduced glycolysis was observed only in ULK1 deficient cells. However, ATG7 deficient cells exhibit reduced glycolysis following treatment with MRT403. Based on that we propose that the reduced glycolysis is an ULK1-dependent effect.

Loss of CD34<sup>+</sup>CD133<sup>+</sup> expressing cells following treatment with MRT403 prompted us to hypothesise that an induction of differentiation might occur as a result of increased mitochondrial respiration and increased ROS levels. Combination treatment using 3  $\mu\text{M}$  MRT403 with low concentration of EPO, confirmed our hypothesis showing that while untreated cells did not respond to EPO, treatment with MRT403 enhanced erythropoiesis measured with increased level of CD44<sup>+</sup>GlyA<sup>+</sup>, CD71<sup>+</sup>GlyA<sup>+</sup> and CD36<sup>+</sup>GlyA<sup>+</sup> cells.

Using ULK1 deficient cells we showed same results as obtained using primary cells, with ULK1 exhibiting increased ROS and erythroid maturation in K562 cells.

Using a leukaemic model expressing inducible BCR-ABL, we showed that following treatment with MRT403, mice exhibit increased MEPs, which led to increased erythroid maturation, inducing BM erythropoiesis.

## Chapter 5 Using MRT403 to target CML LSPCs

Encouraged from our positive results, we tested the combination of MRT403 with TKI *in vitro*, using nilotinib and *in vivo*, using imatinib.

Using 4 different CD34<sup>+</sup> CML samples we showed that treatment with MRT403 inhibited TKI-induced autophagy, measured by accumulation of p62 and LC3B-II. Furthermore, MRT403 treatment enhanced TKI effect in targeting LSPCs with marginal effect on normal CD34<sup>+</sup> cells.

Promising results *in vitro* let us to test the effect of the ULK1/2 inhibitor *in vivo*. A PDX study transplanting CD34<sup>+</sup> CML samples in immune-compromised mice showed that following 5 days treatment, MRT403 was able to target autophagy in transplanted human cells *in vivo*, measured by accumulation of p62 and complex IV of the electron transport chain. Strikingly, combination treatment increased imatinib effect in targeting CD34<sup>+</sup>CD133<sup>+</sup> cells in 2 independent PDX studies using 2 separate CML samples.

Finally, combination treatment using MRT403 and imatinib significantly reduced LT-LSCs (95 %), possibly due to differentiation effect induced followed MRT403 treatment. Furthermore, an increase in MEPs and mature red cells was observed in the BM of treated mice with the combination of MRT403 and imatinib with the mice showing no sign of reduced BM erythropoiesis.

Despite the promising results obtained in this section, it would be interesting to perform some kinetic analysis comparing effect between MRT403 and MRT921 and show reduced unspecific effect with the MRT403. Together with that it would be relevant to perform RNA-seq following treatment using both MRT403 and MRT921 to clarify which gene signature is affected in each treatment and assess any variation.

ULK1 inhibition has been shown to inhibits erythroid maturation during normal haematopoiesis. However, in our study we observe a different phenotype. Understanding if ULK1 has a different role in the contest of CML is a relevant question. It might be that in the case of CML ULK1 is not required for erythroid maturation or LSPCs might adapt the lack of ULK1 switching to different pathways to remove mitochondria such as delivering mitochondria to the lysosomes using

mitochondrial vesicle bodies. Performing treatment using MRT403 in normal mice might clarify this question.

In this section we show for the first-time inhibition of autophagy using a ULK1 inhibitor in vivo. However, due to limitation of engraftment, our studied measured accumulation of p62 only in hCD45 compartment. Despite the progress made with the mouse model to enhance engraftment, human CML cells still have a poor engraftment level which limits our studies. It would be of interest to measure the level of inhibition in more primitive LSCs and compare it with less primitive cells such as CD45. Furthermore, irradiation of NRGW<sup>41</sup> is necessary for engraftment of human CML cells which represent a limitation for our studies since mice never develop the disease but only represent a disease recipient.

## **Chapter 6 Conclusion and future directions**

## 6.1 Conclusions

In this thesis we investigate the effect of inhibiting ULK1-dependent autophagy in CML LSPCs as a potential treatment for CML patients in combination with TKIs. In the paragraphs below we will discuss our findings in relation with latest literature and propose future direction for the work presented in this thesis.

### 6.1.1 Autophagy in HSCs and LSCs

The relevance of autophagy in normal and malignant cells has been of great focus in the past 20 years. Autophagy plays a critical role physiologically, representing one of the main mechanisms that cells use to remove damaged and potentially dangerous waste from the cytoplasm, and provide new building blocks/energy following starvation. However, malignant cancer cells, may hijack this process to sustain their own survival and thereby promote progression of the disease<sup>254-258</sup>.

HSCs are required to produce all the cells circulating in the blood stream for the entire length of an individual life. For that reason, HSCs are protected from any unnecessary need of expansion, located in the hypoxic niche of the BM. Autophagy has been shown to play an important role in normal HSCs. Indeed, autophagy is highly upregulated in quiescent HSCs and plays a critical role in regulating oxidative metabolism and their maintenance<sup>163,165,168</sup>. Evidence indicates that autophagy contributes to mitochondrial removal (to favour glycolytic metabolism) to repress differentiation induced by elevated mitochondrial ROS<sup>30,31,160,163,165,181</sup>. Autophagy not only orientates HSCs to quiescence but also promotes slow cell cycle to ensure preservation and health of long-lived stem cells<sup>167,259</sup>. In fact, fewer replication cycles with minimum telomere shortening ensure that HSCs age more slowly.

CML is a myelo-proliferative disorder which causes the expansion preferentially of granulocytes belonging to the myeloid lineage. The role of autophagy is not as clear in the context of CML. In first instance CML is a 3 stages disease and the role of autophagy could be different, not only within the large heterogeneity of LSPCs, but also in relation to disease progression from CP to AP and finally to BC phase. Recent studies propose that CP LSCs have a higher mitochondrial content together

## Chapter 6 Conclusion and future directions

with an elevated oxidative metabolism compared to HSCs<sup>114</sup>. Based on these findings we hypothesise that CP CML LSPCs have reduced levels of autophagy to favour myeloid expansion and a more pronounced mitochondrial metabolism in comparison to normal HSCs. Furthermore, *Baquero et al.* proposed that the primitive murine LSCs have higher level of autophagy compared to more differentiated cells<sup>193</sup>.

To address our hypothesis and to clarify levels of autophagy between normal and LSPCs, we used CD34<sup>+</sup> normal and CML cells and measured expression of autophagy related genes in both populations. Our result suggests an overall increase in autophagy gene expression in normal CD34<sup>+</sup> cells, with ATG7, ATG16L2 and MAP1LC3A having the highest expression levels. Both ATG7 and ATG16L play an essential role in LC3 lipidation and binding to the autophagosomal membranes<sup>155,156</sup>. Significant increase is also observed in SQSTM1 (p62), a cargo receptor which function is involved in removal of protein-aggregates by direct binding to LC3-II. No significant changes were observed in ATG9 and RPS6KB1. ATG9 has been reported to contribute to lipids supply for the formation of the double membrane vesicles and play a key role in autophagy initiation<sup>260,261</sup>. However, this might not be the case in CD34<sup>+</sup> normal and LSPCs. RPS6KB1 encodes for RPS6K, a down-stream of mTOR, which negatively regulates autophagy<sup>262</sup>. RPS6 is the direct down-stream of RPS6K. mTOR phosphorylation of RPS6K, routinely used to measure of mTOR activity, activates the kinase which phosphorylates RPS6 inducing protein synthesis at the ribosomes. However, kinase activity might not correlate with its gene expression. In this regard it would be informative to measure phosphorylation of mTOR and its down-stream RPS6K and RPS6 to clarify its role in normal and LSCs.

We next performed measurements of autophagic flux, using treatment with lysosomotropic agents, such as HCQ, and inhibitor of the fusion between autophagosome and lysosomes, such as bafilomycin, to repress degradation of LC3-II. Our results indicate that normal CD34<sup>+</sup> cells have higher accumulation of LC3B-II than the leukaemic counterpart. However, these experiments were performed in CD34<sup>+</sup> cells consisting of a mixture of stem and progenitor cells. In this context, it would have been interesting to evaluate in which way HSCs and LSCs upregulate autophagy and to compare it with more differentiated cells. One way to assess this would have been to FACs sort stem and progenitor cells in both

leukemic and normal cells. Comparison of their surface marker expression and evaluation of autophagy in each of these populations. However, the restricted number of primary cells made these experiments challenging and difficult to perform. Further studies are still necessary to elucidate the role of autophagy in CML LSCs and to determine level of autophagy between normal and leukaemic stem and progenitor cells.

### **6.1.2 TKI-induced autophagy in CML**

The introduction of imatinib, first generation TKIs, in the early 2000 for the treatment of CML was defined as “a magic bullet” in the war against cancer. Despite the great success of TKI treatment, leukaemia is not eradicated in the vast majority of patients, and patients can develop sign of resistance and persistence of the disease with time. Among all the signal pathways affected by inhibiting BCR-ABL, leading to inhibition of uncontrolled proliferation of myeloid cells, imatinib activated protective autophagy<sup>263</sup>. Autophagy was therefore proposed to adapt leukaemic cells to the metabolic stress induced by imatinib treatment.

Our attempt to compare level of autophagy between normal and LSCs, showed reduced level of autophagy in leukaemic cells. We hypothesised that this might be due to BCR-ABL signal on mTOR, which negatively regulates autophagy by phosphorylation of ULK1. In this regard, ULK1 might represent the direct link between BCR-ABL, mTOR and autophagy inhibition.

To address the hypothesis that inhibition of BCR-ABL using TKIs leads to an induction of autophagy, we used a second generation TKI, nilotinib (a more potent and cleaner inhibitor of BCR-ABL)<sup>264,265</sup> and showed an increase expression of autophagy genes together with a decrease in p62 levels and an increase in lipidation of LC3 (LC3B-II). Based on that, we confirm that using TKIs to target BCR-ABL results in increased levels of autophagy. We then wanted to clarify the link between BCR-ABL inhibition and autophagy activation. ULK1 was among all the genes that showed a higher expression following nilotinib treatment. Furthermore, we showed that inhibiting the kinase activity of BCR-ABL resulted in activation of AMPK and inhibition of mTOR. Both AMPK and mTOR are the master regulator of cellular energy sensing, emphasising the metabolic stress induced by

TKI treatment<sup>129</sup>. AMPK and mTOR are also the main regulators of autophagy<sup>126,127,266</sup>. Indeed, we showed that inhibition of mTOR and activation of AMPK resulted in increased ULK1 kinase activity measured by its direct phosphorylation of ATG13.

To validate our data, we generated ULK1 deficient cells. Our results indicate that genetic removal of ULK1 leads to a deficiency in autophagy in CML cells, measured with increased level of p62 and accumulation of LC3B-II. Even though we suspect that ULK1 deficient cells might still have residual autophagy, this might not be enough to sustain TKI-induced stress<sup>185</sup>.

Our data, suggesting activation of ULK1 following TKI treatment, are in line with recent publication by *Han et al.*<sup>267</sup>. In their study authors describe a new signalling pathway that leads to ULK1 and autophagy activation following imatinib treatment. They propose that granalcin (GCA) is highly expressed in imatinib-resistant CML cells, demonstrating that GCA results in activation of ULK1 through a positive regulation of the ubiquitin ligase TRAF6.

### **6.1.3 Inhibition of autophagy induces phenotype changes in LSPCs**

Thus far, the limited drugs available to specifically inhibit autophagy has led to use lysosomothropic agents such as HCQ and its derivatives to target autophagy.

In this thesis we investigate for the first time the effect of specific inhibition of autophagy in CML targeting ULK1, a serine/threonine kinase required in the initiation complex of autophagy.

In line with previous published data suggesting that ULK1 plays a central role in regulating clearance of mitochondrial<sup>130,268,269</sup>, we use Parkin-dependent mitophagy to measure autophagic flux following genetic removal of ULK1 and ATG7. In addition to the fact that defective mitophagy was observed in ULK1 and ATG7 deficient cells, we also observed that the clearance of each individual complex of the electron transport chain might be specifically dependent on ULK1 or ATG7. We observed that removal of complex IV is more enhanced in ATG7 deficient cells while a higher accumulation is observed in ULK1 deficient cells. Instead, removal of complex I and II might be more dependent on ATG7. However,

## Chapter 6 Conclusion and future directions

further investigations are required to clarify how individual electron chain complexes are affected by mitophagy.

Measurements of inhibition of basal and stressed induced Parkin-dependent mitophagy was adopted in this study to validate 4 different ULK1 inhibitors provided by LifeArc. Our results indicate that MRT016 has no effect in targeting mitophagy at any concentration used while MRT993 has an effect at the highest concentration used. However, the greatest effect where obtained using MRT921 and MRT403, with significant inhibition of autophagic flux.

Despite the effect shown by inhibition of mitophagy, treatment with MRT921 showed unspecific effects in targeting ULK1 deficient cells. In agreement with the off-targets effect shown using MRT921 at 1  $\mu$ M by *Petherick et al.*, and the reduced toxicity in ULK1 KO cells following treatment with MRT403, we selected MRT403 as our top candidate to inhibit ULK1 in CD34<sup>+</sup> CML cells<sup>200</sup>.

In line with inhibition of mitophagy, pharmacological inhibition of ULK1 /2 in CD34<sup>+</sup> CML cells using MRT403, resulted in increased OCR and ROS levels. Similar results were observed using MRT921 in KCL22 cells. Furthermore, previous work from our lab showed comparable effect in ATG7 deficient cells and using HCQ treatment<sup>189</sup>.

An autophagy-independent role of ULK1 in regulating glucose fluxes between glycolysis and PPP was credited to ULK1<sup>145</sup>. In line with that, we showed that pharmacological inhibition of ULK1 /2 using MRT403 reduces glycolysis and NADPH in CD34<sup>+</sup> CML cells. Similar effect in glycolysis was observed in ULK1 KO cells and using MRT921 in KCL22 cell line. Since ATG7 deficient cells had no changes in glycolysis compared to control cells and that reduction was induced following treatment using MRT403, we also confirmed the specificity of ULK1 in regulating glycolysis.

Increased oxidative stress and ROS are often associated with induced differentiation<sup>189,235,236</sup>. In agreement with previous work from our lab shown using HCQ, or its derivative Lys05, we showed that increase in oxidative metabolism following inhibition of autophagy, led to increased differentiation<sup>189,193</sup>. Using MRT403 treatment induced a rapid loss of CD34<sup>+</sup>CD133<sup>+</sup> cells. We demonstrate that loss of primitive LSPCs was associated with increased response to low units of EPO

following inhibition of ULK1/2, leading to increased erythroid maturation. Same phenotype was observed in leukemic mice, in which anaemia represents a critical side effect of the disease. Despite the fact that rescuing anaemia might be beneficial for CML patients, these results are in disagreement with previous published data<sup>185</sup>. *Kundu et al.* demonstrated that accumulation of immature reticulocytes is observed in ULK1 deficient mice. Given to ULK1's role during red blood cell maturation in normal haematopoiesis, we propose that the scenario might be different during leukemogenesis. Taken into account the anaemic phenotype observed in CML patients and that increased erythroid maturation is observed in an autophagic dependent manner (increased erythropoiesis is observed in ATG7 or ULK1 deficient cells and following treatment with HCQ), we can suggest that the metabolic switch towards oxidative respiration in autophagy deficient CML cells might overcome loss of ULK1 inducing erythroid maturation. It is also possible that erythroid maturation might not be dependent on ULK1 during leukemogenesis and removal of cellular component (such as mitochondria and nucleus) might be happening in an ULK1 independent manner, or other unknown mechanism might overcome loss of ULK1. However further investigations are required to clarify the effect observed.

### **6.1.4 Inhibition of ULK1 to target TKI-induced autophagy and overcome TKI sensitivity in CML LSPCs**

Inhibition of TKI-induced autophagy is considered an attractive target to eradicate LSPCs<sup>192,194,198,270,271</sup>. The value represented by a combination treatment using front line treatment for CML, imatinib and HCQ, an indirect inhibitor of autophagy, provided the rationale for the CHOICES (CHlOroquine and Imatinib Combination to Eliminate Stem cells), a phase II clinical trial. However, recent evidence shows that doses required to target autophagy are not achievable in patients, resulting in limited effectiveness for CML. Furthermore, *Baquero et al.* highlighted the limited efficacy of HCQ when compared to Lys05, a more potent derivative of HCQ<sup>193</sup>. However, targeting lysosomes still remains only an indirect way to block autophagy.

In this study we have tested for the first time the efficacy of targeting TKI-induced autophagy using an inhibitor of the initiation complex of the catabolic process, precisely ULK1.

## Chapter 6 Conclusion and future directions

Using MRT403 treatment, we showed inhibition of TKI-induced autophagy in CD34<sup>+</sup> CML cells. MRT921 treatment also showed similar results. Strikingly, efficacy of MRT403-mediated inhibition of TKI-induced autophagy resulted in enhanced efficacy of combination treatment in targeting LSCs. Together with that, cytotoxic effect shown by MRT921 on normal CD34<sup>+</sup> cells were reduced using MRT403.

Using a PDX model, we showed for the first time that treatment using a ULK1/2 inhibitor, MRT403, targeted autophagy *in vivo* in transplanted human cells. Furthermore, inhibition of ULK1/2 using MRT403 significantly sensitised CD34<sup>+</sup>CD133<sup>+</sup> engrafted cells to imatinib treatment. Of high significance, using a BCR-ABL<sup>+</sup> mouse model, we demonstrate that MRT403-mediated inhibition of ULK1 significantly decreased LT-LSCs when combined with imatinib, increasing number of more differentiated ST-LSCs and MPP cells (**Figure 6.1**).

Of clinical relevance, treatment with MRT403 significantly overcame the reduction of BM erythropoiesis disease and imatinib-induced (**Figure 6.1**).

## 6.2 Future directions

Inhibiting ULK1 has resulted in great success in enhancing TKIs effect both *in vitro* and *in vivo*, making it a good candidate to eradicate LSCs in CML patients (**Figure 6.1**).

Despite the fact that removal of ULK1 has been shown to be deleterious for muscle and brain development, using an inhibitor of ULK1 might not induce similar effects<sup>268,272</sup>. In first instance treatment of a disease would not be permanent, but only for a period of time, and inhibition of ULK1 and autophagy would probably only be partial. In this regard, we must underline the achievability and lack of toxicity effect of the molecule when used *in vivo*. Both normal and leukaemic mice, following a month regime of the inhibitor did not

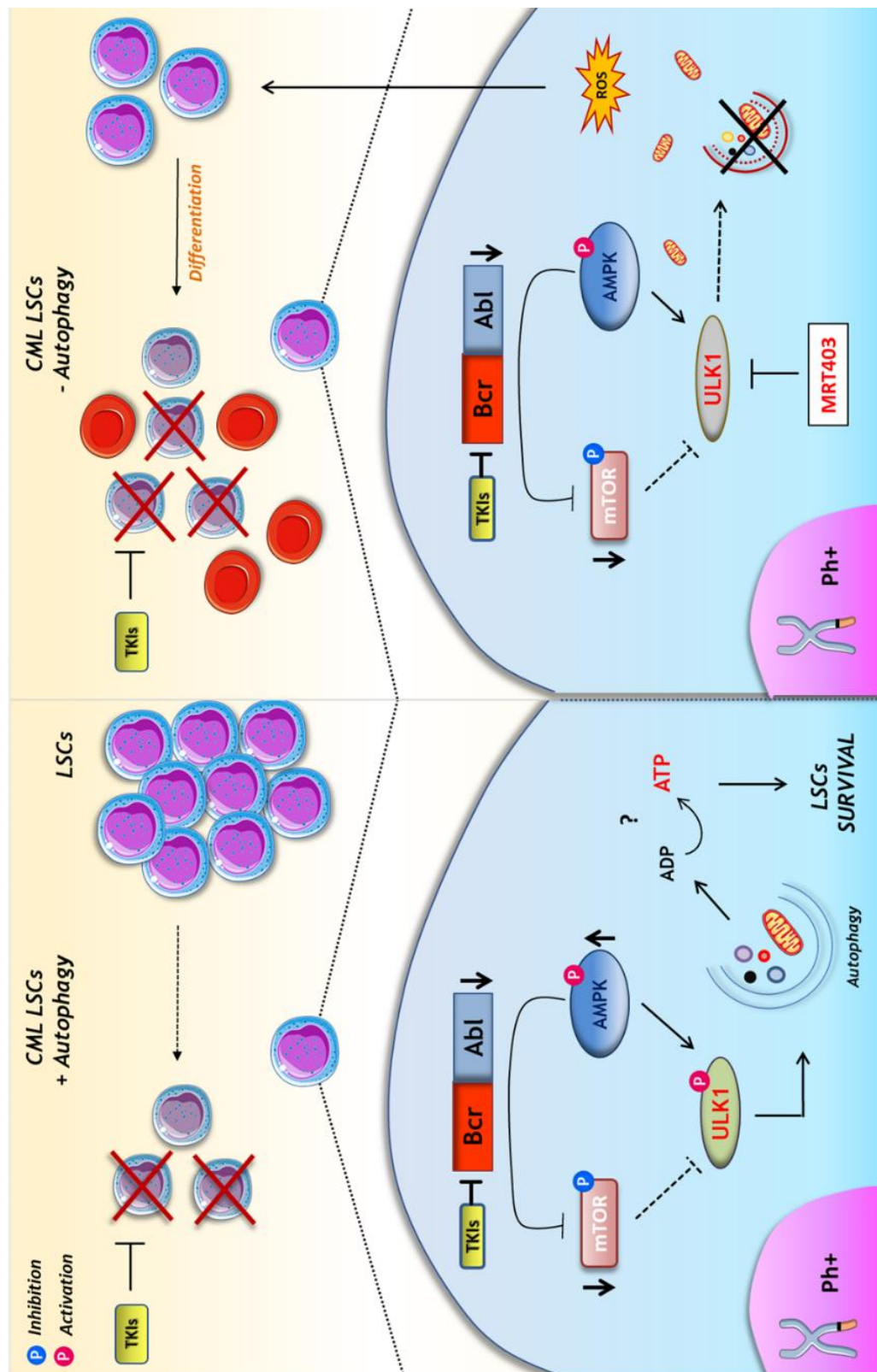


**Figure 6.1: Inhibition of ULK1-dependent autophagy induces differentiation of LSCs potentiating TKI treatment and inducing BM erythropoiesis.**

Schematic representation of main features involved in TKI-induced autophagy in LSCs and how the differentiation induced following treatment using MRT403 enhances TKI efficacy. LSCs upregulate autophagy through activation of ULK1 as a protective mechanism against TKI treatment. Inhibition of ULK1 using MRT403 enables TKI-induced autophagy inducing differentiation of LSCs towards erythroid lineage improving TKI treatment and rescuing TKI-induced reduction of BM erythropoiesis.

## Chapter 6 Conclusion and future directions

show any adverse effect, which further enhance its applicability for treatment of leukaemia, and possibly other malignancies such as anaemias.

Of interest, it would be valuable to further define the effect of using MRT403 on HSCs and erythroid maturation using robust and physiological disease models.

Furthermore, uncover the unknown mechanisms that regulates clearance of mitochondria and other organelles to lead to a mature red cell following inhibition of autophagy is of great interest. This may also reveal novel mechanism(s) that might overcome mitophagy when autophagy is impaired.

## Bibliography

- 1 Zambidis, E. T. *et al.* Emergence of human angiohematopoietic cells in normal development and from cultured embryonic stem cells. *Ann N Y Acad Sci* **1106**, 223-232, doi:10.1196/annals.1392.010 (2007).
- 2 Fukuda, T. Fetal hemopoiesis. I. Electron microscopic studies on human yolk sac hemopoiesis. *Virchows Arch B Cell Pathol* **14**, 197-213 (1973).
- 3 Tavian, M., Robin, C., Coulombel, L. & Peault, B. The human embryo, but not its yolk sac, generates lympho-myeloid stem cells: mapping multipotent hematopoietic cell fate in intraembryonic mesoderm. *Immunity* **15**, 487-495 (2001).
- 4 Julien, E., El Omar, R. & Tavian, M. Origin of the hematopoietic system in the human embryo. *FEBS Lett* **590**, 3987-4001, doi:10.1002/1873-3468.12389 (2016).
- 5 Baum, C. M., Weissman, I. L., Tsukamoto, A. S., Buckle, A. M. & Peault, B. Isolation of a candidate human hematopoietic stem-cell population. *Proc Natl Acad Sci U S A* **89**, 2804-2808, doi:10.1073/pnas.89.7.2804 (1992).
- 6 Hao, Q. L., Thiemann, F. T., Petersen, D., Smogorzewska, E. M. & Crooks, G. M. Extended long-term culture reveals a highly quiescent and primitive human hematopoietic progenitor population. *Blood* **88**, 3306-3313 (1996).
- 7 Doulatov, S. *et al.* Revised map of the human progenitor hierarchy shows the origin of macrophages and dendritic cells in early lymphoid development. *Nat Immunol* **11**, 585-593, doi:10.1038/ni.1889 (2010).
- 8 Adolfsson, J. *et al.* Identification of Flt3<sup>+</sup> lympho-myeloid stem cells lacking erythro-megakaryocytic potential a revised road map for adult blood lineage commitment. *Cell* **121**, 295-306, doi:10.1016/j.cell.2005.02.013 (2005).
- 9 Sanjuan-Pla, A. *et al.* Platelet-biased stem cells reside at the apex of the haematopoietic stem-cell hierarchy. *Nature* **502**, 232-236, doi:10.1038/nature12495 (2013).
- 10 Velten, L. *et al.* Human haematopoietic stem cell lineage commitment is a continuous process. *Nat Cell Biol* **19**, 271-281, doi:10.1038/ncb3493 (2017).
- 11 Laurenti, E. & Gottgens, B. From haematopoietic stem cells to complex differentiation landscapes. *Nature* **553**, 418-426, doi:10.1038/nature25022 (2018).
- 12 Szade, K. *et al.* Where Hematopoietic Stem Cells Live: The Bone Marrow Niche. *Antioxid Redox Signal* **29**, 191-204, doi:10.1089/ars.2017.7419 (2018).
- 13 Cipolleschi, M. G., Dello Sbarba, P. & Olivotto, M. The role of hypoxia in the maintenance of hematopoietic stem cells. *Blood* **82**, 2031-2037 (1993).
- 14 Parmar, K., Mauch, P., Vergilio, J. A., Sackstein, R. & Down, J. D. Distribution of hematopoietic stem cells in the bone marrow according to regional hypoxia. *Proc Natl Acad Sci U S A* **104**, 5431-5436, doi:10.1073/pnas.0701152104 (2007).
- 15 Takubo, K. *et al.* Regulation of the HIF-1 $\alpha$  level is essential for hematopoietic stem cells. *Cell Stem Cell* **7**, 391-402, doi:10.1016/j.stem.2010.06.020 (2010).
- 16 Ianniciello, A., Rattigan, K. M. & Helgason, G. V. The Ins and Outs of Autophagy and Metabolism in Hematopoietic and Leukemic Stem Cells: Food for Thought. *Front Cell Dev Biol* **6**, 120, doi:10.3389/fcell.2018.00120 (2018).

- 17 Takubo, K. *et al.* Regulation of glycolysis by Pdk functions as a metabolic checkpoint for cell cycle quiescence in hematopoietic stem cells. *Cell Stem Cell* **12**, 49-61, doi:10.1016/j.stem.2012.10.011 (2013).
- 18 Luchsinger, L. L., de Almeida, M. J., Corrigan, D. J., Mumau, M. & Snoeck, H. W. Mitofusin 2 maintains haematopoietic stem cells with extensive lymphoid potential. *Nature* **529**, 528-531, doi:10.1038/nature16500 (2016).
- 19 Mohrin, M., Widjaja, A., Liu, Y., Luo, H. & Chen, D. The mitochondrial unfolded protein response is activated upon hematopoietic stem cell exit from quiescence. *Aging Cell* **17**, e12756, doi:10.1111/ace1.12756 (2018).
- 20 Mohrin, M. *et al.* Stem cell aging. A mitochondrial UPR-mediated metabolic checkpoint regulates hematopoietic stem cell aging. *Science* **347**, 1374-1377, doi:10.1126/science.aaa2361 (2015).
- 21 Kim, M., Cooper, D. D., Hayes, S. F. & Spangrude, G. J. Rhodamine-123 staining in hematopoietic stem cells of young mice indicates mitochondrial activation rather than dye efflux. *Blood* **91**, 4106-4117 (1998).
- 22 Piccoli, C. *et al.* Characterization of mitochondrial and extra-mitochondrial oxygen consuming reactions in human hematopoietic stem cells. Novel evidence of the occurrence of NAD(P)H oxidase activity. *J Biol Chem* **280**, 26467-26476, doi:10.1074/jbc.M500047200 (2005).
- 23 Simsek, T. *et al.* The distinct metabolic profile of hematopoietic stem cells reflects their location in a hypoxic niche. *Cell Stem Cell* **7**, 380-390, doi:10.1016/j.stem.2010.07.011 (2010).
- 24 de Almeida, M. J., Luchsinger, L. L., Corrigan, D. J., Williams, L. J. & Snoeck, H. W. Dye-Independent Methods Reveal Elevated Mitochondrial Mass in Hematopoietic Stem Cells. *Cell Stem Cell* **21**, 725-729.e724, doi:10.1016/j.stem.2017.11.002 (2017).
- 25 Folmes, C. D., Dzeja, P. P., Nelson, T. J. & Terzic, A. Metabolic plasticity in stem cell homeostasis and differentiation. *Cell Stem Cell* **11**, 596-606, doi:10.1016/j.stem.2012.10.002 (2012).
- 26 Anso, E. *et al.* The mitochondrial respiratory chain is essential for haematopoietic stem cell function. *Nat Cell Biol* **19**, 614-625, doi:10.1038/ncb3529 (2017).
- 27 Lum, J. J. *et al.* The transcription factor HIF-1alpha plays a critical role in the growth factor-dependent regulation of both aerobic and anaerobic glycolysis. *Genes Dev* **21**, 1037-1049, doi:10.1101/gad.1529107 (2007).
- 28 Ito, K. *et al.* A PML-PPAR-delta pathway for fatty acid oxidation regulates hematopoietic stem cell maintenance. *Nat Med* **18**, 1350-1358, doi:10.1038/nm.2882 (2012).
- 29 Yu, W. M. *et al.* Metabolic regulation by the mitochondrial phosphatase PTPMT1 is required for hematopoietic stem cell differentiation. *Cell Stem Cell* **12**, 62-74, doi:10.1016/j.stem.2012.11.022 (2013).
- 30 Wang, Y. H. *et al.* Cell-state-specific metabolic dependency in hematopoiesis and leukemogenesis. *Cell* **158**, 1309-1323, doi:10.1016/j.cell.2014.07.048 (2014).
- 31 Richardson, C., Yan, S. & Vestal, C. G. Oxidative stress, bone marrow failure, and genome instability in hematopoietic stem cells. *Int J Mol Sci* **16**, 2366-2385, doi:10.3390/ijms16022366 (2015).
- 32 Rimmele, P. *et al.* Mitochondrial metabolism in hematopoietic stem cells requires functional FOXO3. *EMBO Rep* **16**, 1164-1176, doi:10.15252/embr.201439704 (2015).
- 33 Bigarella, C. L. *et al.* FOXO3 Transcription Factor Is Essential for Protecting Hematopoietic Stem and Progenitor Cells from Oxidative DNA Damage. *J Biol Chem* **292**, 3005-3015, doi:10.1074/jbc.M116.769455 (2017).

- 34 Chen, C. *et al.* TSC-mTOR maintains quiescence and function of hematopoietic stem cells by repressing mitochondrial biogenesis and reactive oxygen species. *J Exp Med* **205**, 2397-2408, doi:10.1084/jem.20081297 (2008).
- 35 Luo, Y. *et al.* Rapamycin enhances long-term hematopoietic reconstitution of ex vivo expanded mouse hematopoietic stem cells by inhibiting senescence. *Transplantation* **97**, 20-29, doi:10.1097/TP.0b013e3182a7fcf8 (2014).
- 36 Liu, X. *et al.* Regulation of mitochondrial biogenesis in erythropoiesis by mTORC1-mediated protein translation. *Nat Cell Biol* **19**, 626-638, doi:10.1038/ncb3527 (2017).
- 37 Schofield, R. The relationship between the spleen colony-forming cell and the haemopoietic stem cell. *Blood Cells* **4**, 7-25 (1978).
- 38 Argiropoulos, B. & Humphries, R. K. Hox genes in hematopoiesis and leukemogenesis. *Oncogene* **26**, 6766-6776, doi:10.1038/sj.onc.1210760 (2007).
- 39 Wang, Y. *et al.* The Wnt/beta-catenin pathway is required for the development of leukemia stem cells in AML. *Science* **327**, 1650-1653, doi:10.1126/science.1186624 (2010).
- 40 Rowley, J. D. Letter: A new consistent chromosomal abnormality in chronic myelogenous leukaemia identified by quinacrine fluorescence and Giemsa staining. *Nature* **243**, 290-293, doi:10.1038/243290a0 (1973).
- 41 Raskind, W. H. & Fialkow, P. J. The use of cell markers in the study of human hematopoietic neoplasia. *Adv Cancer Res* **49**, 127-167 (1987).
- 42 Daley, G. Q., Van Etten, R. A. & Baltimore, D. Induction of chronic myelogenous leukemia in mice by the P210bcr/abl gene of the Philadelphia chromosome. *Science* **247**, 824-830, doi:10.1126/science.2406902 (1990).
- 43 Sawyers, C. L. Chronic myeloid leukemia. *N Engl J Med* **340**, 1330-1340, doi:10.1056/nejm199904293401706 (1999).
- 44 Fialkow, P. J., Jacobson, R. J. & Papayannopoulou, T. Chronic myelocytic leukemia: clonal origin in a stem cell common to the granulocyte, erythrocyte, platelet and monocyte/macrophage. *Am J Med* **63**, 125-130, doi:10.1016/0002-9343(77)90124-3 (1977).
- 45 Gunsilius, E. *et al.* Evidence from a leukaemia model for maintenance of vascular endothelium by bone-marrow-derived endothelial cells. *Lancet* **355**, 1688-1691, doi:10.1016/s0140-6736(00)02241-8 (2000).
- 46 Fialkow, P. J., Gartler, S. M. & Yoshida, A. Clonal origin of chronic myelocytic leukemia in man. *Proc Natl Acad Sci U S A* **58**, 1468-1471, doi:10.1073/pnas.58.4.1468 (1967).
- 47 Fialkow, P. J., Faguet, G. B., Jacobson, R. J., Vaidya, K. & Murphy, S. Evidence that essential thrombocythemia is a clonal disorder with origin in a multipotent stem cell. *Blood* **58**, 916-919 (1981).
- 48 Abe, A. *et al.* Retention but significant reduction of BCR-ABL transcript in hematopoietic stem cells in chronic myelogenous leukemia after imatinib therapy. *Int J Hematol* **88**, 471-475, doi:10.1007/s12185-008-0221-1 (2008).
- 49 Chang, J. M., Metcalf, D., Lang, R. A., Gonda, T. J. & Johnson, G. R. Nonneoplastic hematopoietic myeloproliferative syndrome induced by dysregulated multi-CSF (IL-3) expression. *Blood* **73**, 1487-1497 (1989).
- 50 Holyoake, T. L., Jiang, X., Drummond, M. W., Eaves, A. C. & Eaves, C. J. Elucidating critical mechanisms of deregulated stem cell turnover in the chronic phase of chronic myeloid leukemia. *Leukemia* **16**, 549-558, doi:10.1038/sj.leu.2402444 (2002).

- 51 Rohrbacher, M. & Hasford, J. Epidemiology of chronic myeloid leukaemia (CML). *Best Pract Res Clin Haematol* **22**, 295-302, doi:10.1016/j.beha.2009.07.007 (2009).
- 52 Preston, D. L. *et al.* Cancer incidence in atomic bomb survivors. Part III. Leukemia, lymphoma and multiple myeloma, 1950-1987. *Radiat Res* **137**, S68-97 (1994).
- 53 Vlaanderen, J., Lan, Q., Kromhout, H., Rothman, N. & Vermeulen, R. Occupational benzene exposure and the risk of chronic myeloid leukemia: a meta-analysis of cohort studies incorporating study quality dimensions. *Am J Ind Med* **55**, 779-785, doi:10.1002/ajim.22087 (2012).
- 54 Faderl, S., Talpaz, M., Estrov, Z. & Kantarjian, H. M. Chronic myelogenous leukemia: biology and therapy. *Ann Intern Med* **131**, 207-219, doi:10.7326/0003-4819-131-3-199908030-00008 (1999).
- 55 Faderl, S. *et al.* The biology of chronic myeloid leukemia. *N Engl J Med* **341**, 164-172, doi:10.1056/nejm199907153410306 (1999).
- 56 Kantarjian, H. M., Deisseroth, A., Kurzrock, R., Estrov, Z. & Talpaz, M. Chronic myelogenous leukemia: a concise update. *Blood* **82**, 691-703 (1993).
- 57 Perrotti, D., Jamieson, C., Goldman, J. & Skorski, T. Chronic myeloid leukemia: mechanisms of blastic transformation. *J Clin Invest* **120**, 2254-2264, doi:10.1172/jci41246 (2010).
- 58 Pendergast, A. M. *et al.* BCR-ABL-induced oncogenesis is mediated by direct interaction with the SH2 domain of the GRB-2 adaptor protein. *Cell* **75**, 175-185 (1993).
- 59 Cilloni, D. & Saglio, G. Molecular pathways: BCR-ABL. *Clin Cancer Res* **18**, 930-937, doi:10.1158/1078-0432.ccr-10-1613 (2012).
- 60 Naughton, R., Quiney, C., Turner, S. D. & Cotter, T. G. Bcr-Abl-mediated redox regulation of the PI3K/AKT pathway. *Leukemia* **23**, 1432-1440, doi:10.1038/leu.2009.49 (2009).
- 61 de Jong, R., ten Hoeve, J., Heisterkamp, N. & Groffen, J. Tyrosine 207 in CRKL is the BCR/ABL phosphorylation site. *Oncogene* **14**, 507-513, doi:10.1038/sj.onc.1200885 (1997).
- 62 Schaller, M. D. Paxillin: a focal adhesion-associated adaptor protein. *Oncogene* **20**, 6459-6472, doi:10.1038/sj.onc.1204786 (2001).
- 63 Goldman, J. M. Chronic myeloid leukemia: a historical perspective. *Semin Hematol* **47**, 302-311, doi:10.1053/j.seminhematol.2010.07.001 (2010).
- 64 Ghanei, M. & Vosoghi, A. A. An epidemiologic study to screen for chronic myelocytic leukemia in war victims exposed to mustard gas. *Environ Health Perspect* **110**, 519-521, doi:10.1289/ehp.02110519 (2002).
- 65 Rushing, D., Goldman, A., Gibbs, G., Howe, R. & Kennedy, B. J. Hydroxyurea versus busulfan in the treatment of chronic myelogenous leukemia. *Am J Clin Oncol* **5**, 307-313 (1982).
- 66 Pavlu, J., Szydlo, R. M., Goldman, J. M. & Apperley, J. F. Three decades of transplantation for chronic myeloid leukemia: what have we learned? *Blood* **117**, 755-763, doi:10.1182/blood-2010-08-301341 (2011).
- 67 Goldman, J. Hematopoietic stem cell transplantation. *Curr Opin Hematol* **5**, 417-418 (1998).
- 68 Talpaz, M., McCredie, K. B., Mavligit, G. M. & Gutterman, J. U. Leukocyte interferon-induced myeloid cytoreduction in chronic myelogenous leukemia. *Blood* **62**, 689-692 (1983).
- 69 Talpaz, M., Kurzrock, R., Kantarjian, H. & Gutterman, J. Therapy of chronic myelogenous leukaemia with interferons. *Cancer Surv* **8**, 793-798 (1989).

- 70 Druker, B. J. *et al.* Efficacy and safety of a specific inhibitor of the BCR-ABL tyrosine kinase in chronic myeloid leukemia. *N Engl J Med* **344**, 1031-1037, doi:10.1056/nejm200104053441401 (2001).
- 71 Gambacorti-Passerini, C. *et al.* Inhibition of the ABL kinase activity blocks the proliferation of BCR/ABL+ leukemic cells and induces apoptosis. *Blood Cells Mol Dis* **23**, 380-394, doi:10.1006/bcmd.1997.0155 (1997).
- 72 O'Brien, S. G. *et al.* Imatinib compared with interferon and low-dose cytarabine for newly diagnosed chronic-phase chronic myeloid leukemia. *N Engl J Med* **348**, 994-1004, doi:10.1056/NEJMoa022457 (2003).
- 73 Druker, B. J. *et al.* Five-year follow-up of patients receiving imatinib for chronic myeloid leukemia. *N Engl J Med* **355**, 2408-2417, doi:10.1056/NEJMoa062867 (2006).
- 74 Hochhaus, A. *et al.* Six-year follow-up of patients receiving imatinib for the first-line treatment of chronic myeloid leukemia. *Leukemia* **23**, 1054-1061, doi:10.1038/leu.2009.38 (2009).
- 75 Akwa, F. & Liesveld, J. Surrogate end points for long-term outcomes in chronic myeloid leukemia. *Leuk Lymphoma* **54**, 2103-2111, doi:10.3109/10428194.2013.772607 (2013).
- 76 Tura, S. *et al.* Interferon alfa-2a as compared with conventional chemotherapy for the treatment of chronic myeloid leukemia. *N Engl J Med* **330**, 820-825, doi:10.1056/nejm199403243301204 (1994).
- 77 Baccarani, M. *et al.* European LeukemiaNet recommendations for the management of chronic myeloid leukemia: 2013. *Blood* **122**, 872-884, doi:10.1182/blood-2013-05-501569 (2013).
- 78 Branford, S. *et al.* High frequency of point mutations clustered within the adenosine triphosphate-binding region of BCR/ABL in patients with chronic myeloid leukemia or Ph-positive acute lymphoblastic leukemia who develop imatinib (STI571) resistance. *Blood* **99**, 3472-3475, doi:10.1182/blood.v99.9.3472 (2002).
- 79 Gorre, M. E. *et al.* Clinical resistance to STI-571 cancer therapy caused by BCR-ABL gene mutation or amplification. *Science* **293**, 876-880, doi:10.1126/science.1062538 (2001).
- 80 Marin, D. *et al.* Adherence is the critical factor for achieving molecular responses in patients with chronic myeloid leukemia who achieve complete cytogenetic responses on imatinib. *J Clin Oncol* **28**, 2381-2388, doi:10.1200/jco.2009.26.3087 (2010).
- 81 Peng, B. *et al.* Pharmacokinetics and pharmacodynamics of imatinib in a phase I trial with chronic myeloid leukemia patients. *J Clin Oncol* **22**, 935-942, doi:10.1200/jco.2004.03.050 (2004).
- 82 Watkins, D. B., Hughes, T. P. & White, D. L. OCT1 and imatinib transport in CML: is it clinically relevant? *Leukemia* **29**, 1960-1969, doi:10.1038/leu.2015.170 (2015).
- 83 Whang-Peng, J., Broder, S., Lee, E. & Young, R. C. Unusual clonal evolution in a case of chronic myelogenous leukemia. *Acta Haematol* **56**, 345-354, doi:10.1159/000207961 (1976).
- 84 Koschmieder, S. & Vetrie, D. Epigenetic dysregulation in chronic myeloid leukaemia: A myriad of mechanisms and therapeutic options. *Semin Cancer Biol* **51**, 180-197, doi:10.1016/j.semcancer.2017.07.006 (2018).
- 85 Okabe, S. *et al.* Activity of histone deacetylase inhibitors and an Aurora kinase inhibitor in BCR-ABL-expressing leukemia cells: Combination of HDAC and Aurora inhibitors in BCR-ABL-expressing cells. *Cancer Cell Int* **13**, 32, doi:10.1186/1475-2867-13-32 (2013).

- 86 Kantarjian, H. M. *et al.* Efficacy of imatinib dose escalation in patients with chronic myeloid leukemia in chronic phase. *Cancer* **115**, 551-560, doi:10.1002/cncr.24066 (2009).
- 87 Kantarjian, H. M. *et al.* Nilotinib versus imatinib for the treatment of patients with newly diagnosed chronic phase, Philadelphia chromosome-positive, chronic myeloid leukaemia: 24-month minimum follow-up of the phase 3 randomised ENESTnd trial. *Lancet Oncol* **12**, 841-851, doi:10.1016/s1470-2045(11)70201-7 (2011).
- 88 Hochhaus, A. *et al.* Long-term benefits and risks of frontline nilotinib vs imatinib for chronic myeloid leukemia in chronic phase: 5-year update of the randomized ENESTnd trial. *Leukemia* **30**, 1044-1054, doi:10.1038/leu.2016.5 (2016).
- 89 Jorgensen, H. G., Allan, E. K., Jordanides, N. E., Mountford, J. C. & Holyoake, T. L. Nilotinib exerts equipotent antiproliferative effects to imatinib and does not induce apoptosis in CD34+ CML cells. *Blood* **109**, 4016-4019, doi:10.1182/blood-2006-11-057521 (2007).
- 90 Kantarjian, H. *et al.* Dasatinib versus imatinib in newly diagnosed chronic-phase chronic myeloid leukemia. *N Engl J Med* **362**, 2260-2270, doi:10.1056/NEJMoa1002315 (2010).
- 91 Kantarjian, H. M. *et al.* Dasatinib or imatinib in newly diagnosed chronic-phase chronic myeloid leukemia: 2-year follow-up from a randomized phase 3 trial (DASISION). *Blood* **119**, 1123-1129, doi:10.1182/blood-2011-08-376087 (2012).
- 92 Nakamae, H. *et al.* Dasatinib versus imatinib in Japanese patients with newly diagnosed chronic phase chronic myeloid leukemia: a subanalysis of the DASISION 5-year final report. *Int J Hematol* **105**, 792-804, doi:10.1007/s12185-017-2208-2 (2017).
- 93 Puttini, M. *et al.* In vitro and in vivo activity of SKI-606, a novel Src-Abl inhibitor, against imatinib-resistant Bcr-Abl+ neoplastic cells. *Cancer Res* **66**, 11314-11322, doi:10.1158/0008-5472.can-06-1199 (2006).
- 94 Brummendorf, T. H. *et al.* Bosutinib versus imatinib in newly diagnosed chronic-phase chronic myeloid leukaemia: results from the 24-month follow-up of the BELA trial. *Br J Haematol* **168**, 69-81, doi:10.1111/bjh.13108 (2015).
- 95 Gambacorti-Passerini, C. *et al.* Long-term efficacy and safety of bosutinib in patients with advanced leukemia following resistance/intolerance to imatinib and other tyrosine kinase inhibitors. *Am J Hematol* **90**, 755-768, doi:10.1002/ajh.24034 (2015).
- 96 O'Hare, T. *et al.* AP24534, a pan-BCR-ABL inhibitor for chronic myeloid leukemia, potently inhibits the T315I mutant and overcomes mutation-based resistance. *Cancer Cell* **16**, 401-412, doi:10.1016/j.ccr.2009.09.028 (2009).
- 97 Cortes, J. E. *et al.* A phase 2 trial of ponatinib in Philadelphia chromosome-positive leukemias. *N Engl J Med* **369**, 1783-1796, doi:10.1056/NEJMoa1306494 (2013).
- 98 Lipton, J. H. *et al.* Ponatinib versus imatinib for newly diagnosed chronic myeloid leukaemia: an international, randomised, open-label, phase 3 trial. *Lancet Oncol* **17**, 612-621, doi:10.1016/s1470-2045(16)00080-2 (2016).
- 99 Kantarjian, H. M. *et al.* Homoharringtonine: history, current research, and future direction. *Cancer* **92**, 1591-1605, doi:10.1002/1097-0142(20010915)92:6<1591::aid-cncr1485>3.0.co;2-u (2001).

- 100 Ross, D. M. *et al.* Safety and efficacy of imatinib cessation for CML patients with stable undetectable minimal residual disease: results from the TWISTER study. *Blood* **122**, 515-522, doi:10.1182/blood-2013-02-483750 (2013).
- 101 Mahon, F. X. *et al.* Discontinuation of imatinib in patients with chronic myeloid leukaemia who have maintained complete molecular remission for at least 2 years: the prospective, multicentre Stop Imatinib (STIM) trial. *Lancet Oncol* **11**, 1029-1035, doi:10.1016/s1470-2045(10)70233-3 (2010).
- 102 Corbin, A. S. *et al.* Human chronic myeloid leukemia stem cells are insensitive to imatinib despite inhibition of BCR-ABL activity. *J Clin Invest* **121**, 396-409, doi:10.1172/jci35721 (2011).
- 103 Hamilton, A. *et al.* Chronic myeloid leukemia stem cells are not dependent on Bcr-Abl kinase activity for their survival. *Blood* **119**, 1501-1510, doi:10.1182/blood-2010-12-326843 (2012).
- 104 Koschmieder, S. *et al.* Inducible chronic phase of myeloid leukemia with expansion of hematopoietic stem cells in a transgenic model of BCR-ABL leukemogenesis. *Blood* **105**, 324-334, doi:10.1182/blood-2003-12-4369 (2005).
- 105 Pellicano, F., Mukherjee, L. & Holyoake, T. L. Concise review: cancer cells escape from oncogene addiction: understanding the mechanisms behind treatment failure for more effective targeting. *Stem Cells* **32**, 1373-1379, doi:10.1002/stem.1678 (2014).
- 106 Holyoake, T. L. & Vetrie, D. The chronic myeloid leukemia stem cell: stemming the tide of persistence. *Blood* **129**, 1595-1606, doi:10.1182/blood-2016-09-696013 (2017).
- 107 Hurtz, C. *et al.* BCL6-mediated repression of p53 is critical for leukemia stem cell survival in chronic myeloid leukemia. *J Exp Med* **208**, 2163-2174, doi:10.1084/jem.20110304 (2011).
- 108 Pellicano, F. *et al.* The antiproliferative activity of kinase inhibitors in chronic myeloid leukemia cells is mediated by FOXO transcription factors. *Stem Cells* **32**, 2324-2337, doi:10.1002/stem.1748 (2014).
- 109 Naka, K. *et al.* TGF-beta-FOXO signalling maintains leukaemia-initiating cells in chronic myeloid leukaemia. *Nature* **463**, 676-680, doi:10.1038/nature08734 (2010).
- 110 Nowicki, M. O. *et al.* BCR/ABL oncogenic kinase promotes unfaithful repair of the reactive oxygen species-dependent DNA double-strand breaks. *Blood* **104**, 3746-3753, doi:10.1182/blood-2004-05-1941 (2004).
- 111 Ilander, M., Hekim, C. & Mustjoki, S. Immunology and immunotherapy of chronic myeloid leukemia. *Curr Hematol Malig Rep* **9**, 17-23, doi:10.1007/s11899-013-0190-1 (2014).
- 112 Auberger, P. & Puissant, A. Autophagy, a key mechanism of oncogenesis and resistance in leukemia. *Blood* **129**, 547-552, doi:10.1182/blood-2016-07-692707 (2017).
- 113 Henriques Silva, N. *et al.* HLM/OSBP2 is expressed in chronic myeloid leukemia. *Int J Mol Med* **12**, 663-666 (2003).
- 114 Kuntz, E. M. *et al.* Targeting mitochondrial oxidative phosphorylation eradicates therapy-resistant chronic myeloid leukemia stem cells. *Nat Med* **23**, 1234-1240, doi:10.1038/nm.4399 (2017).
- 115 Takeshige, K., Baba, M., Tsuboi, S., Noda, T. & Ohsumi, Y. Autophagy in yeast demonstrated with proteinase-deficient mutants and conditions for its induction. *J Cell Biol* **119**, 301-311, doi:10.1083/jcb.119.2.301 (1992).

- 116 Tsukada, M. & Ohsumi, Y. Isolation and characterization of autophagy-defective mutants of *Saccharomyces cerevisiae*. *FEBS Lett* **333**, 169-174, doi:10.1016/0014-5793(93)80398-e (1993).
- 117 Matsuura, A., Tsukada, M., Wada, Y. & Ohsumi, Y. Apg1p, a novel protein kinase required for the autophagic process in *Saccharomyces cerevisiae*. *Gene* **192**, 245-250, doi:10.1016/s0378-1119(97)00084-x (1997).
- 118 Levine, B. & Klionsky, D. J. Development by self-digestion: molecular mechanisms and biological functions of autophagy. *Dev Cell* **6**, 463-477 (2004).
- 119 Biazik, J., Yla-Anttila, P., Vihinen, H., Jokitalo, E. & Eskelinen, E. L. Ultrastructural relationship of the phagophore with surrounding organelles. *Autophagy* **11**, 439-451, doi:10.1080/15548627.2015.1017178 (2015).
- 120 English, L. *et al.* Autophagy enhances the presentation of endogenous viral antigens on MHC class I molecules during HSV-1 infection. *Nat Immunol* **10**, 480-487, doi:10.1038/ni.1720 (2009).
- 121 Ravikumar, B., Moreau, K., Jahreiss, L., Puri, C. & Rubinsztein, D. C. Plasma membrane contributes to the formation of pre-autophagosomal structures. *Nat Cell Biol* **12**, 747-757, doi:10.1038/ncb2078 (2010).
- 122 Mizushima, N., Yoshimori, T. & Ohsumi, Y. The role of Atg proteins in autophagosome formation. *Annu Rev Cell Dev Biol* **27**, 107-132, doi:10.1146/annurev-cellbio-092910-154005 (2011).
- 123 Ganley, I. G. *et al.* ULK1.ATG13.FIP200 complex mediates mTOR signaling and is essential for autophagy. *J Biol Chem* **284**, 12297-12305, doi:10.1074/jbc.M900573200 (2009).
- 124 Russell, R. C. *et al.* ULK1 induces autophagy by phosphorylating Beclin-1 and activating VPS34 lipid kinase. *Nat Cell Biol* **15**, 741-750, doi:10.1038/ncb2757 (2013).
- 125 Mizushima, N. The role of the Atg1/ULK1 complex in autophagy regulation. *Curr Opin Cell Biol* **22**, 132-139, doi:10.1016/j.ceb.2009.12.004 (2010).
- 126 Kim, J., Kundu, M., Viollet, B. & Guan, K. L. AMPK and mTOR regulate autophagy through direct phosphorylation of Ulk1. *Nat Cell Biol* **13**, 132-141, doi:10.1038/ncb2152 (2011).
- 127 Jung, C. H. *et al.* ULK-Atg13-FIP200 complexes mediate mTOR signaling to the autophagy machinery. *Mol Biol Cell* **20**, 1992-2003, doi:10.1091/mbc.E08-12-1249  
10.1091/mbc.e08-12-1249 (2009).
- 128 Hosokawa, N. *et al.* Nutrient-dependent mTORC1 association with the ULK1-Atg13-FIP200 complex required for autophagy. *Mol Biol Cell* **20**, 1981-1991, doi:10.1091/mbc.E08-12-1248  
10.1091/mbc.e08-12-1248 (2009).
- 129 Garcia, D. & Shaw, R. J. AMPK: Mechanisms of Cellular Energy Sensing and Restoration of Metabolic Balance. *Mol Cell* **66**, 789-800, doi:10.1016/j.molcel.2017.05.032 (2017).
- 130 Egan, D. F. *et al.* Phosphorylation of ULK1 (hATG1) by AMP-activated protein kinase connects energy sensing to mitophagy. *Science* **331**, 456-461, doi:10.1126/science.1196371 (2011).
- 131 Nazio, F. *et al.* mTOR inhibits autophagy by controlling ULK1 ubiquitylation, self-association and function through AMBRA1 and TRAF6. *Nat Cell Biol* **15**, 406-416, doi:10.1038/ncb2708 (2013).
- 132 Lin, S. Y. *et al.* GSK3-TIP60-ULK1 signaling pathway links growth factor deprivation to autophagy. *Science* **336**, 477-481, doi:10.1126/science.1217032 (2012).

- 133 Bach, M., Larance, M., James, D. E. & Ramm, G. The serine/threonine kinase ULK1 is a target of multiple phosphorylation events. *Biochem J* **440**, 283-291, doi:10.1042/bj20101894 (2011).
- 134 Kishi-Itakura, C., Koyama-Honda, I., Itakura, E. & Mizushima, N. Ultrastructural analysis of autophagosome organization using mammalian autophagy-deficient cells. *J Cell Sci* **127**, 4089-4102, doi:10.1242/jcs.156034 (2014).
- 135 Lazarus, M. B., Novotny, C. J. & Shokat, K. M. Structure of the human autophagy initiating kinase ULK1 in complex with potent inhibitors. *ACS Chem Biol* **10**, 257-261, doi:10.1021/cb500835z (2015).
- 136 Liu, C. C. *et al.* Cul3-KLHL20 Ubiquitin Ligase Governs the Turnover of ULK1 and VPS34 Complexes to Control Autophagy Termination. *Mol Cell* **61**, 84-97, doi:10.1016/j.molcel.2015.11.001 (2016).
- 137 Joo, J. H. *et al.* Hsp90-Cdc37 chaperone complex regulates Ulk1- and Atg13-mediated mitophagy. *Mol Cell* **43**, 572-585, doi:10.1016/j.molcel.2011.06.018 (2011).
- 138 Egan, D. F. *et al.* Small Molecule Inhibition of the Autophagy Kinase ULK1 and Identification of ULK1 Substrates. *Mol Cell* **59**, 285-297, doi:10.1016/j.molcel.2015.05.031 (2015).
- 139 Zhou, C. *et al.* Regulation of mATG9 trafficking by Src- and ULK1-mediated phosphorylation in basal and starvation-induced autophagy. *Cell Res* **27**, 184-201, doi:10.1038/cr.2016.146 (2017).
- 140 Di Bartolomeo, S. *et al.* The dynamic interaction of AMBRA1 with the dynein motor complex regulates mammalian autophagy. *J Cell Biol* **191**, 155-168, doi:10.1083/jcb.201002100 (2010).
- 141 Pengo, N., Agrotis, A., Prak, K., Jones, J. & Ketteler, R. A reversible phospho-switch mediated by ULK1 regulates the activity of autophagy protease ATG4B. *Nat Commun* **8**, 294, doi:10.1038/s41467-017-00303-2 (2017).
- 142 Wu, W. *et al.* ULK1 translocates to mitochondria and phosphorylates FUNDC1 to regulate mitophagy. *EMBO Rep* **15**, 566-575, doi:10.1002/embr.201438501 (2014).
- 143 Wold, M. S., Lim, J., Lachance, V., Deng, Z. & Yue, Z. ULK1-mediated phosphorylation of ATG14 promotes autophagy and is impaired in Huntington's disease models. *Mol Neurodegener* **11**, 76, doi:10.1186/s13024-016-0141-0 (2016).
- 144 Xu, J., Fotouhi, M. & McPherson, P. S. Phosphorylation of the exchange factor DENND3 by ULK in response to starvation activates Rab12 and induces autophagy. *EMBO Rep* **16**, 709-718, doi:10.15252/embr.201440006 (2015).
- 145 Li, T. Y. *et al.* ULK1/2 Constitute a Bifurcate Node Controlling Glucose Metabolic Fluxes in Addition to Autophagy. *Mol Cell* **62**, 359-370, doi:10.1016/j.molcel.2016.04.009 (2016).
- 146 Dunlop, E. A., Hunt, D. K., Acosta-Jaquez, H. A., Fingar, D. C. & Tee, A. R. ULK1 inhibits mTORC1 signaling, promotes multisite Raptor phosphorylation and hinders substrate binding. *Autophagy* **7**, 737-747, doi:10.4161/auto.7.7.15491 (2011).
- 147 Gan, W. *et al.* ULK1 phosphorylates Sec23A and mediates autophagy-induced inhibition of ER-to-Golgi traffic. *BMC Cell Biol* **18**, 22, doi:10.1186/s12860-017-0138-8 (2017).
- 148 Li, R. *et al.* Serine/Threonine Kinase Unc-51-like Kinase-1 (Ulk1) Phosphorylates the Co-chaperone Cell Division Cycle Protein 37 (Cdc37) and Thereby Disrupts the Stability of Cdc37 Client Proteins. *J Biol Chem* **292**, 2830-2841, doi:10.1074/jbc.M116.762443 (2017).

- 149 Konno, H., Konno, K. & Barber, G. N. Cyclic dinucleotides trigger ULK1 (ATG1) phosphorylation of STING to prevent sustained innate immune signaling. *Cell* **155**, 688-698, doi:10.1016/j.cell.2013.09.049 (2013).
- 150 Sellier, C. *et al.* Loss of C9ORF72 impairs autophagy and synergizes with polyQ Ataxin-2 to induce motor neuron dysfunction and cell death. *Embo j* **35**, 1276-1297, doi:10.15252/embj.201593350 (2016).
- 151 Lim, J. *et al.* Proteotoxic stress induces phosphorylation of p62/SQSTM1 by ULK1 to regulate selective autophagic clearance of protein aggregates. *PLoS Genet* **11**, e1004987, doi:10.1371/journal.pgen.1004987 (2015).
- 152 Zachari, M. & Ganley, I. G. The mammalian ULK1 complex and autophagy initiation. *Essays Biochem* **61**, 585-596, doi:10.1042/ebc20170021 (2017).
- 153 Backer, J. M. The regulation and function of Class III PI3Ks: novel roles for Vps34. *Biochem J* **410**, 1-17, doi:10.1042/bj20071427 (2008).
- 154 Simonsen, A. & Tooze, S. A. Coordination of membrane events during autophagy by multiple class III PI3-kinase complexes. *J Cell Biol* **186**, 773-782, doi:10.1083/jcb.200907014 (2009).
- 155 Tanida, I., Ueno, T. & Kominami, E. LC3 conjugation system in mammalian autophagy. *Int J Biochem Cell Biol* **36**, 2503-2518, doi:10.1016/j.biocel.2004.05.009 (2004).
- 156 Geng, J. & Klionsky, D. J. The Atg8 and Atg12 ubiquitin-like conjugation systems in macroautophagy. 'Protein modifications: beyond the usual suspects' review series. *EMBO Rep* **9**, 859-864, doi:10.1038/embo.2008.163 (2008).
- 157 Slobodkin, M. R. & Elazar, Z. The Atg8 family: multifunctional ubiquitin-like key regulators of autophagy. *Essays Biochem* **55**, 51-64, doi:10.1042/bse0550051 (2013).
- 158 Jager, S. *et al.* Role for Rab7 in maturation of late autophagic vacuoles. *J Cell Sci* **117**, 4837-4848, doi:10.1242/jcs.01370 (2004).
- 159 Komatsu, M. & Ichimura, Y. Physiological significance of selective degradation of p62 by autophagy. *FEBS Lett* **584**, 1374-1378, doi:10.1016/j.febslet.2010.02.017 (2010).
- 160 Warr, M. R., Kohli, L. & Passegue, E. in *Cell Cycle* Vol. 12 1979-1980 (2013).
- 161 Nguyen-McCarty, M. & Klein, P. S. Autophagy is a signature of a signaling network that maintains hematopoietic stem cells. *PLoS One* **12**, e0177054, doi:10.1371/journal.pone.0177054 (2017).
- 162 Revuelta, M. & Matheu, A. Autophagy in stem cell aging. *Aging Cell* **16**, 912-915, doi:10.1111/accel.12655 (2017).
- 163 Warr, M. R. *et al.* FOXO3A directs a protective autophagy program in haematopoietic stem cells. *Nature* **494**, 323-327, doi:10.1038/nature11895 (2013).
- 164 Liu, F. *et al.* FIP200 is required for the cell-autonomous maintenance of fetal hematopoietic stem cells. *Blood* **116**, 4806-4814, doi:10.1182/blood-2010-06-288589 (2010).
- 165 Mortensen, M. *et al.* The autophagy protein Atg7 is essential for hematopoietic stem cell maintenance. *J Exp Med* **208**, 455-467, doi:10.1084/jem.20101145 (2011).
- 166 Liu, L. & Rando, T. A. Manifestations and mechanisms of stem cell aging. *J Cell Biol* **193**, 257-266, doi:10.1083/jcb.201010131 (2011).
- 167 Cao, Y. *et al.* Autophagy regulates the cell cycle of murine HSPCs in a nutrient-dependent manner. *Exp Hematol* **43**, 229-242, doi:10.1016/j.exphem.2014.11.002 (2015).

- 168 Ho, T. T. *et al.* Autophagy maintains the metabolism and function of young and old stem cells. *Nature* **543**, 205-210, doi:10.1038/nature21388 (2017).
- 169 Montava-Garriga, L. & Ganley, I. G. Outstanding Questions in Mitophagy: What We Do and Do Not Know. *J Mol Biol*, doi:10.1016/j.jmb.2019.06.032 (2019).
- 170 Scott, S. V. & Klionsky, D. J. Delivery of proteins and organelles to the vacuole from the cytoplasm. *Curr Opin Cell Biol* **10**, 523-529, doi:10.1016/s0955-0674(98)80068-9 (1998).
- 171 Zilocchi, M., Fasano, M. & Alberio, T. Mitochondrial Proteins in the Development of Parkinson's Disease. *Adv Exp Med Biol* **1158**, 17-44, doi:10.1007/978-981-13-8367-0\_2 (2019).
- 172 Fu, W., Liu, Y. & Yin, H. Mitochondrial Dynamics: Biogenesis, Fission, Fusion, and Mitophagy in the Regulation of Stem Cell Behaviors. *Stem Cells Int* **2019**, 9757201, doi:10.1155/2019/9757201 (2019).
- 173 Sprenger, H. G. & Langer, T. The Good and the Bad of Mitochondrial Breakups. *Trends Cell Biol*, doi:10.1016/j.tcb.2019.08.003 (2019).
- 174 Kitada, T. *et al.* Mutations in the parkin gene cause autosomal recessive juvenile parkinsonism. *Nature* **392**, 605-608, doi:10.1038/33416 (1998).
- 175 Pickrell, A. M. & Youle, R. J. The roles of PINK1, parkin, and mitochondrial fidelity in Parkinson's disease. *Neuron* **85**, 257-273, doi:10.1016/j.neuron.2014.12.007 (2015).
- 176 Lazarou, M., Jin, S. M., Kane, L. A. & Youle, R. J. Role of PINK1 binding to the TOM complex and alternate intracellular membranes in recruitment and activation of the E3 ligase Parkin. *Dev Cell* **22**, 320-333, doi:10.1016/j.devcel.2011.12.014 (2012).
- 177 Narendra, D., Tanaka, A., Suen, D. F. & Youle, R. J. Parkin is recruited selectively to impaired mitochondria and promotes their autophagy. *J Cell Biol* **183**, 795-803, doi:10.1083/jcb.200809125 (2008).
- 178 Baudot, A. D., Haller, M., Merschtik, M., Tait, S. W. & Ryan, K. M. Using enhanced-mitophagy to measure autophagic flux. *Methods* **75**, 105-111, doi:10.1016/j.ymeth.2014.11.014 (2015).
- 179 Michiorri, S. *et al.* The Parkinson-associated protein PINK1 interacts with Beclin1 and promotes autophagy. *Cell Death Differ* **17**, 962-974, doi:10.1038/cdd.2009.200 (2010).
- 180 Jin, G. *et al.* Atad3a suppresses Pink1-dependent mitophagy to maintain homeostasis of hematopoietic progenitor cells. *Nat Immunol* **19**, 29-40, doi:10.1038/s41590-017-0002-1 (2018).
- 181 Ito, K. *et al.* Self-renewal of a purified Tie2<sup>+</sup> hematopoietic stem cell population relies on mitochondrial clearance. *Science* **354**, 1156-1160, doi:10.1126/science.aaf5530 (2016).
- 182 Iwama, A. *et al.* Molecular cloning and characterization of mouse TIE and TEK receptor tyrosine kinase genes and their expression in hematopoietic stem cells. *Biochem Biophys Res Commun* **195**, 301-309, doi:10.1006/bbrc.1993.2045 (1993).
- 183 Arai, F. *et al.* Tie2/angiopoietin-1 signaling regulates hematopoietic stem cell quiescence in the bone marrow niche. *Cell* **118**, 149-161, doi:10.1016/j.cell.2004.07.004 (2004).
- 184 Zhang, J. *et al.* Mitochondrial clearance is regulated by Atg7-dependent and -independent mechanisms during reticulocyte maturation. *Blood* **114**, 157-164, doi:10.1182/blood-2008-04-151639 (2009).
- 185 Kundu, M. *et al.* Ulk1 plays a critical role in the autophagic clearance of mitochondria and ribosomes during reticulocyte maturation. *Blood* **112**, 1493-1502, doi:10.1182/blood-2008-02-137398 (2008).

- 186 Watson, A. S. *et al.* Autophagy limits proliferation and glycolytic metabolism in acute myeloid leukemia. *Cell Death Discov* **1**, doi:10.1038/cddiscovery.2015.8 (2015).
- 187 Pei, S. *et al.* AMPK/FIS1-Mediated Mitophagy Is Required for Self-Renewal of Human AML Stem Cells. *Cell Stem Cell* **23**, 86-100.e106, doi:10.1016/j.stem.2018.05.021 (2018).
- 188 Rothe, K. *et al.* The core autophagy protein ATG4B is a potential biomarker and therapeutic target in CML stem/progenitor cells. *Blood* **123**, 3622-3634, doi:10.1182/blood-2013-07-516807 (2014).
- 189 Karvela, M. *et al.* ATG7 regulates energy metabolism, differentiation and survival of Philadelphia-chromosome-positive cells. *Autophagy* **12**, 936-948, doi:10.1080/15548627.2016.1162359 (2016).
- 190 Ianniciello, A. *et al.* Chronic myeloid leukemia progenitor cells require autophagy when leaving hypoxia-induced quiescence. *Oncotarget* **8**, 96984-96992, doi:10.18632/oncotarget.18904 (2017).
- 191 Kong, Y. L. *et al.* Expression of autophagy related genes in chronic lymphocytic leukemia is associated with disease course. *Leuk Res* **66**, 8-14, doi:10.1016/j.leukres.2017.12.007 (2018).
- 192 Helgason, G. V. *et al.* Autophagy in chronic myeloid leukaemia: stem cell survival and implication in therapy. *Curr Cancer Drug Targets* **13**, 724-734 (2013).
- 193 Baquero, P. *et al.* Targeting quiescent leukemic stem cells using second generation autophagy inhibitors. *Leukemia* **33**, 981-994, doi:10.1038/s41375-018-0252-4 (2019).
- 194 Bellodi, C. *et al.* Targeting autophagy potentiates tyrosine kinase inhibitor-induced cell death in Philadelphia chromosome-positive cells, including primary CML stem cells. *J Clin Invest* **119**, 1109-1123, doi:10.1172/jci35660 (2009).
- 195 Puissant, A. *et al.* Cathepsin B release after imatinib-mediated lysosomal membrane permeabilization triggers BCR-ABL cleavage and elimination of chronic myelogenous leukemia cells. *Leukemia* **24**, 115-124, doi:10.1038/leu.2009.233 (2010).
- 196 Goussetis, D. J. *et al.* Autophagic degradation of the BCR-ABL oncoprotein and generation of antileukemic responses by arsenic trioxide. *Blood* **120**, 3555-3562, doi:10.1182/blood-2012-01-402578 (2012).
- 197 Crowley, L. C., O'Donovan, T. R., Nyhan, M. J. & McKenna, S. L. Pharmacological agents with inherent anti-autophagic activity improve the cytotoxicity of imatinib. *Oncol Rep* **29**, 2261-2268, doi:10.3892/or.2013.2377 (2013).
- 198 Helgason, G. V., Karvela, M. & Holyoake, T. L. Kill one bird with two stones: potential efficacy of BCR-ABL and autophagy inhibition in CML. *Blood* **118**, 2035-2043, doi:10.1182/blood-2011-01-330621 (2011).
- 199 Dowdle, W. E. *et al.* Selective VPS34 inhibitor blocks autophagy and uncovers a role for NCOA4 in ferritin degradation and iron homeostasis in vivo. *Nat Cell Biol* **16**, 1069-1079, doi:10.1038/ncb3053 (2014).
- 200 Petherick, K. J. *et al.* Pharmacological inhibition of ULK1 kinase blocks mammalian target of rapamycin (mTOR)-dependent autophagy. *J Biol Chem* **290**, 11376-11383, doi:10.1074/jbc.C114.627778 (2015).
- 201 Wu, J. *et al.* CLDN1 induces autophagy to promote proliferation and metastasis of esophageal squamous carcinoma through AMPK/STAT1/ULK1 signaling. *J Cell Physiol*, doi:10.1002/jcp.29133 (2019).

- 202 Jang, J. E. *et al.* AMPK-ULK1-Mediated Autophagy Confers Resistance to  
BET Inhibitor JQ1 in Acute Myeloid Leukemia Stem Cells. *Clin Cancer Res*  
23, 2781-2794, doi:10.1158/1078-0432.ccr-16-1903 (2017).
- 203 Radhi, O. A. *et al.* Inhibition of the ULK1 protein complex suppresses  
Staphylococcus-induced autophagy and cell death. *J Biol Chem*,  
doi:10.1074/jbc.RA119.008923 (2019).
- 204 Martin, K. R. *et al.* A Potent and Selective ULK1 Inhibitor Suppresses  
Autophagy and Sensitizes Cancer Cells to Nutrient Stress. *iScience* 8, 74-84,  
doi:10.1016/j.isci.2018.09.012 (2018).
- 205 Zhang, L. *et al.* Discovery of a small molecule targeting ULK1-modulated  
cell death of triple negative breast cancer in vitro and in vivo. *Chem Sci* 8,  
2687-2701, doi:10.1039/c6sc05368h (2017).
- 206 Zahedi, S. *et al.* Effect of early-stage autophagy inhibition in BRAF(V600E)  
autophagy-dependent brain tumor cells. *Cell Death Dis* 10, 679,  
doi:10.1038/s41419-019-1880-y (2019).
- 207 Palis, J. Primitive and definitive erythropoiesis in mammals. *Front Physiol*  
5, 3, doi:10.3389/fphys.2014.00003 (2014).
- 208 Limpert, A. S. *et al.* Autophagy in Cancer: Regulation by Small Molecules.  
*Trends Pharmacol Sci* 39, 1021-1032, doi:10.1016/j.tips.2018.10.004  
(2018).
- 209 de Back, D. Z., Kostova, E. B., van Kraaij, M., van den Berg, T. K. & van  
Bruggen, R. Of macrophages and red blood cells; a complex love story.  
*Front Physiol* 5, 9, doi:10.3389/fphys.2014.00009 (2014).
- 210 Ji, Y. Q. *et al.* EPO improves the proliferation and inhibits apoptosis of  
trophoblast and decidual stromal cells through activating STAT-5 and  
inactivating p38 signal in human early pregnancy. *Int J Clin Exp Pathol* 4,  
765-774 (2011).
- 211 Zhang, J. & Ney, P. A. Reticulocyte mitophagy: monitoring mitochondrial  
clearance in a mammalian model. *Autophagy* 6, 405-408,  
doi:10.4161/auto.6.3.11245 (2010).
- 212 Nishida, Y. *et al.* Discovery of Atg5/Atg7-independent alternative  
macroautophagy. *Nature* 461, 654-658, doi:10.1038/nature08455 (2009).
- 213 Wang, J. *et al.* Erythroleukemia cells acquire an alternative mitophagy  
capability. *Sci Rep* 6, 24641, doi:10.1038/srep24641 (2016).
- 214 Miller, P. H. *et al.* Analysis of parameters that affect human hematopoietic  
cell outputs in mutant c-kit-immunodeficient mice. *Exp Hematol* 48, 41-  
49, doi:10.1016/j.exphem.2016.12.012 (2017).
- 215 Gregory, C. J., Tepperman, A. D., McCulloch, E. A. & Till, J. E.  
Erythropoietic progenitors capable of colony formation in culture: response  
of normal and genetically anemic W-W-V mice to manipulations of the  
erythron. *J Cell Physiol* 84, 1-12, doi:10.1002/jcp.1040840102 (1974).
- 216 Ratajczak, M. Z. *et al.* Role of the KIT protooncogene in normal and  
malignant human hematopoiesis. *Proc Natl Acad Sci U S A* 89, 1710-1714  
(1992).
- 217 Scudiero, D. A. *et al.* Evaluation of a soluble tetrazolium/formazan assay  
for cell growth and drug sensitivity in culture using human and other tumor  
cell lines. *Cancer Res* 48, 4827-4833 (1988).
- 218 Nakayama, G. R., Caton, M. C., Nova, M. P. & Parandoosh, Z. in *J Immunol*  
*Methods* Vol. 204 205-208 (1997).
- 219 Doudna, J. A. & Charpentier, E. Genome editing. The new frontier of  
genome engineering with CRISPR-Cas9. *Science* 346, 1258096,  
doi:10.1126/science.1258096 (2014).

- 220 Karimian, A. *et al.* CRISPR/Cas9 technology as a potent molecular tool for gene therapy. *J Cell Physiol* **234**, 12267-12277, doi:10.1002/jcp.27972 (2019).
- 221 Kim, J. H. *et al.* Activation of the PI3K/mTOR pathway by BCR-ABL contributes to increased production of reactive oxygen species. *Blood* **105**, 1717-1723, doi:10.1182/blood-2004-03-0849 (2005).
- 222 Airiau, K., Mahon, F. X., Josselin, M., Jeanneteau, M. & Belloc, F. in *Cell Death Dis* Vol. 4 e827- (2013).
- 223 Mitchell, R. *et al.* Targeting BCR-ABL-Independent TKI Resistance in Chronic Myeloid Leukemia by mTOR and Autophagy Inhibition. *J Natl Cancer Inst* **110**, 467-478, doi:10.1093/jnci/djx236 (2018).
- 224 Liang, C., Feng, P., Ku, B., Oh, B. H. & Jung, J. U. UVRAG: a new player in autophagy and tumor cell growth. *Autophagy* **3**, 69-71 (2007).
- 225 Kong-Hap, M. A. *et al.* Regulation of ATG8 membrane association by ATG4 in the parasitic protist *Toxoplasma gondii*. *Autophagy* **9**, 1334-1348, doi:10.4161/auto.25189 (2013).
- 226 Tanida, I., Sou, Y. S., Minematsu-Ikeguchi, N., Ueno, T. & Kominami, E. Atg8L/Apg8L is the fourth mammalian modifier of mammalian Atg8 conjugation mediated by human Atg4B, Atg7 and Atg3. *Febs j* **273**, 2553-2562, doi:10.1111/j.1742-4658.2006.05260.x (2006).
- 227 Mizushima, N. *et al.* A protein conjugation system essential for autophagy. *Nature* **395**, 395-398, doi:10.1038/26506 (1998).
- 228 Tanida, I. *et al.* Apg7p/Cvt2p: A novel protein-activating enzyme essential for autophagy. *Mol Biol Cell* **10**, 1367-1379, doi:10.1091/mbc.10.5.1367 (1999).
- 229 Tanida, I., Ueno, T. & Kominami, E. LC3 and Autophagy. *Methods Mol Biol* **445**, 77-88, doi:10.1007/978-1-59745-157-4\_4 (2008).
- 230 Nath, S. *et al.* Lipidation of the LC3/GABARAP family of autophagy proteins relies upon a membrane curvature-sensing domain in Atg3. *Nat Cell Biol* **16**, 415-424, doi:10.1038/ncb2940 (2014).
- 231 Murphy, M. P. How mitochondria produce reactive oxygen species. *Biochem J* **417**, 1-13, doi:10.1042/bj20081386 (2009).
- 232 Halasi, M. *et al.* ROS inhibitor N-acetyl-L-cysteine antagonizes the activity of proteasome inhibitors. *Biochem J* **454**, 201-208, doi:10.1042/bj20130282 (2013).
- 233 Kirkin, V. *et al.* A role for NBR1 in autophagosomal degradation of ubiquitinated substrates. *Mol Cell* **33**, 505-516, doi:10.1016/j.molcel.2009.01.020 (2009).
- 234 Mancias, J. D., Wang, X., Gygi, S. P., Harper, J. W. & Kimmelman, A. C. Quantitative proteomics identifies NCOA4 as the cargo receptor mediating ferritinophagy. *Nature* **509**, 105-109, doi:10.1038/nature13148 (2014).
- 235 Ji, A. R. *et al.* Reactive oxygen species enhance differentiation of human embryonic stem cells into mesendodermal lineage. *Exp Mol Med* **42**, 175-186, doi:10.3858/emm.2010.42.3.018 (2010).
- 236 Lisowski, P., Kannan, P., Mlody, B. & Prigione, A. Mitochondria and the dynamic control of stem cell homeostasis. *EMBO Rep* **19**, doi:10.15252/embr.201745432 (2018).
- 237 Oburoglu, L. *et al.* Glucose and glutamine metabolism regulate human hematopoietic stem cell lineage specification. *Cell Stem Cell* **15**, 169-184, doi:10.1016/j.stem.2014.06.002 (2014).
- 238 Chen, K. *et al.* Resolving the distinct stages in erythroid differentiation based on dynamic changes in membrane protein expression during

- erythropoiesis. *Proc Natl Acad Sci U S A* **106**, 17413-17418, doi:10.1073/pnas.0909296106 (2009).
- 239 Marsee, D. K., Pinkus, G. S. & Yu, H. CD71 (transferrin receptor): an effective marker for erythroid precursors in bone marrow biopsy specimens. *Am J Clin Pathol* **134**, 429-435, doi:10.1309/ajcpcrk3moaoj6at (2010).
- 240 Mao, B. *et al.* Early Development of Definitive Erythroblasts from Human Pluripotent Stem Cells Defined by Expression of Glycophorin A/CD235a, CD34, and CD36. *Stem Cell Reports* **7**, 869-883, doi:10.1016/j.stemcr.2016.09.002 (2016).
- 241 Chen, L., Gao, Z., Zhu, J. & Rodgers, G. P. Identification of CD13+CD36+ cells as a common progenitor for erythroid and myeloid lineages in human bone marrow. *Exp Hematol* **35**, 1047-1055, doi:10.1016/j.exphem.2007.04.003 (2007).
- 242 Nagata, M., Arimitsu, N., Ito, T. & Sekimizu, K. Antioxidant N-acetyl-L-cysteine inhibits erythropoietin-induced differentiation of erythroid progenitors derived from mouse fetal liver. *Cell Biol Int* **31**, 252-256, doi:10.1016/j.cellbi.2006.11.001 (2007).
- 243 Littlewood, T. & Mandelli, F. The effects of anemia in hematologic malignancies: more than a symptom. *Semin Oncol* **29**, 40-44 (2002).
- 244 Oyekunle, A. A. *et al.* Chronic Myeloid Leukemia in Nigerian Patients: Anemia is an Independent Predictor of Overall Survival. *Clin Med Insights Blood Disord* **9**, 9-13, doi:10.4137/cmbd.s31562 (2016).
- 245 Hellstrom-Lindberg, E. *et al.* Erythroid response to treatment with G-CSF plus erythropoietin for the anaemia of patients with myelodysplastic syndromes: proposal for a predictive model. *Br J Haematol* **99**, 344-351, doi:10.1046/j.1365-2141.1997.4013211.x (1997).
- 246 Ludwig, H. Anemia of hematologic malignancies: what are the treatment options? *Semin Oncol* **29**, 45-54 (2002).
- 247 Oguro, H., Ding, L. & Morrison, S. J. SLAM family markers resolve functionally distinct subpopulations of hematopoietic stem cells and multipotent progenitors. *Cell Stem Cell* **13**, 102-116, doi:10.1016/j.stem.2013.05.014 (2013).
- 248 Kent, D. G. *et al.* Prospective isolation and molecular characterization of hematopoietic stem cells with durable self-renewal potential. *Blood* **113**, 6342-6350, doi:10.1182/blood-2008-12-192054 (2009).
- 249 Moura, M. S. *et al.* Evaluation of anemia after long-term treatment with imatinib in chronic myeloid leukemia patients in chronic phase. *Hematol Transfus Cell Ther*, doi:10.1016/j.htct.2019.03.006 (2019).
- 250 Sakurai, M. *et al.* Renal dysfunction and anemia associated with long-term imatinib treatment in patients with chronic myelogenous leukemia. *Int J Hematol* **109**, 292-298, doi:10.1007/s12185-019-02596-z (2019).
- 251 Ko, P. S. *et al.* Moderate anemia at diagnosis is an independent prognostic marker of the EUTOS, Sokal, and Hasford scores for survival and treatment response in chronic-phase, chronic myeloid leukemia patients with frontline imatinib. *Curr Med Res Opin* **33**, 1737-1744, doi:10.1080/03007995.2017.1356708 (2017).
- 252 Yap, E. *et al.* MicroRNAs that affect the Fanconi Anemia/BRCA pathway are downregulated in imatinib-resistant chronic myeloid leukemia patients without detectable BCR-ABL kinase domain mutations. *Leuk Res* **59**, 32-40, doi:10.1016/j.leukres.2017.05.015 (2017).
- 253 Cortes, J. *et al.* Erythropoietin is effective in improving the anemia induced by imatinib mesylate therapy in patients with chronic myeloid leukemia in chronic phase. *Cancer* **100**, 2396-2402, doi:10.1002/cncr.20292 (2004).

- 254 Fraser, J. *et al.* Targeting of early endosomes by autophagy facilitates EGFR recycling and signalling. *EMBO Rep*, e47734, doi:10.15252/embr.201947734 (2019).
- 255 Vanzo, R. *et al.* Autophagy role(s) in response to oncogenes and DNA replication stress. *Cell Death Differ*, doi:10.1038/s41418-019-0403-9 (2019).
- 256 Yang, Z. J., Chee, C. E., Huang, S. & Sinicrope, F. A. The role of autophagy in cancer: therapeutic implications. *Mol Cancer Ther* **10**, 1533-1541, doi:10.1158/1535-7163.mct-11-0047 (2011).
- 257 Rybstein, M. D., Bravo-San Pedro, J. M., Kroemer, G. & Galluzzi, L. The autophagic network and cancer. *Nat Cell Biol* **20**, 243-251, doi:10.1038/s41556-018-0042-2 (2018).
- 258 Galluzzi, L. *et al.* Autophagy in malignant transformation and cancer progression. *Embo j* **34**, 856-880, doi:10.15252/emboj.201490784 (2015).
- 259 Lee, I. H. *et al.* Atg7 modulates p53 activity to regulate cell cycle and survival during metabolic stress. *Science* **336**, 225-228, doi:10.1126/science.1218395 (2012).
- 260 Yamamoto, H. *et al.* Atg9 vesicles are an important membrane source during early steps of autophagosome formation. *J Cell Biol* **198**, 219-233, doi:10.1083/jcb.201202061 (2012).
- 261 Reggiori, F. & Tooze, S. A. Autophagy regulation through Atg9 traffic. *J Cell Biol* **198**, 151-153, doi:10.1083/jcb.201206119 (2012).
- 262 Datan, E. *et al.* mTOR/p70S6K signaling distinguishes routine, maintenance-level autophagy from autophagic cell death during influenza A infection. *Virology* **452-453**, 175-190, doi:10.1016/j.virol.2014.01.008 (2014).
- 263 Ertmer, A. *et al.* The anticancer drug imatinib induces cellular autophagy. *Leukemia* **21**, 936-942, doi:10.1038/sj.leu.2404606 (2007).
- 264 Weisberg, E. *et al.* Characterization of AMN107, a selective inhibitor of native and mutant Bcr-Abl. *Cancer Cell* **7**, 129-141, doi:10.1016/j.ccr.2005.01.007 (2005).
- 265 Weisberg, E. *et al.* AMN107 (nilotinib): a novel and selective inhibitor of BCR-ABL. *Br J Cancer* **94**, 1765-1769, doi:10.1038/sj.bjc.6603170 (2006).
- 266 Kundu, M. Too sweet for autophagy: hexokinase inhibition of mTORC1 activates autophagy. *Mol Cell* **53**, 517-518, doi:10.1016/j.molcel.2014.02.009 (2014).
- 267 Han, S. H. *et al.* GCA links TRAF6-ULK1-dependent autophagy activation in resistant chronic myeloid leukemia. *Autophagy*, 1-15, doi:10.1080/15548627.2019.1596492 (2019).
- 268 Call, J. A. *et al.* Ulk1-mediated autophagy plays an essential role in mitochondrial remodeling and functional regeneration of skeletal muscle. *Am J Physiol Cell Physiol* **312**, C724-c732, doi:10.1152/ajpcell.00348.2016 (2017).
- 269 Laker, R. C. *et al.* Ampk phosphorylation of Ulk1 is required for targeting of mitochondria to lysosomes in exercise-induced mitophagy. *Nat Commun* **8**, 548, doi:10.1038/s41467-017-00520-9 (2017).
- 270 Calabretta, B. & Salomoni, P. Inhibition of autophagy: a new strategy to enhance sensitivity of chronic myeloid leukemia stem cells to tyrosine kinase inhibitors. *Leuk Lymphoma* **52 Suppl 1**, 54-59, doi:10.3109/10428194.2010.546913 (2011).
- 271 Puissant, A., Robert, G. & Auberger, P. Targeting autophagy to fight hematopoietic malignancies. *Cell Cycle* **9**, 3470-3478, doi:10.4161/cc.9.17.13048 (2010).

- 272 Wang, B. *et al.* The autophagy-inducing kinases, ULK1 and ULK2, regulate axon guidance in the developing mouse forebrain via a noncanonical pathway. *Autophagy* 14, 796-811, doi:10.1080/15548627.2017.1386820 (2018).